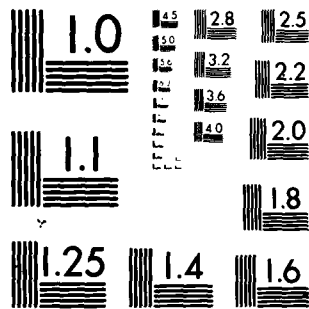


AD-A092 352

CALIFORNIA UNIV BERKELEY EARTHQUAKE ENGINEERING RES--ETC F/G 8/13  
INTERACTION EFFECTS OF SIMULTANEOUS TORSIONAL AND COMPRESSIONAL--ETC(U)  
DEC 79 P M GRIFFIN, W N HOUSTON DAAG29-76-8-0257  
UNCLASSIFIED ICB/EERC-79/34 ARO-13838.1-85 NL

104

2000000



MICROCOPY RESOLUTION TEST CHART  
NATIONAL BUREAU OF STANDARDS 1963-A

SECURITY CLASSIFICATION OF THIS PAGE (When Data Entered)

DTIC  
ELECTE  
DEC 3 1980

UNCLASSIFIED

SECURITY CLASSIFICATION OF THIS PAGE (When Data Entered)

AD A092352

**BMC FILE COPY**

80 12 01 (cont) 142

## 20. ABSTRACT CONTINUED

- 2. Thin-walled Hollow Cylinder tests using longitudinal and torsional cyclic excitation, both separately and in combination.
- 3. Large scale shaking table tests on slope models, using horizontal and vertical cyclic excitation, both separately and in combination.

REPORT NO.  
UCB/EERC-79/34  
DECEMBER 1979

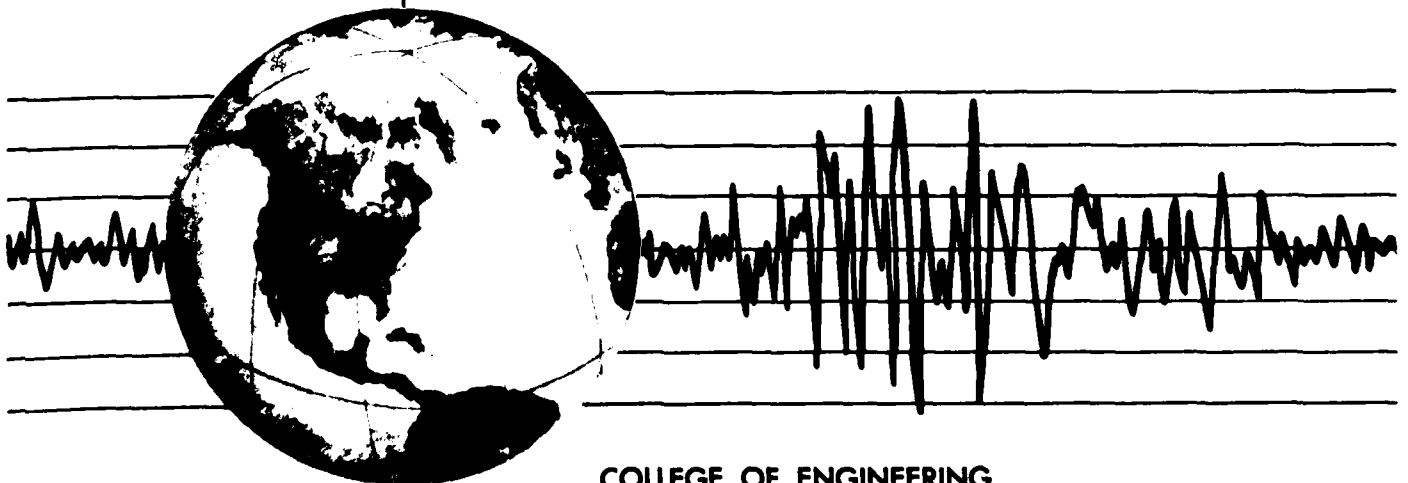
EARTHQUAKE ENGINEERING RESEARCH CENTER

# INTERACTION EFFECTS OF SIMULTANEOUS TORSIONAL AND COMPRESSIONAL CYCLIC LOADING OF SAND

by

PATRICK M. GRIFFIN  
WILLIAM N. HOUSTON

A Report on Research Sponsored by  
the U.S. Army Research Office



COLLEGE OF ENGINEERING  
UNIVERSITY OF CALIFORNIA • Berkeley, California

80 12 01 142

## **DISCLAIMER NOTICE**

**THIS DOCUMENT IS BEST QUALITY  
PRACTICABLE. THE COPY FURNISHED  
TO DTIC CONTAINED A SIGNIFICANT  
NUMBER OF PAGES WHICH DO NOT  
REPRODUCE LEGIBLY.**

EARTHQUAKE ENGINEERING RESEARCH CENTER ✓

INTERACTION EFFECTS OF SIMULTANEOUS TORSIONAL  
AND COMPRESSIONAL CYCLIC LOADING OF SAND

by

Patrick M. Griffin

William N. Houston

Report No. UCB/EERC-79/34 ✓

December 1979

A report on research sponsored by  
the U. S. Army Research Office  
under Grant No. DAAG29-76-G-0257 ✓

College of Engineering  
University of California  
Berkeley, California

APPROVED FOR PUBLIC RELEASE;  
DISTRIBUTION UNLIMITED

### Abstract

An experimental research program based on laboratory test studies and scaled slope model tests was conducted with specimens of Monterey No. 0 sand. The principal objective of the research was to study the effects of interactive coupling during combined compression (normal) and shear loading on the response of sands to dynamic loading. The research program included the following experimental studies:

1. Resonant Column tests on cylindrically shaped specimens using longitudinal and torsional excitation, both separately and in combination.
2. Thin-walled Hollow Cylinder tests using longitudinal and torsional cyclic excitation, both separately and in combination.
3. Large scale shaking table tests on slope models, using horizontal and vertical cyclic excitation, both separately and in combination.

During the course of this research significant effects were observed during combined compression and shear cyclic loading. The primary observed effect of combined loading was the more rapid degradation of modulus with strain than would otherwise occur.

Two methods were developed and presented for calculating the degradation of compression modulus with strain under combined dynamic loading conditions. The first of these, called the Strain Ratio Method, requires the computation of either the instantaneous or an overall average ratio of shear strain amplitude to compression (normal) strain amplitude. The amount of additional degradation in compression modulus due to interactive

coupling may then be determined by reference to a set of typical strain ratio curves which are presented in Figure 7-7 on page 138.

The second method developed is called the Octahedral Shearing Strain Method. This method requires the computation of either the instantaneous or an overall average value of the octahedral shearing strain amplitude. This may be calculated from the strain tensor using either Equation 2-42 on page 18, or Equation 2-44 on page 19. Once this value is determined, the total degradation in compression modulus due to strain, including interactive coupling effects, may be determined by reference to a set of typical octahedral shearing strain curves such as those presented in Figure 7-6 on page 136. Alternatively, a specific set of octahedral shearing strain curves may be developed for any sand by converting the strain amplitude from conventional degradation curves to octahedral shearing strain by use of Equations 2-42 or 2-44 as outlined in the text.

These two methods provide a reasonable estimate of the effects of interactive coupling on the degradation of modulus with strain. Both methods lose accuracy as the straining progresses from elastic to plastic, and as specimens approach failure. Nevertheless, the use of either method under conditions of combined shear and compression loading represents a significant improvement over the practice of neglecting interactive effects.

A series of large scale shaking table tests were conducted upon slope models in an effort to determine when yielding in the slopes began. The slope specimens were subjected to horizontal, and combined horizontal and vertical cyclic excitation. The slopes were thoroughly instrumented to record accelerations and displacements during loading.

Accession For	✓
NTIS GRA&I	
DTIC TAB	
Unannounced	
Justification	
By	
Distribution/	
Avail and/or	
Special	
Dist	
AN	

An analysis method was developed and presented for predicting yield accelerations in granular slopes under combined vertical and horizontal loading conditions. When the shaking table test results were compared with the predicted values of yield acceleration, it was concluded that the predictions were at least as accurate as the empirical measurements could be made. These results were consistent with the conclusion that the effects of combined vertical and horizontal accelerations on yielding of granular slopes may be evaluated using simple superposition.

### Acknowledgments

The authors wish to express their appreciation to the U. S. Army Corps of Engineers for their support and funding for this research.

Valuable assistance during the experimental phases of this study were provided by Mr. C. K. Chan, Research Engineer, and by Messrs. T. W. Pickrell, B. Debeling, M. K. Brock, D. L. Steere, and I. Van Asten of the University of California, Richmond Field Station.

Use of the computer facilities at the University of California Computing Center were subsidized by the Center.

The authors are indebted for numerous stimulating discussions with others, including Drs. F. I. Makdisi, T. C. Kao, and E. Kavazanjian, and with Professors H. B. Seed, J. Lysmer, and J. M. Duncan of the University of California at Berkeley, P. V. Lade of the University of California at Los Angeles, V. P. Drnevich of the University of Kentucky at Lexington, and K. H. Stokoe of the University of Texas at Austin.

Special thanks are extended to Mmes. Pat Clark, Cindy Steen, and Nancy Hoes for their skillful typing of the manuscript, and to Ms. Gloria Pelatowski, for her careful drafting of the numerous figures in this report.

## Table of Contents

	<u>Page</u>
Chapter 1      Introduction	1
Chapter 2      The Strain Tensor	4
Introduction	4
Hooke's Law	4
Hooke's Law in Plane Strain	5
Resonant Column Testing	6
Strain Equations	6
Strain Tensor	8
Hollow Cylinder Testing	9
Strain Equations	9
Tangential Strain Assumption	12
Strain Tensor	13
Incremental Principal Strains	13
Resonant Column	13
Hollow Cylinder	15
Non-Combined Loading	16
Octahedral Strains	18
Octahedral Normal Strain	18
Octahedral Shearing Strain	18
Chapter 3      The State of Stresses	20
Introduction	20
Resonant Column Testing	20
Test Procedure	20
Stress Equations	21

	<u>Page</u>
Vertical Loading Alone	22
Torsional Loading Alone	24
Combined Loading	27
Hollow Cylinder Testing	29
Sample Preparation	29
Consolidation Stress Equations	29
Test Procedure	30
Vertical Loading Alone	32
Torsional Loading Alone	35
Combined Loading	38
Chapter 4      Soil Moduli and Damping Factors	41
Introduction	41
Resonant Column Testing	41
Dynamic Interaction Theory	41
Data Reduction	42
Hollow Cylinder Testing	44
Consolidation Procedure	44
Consolidation Strains	45
Consolidation Modulus Calculation	52
Tangent and Secant Moduli	54
Effect of Torsional Loading on Equations for Moduli	57
Data Reduction	59
Damping	60
Introduction	60
Resonant Column Testing	60
Hollow Cylinder Testing	64

	<u>Page</u>
Chapter 5      Low Strain Combined Cyclic Loading	67
Introduction	67
Vertical Loading Alone	67
Torsional Loading Alone	71
Combined Loading	74
Interaction Effects	74
Strain Ratio Effects	77
Octahedral Shearing Strain Effects	77
Conclusions	91
Strain Ratio Effects	91
Octahedral Shearing Strain Effects	91
Chapter 6      High Strain Combined Cyclic Loading	94
Introduction	94
Vertical Loading Alone	94
Combined Loading	98
Strain Measurements	98
Strain Ratio Effects	102
Octahedral Shearing Strain Effects	108
High Shear Strain Effects	115
Conclusions	124
Strain Ratio Effects	124
Octahedral Shearing Strain Effects	125
High Shear Strain Effects	126
Chapter 7      Comparison of Laboratory Test Results	127
Introduction	127
Vertical Loading Alone	127

	<u>Page</u>
Mean Confining Stress	130
Octahedral Shearing Strain	131
Strain Ratio Effects	135
Conclusions	137
Octahedral Shearing Strain Effects	137
Strain Ratio Effects	139
Chapter 8 Large Scale Model Studies	140
Introduction	140
Test Set-up	141
Test Box	141
Forming Test Specimens	144
Summary of Tests	148
Soil Strength Characteristics	148
Static Slope Failure	148
Direct Shear Tests	150
Shaking Table Tests	157
Test Records	162
Analysis	162
Simplified Analysis	167
Predicted Yield Accelerations	169
Test Results	172
Data Reduction	175
Yield Accelerations	178
Qualitative Observations	181
Additional Observations	183
Analysis of Real Slopes	188

	<u>Page</u>
Displacements	189
Conclusions	191
Chapter 9      Summary and Conclusions	193
Introduction	193
Effects of Combined Cyclic Loading	193
Strain Ratio Method	193
Octahedral Shearing Strain Method	194
Combined Loading Effects on Slope Stability	195
Analysis Method	195
References	197
Appendix A      Testing Equipment	199
Appendix B      Example Test Results	230
Appendix C      Derivations	266
Appendix D      Computer Programs	289

List of Tables

<u>Table No.</u>		<u>Page</u>
4-1	Static Unconstrained Compression Modulus (in psi)	55
5-1	Summary of Resonant Column Tests	69
6-1	Summary of Hollow Cylinder Tests	96
6-2	Maximum Principal Stress Ratios During Cyclic Loading - $(\sigma_1/\sigma_3)_{\max}$ .	99
8-1	Summary of Soil Slope Model Tests	149
8-2	N and S for $D_R \approx 95\%$	152
8-3	N and S for $D_R \approx 80\%$	153
8-4	Predicted Values of Yield Acceleration, $k_y$ , for Various Test Conditions	171
8-5	Summary of Yield Accelerations	180
A2-1	Components of Hollow Cylinder Testing Apparatus	213

### List of Figures

<u>Figure No.</u>		<u>Page</u>
1-1	Gradation Analysis of Monterey No. 0 Sand Used in this Study	3
2-1	Free Body Diagram and State of Strains for Resonant Column Specimens	7
2-2	Free Body Diagram and State of Strains for Hollow Cylinder Specimens	10
2-3	Tangential (a) and Radial (b) Displacement of Hollow Cylinder Specimens Under Load as a Function of Initial Radius	11
2-4	Mohr's Circle in Strain for the " $\theta z$ Plane" for Resonant Column (a) and Hollow Cylinder (b) Specimens Under Dynamic Loading Conditions	14
3-1	Typical Dynamic Loading Sequence for Resonant Column Specimens Under Condition of Vertical Loading Alone: Time Histories of Stress and Strain (a), Mohr's Circle Diagram in Stress (b), and Stress vs Strain Curve (c)	23
3-2	Free Body Diagram (a) and Mohr's Circle in Stress (b) for Resonant Column Specimens Under Condition of Maximum Instantaneous Vertical Stress	25
3-3	Mohr's Circle in Stress (a) and Two-Dimensional Free Body Diagram (b) for Resonant Column Specimens Under Condition of Maximum Instantaneous Torsional Stress	26
3-4	Mohr's Circle in Stress (a) and Stress Time Histories (b) for Simultaneous Dynamic Loading of Resonant Column Specimens Under Condition of Maximum Instantaneous Vertical and Torsional Stress	28
3-5	Free Body Diagram (a) and Mohr's Circles in Stress (b and c) for Hollow Cylinder Specimens Under Condition of Anisotropic Consolidation	31
3-6	Test Records for 4 Typical Hollow Cylinder Tests	33
3-7	Typical Loading Sequence for Hollow Cylinder Specimens Under Condition of Vertical Loading Alone: Time Histories of Stress and Strain (a) and Stress vs Strain Curve (b)	34

<u>Figure No.</u>		<u>Page</u>
3-8	Mohr's Circle in Stress for Hollow Cylinder Specimens Under Condition of Maximum Instantaneous Vertical Stress	36
3-9	Mohr's Circle in Stress (a) and Two-Dimensional Free Body Diagram (b) for Hollow Cylinder Specimens Under Condition of Maximum Instantaneous Torsional Stress	37
3-10	Stress Time Histories (a) and Mohr's Circle in Stress (b) for Simultaneous Dynamic Loading of Hollow Cylinder Specimens Under Condition of Maximum Instantaneous Vertical and Torsional Stress	39
4-1	Effect of the Direction of the Incremental Stresses and Strains on Propagation of Displacements in Cylindrical Resonant Column Samples	43
4-2	Variation of $\epsilon_z$ with Isotropic Increment of Lateral Consolidation Loading, $\sigma_3$ , from 0.5 to 2.0 KSC, for Several Tests	46
4-3	Variation of $\epsilon_z$ with Isotropic Increment of Lateral Consolidation Loading, $\sigma_3$ , from 2.0 to 3.5 KSC, for Several Tests	47
4-4	Summary of Variations of $\epsilon_z$ with Isotropic Increments of Lateral Consolidation Loading, $\sigma_3$ ; and Extrapolation of Initial Increment of Strain from 0 to 0.5 KSC	48
4-5	Variation of $\epsilon_z$ with Both Isotropic and Anisotropic Increments of Vertical Consolidation Loading, $\sigma_z$ , from 0.925 to 3.7 KSC, for Several Tests	50
4-6	Variation of $\epsilon_z$ with Both Isotropic and Anisotropic Increments of Vertical Consolidation Loading, $\sigma_z$ , from 3.7 to 6.475 KSC, for Several Tests	51
4-7	Summary of Variations of $\epsilon_z$ with Isotropic and Anisotropic Increments of Vertical Consolidation Loading, $\sigma_z$ ; and Extrapolation of Initial Increment of Strain from 0 to 0.925 KSC	53
4-8	Mohr's Circle in Strain (a) and in Stress (b) for Hollow Cylinder Test Specimens Under Condition of Maximum Instantaneous Torsional Stress and Strain	58
4-9	Amplitude Decay Method (a) and Magnification Factor Approach (b) for Computing Damping in Resonant Column Tests	62

<u>Figure No.</u>		<u>Page</u>
4-10	Hysteretic Stress-Strain Curve for Dynamic Vertical Loading in Hollow Cylinder Test	65
5-1	Resonant Column Testing Apparatus	68
5-2	Degradation of Compression Modulus with Vertical Strain for Several Tests Under Condition of Vertical Loading Alone	70
5-3	Degradation of Normalized Compression Modulus with Vertical Strain for Several Tests Under Condition of Vertical Loading Alone	72
5-4	Degradation of Shear Modulus with Shear Strain for Several Tests Under Condition of Shear Loading Alone	73
5-5	Degradation of Normalized Shear Modulus with Shear Strain for Several Tests Under Condition of Shear Loading Alone	75
5-6	Degradation of Compression Modulus with Vertical Strain Under Several Levels of Simultaneously Applied Shear Strain	76
5-7	Degradation of Normalized Compression Modulus with Ratio of Shear Strain to Vertical Strain at $\sigma_{3c} = 0.5$ KSC for Several Combined Loading Tests	78
5-8	Degradation of Normalized Compression Modulus with Ratio of Shear Strain to Vertical strain at $\sigma_{3c} = 2.0$ KSC for Several Combined Loading Tests	79
5-9	Degradation of Normalized Compression Modulus with Ratio of Shear Strain to Vertical Strain at $\sigma_{3c} = 3.5$ KSC for Several Combined Loading Tests	80
5-10	Summary of Degradation of Normalized Compression Modulus with Ratio of Shear Strain to Vertical Strain for a Relative Density of 95%	81
5-11	Summary of Degradation of Normalized Compression Modulus with Ratio of Shear Strain to Vertical Strain for All Combined Loading Tests	82
5-12	Degradation of Normalized Compression Modulus with Octahedral Shearing Strain for Condition of Vertical Loading Alone	83

<u>Figure No.</u>		<u>Page</u>
5-13	Degradation of Normalized Compression Modulus with Octahedral Shearing Strain at $\sigma_{3c} = 0.5$ KSC for Several Combined Loading Tests	85
5-14	Degradation of Normalized Compression Modulus with Octahedral Shearing Strain at $\sigma_{3c} = 2.0$ KSC for Several Combined Loading Tests	86
5-15	Degradation of Normalized Compression Modulus with Octahedral Shearing Strain at $\sigma_{3c} = 3.5$ KSC for Several Combined Loading Tests	87
5-16	Degradation of Normalized Compression Modulus with Octahedral Shearing Strain at $\sigma_{3c} = 0.5$ KSC for Both Vertical and Combined Loading Tests	88
5-17	Degradation of Normalized Compression Modulus with Octahedral Shearing Strain at $\sigma_{3c} = 2.0$ KSC for Both Vertical and Combined Loading Tests	89
5-18	Degradation of Normalized Compression Modulus with Octahedral Shearing Strain at $\sigma_{3c} = 3.5$ KSC for Both Vertical and Combined Loading Tests	90
5-19	Summary of Degradation of Normalized Compression Modulus with Octahedral Shearing Strain	92
6-1	Hollow Cylinder Testing Apparatus and Control Panel	95
6-2	Degradation of Compression Modulus with Vertical Strain for Several Tests Under Conditions of Loading Alone	97
6-3	Degradation of Normalized Compression Modulus with Vertical Strain for Several Tests Under Conditions of Vertical Loading Alone	100
6-4	Degradation of Normalized Compression Modulus with Ratio of Shear Strain to Vertical Strain at $\sigma_{3c} = 0.5$ KSC for Several Combined Loading Tests	103
6-5	Degradation of Normalized Compression Modulus with Ratio of Shear Strain to Vertical Strain at $\sigma_{3c} = 2.0$ KSC for Several Combined Loading Tests	104
6-6	Degradation of Normalized Compression Modulus with Ratio of Shear Strain to Vertical Strain at $\sigma_{3c} = 3.5$ KSC for Several Combined Loading Tests	105
6-7	Summary of Degradation of Normalized Compression Modulus with Ratio of Shear Strain to Vertical Strain for All Combined Loading Tests	106

<u>Figure No.</u>		<u>Page</u>
6-8	Effects of Poisson's Ratio, $\mu$ , on the Degradation of the Normalized Compression Modulus with the Ratio of Shear Strain to Vertical Strain for Several Tests	107
6-9	Degradation of Normalized Compression Modulus with Octahedral Shearing Strain for Condition of Vertical Loading Alone	109
6-10	Degradation of Normalized Compression Modulus with Octahedral Shearing Strain at $\sigma_{3c} = 0.5$ KSC for Several Combined Loading Tests with a Constant Vertical Strain of $10^{-1}\%$	110
6-11	Degradation of Normalized Compression Modulus with Octahedral Shearing Strain at $\sigma_{3c} = 2.0$ KSC for Several Combined Loading Tests with a Constant Vertical Strain of $10^{-1}\%$	111
6-12	Degradation of Normalized Compression Modulus with Octahedral Shearing Strain at $\sigma_{3c} = 3.5$ KSC for Several Combined Loading Tests with a Constant Vertical Strain of $10^{-1}\%$	112
6-13	Summary of Degradation of Normalized Compression Modulus with Octahedral Shearing Strain for All Combined Loading Tests at a Constant Vertical Strain of $10^{-1}\%$	113
6-14	Summary of Degradation of Normalized Compression Modulus with Octahedral Shearing Strain for All Combined Loading Tests at a Constant Vertical Strain of $2 \times 10^{-2}\%$	114
6-15	Degradation of Normalized Compression Modulus with Octahedral Shearing Strain at $\sigma_{3c} = 0.5$ KSC for Both Vertical and Combined Loading Tests	116
6-16	Degradation of Normalized Compression Modulus with Octahedral Shearing Strain at $\sigma_{3c} = 2.0$ KSC for Both Vertical and Combined Loading Tests	117
6-17	Degradation of Normalized Compression Modulus with Octahedral Shearing Strain at $\sigma_{3c} = 3.5$ KSC for Both Vertical and Combined Loading Tests	118
6-18	Degradation of Normalized Compression Modulus with Octahedral Shearing Strain for All Vertical and Combined Loading Tests	119

<u>Figure No.</u>		<u>Page</u>
6-19	Summary of Degradation of Normalized Compression Modulus with Octahedral Shearing Strain	120
6-20	Typical Stress vs Strain Curves in Vertical Compression Under Condition of Simultaneous Very High Relative Shear Strain	122
6-21	Matrix of a Uniformly Graded Granular Material (a) and Detail of Vertical Normal Strain Resulting from Application of Shear Stress (b) Including Time Histories (c)	123
7-1	Summary of Degradation of Normalized Compression Modulus with Vertical Strain for Resonant Column and Hollow Cylinder Tests Under Condition of Vertical Loading Alone	128
7-2	Degradation of Normalized Compression Modulus with Vertical Strain Under Condition of Vertical Loading Alone at Lateral Confining Pressures, $\sigma_{3c}$ , of 0.5, 2.0, and 3.5 KSC	129
7-3	Interpolation of Normalized Compression Modulus Values for Mean Confining Pressures, $\sigma_m$ , of 0.5, 2.0, and 3.5 KSC	132
7-4	Degradation of Normalized Compression Modulus with Vertical Strain for Hollow Cylinder Tests Under Condition of Vertical Loading Alone for Mean Confining Pressure, $\sigma_m$ , of 0.5, 2.0, and 3.5 KSC	133
7-5	Degradation of Normalized Compression Modulus with Vertical Strain Under Condition of Vertical Loading Alone at Mean Confining Pressures, $\sigma_m$ , of 0.5, 2.0, and 3.5 KSC	134
7-6	Degradation of Normalized Compression Modulus with Octahedral Shearing Strain at Mean Confining Pressures, $\sigma_m$ , of 0.5, 2.0, and 3.5 KSC	136
7-7	Summary of Degradation of Normalized Compression Modulus with Ratio of Shear Strain to Normal Strain	138
8-1	Cut-Away View of Typical Slope Specimen Showing Location of Instrumentation	142
8-2	Detail of Test Box (a) and Bracing Behind Spacer Board (b)	143
8-3	Two Views of Forming Mold Assembly Used When Constructing Slope Specimens	145

<u>Figure No.</u>		<u>Page</u>
8-4	Two Views of a Completed, Instrumented Slope Specimen Ready to be Tested	146
8-5	Detail of Placement of DCDT Core Probes on the Surface of a Slope Specimen (a), and of Sand-Epoxy Bond on Wire Pertusion (b)	147
8-6	Diagram of Forces Acting on the Sliding Block Used in Surface Direct Shear Tests Performed on Slope Specimens	151
8-7	Variation of N and S for Slope Specimen Sands with an Average Relative Density, $D_R = 95\%$	155
8-8	Variation of N and S for Slope Specimen Sands with an Average Relative Density, $D_R = 80\%$	156
8-9	Comparison of Gradation Analyses for Monterey No. 20 and Monterey No. 0 Sands	158
8-10	Relationship Between Shear Strength Intercept and Mean Grain Size for Uniformly Graded Sands (after Seed and Goodman)	159
8-11	Illustration of In-Phase Combined Horizontal and Vertical Loading Used in Slope Tests	160
8-12	Graphical Illustration of Application of Horizontal Acceleration Alone (a) and Combined Horizontal and Vertical Acceleration (b) on Slope Specimens	161
8-13	Examples of Two Acceleration Records Used in Slope Tests	163
8-14	Diagram of Forces Along Sliding Surface at Limiting Equilibrium for Slope Specimens	164
8-15	Variation of Components of Equation 8.18 with the Angle, $\omega$ , of Application of Yield Acceleration, $k_y$	168
8-16	Relationship Between Slope Length, Shear Strength Intercept, and Angle $\phi_{SL}$ (after Seed and Goodman)	170
8-17	Acceleration Test Records for Tests 2 and 3	173
8-18	Acceleration Test Records for Tests 7X and 8Y	174
8-19	Acceleration and DCDT Test Records for Test No. 1	176

<u>Figure No.</u>		<u>Page</u>
8-20	Acceleration and DCDT Test Records for Test No. 4	177
8-21	DCDT Test Records for Test No. 3	182
8-22	DCDT Test Records for Test No. 7X	184
8-23	DCDT Test Records for Test No. 8X	185
8-24	DCDT Test Records for Test No. 8Y	186
8-25	DCDT Test Records for Test No. 8Z	187
A1-1	Resonant Column Testing Apparatus and Setup (a) and Close-up of Sample Prepared for Testing (b)	201
A1-2	Data Sheet for Resonant Column Test No. 1A-3	205
A1-3	Data Sheet for Resonant Column Test No. 12B-2	206
A1-4	Data Sheet for Resonant Column Test No. 18C-3	209
A2-1	Hollow Cylinder Testing Apparatus and Control Panel	211
A2-2	Detail of Load Chain of Hollow Cylinder Testing Apparatus	212
A2-3	View of Left Side of Hollow Cylinder Testing Apparatus (a) and Close-up of Dynamic Load Control System (b)	216
A2-4	View of Rear (a) and Right Side of Hollow Cylinder Testing Apparatus Showing Torsional Loading Cylinders (b)	219
A2-5	Test Records for 4 Typical Hollow Cylinder Tests	222
A3-1	Cut-Away View of Typical Slope Specimen Showing Location of Instrumentation	224
A3-2	View of Test Box on Shaking Table (a) and Close-up of Steel Plate and Spacer Board in Test Box (b)	225
A3-3	View of Specimen Forming Mold in Place within Test Box (a) and View of DCDT's on Mounting Frame and Failed Slope After Testing (b)	227
C4-1	Mohr's Circle in Stress (a) and Stress Time Histories (b) for Simultaneous Dynamic Loading of Resonant Column Specimens Under Condition of Maximum Instantaneous Vertical and Torsional Stress	277

<u>Figure No.</u>		<u>Page</u>
C5-1	Stress Time Histories (a) and Mohr's Circle in Stress (b) for Simultaneous Dynamic Loading of Hollow Cylinder Specimens Under Condition of Maximum Instantaneous Vertical and Torsional Stress	280
C7-1	Free Body Diagram and State of Strains for Hollow Cylinder Specimens	284
C8-1	Gradation Analysis of Monterey No. 0 Sand Used in This Study	287

# LIST OF SYMBOLS

## Roman Letters

$A_{ABO}, A_{A'B'O}$	Area of triangles ABO and A'B'O
$A_l$	Area of hysteresis loop
$a, ACC1, ACC2$	Variable of acceleration, accelerometers 1 and 2
$a_h, a_v$	Horizontal and vertical accelerations
$a_{max}, a_0, a_1$	Peak acceleration response at frequencies $f_{res}, f_0$ , and $f_1$ , respectively
$a_0, a_n$	Acceleration amplitude of 0-th and n-th cycles
$b$	Length of free body sliding block in slope
$C$	Notation indicating combined vertical and torsional loading
$D$	Ratio of critical damping
$DCDT1, DCDT2$	DC linear differential transformers 1 and 2
$D_R$	Relative density
$d$	Depth of free body sliding block in slope
$E, E_{ps}$	Dynamic Young's Modulus and Dynamic Young's Modulus in plane strain
$E \ll \gamma_{\theta z}$	Dynamic Young's Modulus at very low shear strain
$e, e_{min}, e_{max}$	Void ratio, minimum and maximum void ratios
$F_d, F_u$	Lower and upper normal forces acting on free body sliding block in slope
$f_z, f_T$	Vertical and torsional frequency of loading
$f_{res}, f_0, f_1, f_2$	Resonant frequency and frequencies 0, 1, and 2
$G$	Dynamic shear modulus

$G_s$	Unit weight of soil solids
$g$	Acceleration of gravity
$H, H_o, H_N$	Height of specimen, old height, and new height
$H$	Notation indicating horizontal acceleration alone
$I_1, I_2$	First and second invariants of strain
$J, J_o$	Torsional moment of inertia of specimen and top cap system
$k_y$	Yield acceleration
$L$	Length or height of cylindrical specimen
$l, l_{AB}, l_{BC}$	Length, length from A to B, and length from B to C
$M$	Constrained compression modulus
$N, N_w$	Normal stress on failure surface at impending failure and normal stress due to weight of sliding block on slope
$n$	A positive integer
$P$	Normal force exerted by passive wedge at toe of slope
$R$	Radius of specimen
$R$	Resultant force in diagram of forces on free body at toe of slope
$R_{AVG}, R_1, R_2$	Average, inner, and outer radius of hollow
$R_o, R_N$	Old and new radius of cylinder specimen
$r$	Variable in radial direction
$S, S_w$	Shear stress on failure surface at impending failure and shear stress due to weight of sliding block on slope
$s_i$	Shear strength intercept on Mohr's circle diagram
$T$	Notation indicating torsional loading alone
$T$	Upward force applied to sliding block on slope
$T$	Thickness of hollow cylinder specimen

$t$	Variable of time
$u$	Displacement in radial direction
$V$	Notation indicating vertical loading alone
$V_O, V_N$	Old volume and new volume
$V_P, V_S$	Velocity of propagation of "p-wave" and "s-wave"
$V, V_V, V_S$	Volume, volume of voids, and volume of solids
$v$	Displacement in tangential direction
$W, W_S$	Weight of soil
$W_{TOP}$	Weight of top cap system
$w$	Displacement in vertical direction
$x$	Variable in "x" direction
$y$	Variable in "y" direction
$z$	Variable in "z" or vertical direction

### Greek Letters

$\alpha$	A constant
$\alpha$	Phase lag between vertical and torsional loading
$\alpha$	Angle of slope
$\beta$	Angle of reorientation of the principal stresses
$\gamma_d$	Unit weight of dry soil
$\gamma_{OCT}$	Octahedral shearing strain
$\gamma_{xy}, \gamma_{yz}, \gamma_{xz}$	Shear strains within the "xy", "yz", and "xz" planes
$\delta$	Damping calibration factor
$\Delta$	Amplitude decay damping
$\Delta z_o, \Delta \theta_o$	Peak vertical and torsional displacement
$\Delta \gamma_{R\theta}, \Delta \gamma_{Rz}, \Delta \gamma_{\theta z}$	Peak-to-peak or single amplitude shear strain in "R $\theta$ ", "Rz", and " $\theta$ z" planes
$\Delta \epsilon_R, \Delta \epsilon_\theta, \Delta \epsilon_z$	Peak-to-peak or single amplitude normal strain in "R", " $\theta$ ", and "z" directions
$\Delta \sigma_R, \Delta \sigma_\theta, \Delta \sigma_z$	Peak-to-peak or single amplitude normal stress in the "R", " $\theta$ ", and "z" directions
$\Delta \sigma_{a_1}, \Delta \sigma_{a_{max}}$	Driving stress when acceleration response is $a_1$ and $a_{max}$
$\Delta \tau_{R\theta}, \Delta \tau_{Rz}, \Delta \tau_{\theta z}$	Peak-to-peak or single amplitude shear stress in "R $\theta$ ", "Rz", and " $\theta$ z" planes
$\epsilon, \epsilon_x, \epsilon_y, \epsilon_z$	Normal strain and normal strain in the "x", "y", and "z" directions
$\epsilon_{ct}$	Center of Mohr's circle in strain
$\epsilon_{OCT}$	Octahedral normal strain
$\epsilon_{R\theta}, \epsilon_{Rz}, \epsilon_{\theta z}$	Shear strains within "R $\theta$ ", "Rz", and " $\theta$ z" planes

$\epsilon_{vol}$	Volumetric strain
$\epsilon_1, \epsilon_2, \epsilon_3$	Principal strains
$\epsilon_{1c}, \epsilon_{2c}, \epsilon_{3c}$	Principal strains during consolidation
$\lambda$	A constant
$\lambda$	Hysteretic damping
$\pi$	The constant " $\pi$ "
$\rho$	A constant
$\rho$	Mass density of specimen material
$\mu$	Poisson's ratio
$\sigma, \sigma_x, \sigma_y, \sigma_z,$ $\sigma_R, \sigma_\theta$	Normal stress and normal stress in the "x", "y", "z", "R", and " $\theta$ " directions
$\sigma_{ct}$	Center of Mohr's circle in stress
$\sigma_a$	Variable of principal stress
$\sigma_m$	Mean confining stress
$\sigma_1, \sigma_2, \sigma_3$	Principal stresses
$\sigma_{1c}, \sigma_{2c}, \sigma_{3c}$	Principal stresses during consolidation
$\phi, \phi_{ps}$	Angle of internal friction, angle of internal friction in plane strain
$\phi_{max}$	Maximum angle of internal friction
$\phi_{SL}$	Factor in simplified yield acceleration equation
$\tau_{xy}, \tau_{xz}, \tau_{yz}$	Shear stress in the "xy", "xz", and "yz" planes
$\tau_{\theta z}$	Shear stress in the " $\theta z$ " plane
$\theta$	A constant
$\theta$	Angle of passive wedge at toe of slope
$\omega$	Angle of application of resultant acceleration
$\omega_z, \omega_T$	Rotational velocity in vertical and torsional directions

$\psi$

Angle of reorientation of the principal strains

## Chapter 1

### Introduction

The objective of this research was to study the interaction effects of combined compression and shear loading on the response of sands to dynamic loading. This research included the following experimental studies:

1. Resonant Column tests on cylindrically shaped specimens of sand using longitudinal and torsional excitation, separately and in combination (Chapter 5).
2. Thin-walled Hollow Cylinder tests on sand specimens using longitudinal and torsional cyclic excitation, both separately and in combination (Chapter 6).
3. Large scale shaking table tests on slope models constructed with sand, using horizontal and vertical cyclic excitation, both separately and in combination (Chapter 8).

A review of available theories for analyzing soil behavior under dynamic loading conditions was made, and the strain tensor (Chapter 2) and state of stresses (Chapter 3) were developed for the specimens under test in the first two of these studies. Formulae for calculating moduli and damping factors from the results of those studies were developed and presented in Chapter 4. The results of these first two studies were further analyzed and combined in Chapter 7.

The details of the large scale shaking table testing program, including the development of an analysis technique and evaluation of the test results, were presented in Chapter 8.

The mechanical and testing details of the various equipment used in

these experimental studies are presented in Appendix A. Derivations (Appendix C), computer programs (Appendix D), and example test results (Appendix B) are also included.

These experimental studies were performed on specimens constructed of Monterey No. 0 sand, a uniformly graded, fine grained quartz sand processed from beach sand. A gradation analysis of the sand used in these studies is shown in Figure 1-1. The maximum and minimum densities of this sand were found to be as follows:

$$\gamma_{d \max} = 1.707 \text{ gm/cc}, \quad (1.1)$$

and  $\gamma_{d \min} = 1.425 \text{ gm/cc}, \quad (1.2)$

Experimental studies were performed at a variety of densities and confining pressures so that the effects of these variables could be evaluated as well.

## Chapter 1

### Introduction

The objective of this research was to study the interaction effects of combined compression and shear loading on the response of sands to dynamic loading. This research included the following experimental studies:

1. Resonant Column tests on cylindrically shaped specimens of sand using longitudinal and torsional excitation, separately and in combination (Chapter 5).
2. Thin-walled Hollow Cylinder tests on sand specimens using longitudinal and torsional cyclic excitation, both separately and in combination (Chapter 6).
3. Large scale shaking table tests on slope models constructed with sand, using horizontal and vertical cyclic excitation, both separately and in combination (Chapter 8).

A review of available theories for analyzing soil behavior under dynamic loading conditions was made, and the strain tensor (Chapter 2) and state of stresses (Chapter 3) were developed for the specimens under test in the first two of these studies. Formulae for calculating moduli and damping factors from the results of those studies were developed and presented in Chapter 4. The results of these first two studies were further analyzed and combined in Chapter 7.

The details of the large scale shaking table testing program, including the development of an analysis technique and evaluation of the test results, were presented in Chapter 8.

The mechanical and testing details of the various equipment used in

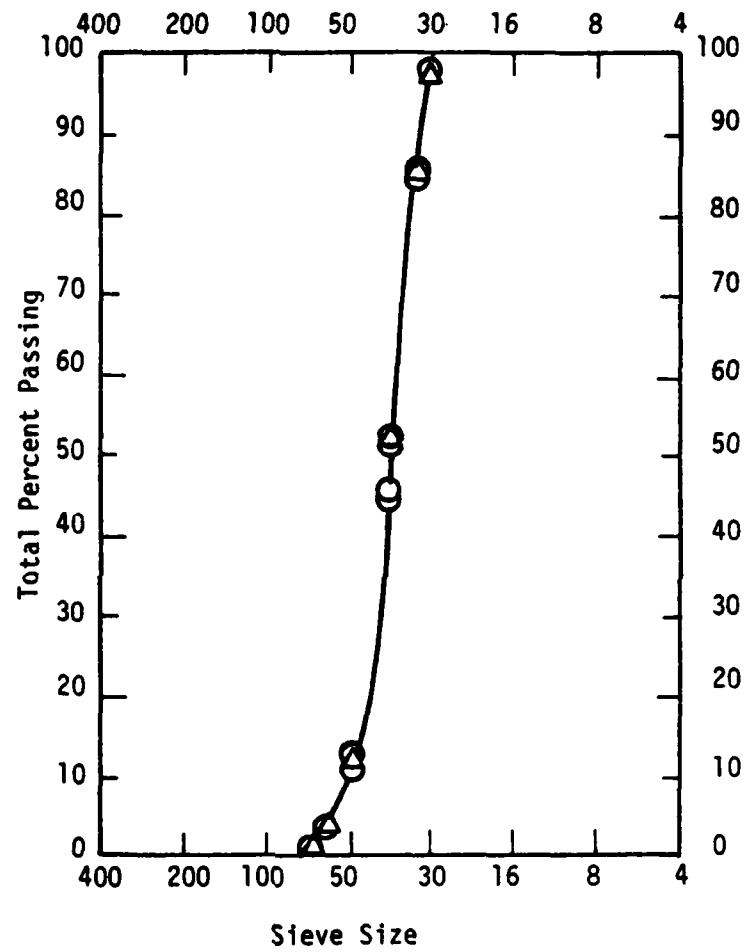


FIGURE 1-1 GRADATION ANALYSIS OF MONTEREY  
NO. 0 SAND USED IN THIS STUDY

## Chapter 2

### The Strain Tensor

#### Introduction

In both the triaxial resonant-column and the thin-walled hollow cylinder testing series forces and displacements are measured in the vertical and torsional directions. However, because of the geometry and complex loading of these specimens, the principal stresses and strains are not directly measurable. It is the purpose of this chapter to describe the strain tensor for these two testing series so that the complete state of strains may be determined from those strains which are directly measurable.

During the two testing series, the maximum strains measured were in the order of  $10^{-1}$ , so that a linear distribution of strains may be assumed. An elastic analysis of the stress-strain response of these soil specimens may be performed with the use of Hooke's Law.

#### Hooke's Law

In its simplest form, Hooke's Law for a homogeneous, isotropic body may be expressed as follows:

$$\begin{Bmatrix} \epsilon_x \\ \epsilon_y \\ \epsilon_z \\ \gamma_{yz} \\ \gamma_{xz} \\ \gamma_{xy} \end{Bmatrix} = \begin{bmatrix} \frac{1}{E} & -\frac{\mu}{E} & -\frac{\mu}{E} & 0 & 0 & 0 \\ -\frac{\mu}{E} & \frac{1}{E} & -\frac{\mu}{E} & 0 & 0 & 0 \\ -\frac{\mu}{E} & -\frac{\mu}{E} & \frac{1}{E} & 0 & 0 & 0 \\ 0 & 0 & 0 & \frac{2(1+\mu)}{E} & 0 & 0 \\ 0 & 0 & 0 & 0 & \frac{2(1+\mu)}{E} & 0 \\ 0 & 0 & 0 & 0 & 0 & \frac{2(1+\mu)}{E} \end{bmatrix} \begin{Bmatrix} \sigma_x \\ \sigma_y \\ \sigma_z \\ \tau_{yz} \\ \tau_{xz} \\ \tau_{xy} \end{Bmatrix} \quad (2.1)$$

The use of Hooke's Law for modeling the stress-strain behavior of a material implies several assumptions. The material is assumed to behave linearly and elastically during loading, so that the strains considered must be small enough so that changes in shape and size are negligible. Hooke's Law further implies that superposition of loading effects is valid, and that the principal stresses and strains are in the same directions.

#### Hooke's Law in Plane Strain

For the special case of plane strain in the xy plane, Hooke's Law reduces to the following expressions.

$$\left. \begin{aligned} \epsilon_z &\approx 0 \\ \gamma_{xz} &\approx 0 \\ \gamma_{yz} &\approx 0 \end{aligned} \right\} \quad (2.2)$$

$\sigma_z$  can be expressed as:

$$\sigma_z = \mu \cdot (\sigma_x + \sigma_y) \quad (2.3)$$

And:

$$\begin{Bmatrix} \epsilon_x \\ \epsilon_y \\ \gamma_{xy} \end{Bmatrix} = \begin{bmatrix} \frac{1}{E}(1-\mu^2) & -\frac{1}{E}(\mu+\mu^2) & 0 \\ -\frac{1}{E}(\mu+\mu^2) & \frac{1}{E}(1-\mu^2) & 0 \\ 0 & 0 & \frac{2(1+\mu)}{E} \end{bmatrix} \begin{Bmatrix} \sigma_x \\ \sigma_y \\ \tau_{xy} \end{Bmatrix} \quad (2.4)$$

### Resonant-Column Testing

The strain tensor for the triaxial resonant-column testing series may be expressed in "cylindrical" coordinates in the following form:

$$\epsilon = \begin{bmatrix} \epsilon_R & \epsilon_{R\theta} & \epsilon_{Rz} \\ \epsilon_{\theta R} & \epsilon_\theta & \epsilon_{\theta z} \\ \epsilon_{zR} & \epsilon_{z\theta} & \epsilon_z \end{bmatrix} \quad (2.5)$$

where the  $R$ ,  $\theta$ , and  $z$  directions are as shown in Figure 2-1(c) and  $\epsilon_{\theta z} = \gamma_{\theta z}$ ,  $\epsilon_{R\theta} = \gamma_{R\theta}$ , and  $\epsilon_{zR} = \gamma_{zR}$ . To maintain equilibrium, we can see from Figure 2-1(b) that  $|\epsilon_{R\theta}| = |\epsilon_{\theta R}|$ ,  $|\epsilon_{Rz}| = |\epsilon_{zR}|$ , and  $|\epsilon_{z\theta}| = |\epsilon_{\theta z}|$ ; and so  $[\epsilon]$  must be a symmetrical matrix which is uniquely defined by six strains.

### Strain Equations

If the displacements  $u$ ,  $v$ , and  $w$  are defined as shown in Figure 2-1(c), the strains can be defined as follows:

$$\epsilon_R = \frac{du}{dr} \quad (2.6)$$

$$\epsilon_\theta = \frac{u}{r} + \frac{dv}{d\theta} \quad (2.7)$$

$$\epsilon_z = \frac{dw}{dz} \quad (2.8)$$

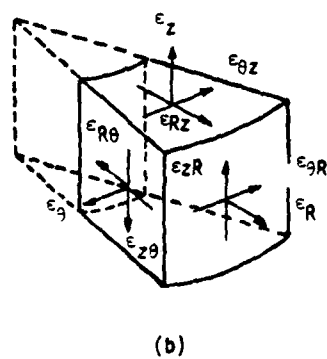
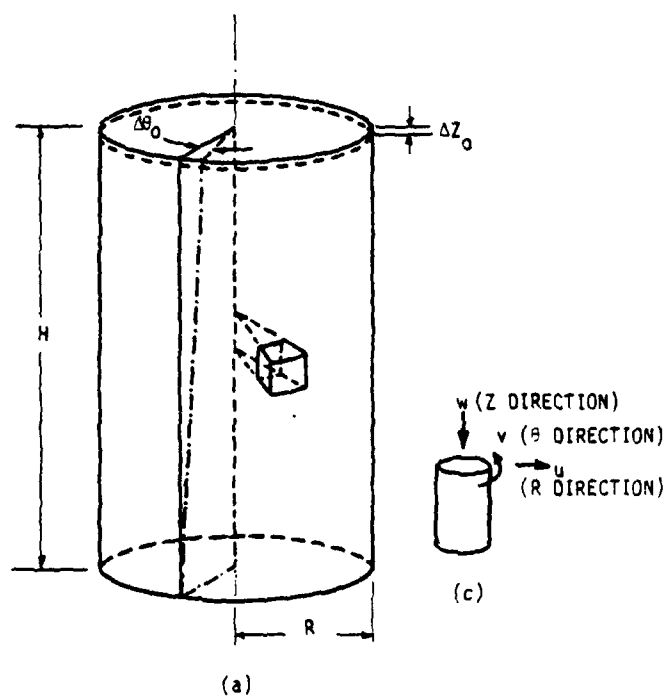


FIGURE 2-1 FREE BODY DIAGRAM AND STATE OF STRAINS  
FOR RESONANT COLUMN SPECIMENS

$$\epsilon_{R\theta} = \epsilon_{\theta R} = \frac{1}{2} \left( \frac{1}{r} \frac{du}{d\theta} + \frac{dv}{dr} - \frac{v}{r} \right) \quad (2.9)$$

$$\epsilon_{z\theta} = \epsilon_{\theta z} = \frac{1}{2} \left( \frac{dv}{dz} + \frac{1}{r} \frac{dw}{d\theta} \right) \quad (2.10)$$

$$\epsilon_{Rz} = \epsilon_{zR} = \frac{1}{2} \left( \frac{du}{dz} + \frac{dw}{dr} \right) \quad (2.11)$$

For this testing series, the following boundary conditions exist:

$$1. \quad w = \alpha \cdot z, \quad \alpha = \epsilon_z \quad (2.12)$$

$$2. \quad v = r \cdot z \cdot \Delta\theta_0 \quad (2.13)$$

Equation 2.12, states that the vertical strain is known. This is true because it is directly calculated in all of the tests. The assumption expressed in Equation 2.13 is that the torsional displacement  $v$  varies linearly in both the  $r$  and  $z$  directions. This condition is illustrated in Figure 2-1(a).

#### Strain Tensor

Applying boundary conditions 1 and 2 (Equations 2.12 and 2.13) to the six strains which define the strain tensor (Equations 2.6 through 2.11) yields the following:

$$\epsilon = \begin{bmatrix} -\mu\epsilon_z & 0 & 0 \\ 0 & -\mu\epsilon_z & \frac{1}{2}r\Delta\theta_0 \\ 0 & \frac{1}{2}r\Delta\theta_0 & \epsilon_z \end{bmatrix} \quad (2.14)$$

A detailed derivation of the above expression appears in Appendix C-1.

### Hollow Cylinder Testing

In the case of the thin-walled hollow cylinder testing series the strain tensor may be expressed in the same form as Equation 2.5, but the strains are now as shown in Figure 2-2.

#### Strain Equations

As with the resonant-column testing series,  $[\epsilon]$  is a symmetric matrix about the normal strain diagonal, and is uniquely defined by six strains. From Figures 2-2 and 2-3 those strains can be defined as follows:

$$\epsilon_z = \frac{dw}{dz} \quad (2.8)$$

$$\epsilon_\theta = \left[ \frac{(1 - R_{AVG}/r)}{(1 - R_{AVG}/R_2)} \cdot \left( \frac{R_{2NEW}}{R_{2OLD}} - 1 \right) \right]_{R_{AVG} < r < R_2} \quad (2.15)$$

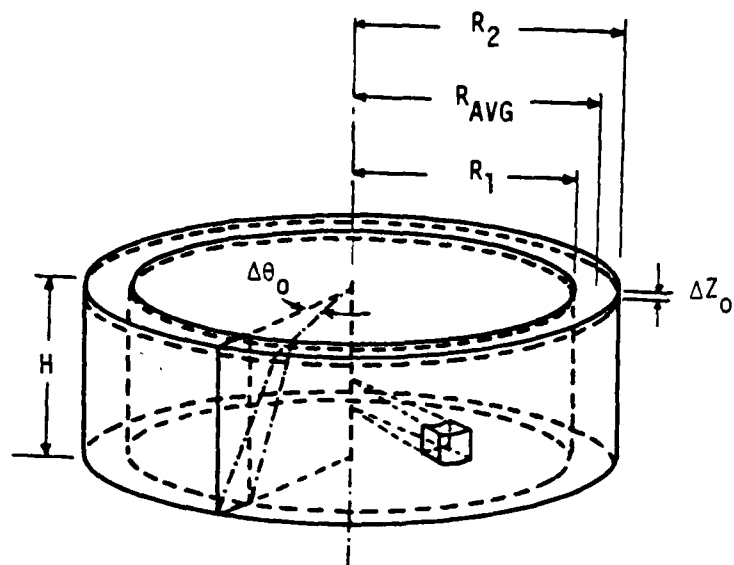
$$\epsilon_\theta \Big|_{R_{AVG} < r < R_2} = -\epsilon_\theta \Big|_{R_1 < r < R_{AVG}}$$

$$\epsilon_R = \left[ \frac{R_{2NEW} - R_{AVG}}{R_{2OLD} - R_{AVG}} - 1 \right]_{R_1 < r < R_2} \quad (2.16)$$

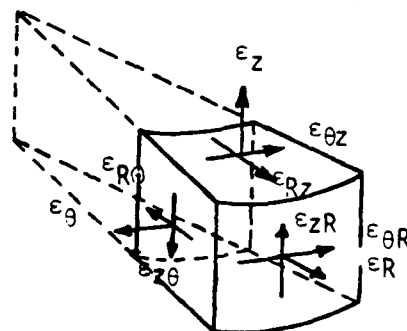
$$\epsilon_{R\theta} = \frac{1}{2} \left( \frac{1}{r} \frac{du}{d\theta} + \frac{dv}{dr} - \frac{v}{r} \right) \quad (2.9)$$

$$\epsilon_{z\theta} = \frac{1}{2} \left( \frac{dv}{dz} + \frac{dw}{d\theta} \right) \quad (2.10)$$

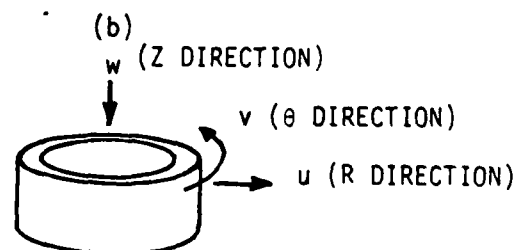
$$\epsilon_{Rz} = \frac{1}{2} \left( \frac{du}{dz} + \frac{dw}{dr} \right) \quad (2.11)$$



(a)

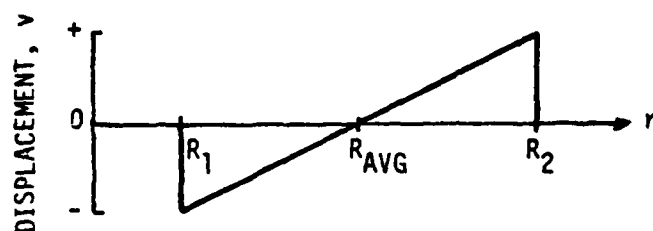


(b)

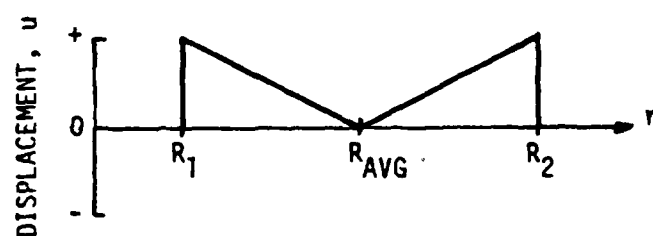


(c)

FIGURE 2-2 FREE BODY DIAGRAM AND STATE OF STRAINS FOR HOLLOW CYLINDER SPECIMENS



(a) TANGENTIAL DISPLACEMENT,  $v$



(b) RADIAL DISPLACEMENT,  $u$

FIGURE 2-3 TANGENTIAL (a) AND RADIAL (b) DISPLACEMENT OF HOLLOW CYLINDER SPECIMENS UNDER LOAD AS A FUNCTION OF INITIAL RADIUS

### Tangential Strain Assumption

Note that Equations 2.8 through 2.11 are identical to the expressions developed for the resonant-column testing series. The assumption implicit in Equations 2.15 and 2.16 and in Figure 2-3 is that the thin-walled hollow cylinder specimen will strain in such a way that the average radius,  $R_{AVG}$ , remains unchanged during loading. This assumption is equivalent to the assumption that  $\epsilon_\theta = 0$ . If  $\gamma_{R\theta} = \gamma_{z\theta} = 0$ , such as during consolidation or vertical loading alone, a plane strain condition exists.

Because of the geometry and the end platen boundary conditions of the thin-walled hollow cylinder specimen, the assumption of  $\epsilon_\theta = 0$  is reasonable. As the specimen is loaded compressively in the vertical direction, the specimen will compress vertically and bulge radially. This radial straining will appear as a bulging on both the inner and outer walls of the cylinder. At some radius within the specimen the radial (and tangential) displacement will be zero. If that radius is the average radius,  $R_{AVG}$ , then the net tangential strain will be zero, as illustrated in Figure 2-3(a). If the no-strain radius is some other value, the net tangential strain will not be zero, but will be very small when compared with the net radial strain. Marachi et al, (1969) have shown that under this type of net strain condition the stress-strain response is essentially that of plane strain.

For this testing series the following boundary conditions exist:

1.  $w = \alpha \cdot z, \alpha = \epsilon_z$  (2.12)
2.  $v = r \cdot z \cdot \Delta\theta_0$

Note that these are identical to the boundary conditions for the triaxial resonant-column testing series.

### Strain Tensor

Applying these boundary conditions to the six strain equations defining the strain tensor (Equations 2.8 through 2.11, 2.15, and 2.16) gives the following expression for the strain tensor:

$$\epsilon = \begin{bmatrix} -\left(\frac{\mu+\mu^2}{1-\mu^2}\right)\epsilon_z & 0 & 0 \\ 0 & 0 & \frac{1}{2}R_{AVG}\Delta\theta_0 \\ 0 & \frac{1}{2}R_{AVG}\Delta\theta_0 & \epsilon_z \end{bmatrix} \quad (2.17)$$

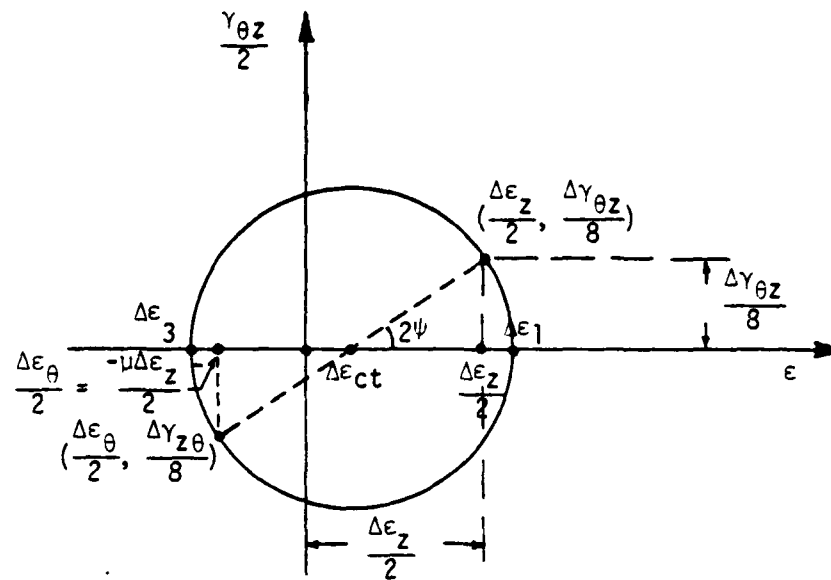
A detailed derivation of the above expression appears in Appendix C-2. It was assumed that  $\epsilon_\theta = 0$  for this derivation.

### Incremental Principal Strains

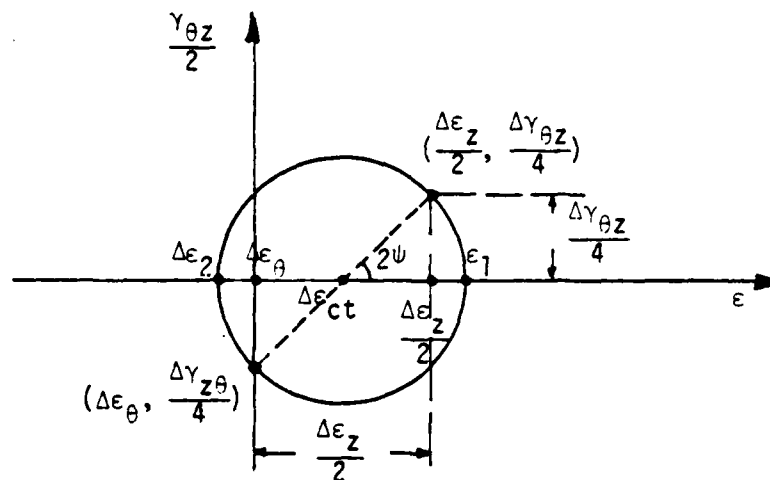
Incremental principal strains may be evaluated using the strain tensors developed in Equations 2.14 and 2.17.

### Resonant Column

In the case of the triaxial resonant column specimens, whose strain tensor is given in Equation 2.14, the Mohr's circle in strain for the  $\theta z$  "plane" is shown in Figure 2-4(a). The condition illustrated in this figure is the case in which the maximum vertical normal strain,  $\frac{\Delta\epsilon_z}{2}$ , is occurring simultaneously with the average shear strain,  $\frac{\Delta\gamma_{\theta z}}{4}$ . As recorded,  $\Delta\gamma_{\theta z}$  and  $\Delta\epsilon_z$  are "peak-to-peak" or double amplitude values. Thus the single amplitude values are  $\Delta\gamma_{\theta z}/2$  and  $\Delta\epsilon_z/2$ . Because the compressional and torsional strains were out of phase and at different frequencies, the average value of  $\Delta\gamma_{\theta z}$  occurring simultaneously with  $\Delta\epsilon_z$



(a)



(b)

FIGURE 2-4 MOHR'S CIRCLE IN STRAIN FOR THE " $\theta z$  PLANE" FOR RESONANT COLUMN (a) AND HOLLOW CYLINDER (b) SPECIMENS UNDER DYNAMIC LOADING CONDITIONS

was approximated as  $\Delta\gamma_{\theta z}/2$ . Thus  $\Delta\gamma_{\theta z}/4$  is used as the average single amplitude value. Because the vertical axis of Mohr's circle is equal to half the shear strain in any direction, the plotted value of shear strain on the  $\theta z$  "plane" is  $\frac{\Delta\gamma_{\theta z}}{8}$ .

From Figure 2-4(a), and the strain tensor (Equation 2.14) the principal strains may be expressed as follows:

$$\Delta\epsilon_1 = \frac{\Delta\epsilon_z}{2} + \frac{\Delta\gamma_{\theta z}}{8} \cdot \tan\psi \quad (2.20)$$

$$\Delta\epsilon_2 = \frac{\Delta\epsilon_R}{2} = -\mu \frac{\Delta\epsilon_z}{2} \quad (2.21)$$

$$\Delta\epsilon_3 = -(\mu \frac{\Delta\epsilon_z}{2} + \frac{\Delta\gamma_{\theta z}}{8} \cdot \tan\psi) \quad (2.22)$$

where,

$$\psi = \begin{cases} \text{angle of orientation of the principal strains} \\ \frac{1}{2} \tan^{-1} \frac{\Delta\gamma_{\theta z}}{8(\frac{\Delta\epsilon_z}{2} - \Delta\epsilon_{ct})} \end{cases} \quad (2.23)$$

and,

$$\Delta\epsilon_{ct} = \left(\frac{1-\mu}{4}\right)\Delta\epsilon_z \quad (2.24)$$

#### Hollow Cylinder

For the case of the thin-walled hollow cylinder testing series, whose strain tensor is presented in Equation 2.17, the Mohr's circle of strain for the  $\theta z$  "plane" is shown in Figure 2-4(b). In this figure the condition of maximum vertical normal strain and simultaneous maximum shear strain is illustrated. In the hollow cylinder series the measured value of  $\Delta\gamma_{\theta z}$  is the double amplitude value, so  $\Delta\gamma_{\theta z}/2$  is the single amplitude value. However, the compressional and torsional strains had

the same frequency. If they were also in phase, as depicted in Figure 2-4(b), then the maximum value of  $\Delta\gamma_{\theta z}$  would always occur when  $\Delta\epsilon_z$  is maximum. Thus it is not necessary to divide  $\Delta\gamma_{\theta z}$  by an additional factor of 2 to get the average value of the shear strain accompanying the maximum value of vertical normal strain, as was done for the resonant column specimens.

Because the vertical axis of the Mohr's circle in strain is equal to one-half the shear strain in any direction, the plotted value of shear strain in the  $\theta z$  "plane" in Figure 2.4(b) is  $\frac{\Delta\gamma_{\theta z}}{4}$ . From the figure the following equations may be written:

$$\Delta\epsilon_1 = \frac{\Delta\epsilon_z}{2} + \frac{\Delta\gamma_{\theta z}}{4} \cdot \tan\psi \quad (2.25)$$

$$\Delta\epsilon_2 = -\frac{\Delta\gamma_{\theta z}}{4} \cdot \tan\psi \quad (2.26)$$

$$\Delta\epsilon_3 = -\left[\frac{\mu + \mu^2}{1 - \mu^2}\right] \frac{\Delta\epsilon_z}{2} \quad (2.27)$$

and, 
$$\psi = \frac{1}{2} \tan^{-1} \left[ \frac{\Delta\gamma_{\theta z}}{\frac{\Delta\epsilon_z}{2} - \Delta\epsilon_{ct}} \right] \quad (2.28)$$

$$\Delta\epsilon_{ct} = \frac{\Delta\epsilon_z}{4} \quad (2.29)$$

#### Non-Combined Loading

For the special case of vertical loading alone, Equations 2.20 through 2.22 reduce to the following:

$$\Delta\epsilon_1 = \frac{\Delta\epsilon_z}{2} \quad (2.30)$$

$$\Delta\epsilon_2 = \Delta\epsilon_3 = -\frac{\mu\Delta\epsilon_z}{2} \quad (2.31)$$

and Equations 2.25 through 2.28 become:

$$\Delta\epsilon_1 = \frac{\Delta\epsilon_z}{2} \quad (2.32)$$

$$\Delta\epsilon_2 = 0 \quad (2.33)$$

$$\Delta\epsilon_3 = -\left[\frac{\mu + \mu^2}{1 - \mu^2}\right] \frac{\Delta\epsilon_z}{2} \quad (2.34)$$

and  $\psi = 0 \quad (2.35)$

In the special loading case of torsional loading alone Equations 2.20 through 2.23 become:

$$\Delta\epsilon_1 = \frac{\Delta\gamma_{\theta z}}{4} \quad (2.36)$$

$$\Delta\epsilon_2 = 0 \quad (2.37)$$

$$\Delta\epsilon_3 = -\frac{\Delta\gamma_{\theta z}}{4} \quad (2.38)$$

$$\psi = 45^\circ \quad (2.39)$$

In the absence of vertical loading it is not necessary to divide  $\Delta\gamma_{\theta z}$  by two to get the average value associated with  $\Delta\epsilon_z$ . Thus the denominator in Equations 2.36 and 2.38 is 4 rather than 8.

Although torsional loading alone was not performed in the hollow cylinder test series, the applicable equations can be derived from Equations 2.25 through 2.29.

Because  $\Delta\epsilon_z/2 = 0$ , Equation 2.27 now defines  $\Delta\epsilon_z$ , which is zero, and

$\Delta\epsilon_3$  is obtained from Equation 2.26. Thus the expressions for  $\Delta\epsilon_1$ ,  $\Delta\epsilon_2$ ,  $\Delta\epsilon_3$  and  $\psi$  become identical to Equations 2.36 through 2.39.

### Octahedral Strains

The nonlinearity of the stress-strain response for soil has been recognized for some time. Researchers have often referred to this nonlinearity as the "degradation of modulus with increasing strain amplitude." The octahedral strains are a very useful tool in evaluating the effects of strain amplitude on modulus because they are both dimensionless and bring into consideration the complete state of strain, and are independent of the orientation of the coordinate system.

#### Octahedral Normal Strain

There are two octahedral strains: the hydrostatic component and the shearing component. The first of these,  $\epsilon_{OCT}$ , is also called the octahedral strain or the octahedral normal strain; and may be computed from the following expression:

$$\epsilon_{OCT} = \frac{I_1}{3} \quad (2.40)$$

where  $I_1$  is the first strain invariant, and may be written:

$$I_1 = \epsilon_x + \epsilon_y + \epsilon_z = \epsilon_\theta + \epsilon_R + \epsilon_z = \epsilon_1 + \epsilon_2 + \epsilon_3 = \epsilon_{vol} \quad (2.41)$$

#### Octahedral Shearing Strain

The second octahedral strain,  $\gamma_{OCT}$ , is also called the octahedral shearing strain; and may be computed from the following:

$$\gamma_{OCT} = \frac{2\sqrt{2}}{3} \cdot \left[ I_1^2 + 3I_2 \right]^{1/2} \quad (2.42)$$

where  $I_2$  is the second strain invariant, and may be written:

$$\begin{aligned}
 I_2 &= -(\epsilon_y \epsilon_z + \epsilon_z \epsilon_x + \epsilon_x \epsilon_y) + \frac{1}{4} \gamma_{yz}^2 + \frac{1}{4} \gamma_{zx}^2 + \frac{1}{4} \gamma_{xy}^2 \\
 &= -(\epsilon_\theta \epsilon_z + \epsilon_z \epsilon_R + \epsilon_\theta \epsilon_R) + \frac{1}{4} \gamma_{\theta z}^2 + \frac{1}{4} \gamma_{zR}^2 + \frac{1}{4} \gamma_{\theta R}^2 \\
 &= -(\epsilon_1 \epsilon_2 + \epsilon_2 \epsilon_3 + \epsilon_1 \epsilon_3)
 \end{aligned} \tag{2.43}$$

In terms of the principal strains, Equation 2.42 may be written as follows:

$$\gamma_{OCT} = \frac{2}{3} \sqrt{(\epsilon_1 - \epsilon_3)^2 + (\epsilon_1 - \epsilon_2)^2 + (\epsilon_2 - \epsilon_3)^2} \tag{2.44}$$

This shearing component has the effect of causing shearing or distortional deformation of a material, whereas the octahedral normal strain has the effect of causing purely normal or compressive deformations.

When considering the process of degradation of modulus with increasing strain amplitude, it is clearly the shearing strain component of the state of strain which causes the degradation. The normal component of the strain tends to increase the modulus with increasing strain amplitude.

For soils assumed to be isotropic the octahedral shearing strain,  $\gamma_{OCT}$ , would appear to be a very useful tool in evaluating the effects of strain on modulus for these testing series since it will bring into consideration both the effect of the dynamic shear strains,  $\Delta \gamma_{\theta z}$ , and the shear strain component of the anisotropic dynamic vertical loading, represented by the diameter of the Mohr's circle in strain in Figure 2-4.

### Chapter 3

#### The State of Stresses

##### Introduction

It is the purpose of this chapter to describe the complete state of stresses of the various soil samples used in both the triaxial resonant-column and the thin-walled hollow cylinder testing series. This presentation will include the magnitude and direction of the principal stresses throughout the load history of the specimens.

Assuming that the material is behaving both linearly and elastically, the principal stresses and directions may be easily calculated if the values of all stresses on three mutually perpendicular planes are known. In the two testing series conducted, the stresses were measured in different manners and the specimens were subjected to different pre-loading consolidation stress histories; therefore, the state of stress will be discussed separately for each series.

##### Resonant-Column Testing

###### Test Procedure

In this testing series cylindrically shaped specimens of sand were isotropically consolidated to one of the following confining pressure: 0.5 KSC, 2.0 KSC, and 3.5 KSC ( $1 \text{ KSC} = 1 \text{ kg/cm}^2 = 98.07 \text{ kN/m}^2$ ). The samples were then fixed at the base and excited from the cap with a pure sinusoidal force of very low amplitude. The frequency of this excitation was adjusted to the undamped natural frequency (also called the resonant frequency) of the soil column. The acceleration response of the

soil column was measured with a calibrated accelerometer mounted in the cap of the specimen.

The resonant frequency was obtained with the use of an oscilloscope by displaying a Lissajous figure of the excitation and the acceleration response. When the two axes of the elliptical Lissajous figure are in the same directions as the input axes (i.e.: the vertical and horizontal plates), then the two signals are at the same frequency but  $90^\circ$  out of phase. For the resonant-column sample, the frequency at which the input excitation and the acceleration response are  $90^\circ$  out of phase is by definition the undamped natural frequency.

From the calibrated acceleration response and the geometry of the specimen, the peak-to-peak strain response may be easily calculated.

During testing of a specimen the excitation may be axial (vertical), torsional, or both simultaneously. In a typical test the specimen will be loaded with a particular excitation for less than two minutes, then the excitation amplitude is increased and the process repeated.

Values of dynamic unconstrained compression modulus (also called dynamic Young's modulus) and dynamic shear modulus are calculated from the resonant frequency, the sample geometry and weight and the dynamic response characteristics of the testing apparatus. A more detailed discussion of this calculation is included in Appendix C-3.

#### Stress Equations

The net, peak-to-peak vertical and torsional stress may be calculated by multiplying the calculated modulus by the calculated peak-to-peak strain as follows:

$$\Delta\sigma_z = E \cdot \Delta\epsilon_z \quad (3.1)$$

$$\text{and} \quad \Delta\tau_{z\theta} = G \cdot \Delta\gamma_{z\theta} \quad (3.2)$$

where:

- $E$  = unconstrained compression modulus,
- $G$  = shear modulus,
- $\Delta\sigma_z$  = peak-to-peak vertical stress,
- $\Delta\epsilon_z$  = peak-to-peak vertical strain,
- $\Delta\tau_{z\theta}$  = peak-to-peak torsional stress,
- and  $\Delta\gamma_{z\theta}$  = peak-to-peak torsional strain.

#### Vertical Loading Alone

The typical loading sequence for the case of vertical loading alone is shown in Figure 3-1. In this figure it can be seen that the calculation of the magnitude and direction of the principal stresses is greatly simplified. The principal stress directions are coincident with the directions of the cylindrical coordinate system shown in Figure 2-1; thus their values are equal to the values of  $\sigma_z$ ,  $\sigma_R$ , and  $\sigma_\theta$  as a function of time, where,

- $\sigma_z$  = vertical normal stress,
- $\sigma_R$  = radial normal stress,
- $\sigma_\theta$  = tangential normal stress.

The mathematical expression for the vertical principal stress,  $\sigma_a$ , is as follows:

$$\sigma_a = \sigma_{1c} + \frac{\Delta\sigma_z}{2} \cdot \sin(\omega_z \cdot t) \quad (3.3)$$

where  $\sigma_{1c}$  = vertical principal stress during consolidation

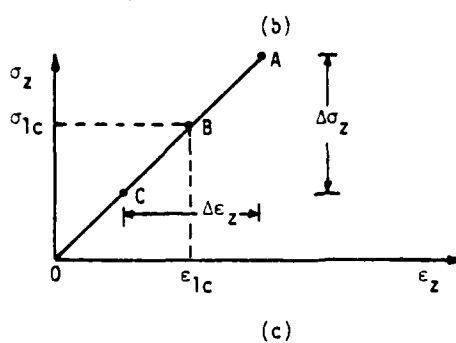
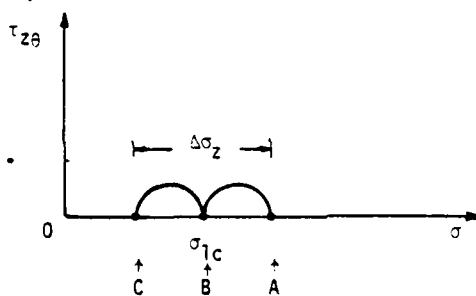
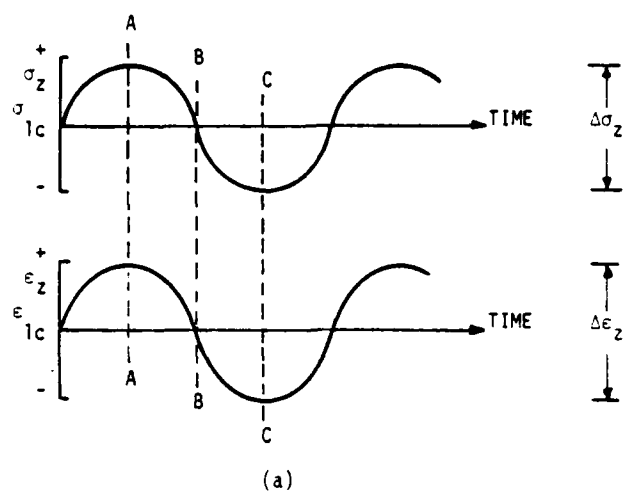


FIGURE 3-1 TYPICAL DYNAMIC LOADING SEQUENCE FOR RESONANT COLUMN SPECIMENS UNDER CONDITION OF VERTICAL LOADING ALONE: TIME HISTORIES OF STRESS AND STRAIN (a), MOHR'S CIRCLE DIAGRAM IN STRESS (b), AND STRESS VS STRAIN CURVE (c)

and 
$$\omega_z = 2 \cdot \pi \cdot f_z \quad (3.4)$$

with  $f_z$  as the vertical resonant frequency.

If a free-body is isolated as was done in Figure 2-1, and the maximum vertical stress condition is plotted upon it, the illustration in Figure 3-2(a) is obtained. Figure 3-2(b) shows the Mohr's circle plot for this loading condition. Note from this figure that:

$$\sigma_1 = \sigma_z = \sigma_R + \frac{\Delta\sigma_z}{2} \quad (3.5)$$

$$\sigma_2 = \sigma_3 = \sigma_R = \sigma_\theta \quad (3.6)$$

where,

$\sigma_1$  = major principal stress,

$\sigma_2$  = intermediate principal stress,

$\sigma_3$  = minor principal stress.

#### Torsional Loading Alone

Under the condition of torsional stress alone, the maximum principal stress Mohr's circle is shown in Figure 3-3(a). With these loading conditions, the principal stresses in the  $\theta z$  "plane" are oriented  $45^\circ$  from the axes in cylindrical coordinates. These principal stress values may be expressed as follows:

$$\sigma_1 = \sigma_{1c} + \left[ \frac{\Delta\tau_{\theta z}}{2} \cdot \sin(\omega_T \cdot t) \right] \quad (3.7)$$

$$\sigma_2 = \sigma_{2c} = \sigma_R \quad (3.8)$$

$$\sigma_3 = \sigma_{3c} - \left[ \frac{\Delta\tau_{\theta z}}{2} \cdot \sin(\omega_T \cdot t) \right] \quad (3.9)$$

where  $\sigma_{1c}$ ,  $\sigma_{2c}$ , and  $\sigma_{3c}$  are the principal stresses during consolidation.

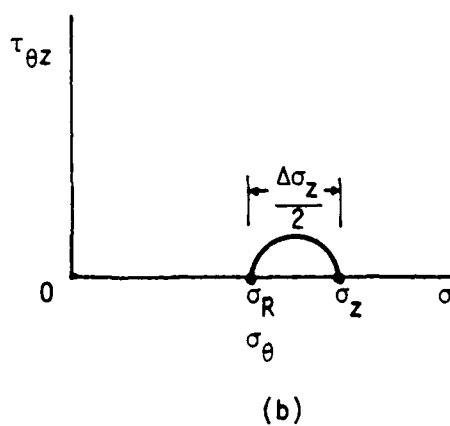
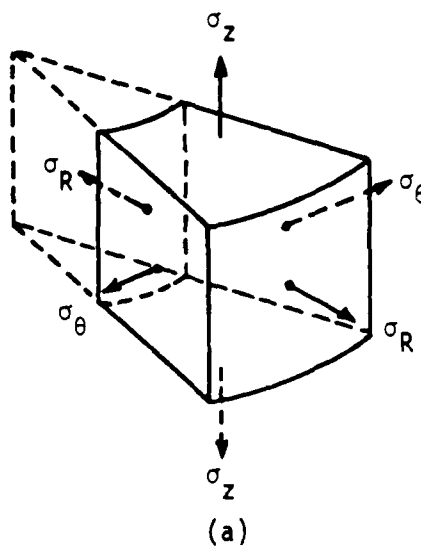


FIGURE 3-2 FREE BODY DIAGRAM (a) AND MOHR'S CIRCLE IN STRESS (b) FOR RESONANT COLUMN SPECIMENS UNDER CONDITION OF MAXIMUM INSTANTANEOUS VERTICAL STRESS

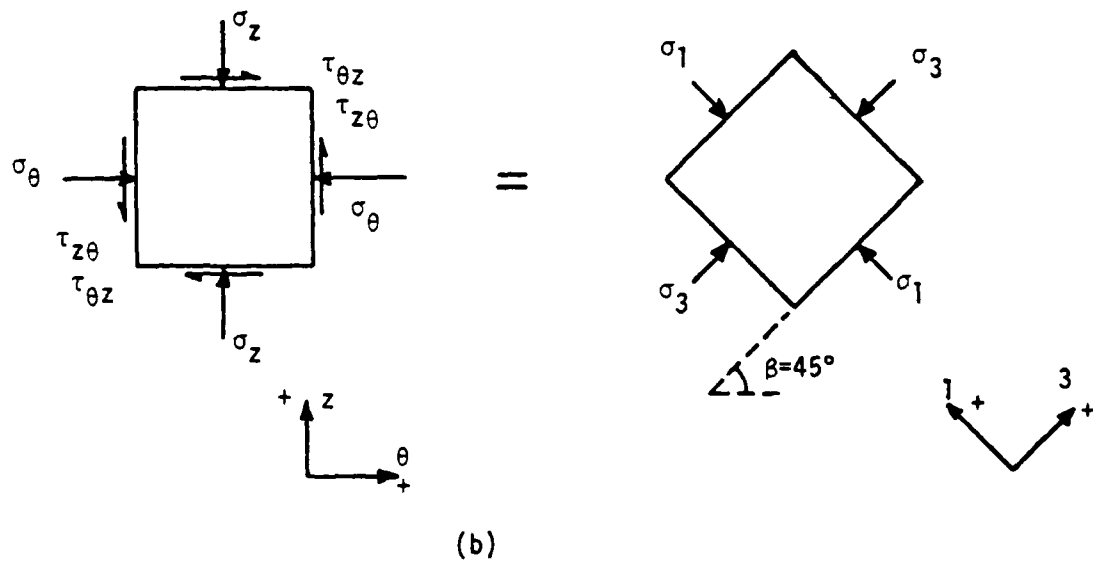
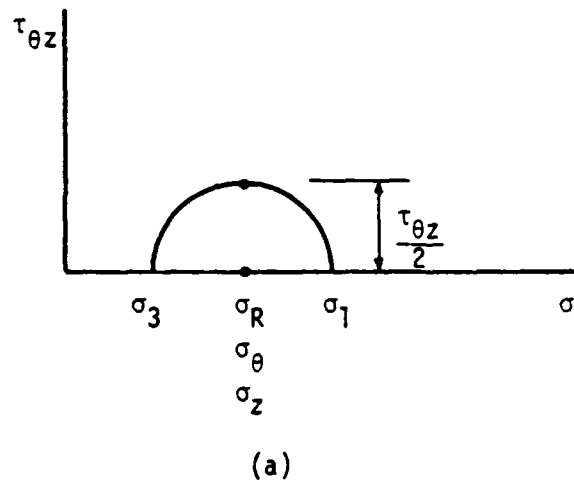


FIGURE 3-3 MOHR'S CIRCLE IN STRESS (a) AND TWO-DIMENSIONAL FREE BODY DIAGRAM (b) FOR RESONANT COLUMN SPECIMENS UNDER CONDITION OF MAXIMUM INSTANTANEOUS TORSIONAL STRESS

and 
$$\omega_T = 2 \cdot \pi \cdot f_T \quad (3.10)$$

with  $f_T$  as the torsional resonant frequency. The relationship between the applied torsional stress and the principal stresses is further illustrated in Figure 3-3(b), which is a two-dimensional free-body diagram in the  $\theta z$  "plane".

### Combined Loading

In the case of simultaneous vertical and torsional excitation conditions become more complicated. The resonant frequencies  $f_z$  and  $f_T$  are different, and are normally not an integer multiple of one another. As seen above, the principal stress directions are different for the two types of loading, and will vary as a function of time. Figure 3-4 shows a Mohr's circle diagram in the  $\theta z$  "plane" for the condition (and at the time of occurrence) of the maximum  $\sigma_1$ . The angle  $\beta$  is the angle of re-orientation of the principal stresses in the  $\theta z$  "plane" from the  $\theta z$  axes.

If we establish a constant,  $\rho$ , such that:

$$\rho = \frac{f_T}{f_z} \quad (3.11)$$

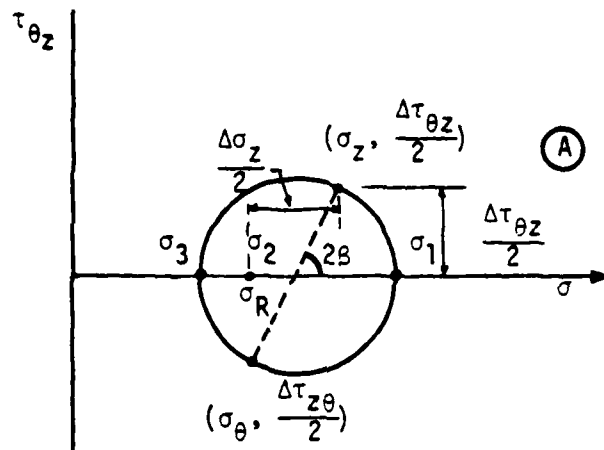
the stresses may be expressed in the following mathematical form:

$$\sigma_z = \sigma_R + \left[ \frac{\Delta\sigma_z}{2} \cdot \sin(\omega_z \cdot t) \right] \quad (3.12)$$

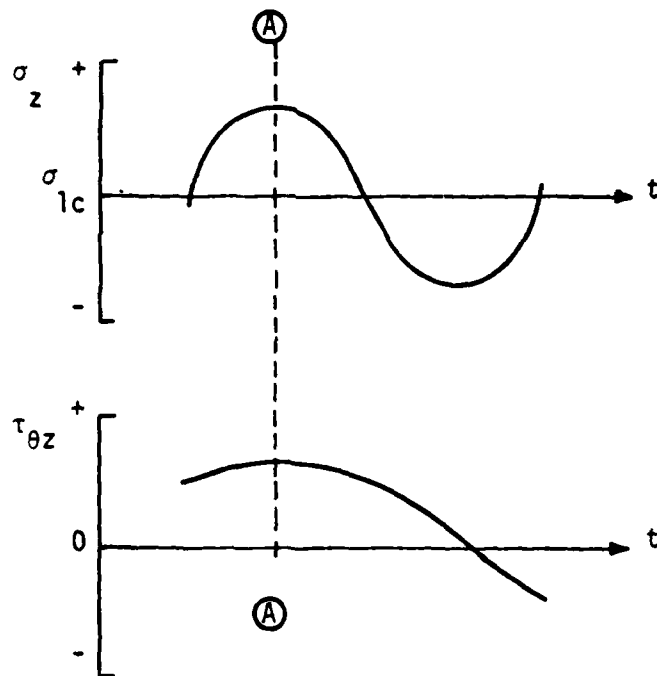
and 
$$\tau_{\theta z} = \frac{\Delta\tau_{\theta z}}{2} \cdot \sin(\rho \cdot \omega_z \cdot t) \quad (3.13)$$

From these equations the following expressions were derived for the principal stresses and directions:

$$\sigma_1 = \sigma_R + \left[ \frac{\Delta\sigma_z}{2} \cdot \sin(\omega_z \cdot t) \right] + \left[ \frac{\Delta\tau_{\theta z}}{2} \cdot \sin(\rho \cdot \omega_z \cdot t) \cdot \tan(\beta) \right] \quad (3.14)$$



(a)



(b)

FIGURE 3-4 MOHR'S CIRCLE IN STRESS (a) AND STRESS TIME HISTORIES (b) FOR SIMULTANEOUS DYNAMIC LOADING OF RESONANT COLUMN SPECIMENS UNDER CONDITION OF MAXIMUM INSTANTANEOUS VERTICAL AND TORSIONAL STRESS

$$\sigma_2 = \sigma_R \quad (3.15)$$

$$\sigma_3 = 2\sigma_{ct} - \sigma_1 \quad (3.16)$$

$$\beta = \frac{1}{2} \tan^{-1} \left[ \frac{\Delta\tau_{\theta z} \cdot \sin(\rho \cdot \omega_z \cdot t)}{\frac{\Delta\sigma_z}{2} \cdot \sin(\omega_z \cdot t)} \right] \quad (3.17)$$

$$\text{and} \quad \sigma_{ct} = \sigma_R + \left[ \frac{\Delta\sigma_z}{4} \cdot \sin(\omega_z \cdot t) \right] \quad (3.18)$$

where  $\sigma_{ct}$  is the center of the  $\theta z$  Mohr's circle.

A more detailed derivation of the above expressions appears in Appendix C-4.

### Hollow Cylinder Testing

#### Sample Preparation

In these testing series thin walled hollow cylinder specimens of sand were anisotropically consolidated with a principal stress ratio of 0.54. The minor principal stress during consolidation was set at one of the following values: 0.5 KSC, 2.0 KSC, or 3.5 KSC.

#### Consolidation Stress Equations

As discussed in Chapter 2, the load response of the hollow cylinder specimen is closely analogous to plane strain type loading in the  $zR$  plane during consolidation. If we apply the expressions for Hooke's Law in the special case of plane strain loading (Equations 2.2 through 2.4) to the present example, we obtain the following expression for the intermediate principal stress during consolidation:

$$\sigma_{2c} = \mu(\sigma_{1c} + \sigma_{3c}) \quad (3.19)$$

where:

$$\sigma_{1c} = \text{major principal stress during consolidation}$$

$$\sigma_{2c} = \text{intermediate principal stress during consolidation}$$

$$\sigma_{3c} = \text{minor principal stress during consolidation}$$

and

$$\mu = \text{Poisson's ratio}$$

Because the directions of the principal stresses are coincident with the directions of the axes in cylindrical coordinates, and because the principal stress ratio during consolidation is known, the consolidation stress state for the hollow cylinder test may be stated as follows:

$$\sigma_{1c} = \sigma_z = 1.85 \cdot \sigma_{3c} \quad (3.20)$$

$$\sigma_{2c} = \sigma_\theta = 2.85 \cdot \mu \cdot \sigma_{3c} \quad (3.21)$$

$$\sigma_{3c} = \sigma_R \quad (3.22)$$

It is noteworthy that, should the Poisson's ratio be less than 0.35, then the tangential principal stress would actually be the minor principal stress and the radial stress would be the intermediate principal stress. This consolidation stress state is illustrated graphically in Figure 3-5.

#### Test Procedure

Following consolidation, the hollow cylinder specimens were excited at a frequency of approximately 0.33 hertz with a moderate amplitude sinusoidal force. The loading excitation was applied in the vertical direction, the torsional direction, or in both the vertical and torsional directions simultaneously.

During the excitation, which was applied for 10 to 20 cycles, the

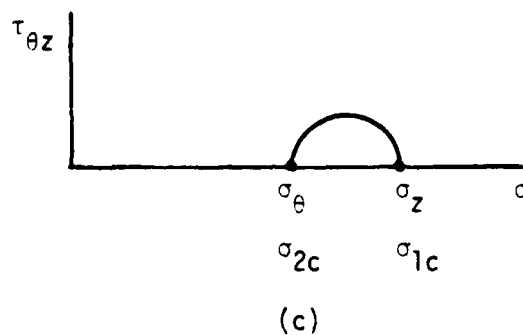
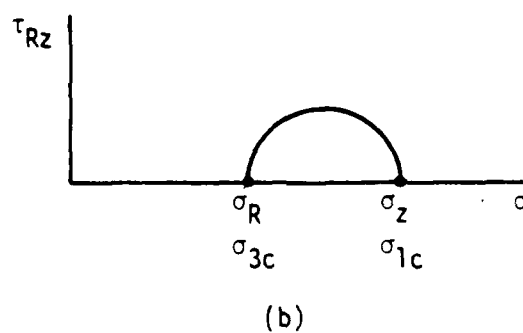
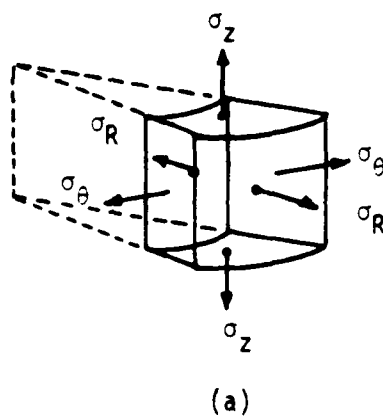


FIGURE 3-5 FREE BODY DIAGRAM (a) AND MOHR'S CIRCLES IN STRESS (b AND c) FOR HOLLOW CYLINDER SPECIMENS UNDER CONDITION OF ANISOTROPIC CONSOLIDATION

vertical stress and strain were recorded directly on an XY recorder, and the vertical stress, torsional stress, and torsional strain were plotted as a function of time on a strip chart recorder. Several typical load records are shown in Figure 3-6. After loading, the cyclic stress levels were adjusted, and the process repeated.

#### Vertical Loading Alone

The typical loading sequence for the case of vertical excitation alone is illustrated in Figure 3-7(a). In this figure we can observe several differences from the case of the resonant-column testing series that was shown in Figure 3-1. The peak stresses and strains occur essentially at the same time, but the zero crossings indicate a phase lag of strain behind stress. This is further illustrated in Figure 3-7(b), as a hysteretical stress-strain response. This hysteresis represents an energy loss during loading and is a measure of damping during the loading sequence. Although some non-elastic response occurs in all loading, it is relatively insignificant at the very low levels of loading encountered during the resonant-column testing series. At the higher strains seen in the hollow cylinder testing series, however, hysteretic stress-strain response is common. This damping effect will be discussed in more detail in Chapter 4.

A second peculiarity of this testing series is the anisotropic consolidation which the samples have undergone. This has the primary effect of moving the dynamic loading effects higher up the stress-strain response curve to a region where higher total strains (and the resultant non-linear, inelastic load response) are seen. In this region of the

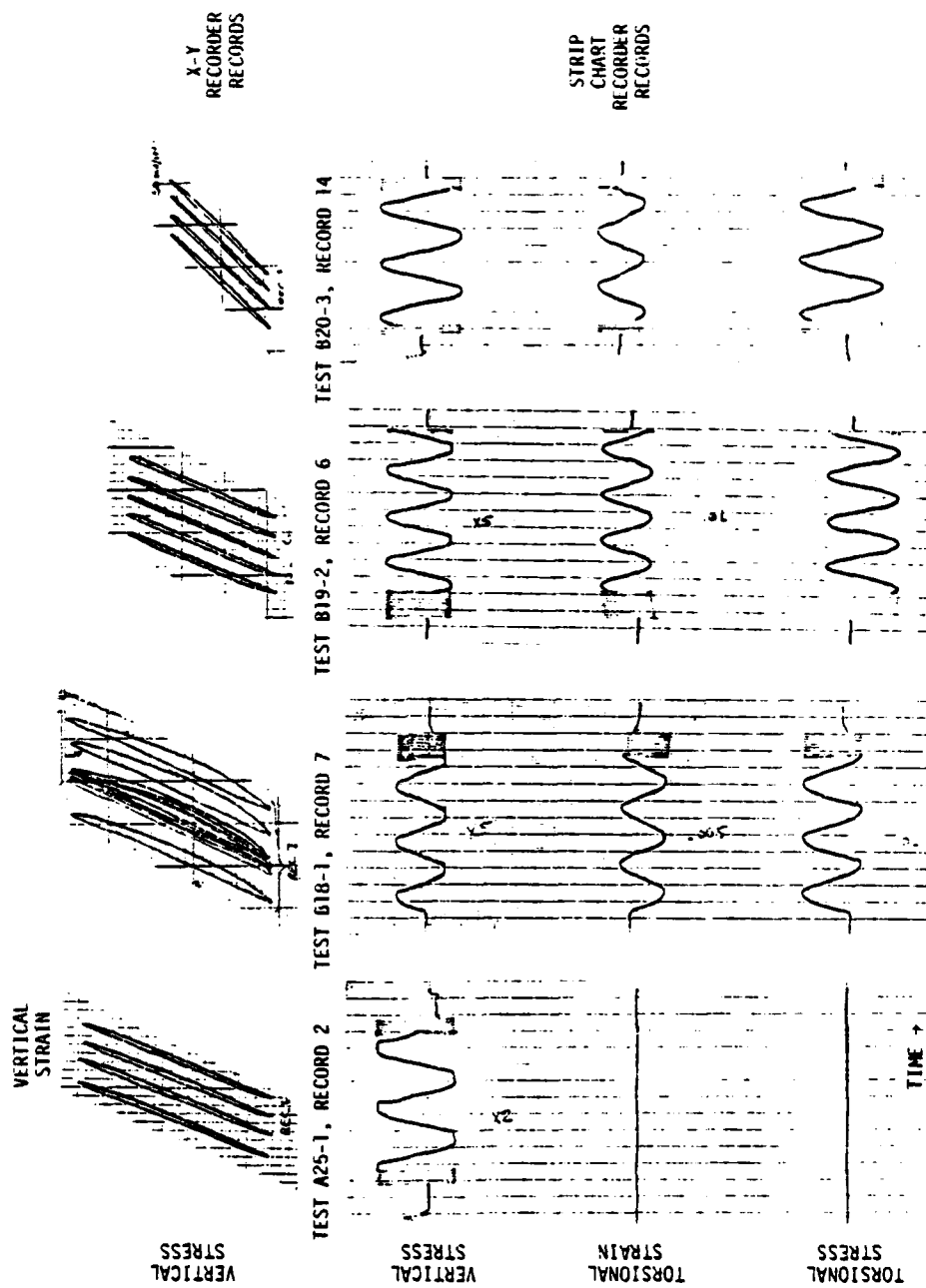
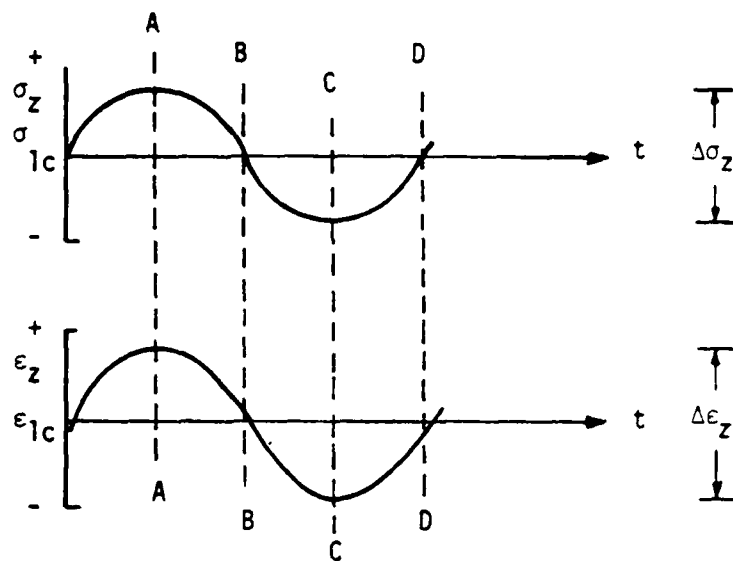
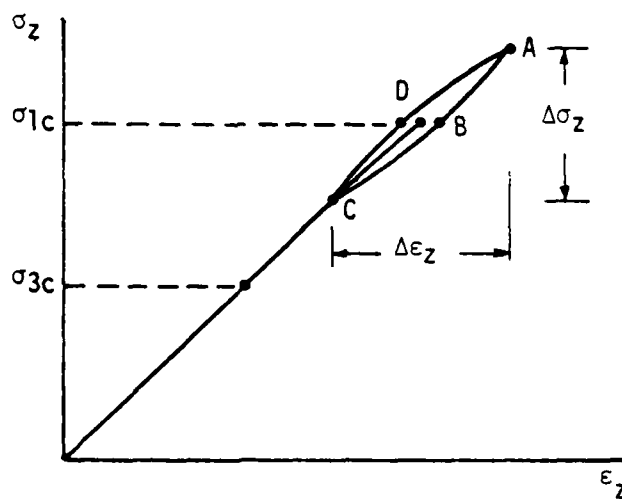


FIGURE 3-6 TEST RECORDS FOR 4 TYPICAL HOLLOW CYLINDER TESTS



(a)



(b)

FIGURE 3-7 TYPICAL LOADING SEQUENCE FOR HOLLOW CYLINDER SPECIMENS UNDER CONDITION OF VERTICAL LOADING ALONE: TIME HISTORIES OF STRESS AND STRAIN (a) AND STRESS VS STRAIN CURVE (b)

material response, a significant level of load resisting stress has been mobilized in the specimen.

In addition, because of the nearly plane strain type load response of the hollow cylinder specimen, the tangential normal stress varies with the vertical normal stress and the Poisson's ratio. This effect is illustrated schematically in a Mohr's circle diagram in the  $\theta z$  "plane" in Figure 3-8.

The mathematical expressions for the principal stresses under this loading condition are as follows:

$$\sigma_z = \sigma_{1c} + \left[ \frac{\Delta\sigma_z}{2} \cdot \sin(\lambda \cdot t) \right] \quad (3.23)$$

$$\sigma_\theta = \sigma_{2c} + \left[ \frac{\Delta\sigma_\theta}{2} \cdot \sin(\lambda \cdot t) \right] \quad (3.24)$$

$$\text{and} \quad \sigma_R = \sigma_{3c} \quad (3.25)$$

where  $\lambda$  is a constant. These equations further reduce to the following:

$$\sigma_z = 1.85 \cdot \sigma_{3c} + \left[ \frac{\Delta\sigma_z}{2} \cdot \sin(\lambda \cdot t) \right] \quad (3.26)$$

$$\sigma_\theta = 2.85 \cdot \mu \cdot \sigma_{3c} + \left[ \mu \cdot \frac{\Delta\sigma_z}{2} \cdot \sin(\lambda \cdot t) \right] \quad (3.27)$$

$$\text{and} \quad \sigma_R = \sigma_{3c} \quad (3.25)$$

#### Torsional Loading Alone

Under the condition of torsional stress alone, the maximum principal stress Mohr's circle in the  $\theta z$  plane is shown in Figure 3-9(a). Unlike the case with the resonant-column testing series, the principal stresses in the " $\theta z$ " plane are not oriented at an angle of  $45^\circ$  from the cylindrical coordinate axes. Indeed, the angle of orientation,  $\beta$ , varies both

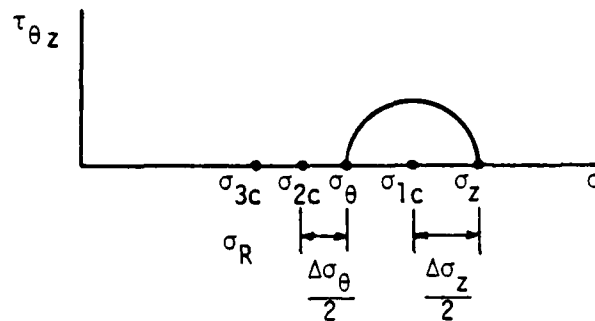


FIGURE 3-8 MOHR'S CIRCLE IN STRESS FOR HOLLOW CYLINDER SPECIMENS UNDER CONDITION OF MAXIMUM INSTANTANEOUS VERTICAL STRESS

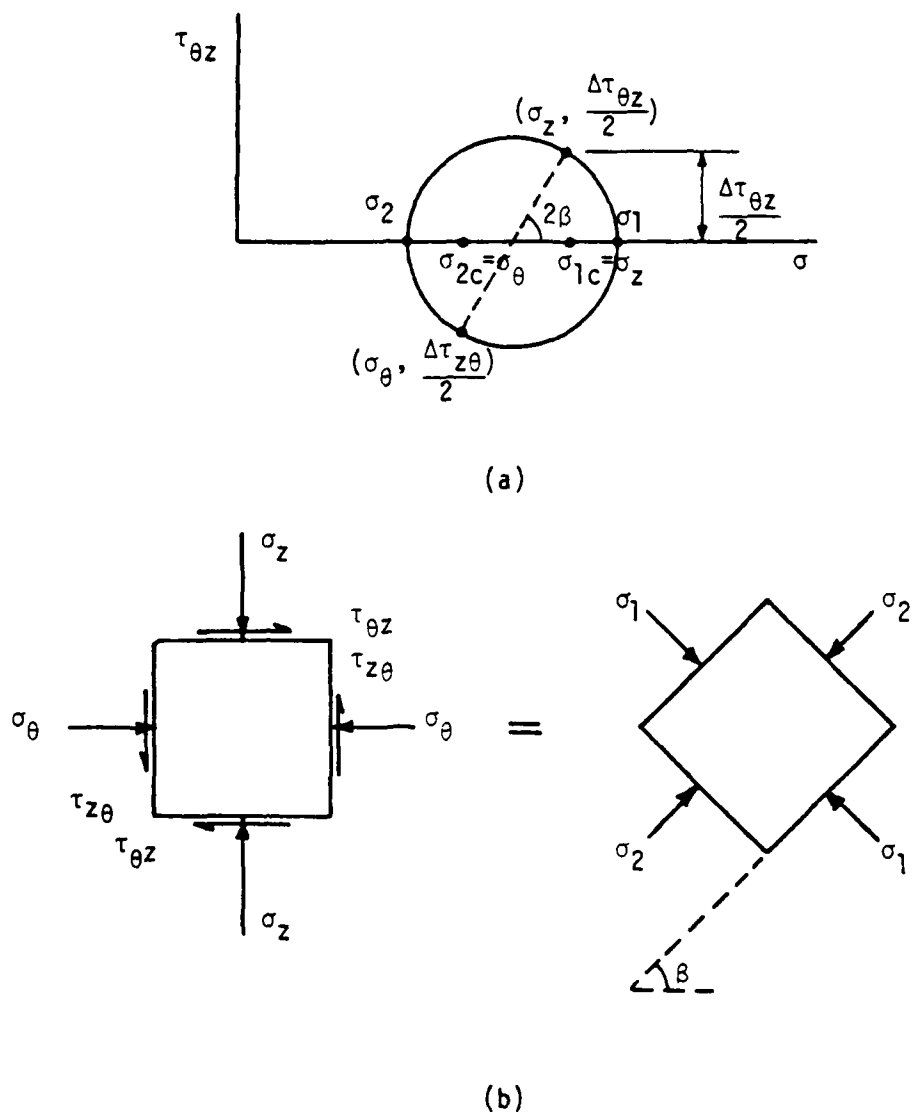


FIGURE 3-9 MOHR'S CIRCLE IN STRESS (a) AND TWO-DIMENSIONAL FREE BODY DIAGRAM (b) FOR HOLLOW CYLINDER SPECIMENS UNDER CONDITION OF MAXIMUM INSTANTANEOUS TORSIONAL STRESS

with Poisson's ratio and with time. This orientation effect is illustrated in Figure 3-9(b), which is a two-dimensional free-body diagram in the  $\theta z$  "plane".

Under these conditions of loading, the state of stresses is defined by the following equations:

$$\sigma_1 = \sigma_{1c} + \left[ \frac{\Delta \tau_{\theta z}}{2} \cdot \sin(\lambda \cdot t) \cdot \tan \beta \right] \quad (3.28)$$

$$\sigma_2 = \sigma_1 - 2(\sigma_1 - \sigma_{CT}) \quad (3.29)$$

$$\sigma_3 = \sigma_{3c} \quad (3.30)$$

and

$$\beta = \frac{1}{2} \tan^{-1} \left[ \frac{(\tau_{\theta z}/2) \cdot \sin(\lambda \cdot t)}{\sigma_{1c} - \sigma_{ct}} \right] \quad (3.31)$$

where

$$\sigma_{ct} = \left[ \left( \frac{1 + \mu}{2} \right) \cdot \sigma_{1c} \right] + \left[ \frac{\mu}{2} \cdot \sigma_{3c} \right] \quad (3.32)$$

and

$$\sigma_{1c} = 1.85 \cdot \sigma_{3c} \quad (3.20)$$

#### Combined Loading

In the case of simultaneous vertical and torsional excitation, the loading sequence is shown in Figure 3-10. The greatest complication in this stress state occurs because, although the two excitations are at the same frequency, they may be at different phases. This condition is shown in Figure 3-10(a). The maximum principal stress Mohr's circle in the  $\theta z$  "plane" is shown in Figure 3-10(b). The following equations define the state of stresses under these loading conditions:

$$\begin{aligned} \sigma_1 = \sigma_{1c} &+ \left[ \frac{\Delta \sigma_z}{2} \cdot \sin(\lambda \cdot t) \right] \\ &+ \left[ \frac{\Delta \tau_{\theta z}}{2} \cdot \sin[(\lambda - \alpha) \cdot t] \cdot \tan(\beta) \right] \end{aligned} \quad (3.33)$$

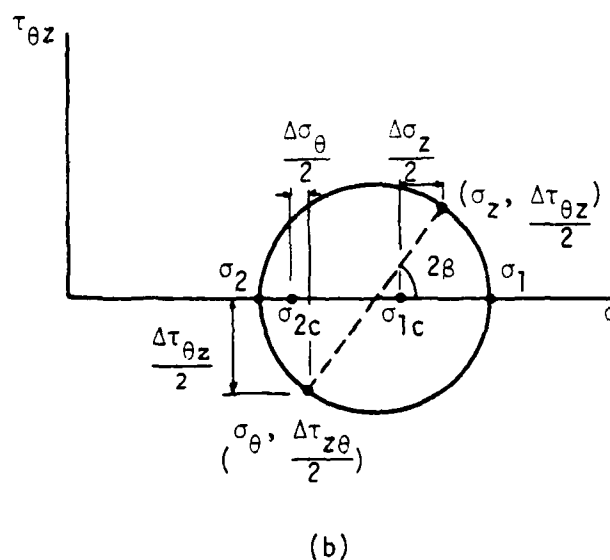
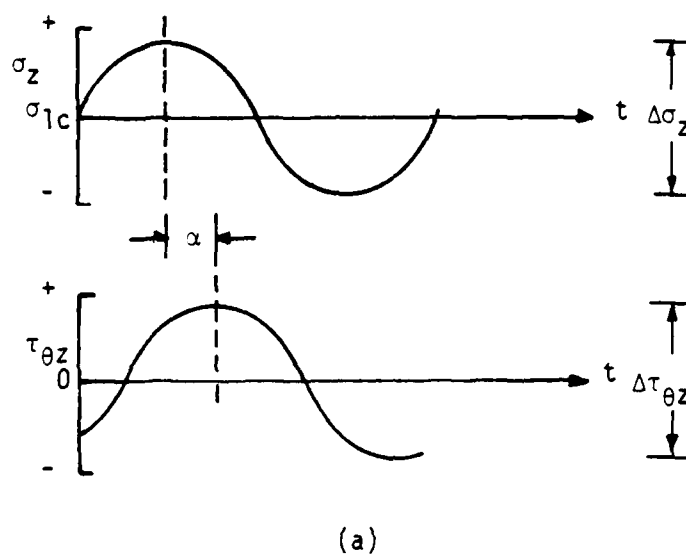


FIGURE 3-10 STRESS TIME HISTORIES (a) AND MOHR'S CIRCLE IN STRESS (b) FOR SIMULTANEOUS DYNAMIC LOADING OF HOLLOW CYLINDER SPECIMENS UNDER CONDITION OF MAXIMUM INSTANTANEOUS VERTICAL AND TORSIONAL STRESS

$$\sigma_2 = \sigma_1 - 2(\sigma_1 - \sigma_{ct}) \quad (3.34)$$

$$\sigma_3 = \sigma_{3c} \quad (3.35)$$

$$\beta = \frac{1}{2} \tan^{-1} \left[ \frac{\Delta\tau_{\theta z} \cdot \sin[(\lambda - \alpha) \cdot t]}{2 \left[ \sigma_{1c} + \frac{\Delta\sigma_z}{2} \cdot \sin(\lambda \cdot t) - \sigma_{ct} \right]} \right] \quad (3.36)$$

where

$$\sigma_{ct} = \left[ \left( \frac{1 + \mu}{2} \right) \cdot \sigma_{1c} \right] + \left[ \left( \frac{1 + \mu}{4} \right) \cdot \Delta\sigma_z \cdot \sin(\lambda \cdot t) \right] + \left[ \frac{\mu \cdot \sigma_{3c}}{2} \right] \quad (3.37)$$

$$\sigma_{1c} = 1.85 \cdot \sigma_{3c} \quad (3.20)$$

and  $\alpha$  is the phase lag of torsional loading to vertical loading.

A more detailed derivation of these equations appears in Appendix C-5.

## Chapter 4

### Soil Moduli and Damping Factors

#### Introduction

In this chapter the strain tensor developed in Chapter 2 and the state of stresses described in Chapter 3 will be further developed and combined to produce a complete picture of the stress-strain behavior of triaxial resonant-column and thin-walled hollow cylinder test specimens under dynamic loading conditions.

#### Resonant Column Testing

In the triaxial resonant-column testing series, the moduli are determined directly in the manner described in Chapter 3. Damping factors are also obtained during this testing series using either the amplitude decay technique or the logarithmic decrement approach.

#### Dynamic Interaction Theory

When evaluating the stress-strain response of these specimens under combined vertical and torsional loading, it is necessary to consider the effects of the reorientation of the principal stress directions during loading to evaluate the interaction.

As described in Chapter 3, the principal stresses and their directions will change throughout each combined loading test because the two excitations are at two independent frequencies. As a test is conducted, any interaction effects resulting from the reorientation of the principal stress directions will vary continuously, and the

Lissajous figure observed on the oscilloscope will be an integration of the combined excitation and response over time. The modulus and damping factor calculated from this Lissajous figure will be "weighted average" values, averaging any interaction effects.

Because it is being assumed that the specimen is behaving as a linear, elastic, isotropic material, the direction of incremental strains during loading will coincide with the direction of incremental stresses, and the principal strain and stress directions will coincide. Consequently, the path of travel of the dynamic waves will be distorted to follow the direction of the principal stresses, and the effective velocity of propagation through the material will be decreased. This effect will evidence as a decrease in the resonant frequency of the specimen, and a decrease in the effective modulus of the material. This principle is illustrated graphically in Figure 4-1.

#### Data Reduction

A computer program has been developed which reduces the raw data from the resonant-column testing series to produce values of the moduli and damping factors under combined vertical and torsional dynamic loading conditions, and to calculate the values and directions of the maximum principal stresses during loading. This computer program, called Program RC, is included as Appendix D-1.

Example results of this testing series, as reduced by Program RC are presented in Appendices B-1 through B-3, and summaries of the results are given in Chapter 5. The complete results are available in Griffin (1980).

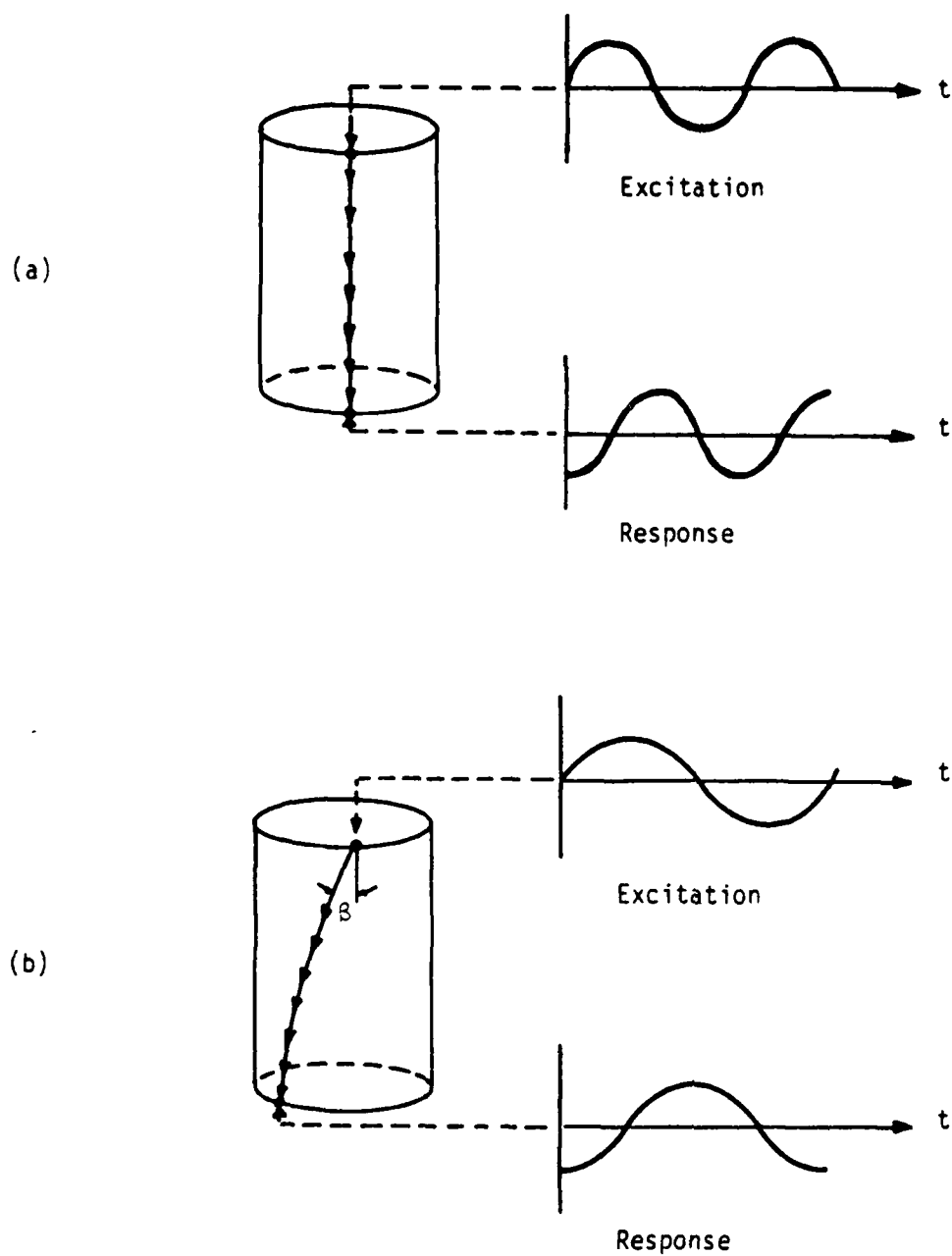


FIGURE 4-1 EFFECT OF THE DIRECTION OF THE INCREMENTAL STRESSES AND STRAINS ON PROPAGATION OF DISPLACEMENTS IN CYLINDRICAL RESONANT COLUMN SAMPLES

### Hollow Cylinder Testing

In the thin-walled hollow cylinder testing series, the vertical and torsional stresses and strains were measured directly as described in Chapter 3. Moduli and damping factors may be calculated from this data provided the complete state of stresses and strains are known.

#### Consolidation Procedure

During each test, a test specimen was first isotropically consolidated to 0.5 KSC confining pressure by intercell vacuum. The specimen was then loaded vertically with an additional compressive stress to provide an anisotropic consolidation ratio,  $\sigma_{3c}/\sigma_{1c}$ , of 0.54. This occurred when the total vertical compressive stress was 0.925 KSC. While several tests were conducted upon specimens in this consolidation state, a number of tests received further consolidation preparation before dynamic testing was performed. As discussed earlier, tests were performed upon samples with consolidation lateral confining pressures of 0.5, 2.0, and 3.5 KSC.

For those tests conducted at the two higher confining pressures, the above consolidation process was continued in the same sequence as described above. First the effective cell pressure was increased from 0.5 KSC to 2.0 KSC, then the additional vertical compressive stress was increased from 0.425 KSC to the value causing an anisotropic consolidation ratio of 0.54. This additional vertical stress value was 1.7 KSC, resulting in a total vertical stress of 3.7 KSC.

Similarly, for specimens to be tested at a lateral confining pressure of 3.5 KSC, the effective cell pressure was increased to that

value, then the additional vertical stress was increased from 1.7 KSC to 2.975 KSC to create an anisotropic consolidation ratio of 0.54.

#### Consolidation Strains

During this consolidation process, the vertical displacement proximeter was installed immediately following the initial consolidation steps. It was therefore possible to record the vertical strain,  $\epsilon_z$ , during the remaining consolidation steps where lateral confining pressures greater than 0.5 KSC were used. This record was made on the XY recorder for a number of tests, and the summary of these records are shown in Figures 4-2 through 4-7.

In Figures 4-2 and 4-3, the variation in vertical strain,  $\epsilon_z$ , is shown for the increment of consolidation loading resulting from the change in intercell vacuum only. This change in stress corresponds to an isotropic increment of loading applied to a specimen which is already at some anisotropic state of stress. Since the XY recorder used to measure this strain increment was plotting it against the additional vertical stress change, which was zero for this increment of loading, it was not possible to show the true shape of the stress-strain response. The stress-strain response is therefore shown as a dashed line between the known values.

Figure 4-4 provides a summary of the data presented in Figures 4-2 and 4-3, and an extrapolation to allow for predicting the total consolidation strains. The predicted isotropic increments of vertical strain shown in Figure 4-4 are as follows:

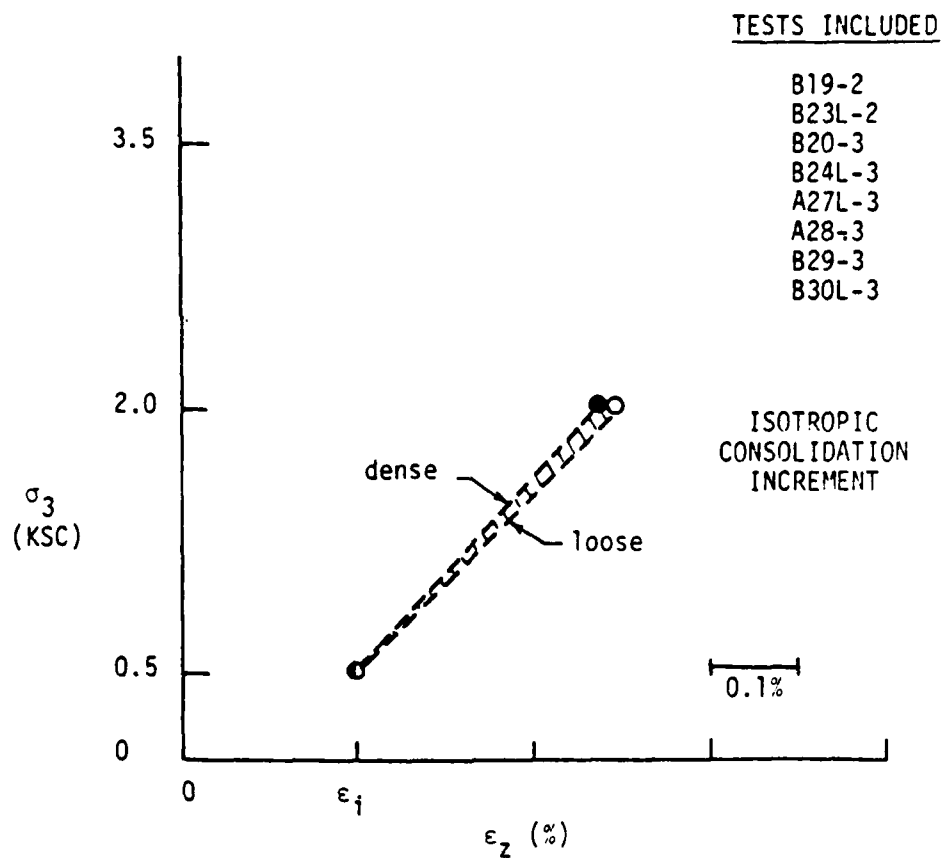


FIGURE 4-2 VARIATION OF  $\epsilon_z$  WITH ISOTROPIC INCREMENT OF LATERAL CONSOLIDATION LOADING,  $\sigma_3$ , FROM 0.5 TO 2.0 KSC, FOR SEVERAL TESTS

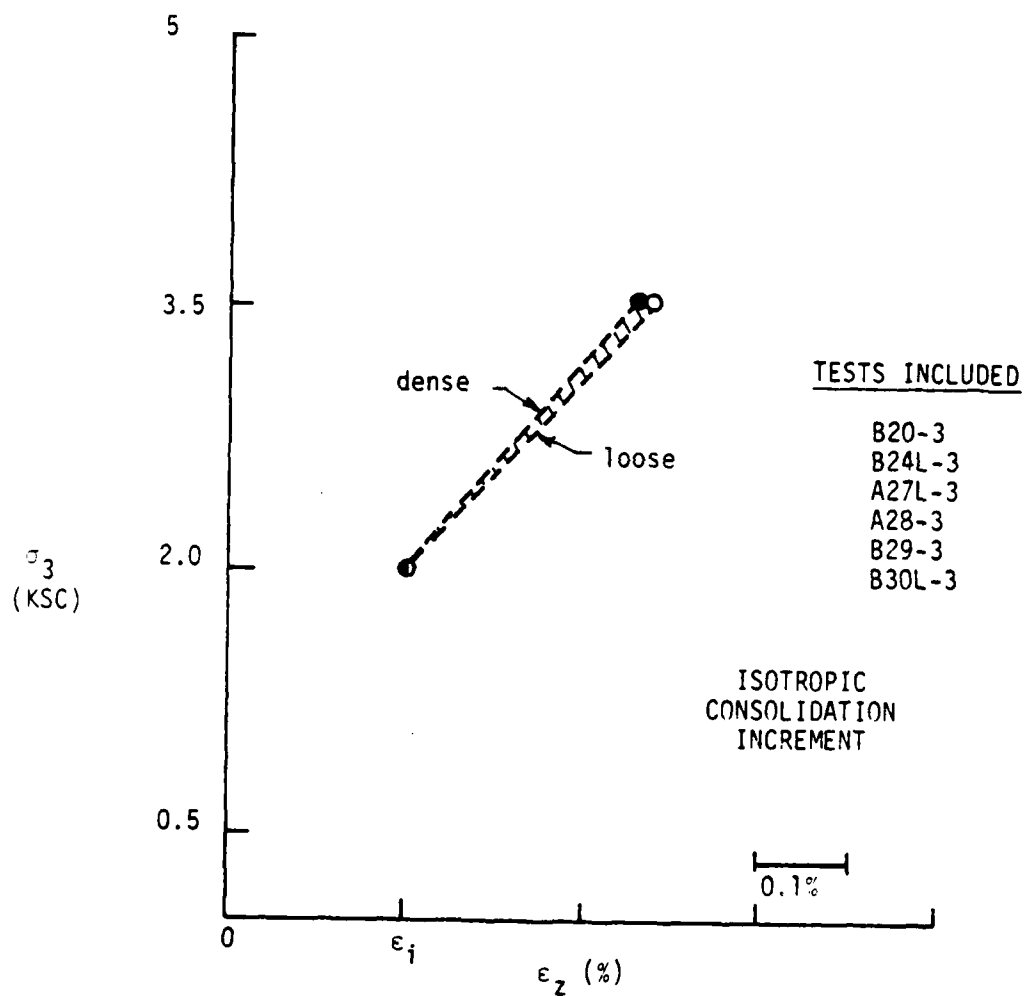


FIGURE 4-3 VARIATION OF  $\epsilon_z$  WITH ISOTROPIC INCREMENT OF LATERAL CONSOLIDATION LOADING,  $\sigma_3$ , FROM 2.0 TO 3.5 KSC, FOR SEVERAL TESTS

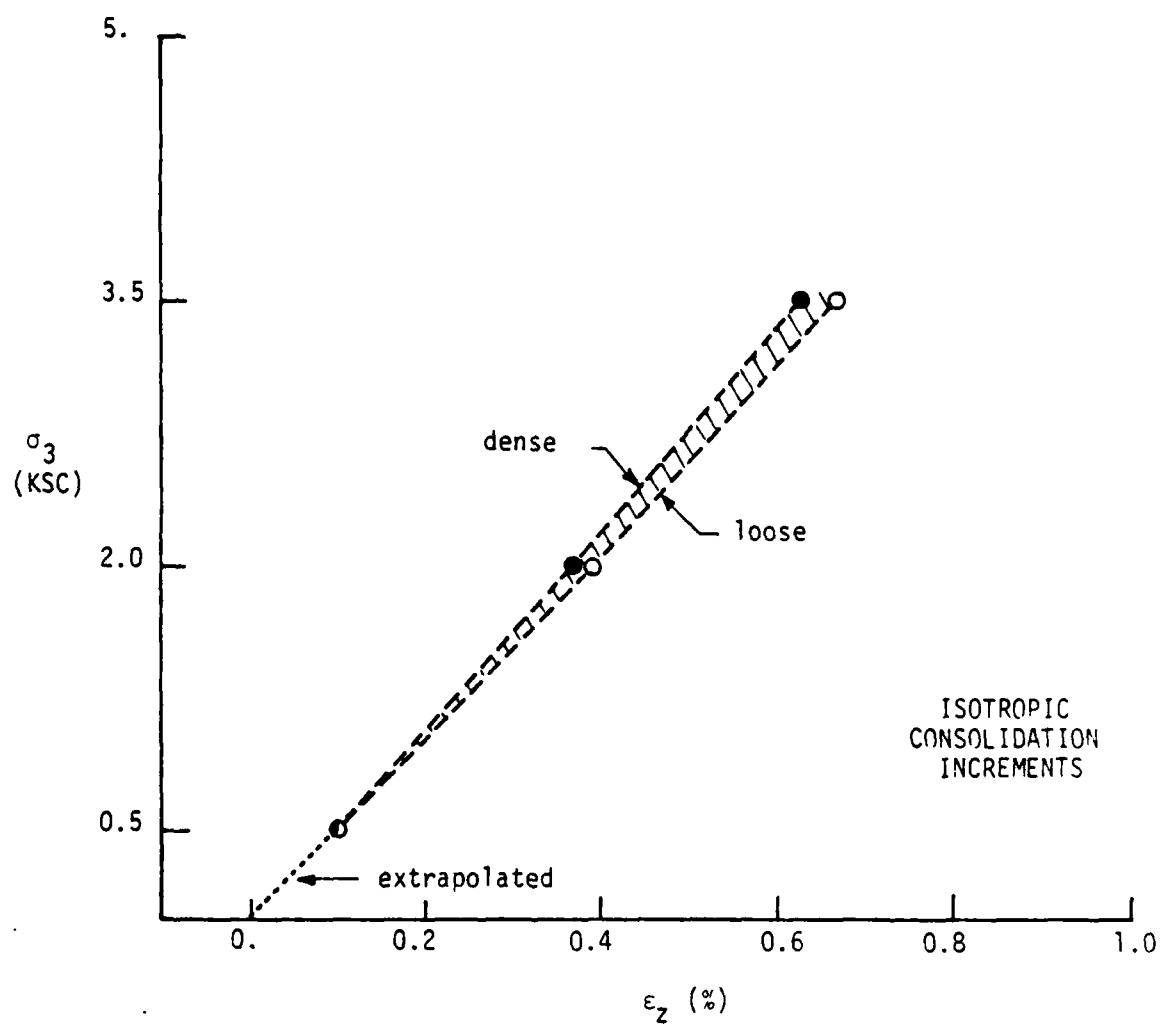


FIGURE 4-4 SUMMARY OF VARIATIONS OF  $\epsilon_z$  WITH ISOTROPIC INCREMENTS OF LATERAL CONSOLIDATION LOADING,  $\sigma_3$ ; AND EXTRAPOLATION OF INITIAL INCREMENT OF STRAIN FROM 0 TO 0.5 KSC

$$\epsilon_z (\sigma_{3c} = 0.5 \text{ KSC}) \approx 0.10\% \quad (4.1)$$

$$\epsilon_z (\sigma_{3c} = 2.0 \text{ KSC}) \approx 0.37\% \quad (4.2)$$

$$\text{and} \quad \epsilon_z (\sigma_{3c} = 3.5 \text{ KSC}) \approx 0.65\% \quad (4.3)$$

The short extrapolated line in this figure is an estimate of the amount of vertical straining resulting from the initial application of 0.5 KSC of intercell vacuum upon the sample. This value could not be directly measured as the sample was still in the forming mold at the time of application of the intercell vacuum.

It should be emphasized that the stress-strain response approximated in Figure 4-4 is not truly representative of the stress-strain response of the samples to isotropic loading. Because all samples were in an anisotropic state of stress before the various isotropic loading increments were applied, the lateral stresses were increasing disproportionately with the vertical stress during the loading increment. The primary purpose of plotting this figure was to allow an extrapolation of the initial vertical strain increment value and the estimation of total consolidation strains.

For the anisotropic consolidation increments of stress, the vertical compressive stress was adjusted as described earlier to provide an anisotropic consolidation ratio of 0.54. Since both the change in vertical stress,  $\Delta\sigma_z$ , and the change in vertical strain,  $\Delta\epsilon_z$ , were plotted on the XY recorder for this stress-strain increment, the actual shape of the stress-strain response is known.

In Figures 4-5 and 4-6 the anisotropic stress-strain increments are shown combined with the isotropic stress increments. The solid lines

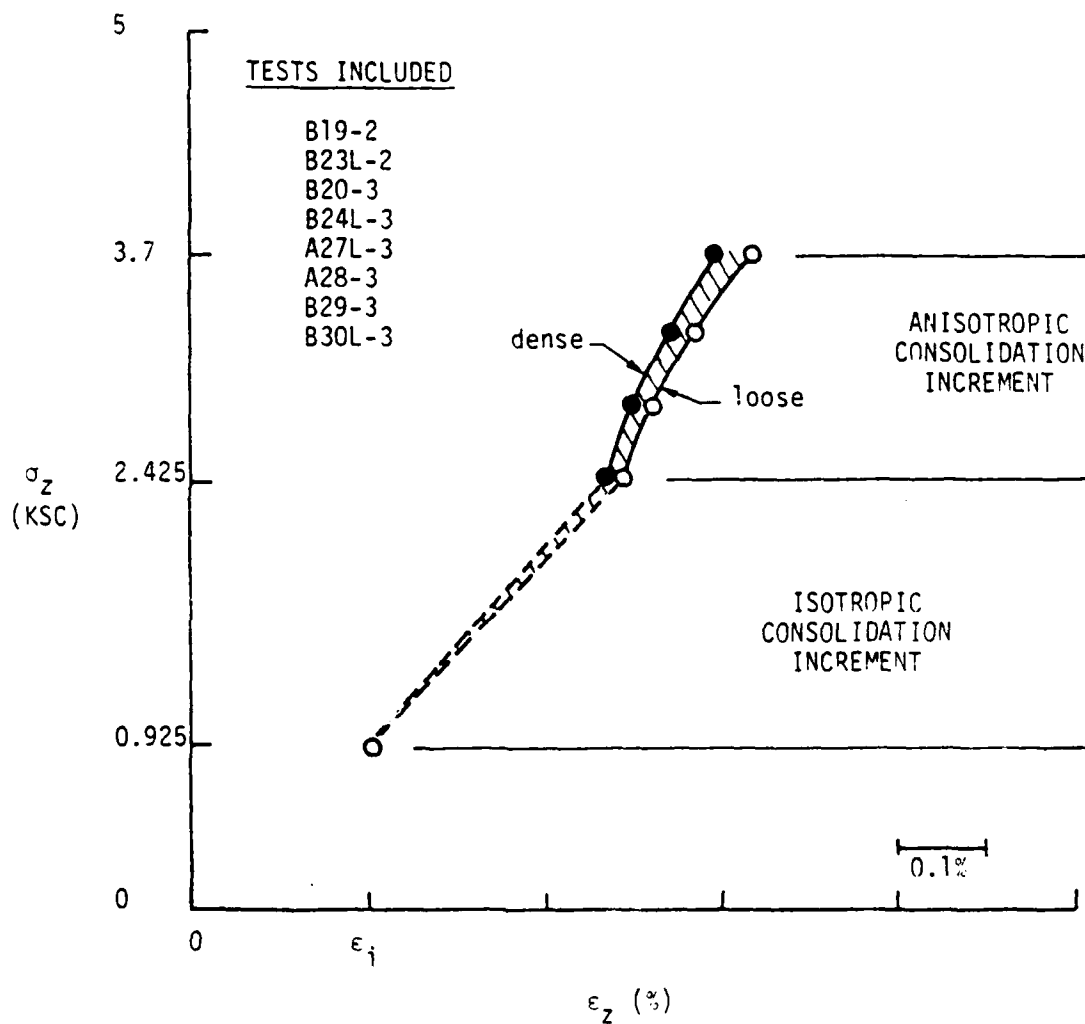


FIGURE 4-5 VARIATION OF  $\epsilon_z$  WITH BOTH ISOTROPIC AND ANISOTROPIC INCREMENTS OF VERTICAL CONSOLIDATION LOADING,  $\sigma_z$ , FROM 0.925 TO 3.7 KSC, FOR SEVERAL TESTS

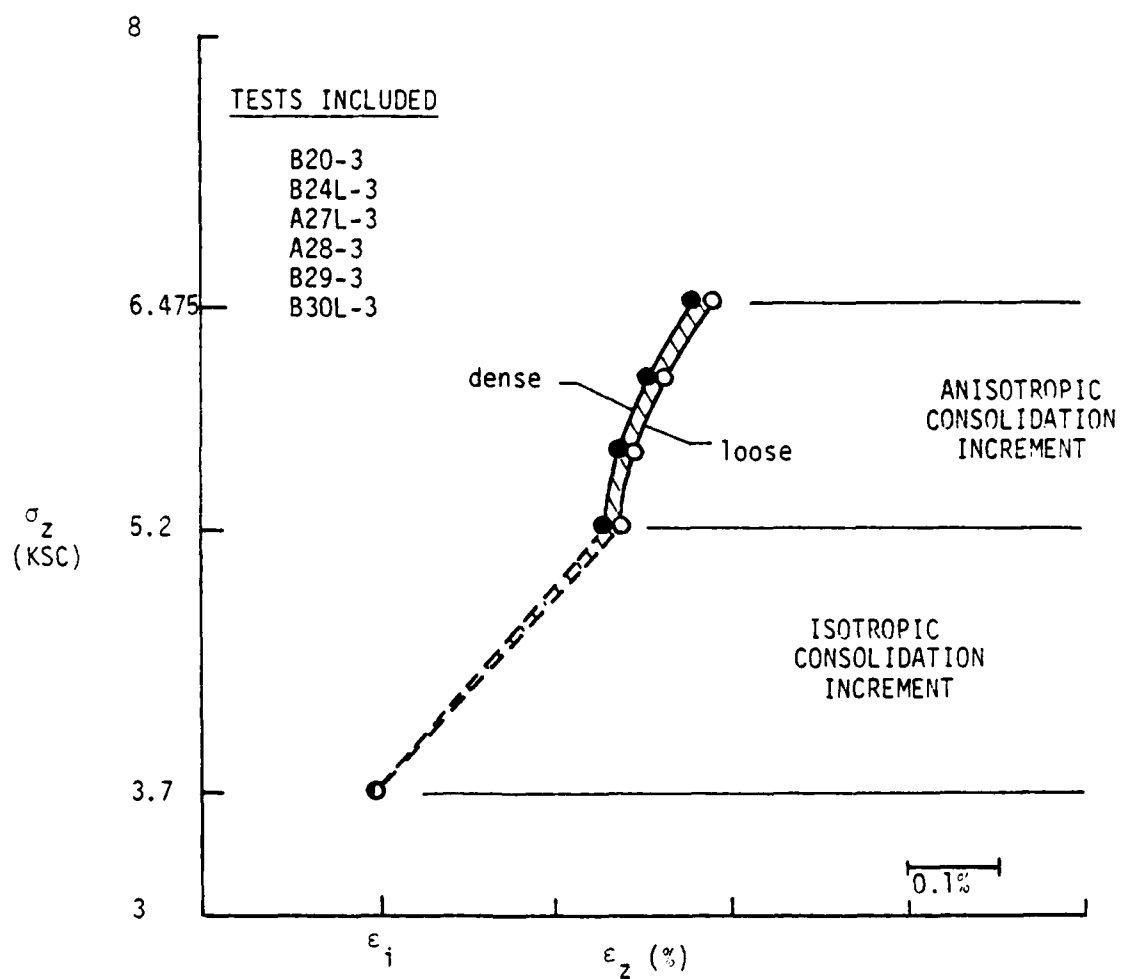


FIGURE 4-6 VARIATION OF  $\epsilon_z$  WITH BOTH ISOTROPIC AND ANISOTROPIC INCREMENTS OF VERTICAL CONSOLIDATION LOADING,  $\sigma_z$ , FROM 3.7 TO 6.475 KSC, FOR SEVERAL TESTS

shown in these curves correspond to the actual anisotropic stress-strain response of the soil recorded by the XY recorder. The data on these two figures are summarized in Figure 4-7, along with an extrapolation to estimate the total consolidation strain values. The extrapolated line on Figure 4-7 includes the earlier isotropic increment extrapolation from Figure 4-4, and an anisotropic increment extrapolation deduced from the anisotropic loading increment data shown in the figure. The total consolidation vertical strains may now be estimated as follows:

$$\epsilon_z(\sigma_{3c} = 0.5 \text{ KSC}) \approx 0.15\% \quad (4.4)$$

$$\epsilon_z(\sigma_{3c} = 2.0 \text{ KSC}) \approx 0.56\% \quad (4.5)$$

$$\epsilon_z(\sigma_{3c} = 3.5 \text{ KSC}) \approx 0.93\% \quad (4.6)$$

It is interesting to note that for all of the tests shown, which represent a wide range of densities, the recorded values of the total vertical strain under anisotropic consolidation conditions fall within a few percent of the average values in Equations 4.4 through 4.6.

#### Consolidation Modulus Calculation

From the strain tensor developed in Equation 2.17, we can calculate the volumetric strain as follows:

$$\epsilon_{vol} = \left(1 - \frac{\mu + \mu^2}{1 - \mu^2}\right) \cdot \epsilon_z \quad (4.7)$$

and from Hooke's Law (Equation 2.4),

$$\epsilon_z = \left(\frac{1 - \mu^2}{E}\right) \cdot \sigma_z - \left(\frac{\mu + \mu^2}{E}\right) \cdot \sigma_R \quad (4.8)$$

and

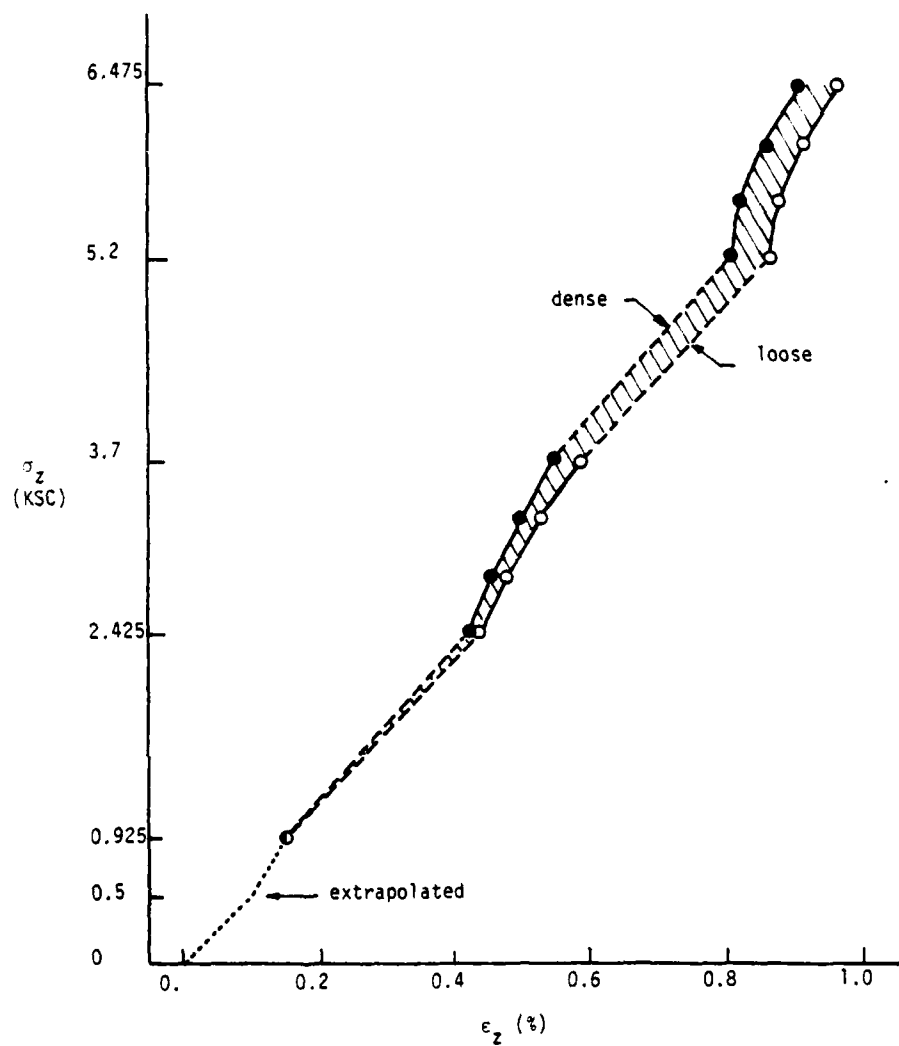


FIGURE 4-7 SUMMARY OF VARIATIONS OF  $\epsilon_z$  WITH ISOTROPIC AND ANISOTROPIC INCREMENTS OF VERTICAL CONSOLIDATION LOADING,  $\sigma_z$ ; AND EXTRAPOLATION OF INITIAL INCREMENT OF STRAIN FROM 0 TO 0.925 KSC

$$\epsilon_R = \left( \frac{1 - \mu^2}{E} \right) \cdot \sigma_R - \left( \frac{\mu + \mu^2}{E} \right) \cdot \sigma_z \quad (4.9)$$

which reduces to:

$$\epsilon_{vol} = \left( \frac{1 - \mu - 2\mu^2}{E} \right) (\sigma_z + \sigma_R) \quad (4.10)$$

Combining Equations 4.7 and 4.10 gives:

$$\left( 1 - \frac{\mu + \mu^2}{1 - \mu^2} \right) \epsilon_z = \left( \frac{1 - \mu - 2\mu^2}{E} \right) (\sigma_z + \sigma_R) \quad (4.11)$$

which reduces to:

$$E = \frac{(1 - \mu - 2\mu^2) \cdot (\sigma_z + \sigma_R)}{\left[ 1 - \left( \frac{\mu + \mu^2}{1 - \mu^2} \right) \right] \cdot \epsilon_z} \quad (4.12)$$

The static compression modulus  $E$  was calculated from Equation 4.12 for a variety of values of Poisson's ratio and the results are shown in Table 4-1. The similarity in the calculated moduli for a specific Poisson's ratio is a measure of the similarity in the principal stress ratio during consolidation, and of linearity of the stress-strain response.

#### Tangent and Secant Moduli

During dynamic excitation, the dynamic vertical stress and strain will be superimposed upon the consolidation stress-strain condition. Consequently, it is possible to view either the tangent modulus or the secant modulus under these loading conditions.

Vertical straining during dynamic loading will be in accordance with the strain tensor developed in Equation 2.17 and Hooke's Law as presented in Equation 2.4. The dynamic tangent compression modulus

TABLE 4-1

Static Unconstrained Compression Modulus (in psi)

$\mu$	$E(\sigma_{3c} = 0.5 \text{ KSC})$	$E(\sigma_{3c} = 2.0 \text{ KSC})$	$E(\sigma_{3c} = 3.5 \text{ KSC})$
0.49	10,612.	11,370.	11,981.
0.44	11,261.	12,066.	12,714.
0.39	11,841.	12,687.	13,369.
0.34	12,351.	13,233.	13,944.
0.29	12,791.	13,704.	14,441.
0.24	13,161.	14,101.	14,859.

under vertical or combined vertical and torsional dynamic loading conditions may be calculated by the following expression:

$$E = (1 - \mu^2) \frac{\Delta \sigma_z}{\Delta \epsilon_z} \quad (4.13)$$

A derivation of this expression is given in Appendix C-6.

Similarly, Equation 4.12 may be rewritten to provide a means for calculating the dynamic secant compression modulus, producing the following:

$$E = \left[ \frac{1 - \mu - 2\mu^2}{1 - \left( \frac{\mu + \mu^2}{1 - \mu^2} \right)} \right] \cdot \frac{\sigma_z + \sigma_R + \frac{\Delta \sigma_z}{2}}{\epsilon_z + \frac{\Delta \epsilon_z}{2}} \quad (4.14)$$

where  $\sigma_z = \sigma_{1c}$ ,  $\sigma_R = \sigma_{3c}$ , and  $\epsilon_z = \epsilon_{1c}$ .

The secant compression modulus may be simply calculated using Equation 4.14. Because this modulus is an overall average modulus from the preconsolidation state, the values will not vary greatly from those values in Table 4-1 except under conditions of very high dynamic straining.

If the soil sample is considered representative of soil conditions in the field, with anisotropic consolidation, then the compression modulus of interest is the tangent compression modulus determined using Equation 4.13. This modulus will reflect the dynamic stress-strain behavior of soil which has reached a steady-state consolidation condition, and whose strain will vary throughout the range of strains imposed in this testing program.

### Effect of Torsional Loading on Equations for Moduli

Under conditions of torsional dynamic loading alone, the principal stress and strain directions will change during loading as discussed in Chapter 3. The Mohr's circles in strain and stress for this condition are indicated in Figure 4-8, with the reorientation of the principal strains in the  $\theta z$  "plane" indicated by the angle  $\psi$ . If the material behaves linearly and elastically, then  $\psi$  must equal  $\beta$ .

Note from Figure 4-8(a) that the principal strains may now be written as follows:

$$\epsilon_1 = \epsilon_{1c} + \left[ \frac{\Delta\gamma_{\theta z}}{4} \cdot \sin(\lambda \cdot t) \cdot \tan\psi \right] \quad (4.15)$$

$$\epsilon_2 = 0 - \left[ \frac{\Delta\gamma_{\theta z}}{4} \cdot \sin(\lambda \cdot t) \cdot \tan\psi \right] \quad (4.16)$$

$$\epsilon_3 = \epsilon_{3c} \quad (4.17)$$

and 
$$\psi = \frac{1}{2} \tan^{-1} \left[ \frac{\Delta\gamma_{\theta z} \cdot \sin(\lambda t)}{2\epsilon_{1c}} \right] \quad (4.18)$$

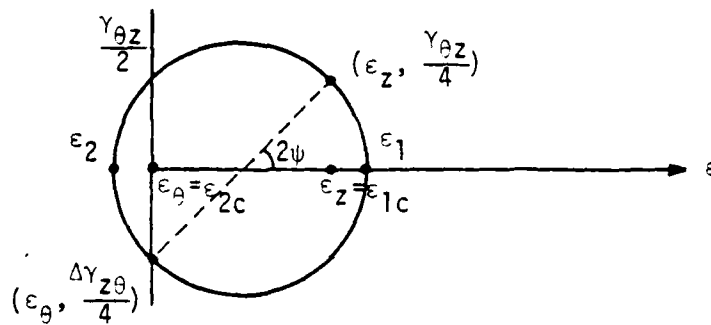
where  $\epsilon_{1c} = \epsilon_z$ ,  $\epsilon_{2c} = \epsilon_{\theta} = 0$ , and  $\epsilon_{3c} = \epsilon_R$ .

The volumetric strain may now be written:

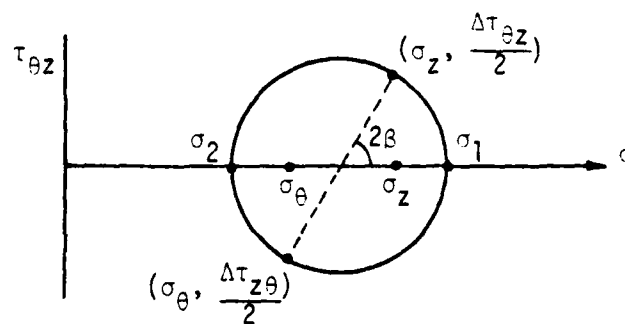
$$\epsilon_{vol} = \epsilon_1 + \epsilon_2 + \epsilon_3 = \epsilon_{1c} + \epsilon_{3c} \quad (4.19)$$

$$= \left[ 1 - \frac{\mu + \mu^2}{1 - \mu^2} \right] \epsilon_z$$

Because Equation 4.19 is exactly equal to Equation 4.7, the expression for the volumetric strain during dynamic loading is shown to be independent of reorientation of the principal stress and strain directions. The expressions for the compression modulus (Equations 4.13 and 4.14) are derived from the expression for volumetric strain,



(a)



(b)

FIGURE 4-8 MOHR'S CIRCLE IN STRAIN (a) AND IN STRESS (b) FOR HOLLOW CYLINDER TEST SPECIMENS UNDER CONDITION OF MAXIMUM INSTANTANEOUS TORSIONAL STRESS AND STRAIN

thus those expressions are also independent of reorientation of the principal stress and strain directions.

The dynamic shear modulus under torsional loading conditions may be calculated by the following expression:

$$G = \frac{\Delta \tau_{\theta z}}{\Delta \gamma_{\theta z}} \quad (4.20)$$

Under conditions where only one modulus can be directly calculated from the data presented, or where it is desired to predict the effective Poisson's ratio under combined vertical and torsional loading conditions, the following expression may be used:

$$E = 2(1 + \mu) \cdot G \quad (4.21)$$

#### Data Reduction

A computer program has been written which calculates values of the tangent and secant dynamic compression moduli, the dynamic shear modulus, and the magnitude and direction of the maximum principal stresses and strains from the raw test data as a function of the Poisson's ratio. This computer program is called Program HC, and is included as Appendix D-2.

Example results of this testing series, as reduced from Program HC, are presented in Appendices B-4 through B-6, and complete results are summarized in Chapter 6. The complete results are available in Griffin (1980).

## Damping

### Introduction

In both the triaxial resonant-column and the thin-walled hollow cylinder testing series energy is dissipated during dynamic loading due to damping. Generally speaking, the greater the strain amplitude, the greater will be this energy loss. With closely monitored laboratory tests such as these, the energy loss measured is due solely to the inelastic response of the materials under test, and is sometimes referred to as hysteretic damping or friction damping. If the material behaves linearly and elastically, the energy loss and thus the damping, will be zero. As long as the damping is small, it is quite possible (and common practice) to treat the peak-to-peak stress strain response as an "equivalent-linear" modulus, and introduce damping as an energy dissipation over time.

### Resonant Column Testing

In the triaxial resonant-column testing series, the damping was measured using either the amplitude decay technique or the multiplication factor approach. The first of these involves the excitation of the specimen at its resonant frequency and observing the acceleration response as a function of time. When the driving force is abruptly stopped, the sample will continue to oscillate freely, but the acceleration amplitude will decay with time because of damping. The value of the damping may be calculated as follows:

$$\Delta = \frac{1}{n} \left( \ln \frac{a_o}{a_n} \right) \quad (4.22)$$

where  $\Delta$  = amplitude decay damping

$n$  = number of cycles, where  $n \geq 1$

$a_0$  = acceleration amplitude of the 0 - th cycle

$a_n$  = acceleration amplitude of the  $n$  - th cycle

This is illustrated graphically in Figure 4-9(a).

The amplitude decay damping is related to the ratio of critical damping,  $D$ , by the following expression:

$$\Delta = \frac{2\pi D}{\sqrt{1 - D^2}} \quad (4.23)$$

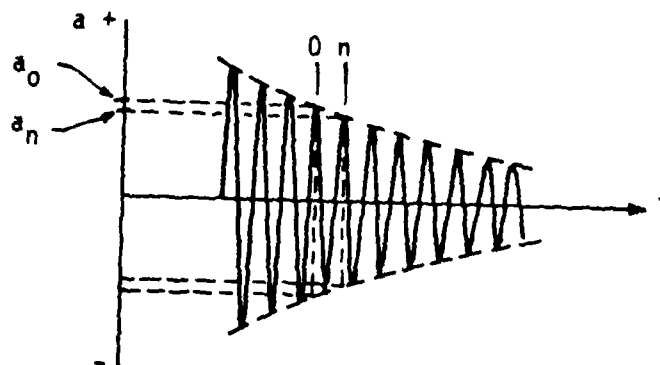
and, for small values of damping,  $D$  may be expressed in percent as follows:

$$D(\%) \approx \frac{\Delta}{2\pi} \cdot 100\% \quad (4.24)$$

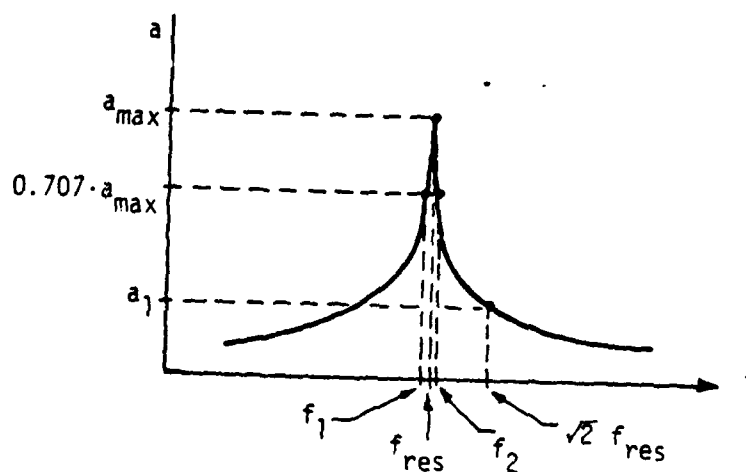
The use of the multiplication factor approach requires a look at the response spectrum for the specimen as shown in Figure 4-9(b). The resonant frequency is obtained as described in Chapter 3; then frequencies and amplitudes may be determined from other points along the "bell shaped curve," as shown in Figure 4-9(b).

The sharpness of the "bell" is an indication of the energy dissipation of the sample. A perfectly linear, elastic material would respond at one precise resonant frequency, and would have a response spectrum which is just a vertical line at the resonant frequency.

The values of frequency and response shown in Figure 4-9(b) are convenient because they lead to relatively simple expressions for calculating the damping. The values of  $f_1$  and  $f_2$  were selected such that the acceleration response at those frequencies was  $1/\sqrt{2}$  times the



(a)



(b)

FIGURE 4-9 AMPLITUDE DECAY METHOD (a) AND MULTIPLICATION FACTOR APPROACH (b) FOR COMPUTING DAMPING IN RESONANT COLUMN TESTS

maximum acceleration response occurring at or near resonance. Using these frequencies, the damping may be expressed as follows:

$$\Delta = \frac{\pi(f_2 - f_1)a_{\max}}{f_{\text{res}}} \quad (4.25)$$

or

$$D(\%) \approx \frac{(f_2 - f_1) \cdot a_{\max}}{2 f_{\text{res}}} \cdot 100\% \quad (4.26)$$

The value  $a_1$  was selected such that the frequency at which it occurred is equal to  $\sqrt{2}$  times the resonant frequency. In this case the damping may be calculated as follows:

$$\Delta = \frac{\pi}{2} \cdot \left[ \frac{\Delta\sigma_{\max}}{a_{\max}} \right] \cdot \left[ \frac{a_1}{\Delta\sigma_{a1}} \right] \quad (4.27)$$

or

$$D(\%) \approx \frac{1}{4} \left[ \frac{\Delta\sigma_{\max}}{a_{\max}} \right] \left[ \frac{a_1}{\Delta\sigma_{a1}} \right] \cdot 100\% \quad (4.28)$$

where  $\Delta\sigma_{\max}$  = driving stress at  $a_{\max}$  response

$\Delta\sigma_{a1}$  = driving stress at  $a_1$  response

If the driving force is held constant throughout the response spectrum, which is usually the case, Equations 4.27 and 4.28 reduce to the following:

$$\Delta = \frac{\pi a_1}{2a_{\max}} \quad (4.29)$$

and

$$D = \frac{a_1}{4a_{\max}} \cdot 100\% \quad (4.30)$$

The practical advantage to using Equations 4.27 and 4.28 in the form presented is that the factor  $\left[ \frac{a_1}{\Delta\sigma_{a1}} \right]$  does not change appreciably

during testing, and normally needs to be measured only once. The damping may then be calculated by merely knowing the acceleration response and the driving stress at resonance throughout testing. The damping equations may thus be rewritten as follows:

$$\Delta = \frac{2\pi\delta}{100\%} \cdot \left( \frac{\Delta\sigma_{\text{amax}}}{a_{\text{max}}} \right) \quad (4.31)$$

and

$$D(\%) = \delta \cdot \left( \frac{\Delta\sigma_{\text{amax}}}{a_{\text{max}}} \right) \quad (4.32)$$

where

$$\delta = \begin{cases} \frac{100\%}{4} \cdot \left[ \frac{a_1}{\Delta\sigma_{a1}} \right] \\ \text{damping calibration factor} \end{cases} \quad (4.33)$$

#### Hollow Cylinder Testing

In the thin-walled hollow cylinder testing series, the energy dissipation is seen as a hysteresis loop stress-strain response, as shown in Figure 4-10. The "equivalent linear" modulus is shown as the ratio of peak-to-peak stress to peak-to-peak strain. In Figure 4-10, the following equations may be written:

$$\overline{AB} = \overline{A'B'} = \frac{\Delta\sigma}{2} \quad (4.34)$$

$$\overline{OB} = \overline{B'O} = \frac{\Delta\epsilon}{2} \quad (4.35)$$

$$E_{ps} = \frac{\overline{AB}}{\overline{OB}} = \frac{\overline{A'B'}}{\overline{B'O}} \quad (4.36)$$

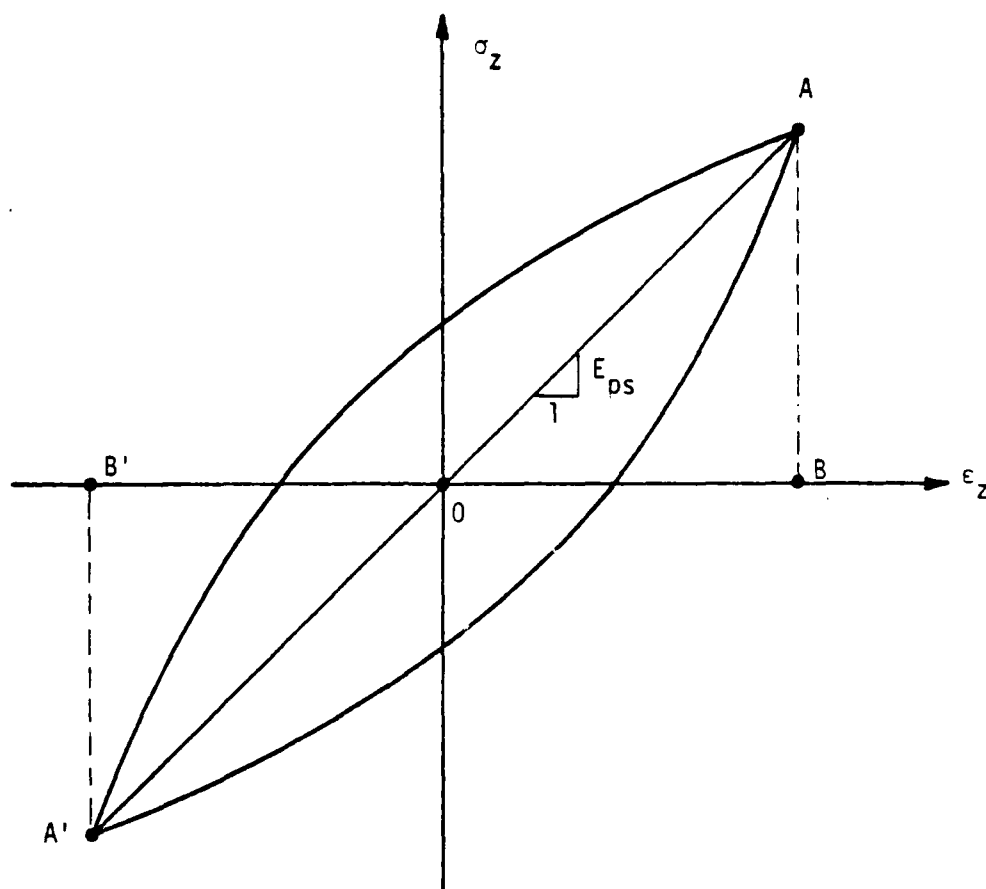


FIGURE 4-10 HYSTERETIC STRESS-STRAIN CURVE FOR DYNAMIC VERTICAL LOADING IN HOLLOW CYLINDER TEST

AD-A092 352

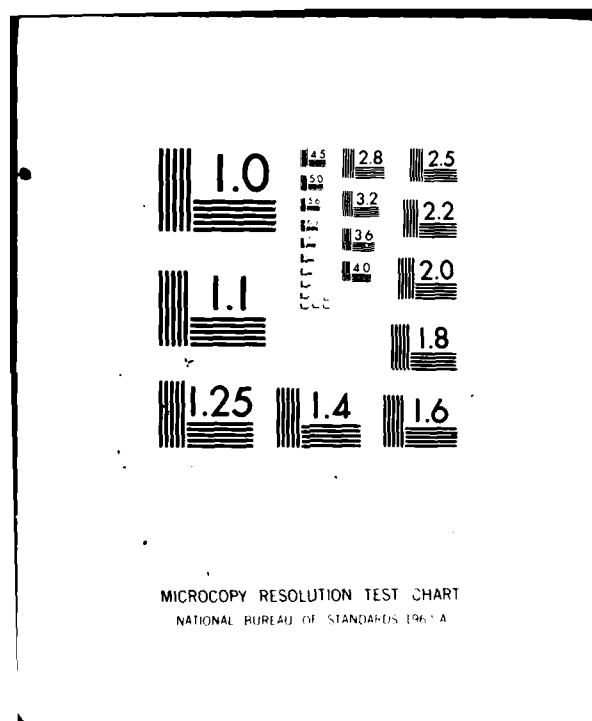
CALIFORNIA UNIV BERKELEY EARTHQUAKE ENGINEERING RES--ETC F/6 8/13  
INTERACTION EFFECTS OF SIMULTANEOUS TORSIONAL AND COMPRESSIONAL--ETC(U)  
DEC 79 P M GRIFFIN, W N HOUSTON DAA029-76-6-0257  
UCB/EERC-79/34 ARO-13838,1-85 NL

UNCLASSIFIED

204

204





The damping may be expressed as follows:

$$\lambda = \frac{A_{\ell}}{A_{ABO} + A_{A'B'O}} \quad (4.37)$$

where  $A_{\ell}$  = area of the loop

$A_{ABO}$  = area of the triangle ABO

$A_{A'B'O}$  = area of the triangle A'B'O

This value of hysteretic damping is related to the ratio of critical damping by the following relationship:

$$\lambda = \frac{2 \pi D}{\sqrt{1 - D^2}} \quad (4.38)$$

or, for small values of damping,

$$D(\%) \approx \frac{\lambda}{2\pi} \cdot 100\% \quad (4.39)$$

## Chapter 5

### Low Strain Combined Cyclic Loading

#### Introduction

In this chapter the actual laboratory test results reduced from the triaxial resonant column series will be presented. Shown in Figure 5-1 is a photograph of the resonant column testing device with a specimen in place. Listed in Table 5-1 is a summary of the seventeen tests which have been analyzed for this presentation.

As discussed previously, the moduli during dynamic combined loading will change both with vertical strain amplitude and with compression-shear interaction. The data will be presented in such a way that the two effects may be seen both separately and together. The results will also be presented as a function of the octahedral shearing strain.

#### Vertical Loading Alone

The dynamic compression modulus is shown as a function of the cyclic vertical strain under conditions of vertical loading alone in Figure 5-2. It should be noted that for all values of strain referred to hereafter, the single-amplitude values are used. The cyclic stress amplitudes shown on drawings, however, are peak-to-peak values. This Figure includes data from a variety of samples at various densities and confining pressures. Superimposed upon the drawing are contour lines showing values of equal vertical normal cyclic stress,  $\Delta\sigma_z$ . From this Figure we can see that the range of cyclic vertical normal stress used in this testing series was from approximately 0.02 psi to 25 psi. The corresponding vertical

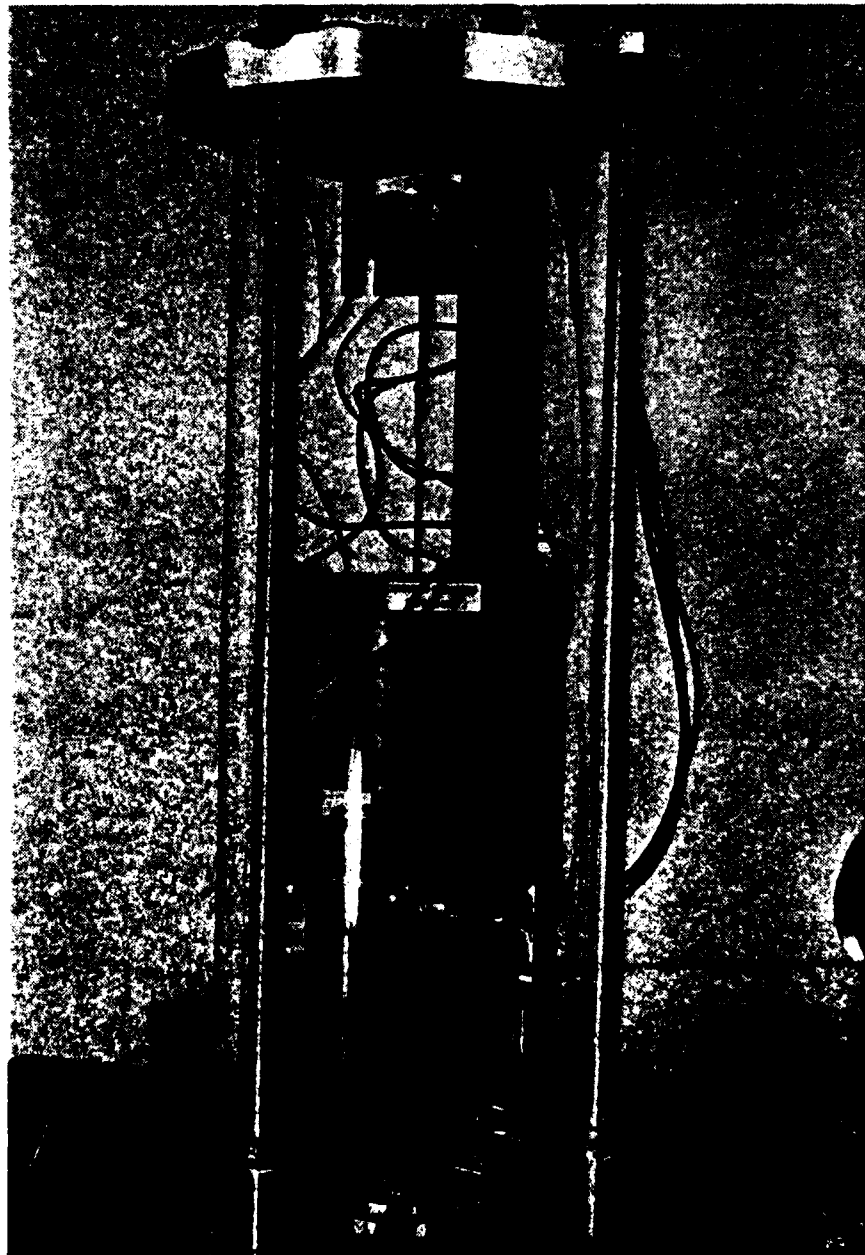


FIGURE 5-1 RESONANT COLUMN TESTING APPARATUS

TABLE 5-1  
Summary of Resonant Column Tests

TEST NO.	$\gamma_d$ (g/cc)	$D_R$ (%)	$\sigma_{3c}$ (KSC)	MODE V-VERTICAL T-TORSIONAL C-COMBINED
1A-3	1.70	97.9	3.5	V
2AL-3	1.61	69.5	3.5	V
3AL-3	1.61	69.5	3.5	V
4AL-2	1.63	76.1	2.0	V
5A-2	1.69	94.9	2.0	V
6A-1	1.69	94.9	0.5	V
7AL-1	1.62	72.8	0.5	V
9BL-1	1.62	72.8	0.5	C
10B-1	1.70	97.9	0.5	C
11BL-2	1.64	79.3	2.0	C
12B-2	1.69	94.9	2.0	C
13BL-3	1.64	79.3	3.5	C
14B-3	1.68	91.8	3.5	C
15CM-1	1.68	91.8	0.5	T
16CL-1	1.64	79.3	0.5	T
17CL-3	1.64	79.3	3.5	T
18C-3	1.67	88.8	3.5	T

$\gamma_d$  = dry density of soil

$D_R$  = relative density

$\sigma_{3c}$  = lateral confining pressure

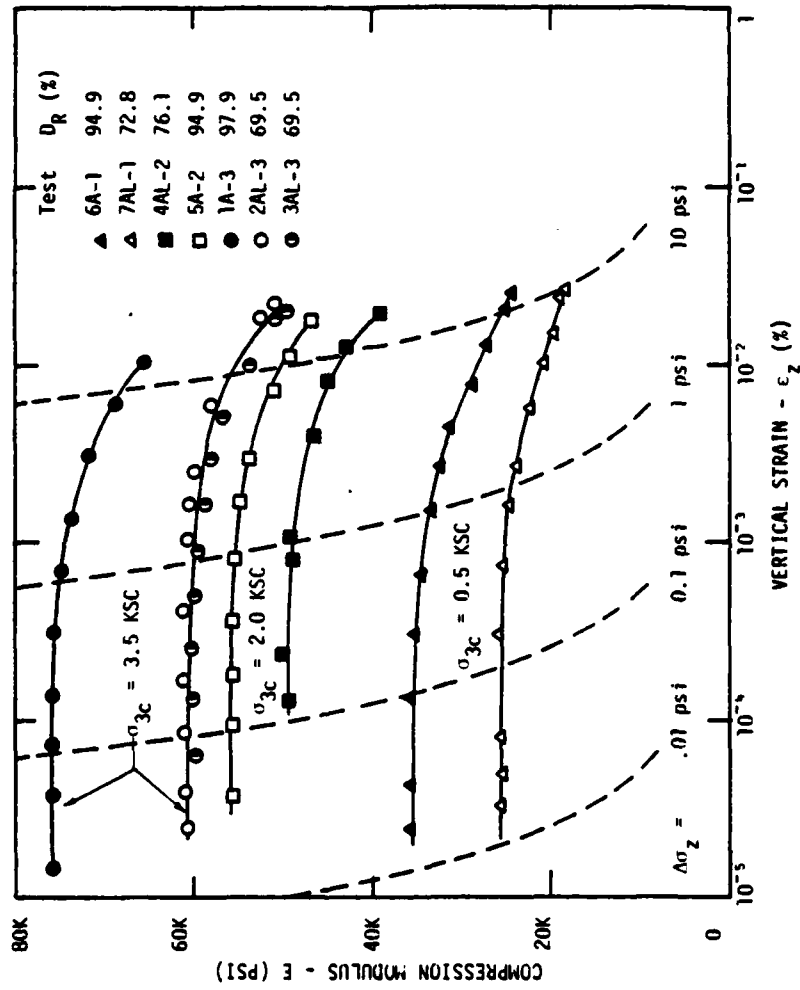


FIGURE 5-2 DEGRADATION OF COMPRESSION MODULUS WITH VERTICAL STRAIN FOR SEVERAL TESTS UNDER CONDITION OF VERTICAL LOADING ALONE

strain amplitudes were in the range of from approximately  $10^{-5}\%$  to  $3 \times 10^{-2}\%$ . It is interesting to note the steepness of the stress contours, indicating that relatively small variations in strain amplitude will yield relatively large variations in moduli.

To eliminate variations in the modulus-strain curves due to sample peculiarities, density variations, and small measurement errors, it is desirable to "normalize" these curves by plotting a "relative modulus" in place of the absolute value of modulus. This technique allows a direct evaluation of the relative variation of modulus with strain amplitude.

In Figure 5-3 six tests are normalized to the value of the modulus at a single amplitude vertical strain of  $5 \times 10^{-3}\%$ . This value was selected to allow for comparison of these test results with those of the higher strain, thin-walled hollow cylinder testing series which will be presented in Chapter 6.

From Figure 5-3 it can be seen that the greatest rate of change of modulus with strain amplitude occurs at the lowest confining pressures. Although there is some variation in this rate as a function of density, this variation is small when compared with the influence of the confining pressure on the rate of variation.

#### Torsional Loading Alone

The results of four tests in which pure torsional loading was applied to samples are presented in Figure 5-4. As with Figure 5-2, the modulus (in this case the Shear Modulus) is seen to change as a function of the strain amplitude. In these tests the range of the cyclic torsional shear stress was from approximately .01 psi to 15 psi, very similar to

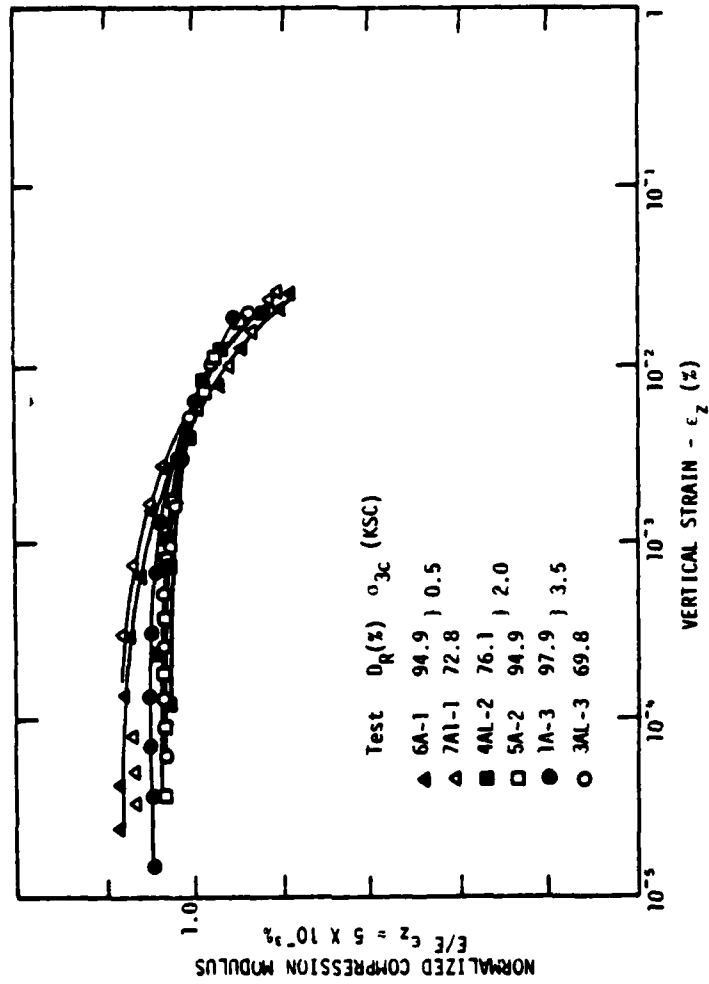


FIGURE 5-3 DEGRADATION OF NORMALIZED COMPRESSION MODULUS WITH VERTICAL STRAIN FOR SEVERAL TESTS UNDER CONDITION OF VERTICAL LOADING ALONE

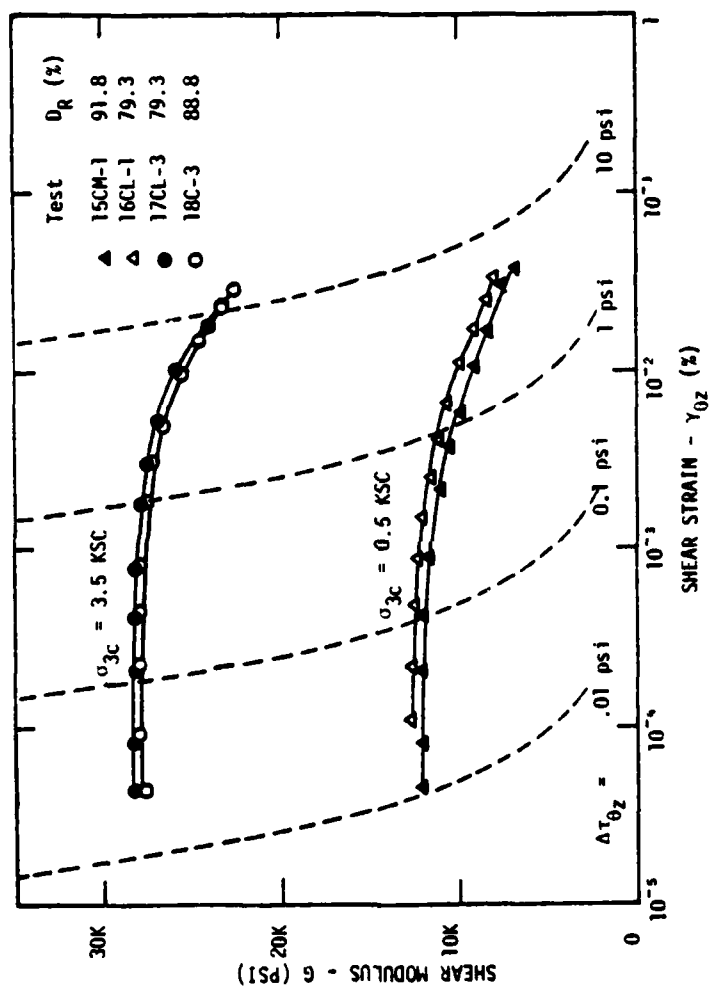


FIGURE 5-4 DEGRADATION OF SHEAR MODULUS WITH SHEAR STRAIN FOR SEVERAL TESTS UNDER CONDITION OF SHEAR LOADING ALONE

the load range in vertical compression. The corresponding torsional shear strain amplitudes were in the range of from approximately  $4 \times 10^{-5}\%$  to  $4 \times 10^{-2}\%$ .

The shear modulus-shear strain curves were normalized to the modulus at a shear strain of  $5 \times 10^{-3}\%$  and presented in Figure 5-5. In this Figure it can be seen that the relative variation of shear modulus with strain amplitude is somewhat greater than the variation of compression modulus shown in Figure 5-3 over a similar strain range.

#### Combined Loading

Under conditions of simultaneous vertical and torsional dynamic loading, the modulus will vary both as a function of the vertical strain amplitude and as a function of the compression-shear interaction effects. As indicated in Table 5-1, six tests performed under simultaneous combined loading conditions have been presented and analyzed. These tests represented two different densities and three different confining pressures.

#### Interaction Effects

The effects of this interaction on two of these tests are shown in Figure 5-6. In this Figure modulus-strain amplitude curves are plotted for the two test specimens, with contours of equal shear strain amplitude superimposed on the drawing. The curves labeled  $\gamma_{\theta z} < 10^{-4}\%$  are those corresponding to the "virgin" modulus-strain curve in which no measurable compression-shear interaction effects are present. These are the solid lines in this Figure.

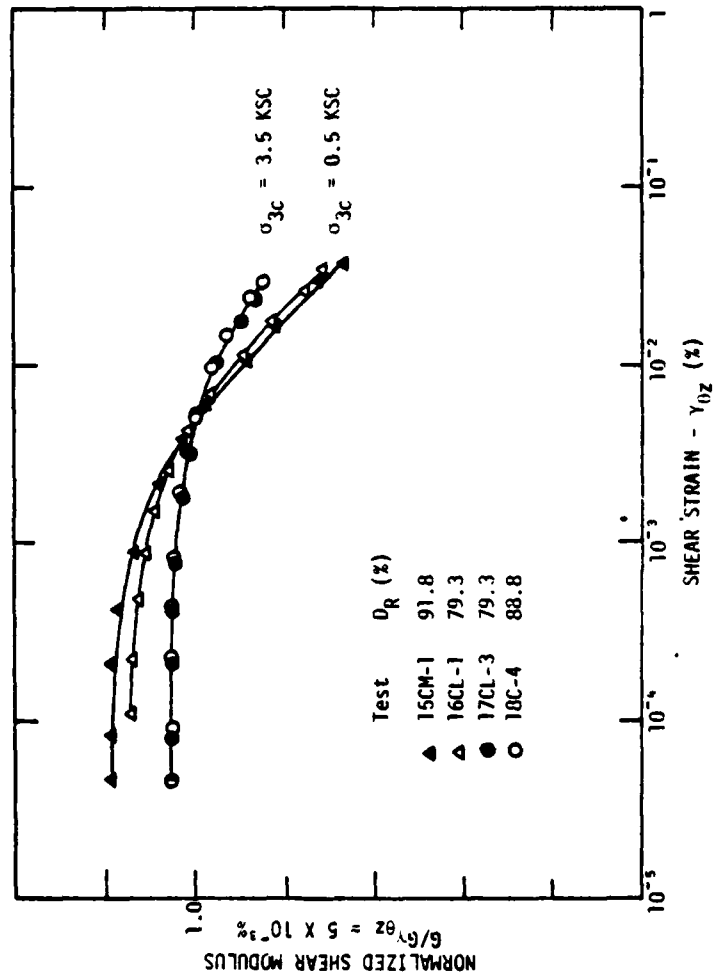


FIGURE 5-5 DEGRADATION OF NORMALIZED SHEAR MODULUS WITH SHEAR STRAIN FOR SEVERAL TESTS UNDER CONDITION OF SHEAR LOADING ALONE

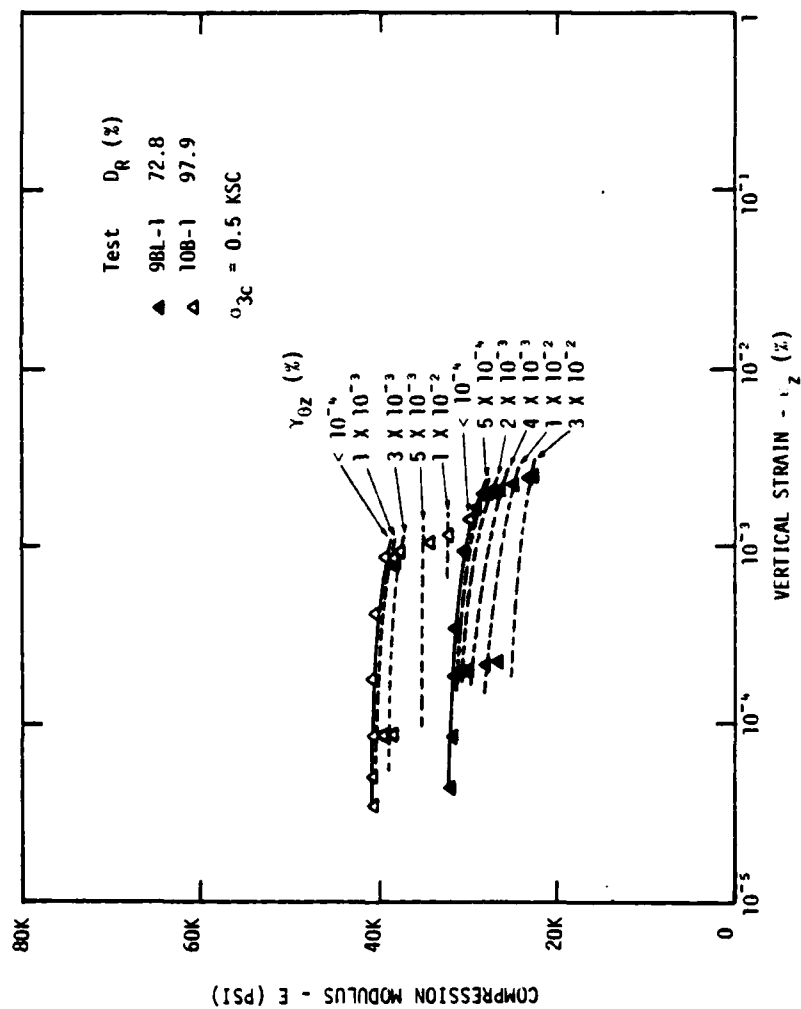


FIGURE 5-6 DEGRADATION OF COMPRESSION MODULUS WITH VERTICAL STRAIN UNDER SEVERAL LEVELS OF SIMULTANEOUSLY APPLIED SHEAR STRAIN

### Strain Ratio Effects

These interaction effects can be isolated from the other factors influencing the modulus value by plotting a normalized modulus vs. the ratio of average shear strain,  $\gamma_{\theta z}$ , (see Chapter 2 for definition) to the vertical normal strain,  $\epsilon_z$ . The modulus should be normalized to the modulus at that vertical strain amplitude on the "virgin" modulus-strain curve,  $E_{<\gamma_{\theta z}}$ .

These normalized plots were prepared for all of the combined loading tests in this series, and are presented in Figures 5-7, 5-8, and 5-9, for confining pressures of 0.5, 2.0, and 3.5 KSC, respectively. These normalized curves are combined and summarized for those tests with a relative density of 95% in Figure 5-10; and for all combined loading tests in Figure 5-11.

### Octahedral Shearing Strain Effects

As discussed in Chapter 2, the octahedral shearing strain,  $\gamma_{OCT}$ , is a very useful tool in evaluating the degradation of modulus with strain amplitude. For these testing series a degradation of modulus has been observed both with increasing dynamic axial strain,  $\Delta\epsilon_z$ , and with increasing dynamic shear strain,  $\Delta\gamma_{\theta z}$ . The octahedral shearing strain combines both of these types of straining, and should be very useful in studying the combined degradation effects.

It should be noted that if the material is homogeneous and isotropic, then the degradation of modulus with octahedral shearing strain,  $\gamma_{OCT}$ , will be independent of how the strain was developed; i.e., from axial or torsional straining.

In Figure 5-12 are shown the "virgin" normalized compression moduli,

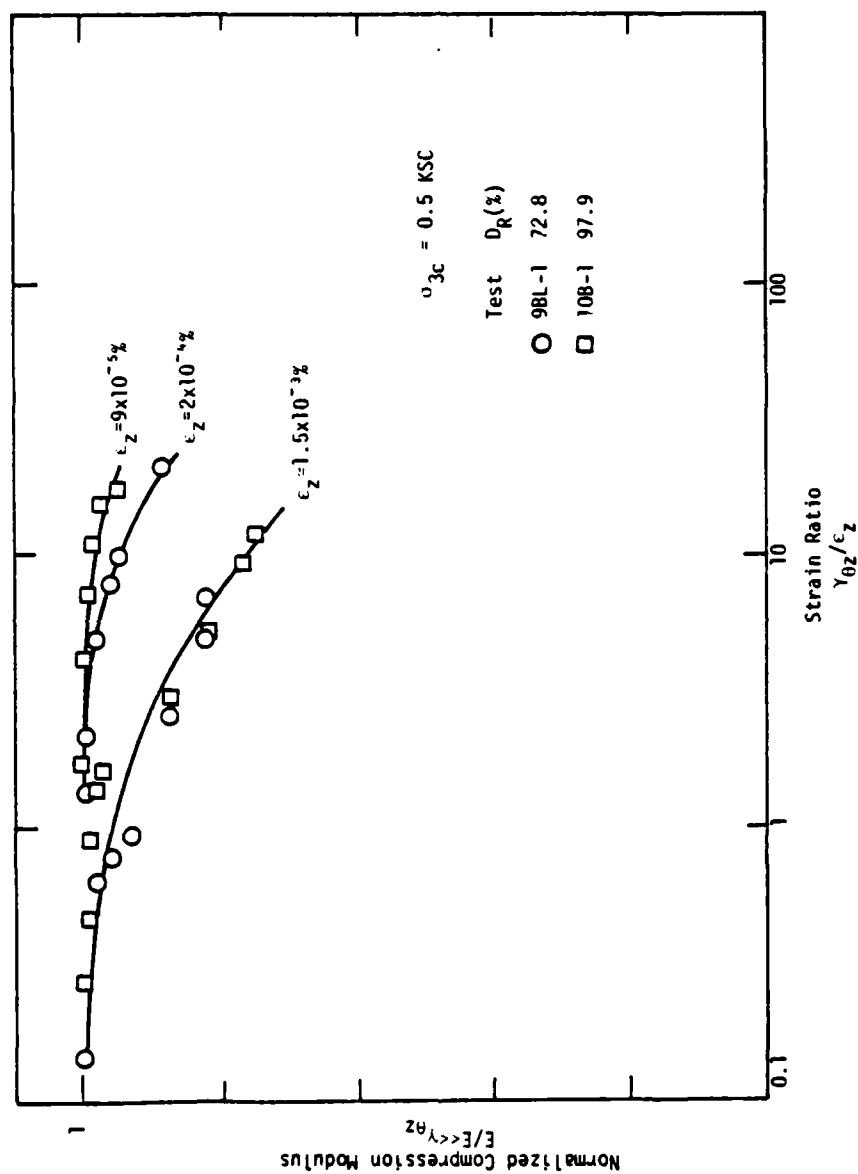


FIGURE 5-7 DEGRADATION OF NORMALIZED COMPRESSION MODULUS WITH RATIO OF SHEAR STRAIN TO VERTICAL STRAIN AT  $\sigma_{3c} = 0.5 \text{ KSC}$  FOR SEVERAL COMBINED LOADING TESTS

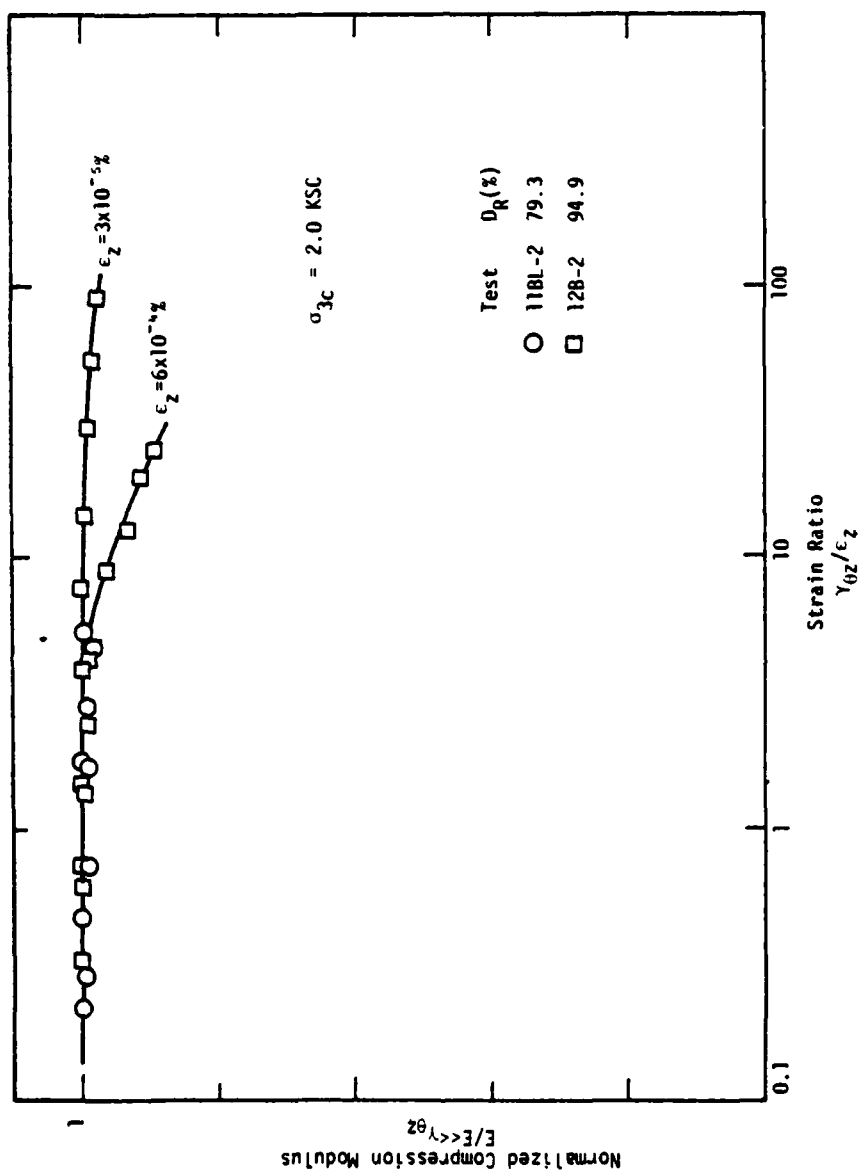


FIGURE 5-8 DEGRADATION OF NORMALIZED COMPRESSION MODULUS WITH RATIO OF SHEAR STRAIN TO VERTICAL STRAIN AT  $\sigma_{3c} = 2.0 \text{ KSC}$  FOR SEVERAL COMBINED LOADING TESTS

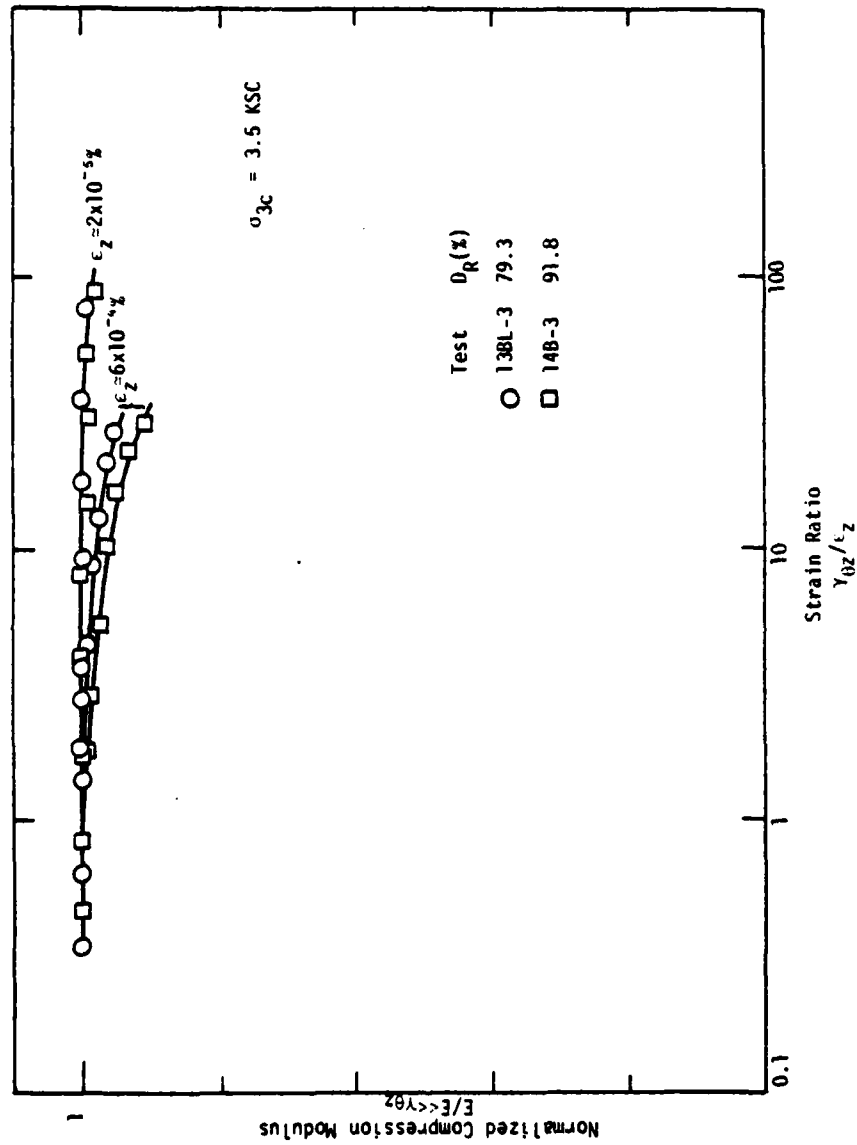


FIGURE 5-9 DEGRADATION OF NORMALIZED COMPRESSION MODULUS WITH RATIO OF SHEAR STRAIN TO VERTICAL STRAIN AT  $\sigma_{3c} = 3.5 \text{ KSC}$  FOR SEVERAL COMBINED LOADING TESTS

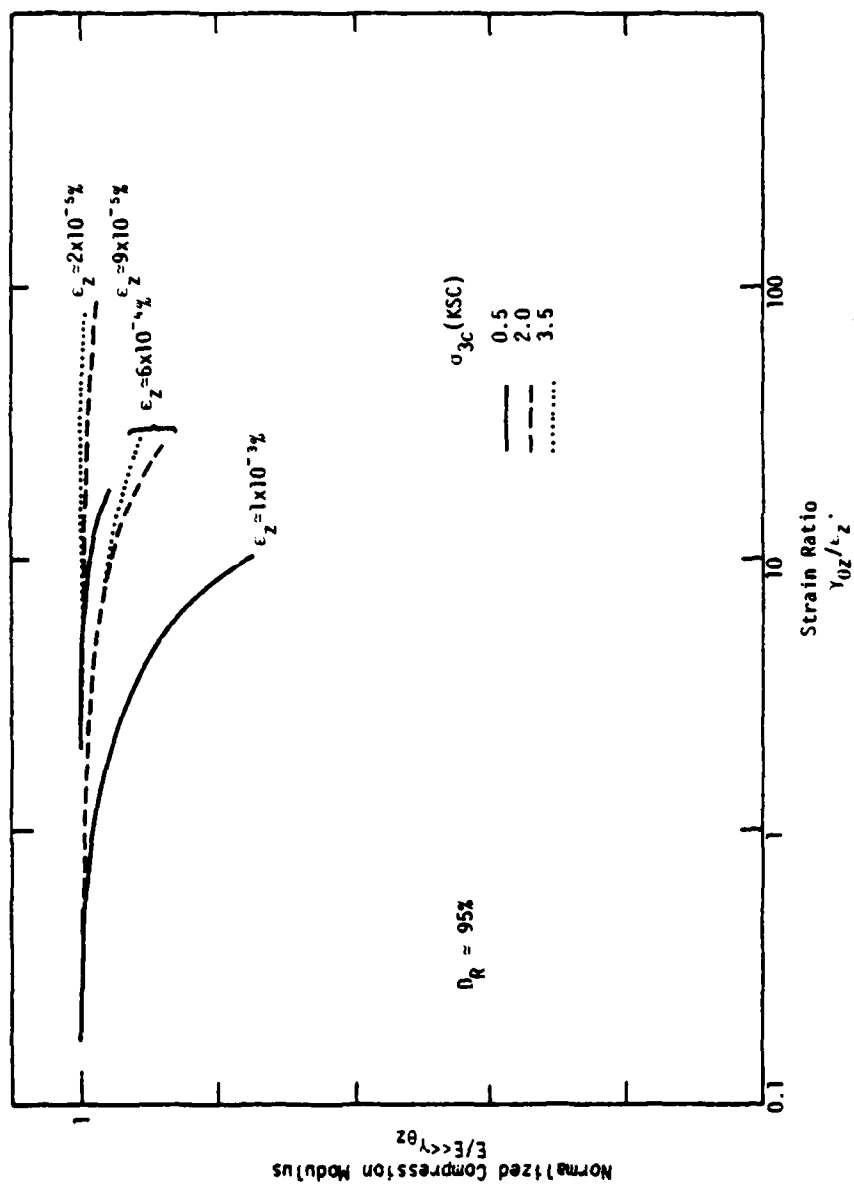


FIGURE 5-10 SUMMARY OF DEGRADATION OF NORMALIZED COMPRESSION MODULUS WITH RATIO OF SHEAR STRAIN TO VERTICAL STRAIN FOR A RELATIVE DENSITY OF 95%

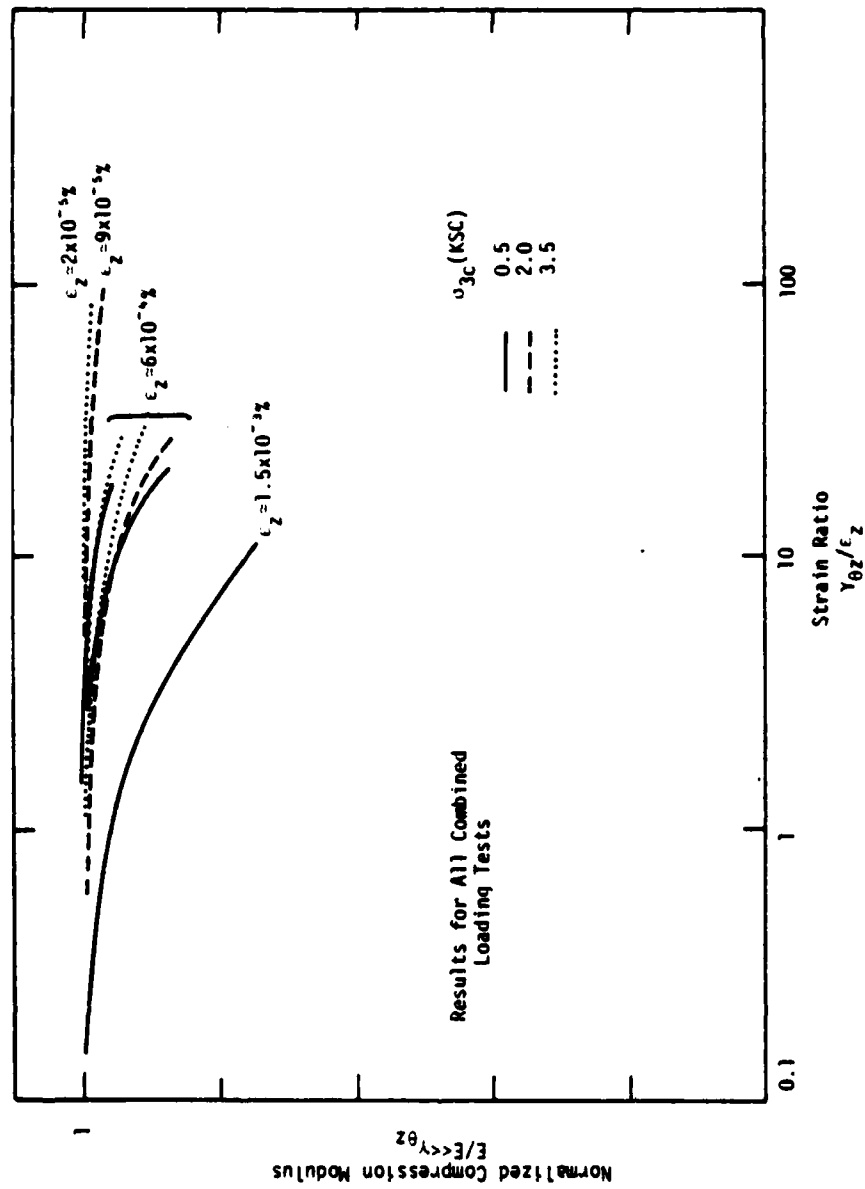


FIGURE 5-11 SUMMARY OF DEGRADATION OF NORMALIZED COMPRESSION MODULUS WITH RATIO OF SHEAR STRAIN TO VERTICAL STRAIN FOR ALL COMBINED LOADING TESTS

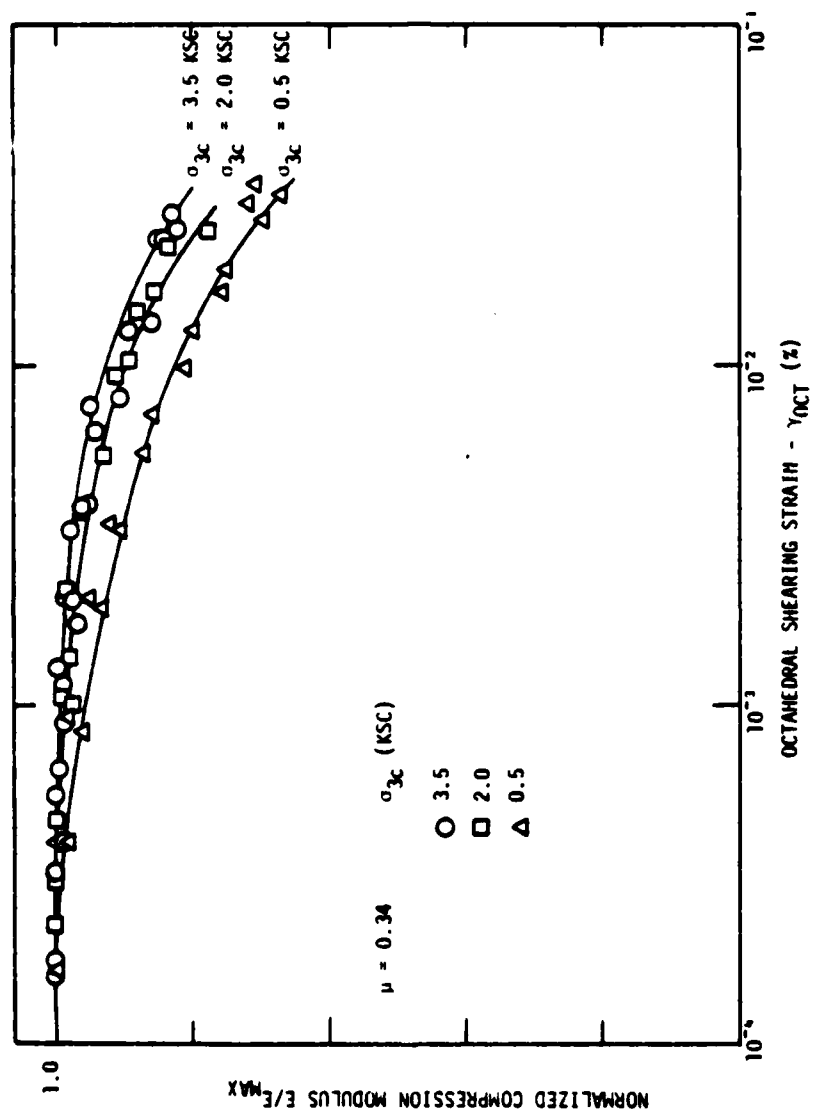


FIGURE 5-12 DEGRADATION OF NORMALIZED COMPRESSION MODULUS WITH OCTAHEDRAL SHEARING STRAIN FOR CONDITION OF VERTICAL LOADING ALONE

$E/E_{MAX}$ , plotted vs.  $\gamma_{OCT}$ . Because these curves were developed by applying vertical loading alone to the soil specimens, the octahedral shearing strain in that Figure is developed purely from vertical, radial, and tangential normal straining. These normal strains correspond to the principal strains in this case.

In the combined loading case, shear strains introduced in the  $\theta_z$  "plane" result in a reorientation of the principal strain directions; thus, the octahedral shearing strain in this case is developed from the combination of vertical, radial, and tangential normal strains, plus  $\theta_z$  "plane" shear strains.

The variation of compression moduli with the virgin compression moduli, as a function of octahedral shearing strain is shown in Figures 5-13, 5-14, and 5-15 for confining pressures of 0.5, 2.0, and 3.5 KSC, respectively. These curves are combined with the virgin curves from Figure 5-12 to determine the effects of shear-compression interaction, and are presented in Figures 5-16, 5-17, and 5-18 for the same three confining pressures. For the dashed curves the increases in  $\gamma_{OCT}$  arise from increases in  $\gamma_{\theta_z}$  with  $\epsilon_z$  held constant as shown. For the solid curves, the increases in  $\gamma_{OCT}$  arise from increases in  $\epsilon_z$  with  $\gamma_{\theta_z}$  held as small as possible, typically less than  $10^{-4}\%$  as shown. The intersection of the dashed curves and the solid curve occurs when the contribution of  $\gamma_{\theta_z}$  to  $\gamma_{OCT}$  is small compared to the contribution of  $\epsilon_z$  for these tests. Therefore the value of  $\gamma_{OCT}$  at which the intersection occurs can be computed directly from  $\epsilon_z$  for practical purposes.

In these Figures it is apparent that the two types of curves are essentially coincident, and thus any shear-compression interaction effect which is not accounted for by the use of the octahedral shearing strain

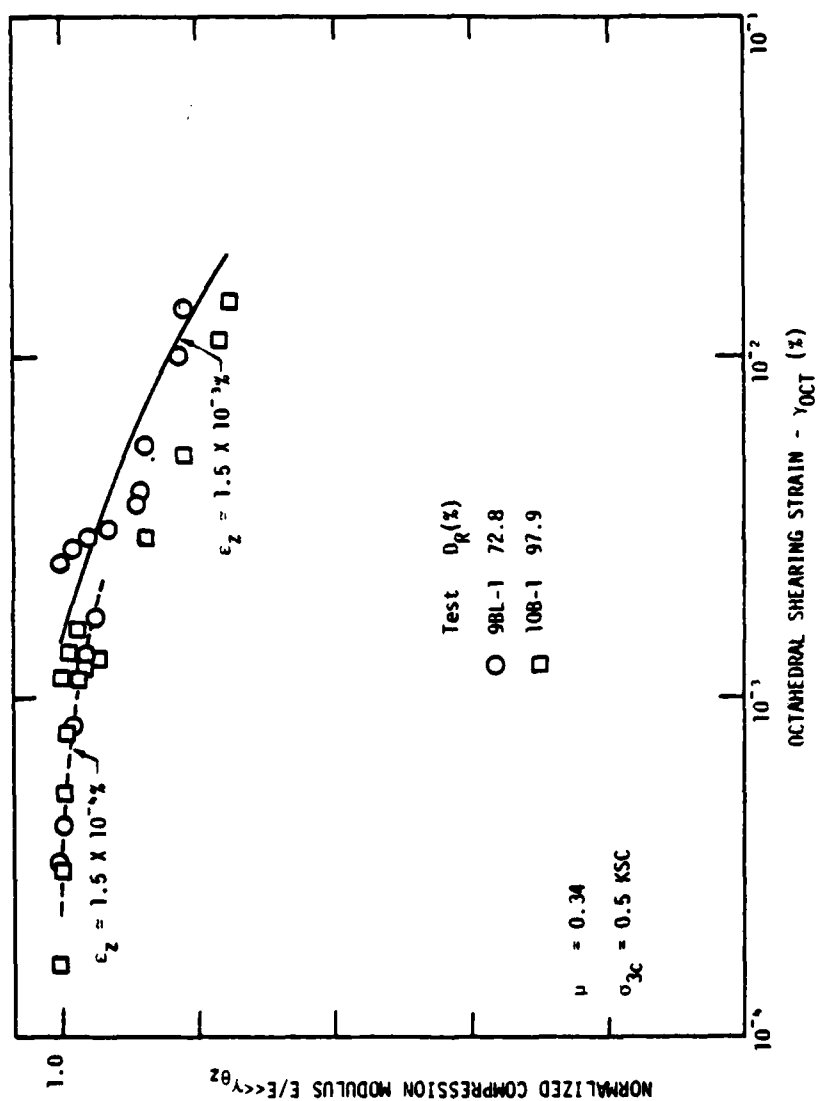


FIGURE 5-13 DEGRADATION OF NORMALIZED COMPRESSION MODULUS WITH OCTAHEDRAL SHEARING STRAIN AT  $\sigma_{3c} = 0.5 \text{ KSC}$  FOR SEVERAL COMBINED LOADING TESTS

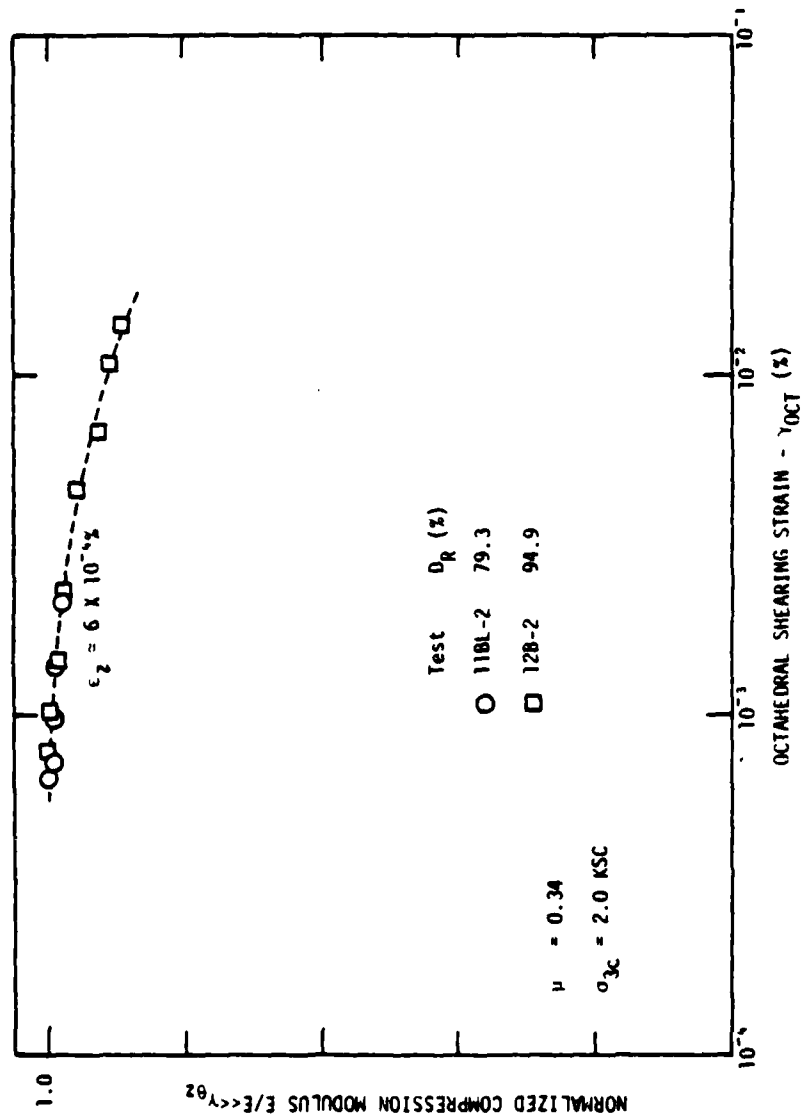


FIGURE 5-14 DEGRADATION OF NORMALIZED COMPRESSION MODULUS WITH OCTAHEDRAL SHEARING STRAIN AT  $\sigma_{3c} = 2.0 \text{ KSC}$  FOR SEVERAL COMBINED LOADING TESTS

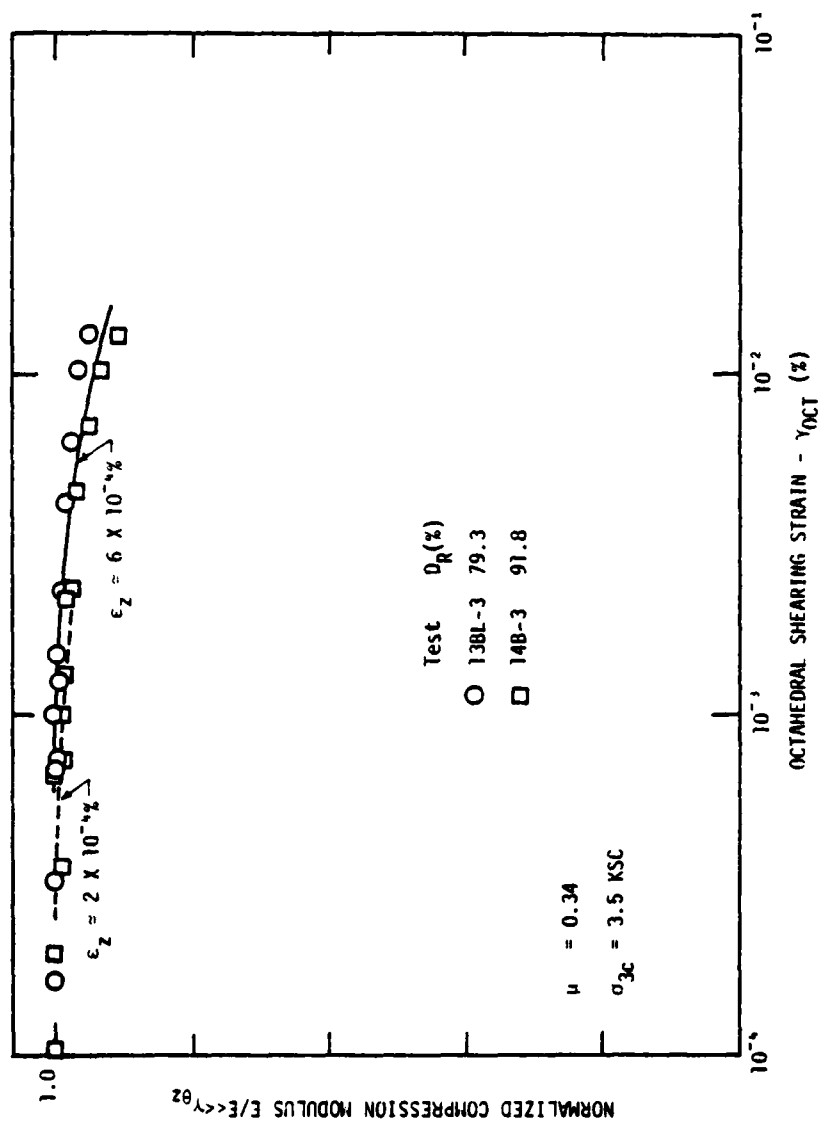


FIGURE 5-15 DEGRADATION OF NORMALIZED COMPRESSION MODULUS WITH OCTAHEDRAL SHEARING STRAIN AT  $\sigma_{3c} = 3.5 \text{ KSC}$  FOR SEVERAL COMBINED LOADING TESTS

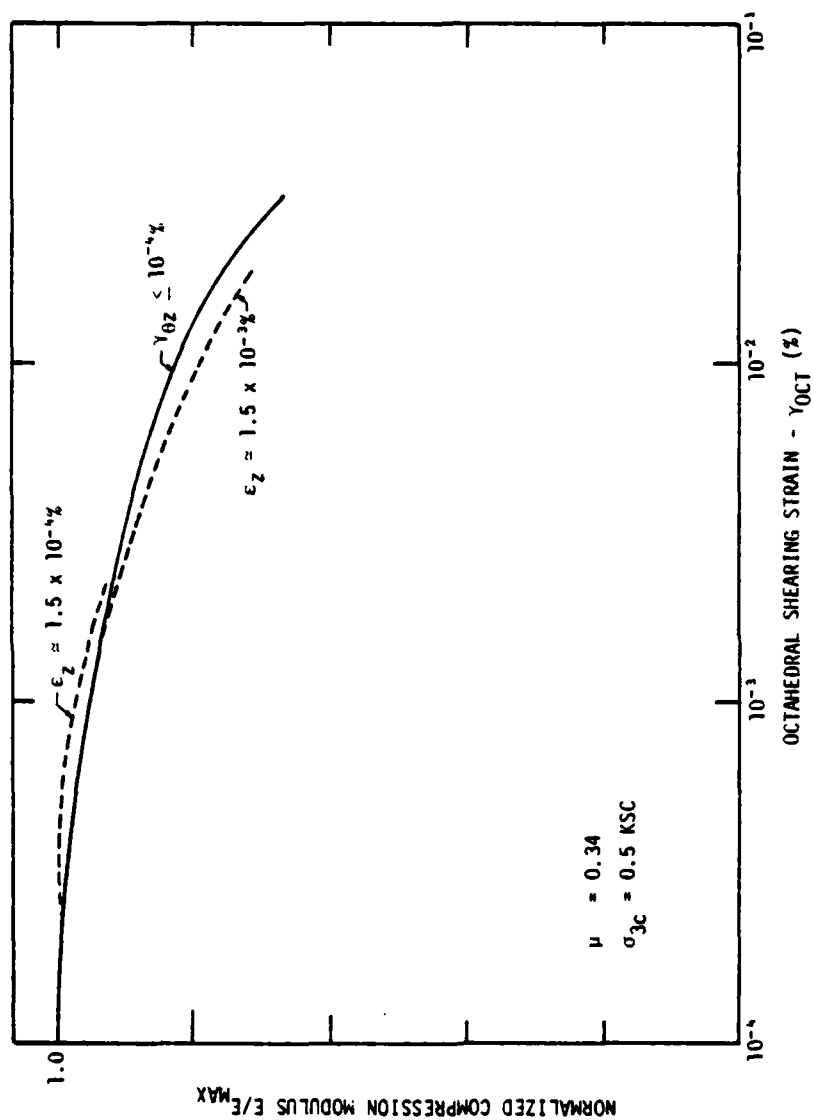


FIGURE 5-16 DEGRADATION OF NORMALIZED COMPRESSION MODULUS WITH OCTAHEDRAL SHEARING STRAIN AT  $\sigma_{3c} = 0.5 \text{ KSC}$  FOR BOTH VERTICAL AND COMBINED LOADING TESTS

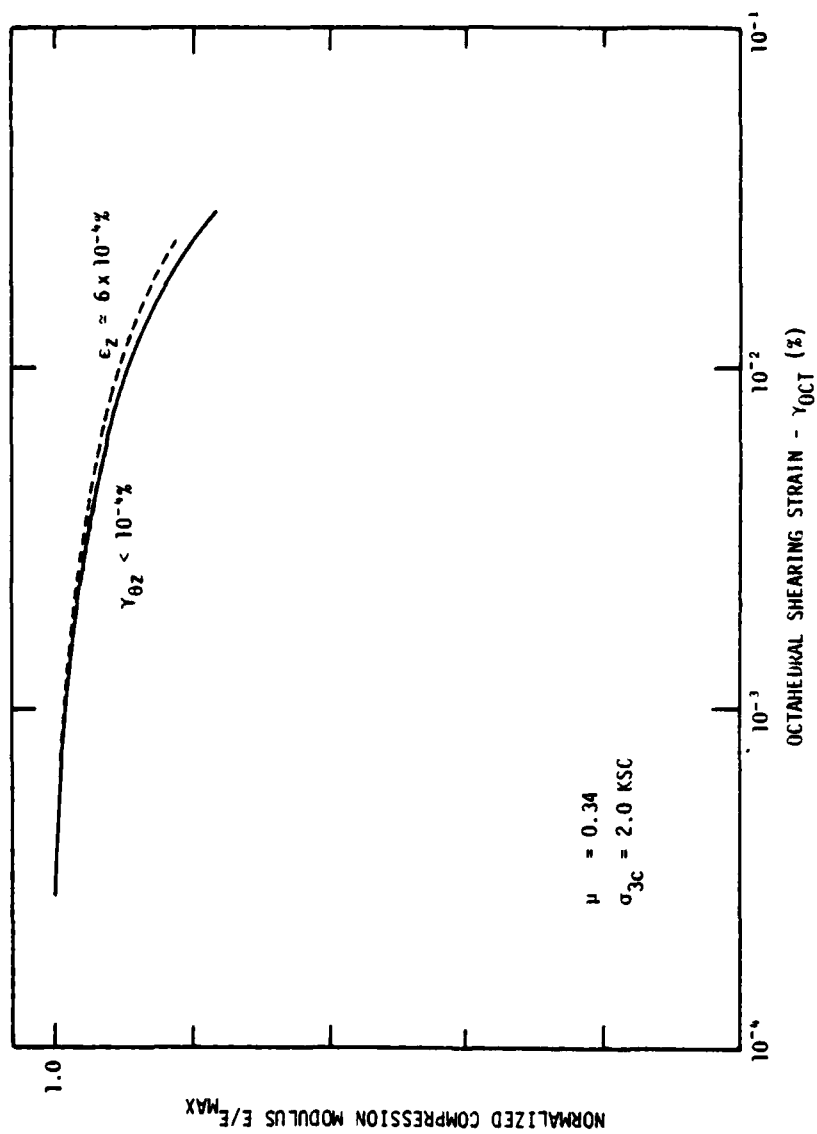


FIGURE 5-17 DEGRADATION OF NORMALIZED COMPRESSION MODULUS WITH OCTAHEDRAL SHEARING STRAIN AT  $\sigma_{3c} = 2.0 \text{ KSC}$  FOR BOTH VERTICAL AND COMBINED LOADING TESTS

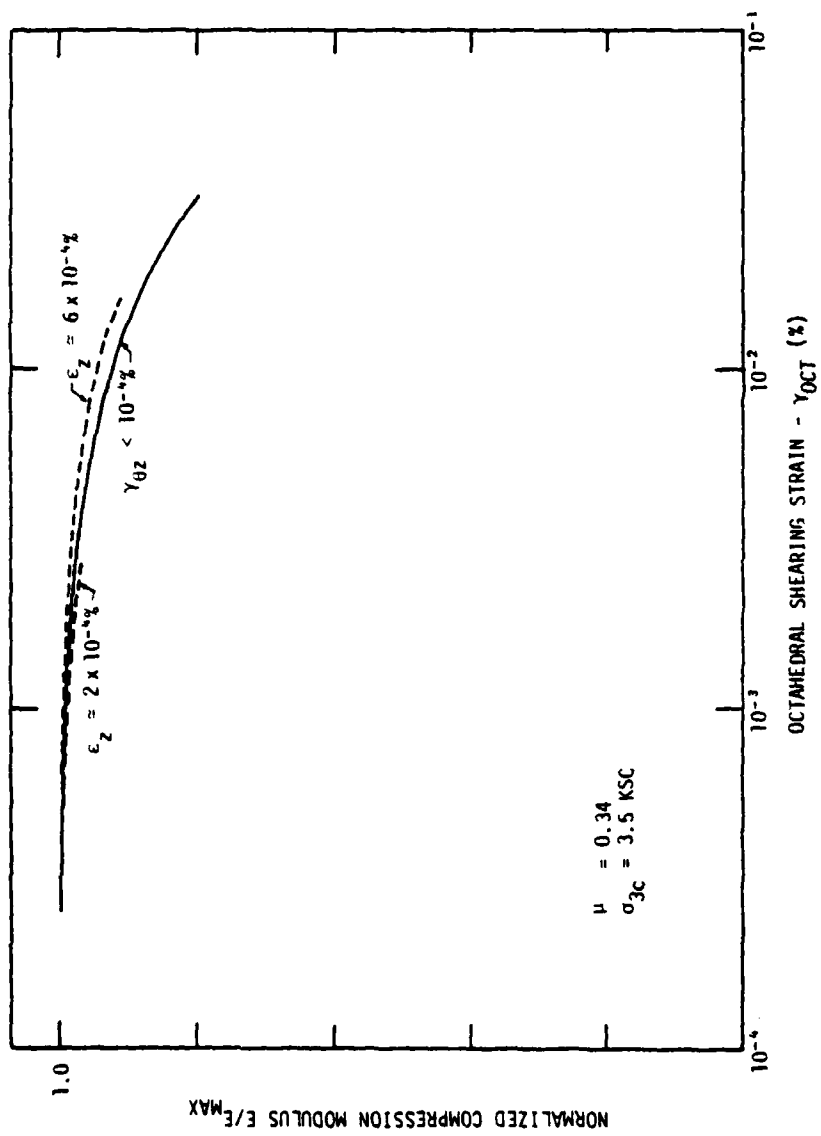


FIGURE 5-18 DEGRADATION OF NORMALIZED COMPRESSION MODULUS WITH OCTAHEDRAL SHEARING STRAIN AT  $\sigma_{3c} = 3.5 \text{ KSC}$  FOR BOTH VERTICAL AND COMBINED LOADING TESTS

is negligible.

The resultant best-fit normalized moduli-octahedral shearing strain curves are presented in Figure 5-19.

### Conclusions

The various test results were presented in different ways to evaluate the relative compression-shear interaction under combined loading conditions.

#### Strain Ratio Effects

From the results of the presentation of the relative normalized compression moduli plotted against the ratio of average shear strain,  $\gamma_{\theta z}$ , to vertical normal strain,  $\epsilon_z$ , in Figure 5-11, it is apparent that there exists a "threshold" strain ratio below which negligible interaction effects are observed. It appears that the minimum threshold strain ratio in this testing program was approximately 1, where the average shear strain equaled the vertical normal strain. This means that when the shear strain,  $\gamma_{\theta z}$ , was numerically smaller than the vertical normal strain the degradation of modulus due to  $\gamma_{\theta z}$  was negligible.

Also apparent is the fact that the moduli-strain ratio curve and the threshold strain ratio depend primarily upon the vertical normal strain amplitude. The effects of confining pressure and relative density upon these curves appears to be very small.

#### Octahedral Shearing Strain Effects

From the results of the presentation of normalized compression

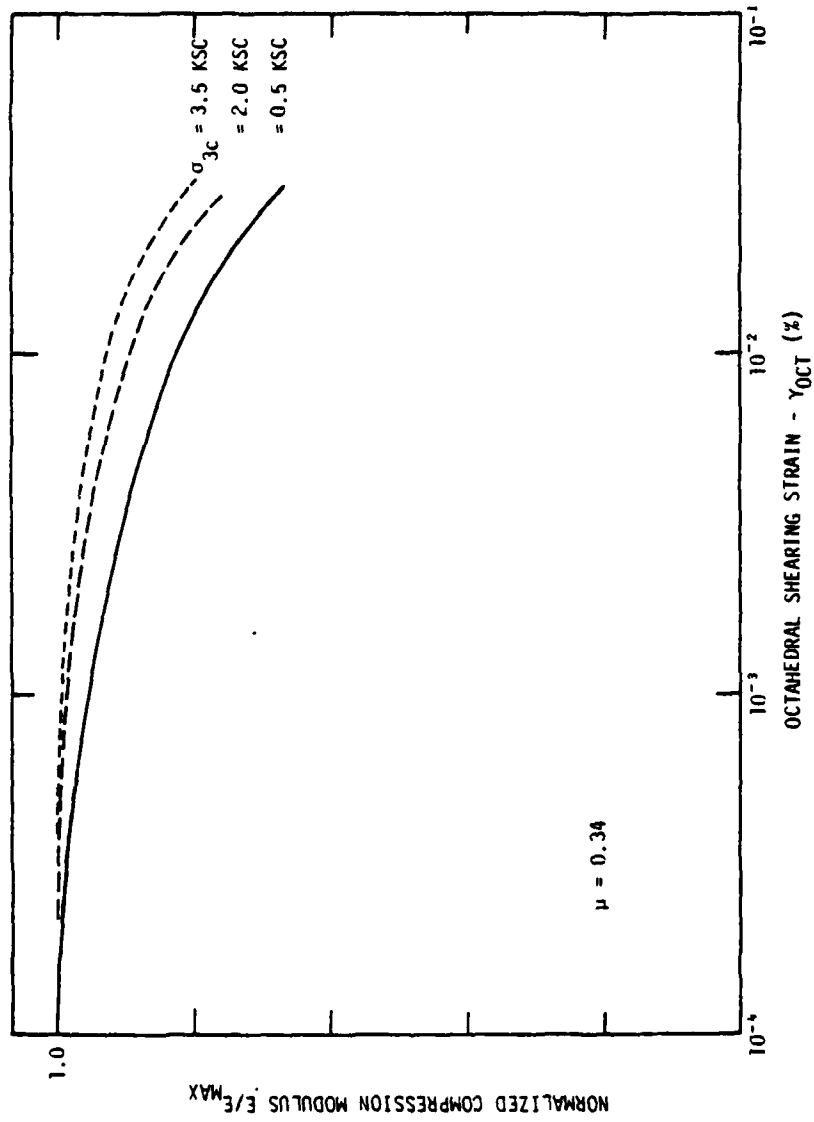


FIGURE 5-19 SUMMARY OF DEGRADATION OF NORMALIZED COMPRESSION MODULUS WITH OCTAHEDRAL SHEARING STRAIN

moduli plotted against the octahedral shearing strain in Figure 5-19 it appears that the compression-shear interaction is directly predictable or "expressible" by use of the octahedral shearing strain.

The maximum octahedral shearing strain developed in this testing series was approximately  $3 \times 10^{-2}\%$ .

## Chapter 6

### High Strain Combined Cyclic Loading

#### Introduction

In this chapter the results of the thin-walled hollow cylinder testing program will be presented. A photograph of the testing apparatus is shown in Figure 6-1. A summary of the twenty-one tests which make up this testing series is presented in Table 6-1.

As with the low strain triaxial resonant column testing program, the data is presented in such a manner that changes in the dynamic compression modulus due to vertical strain amplitude and due to combined loading interaction may be evaluated separately and independently of one another. Additionally, the vertical compression stress-strain response under conditions of very high shear loading will be presented and discussed.

#### Vertical Loading Alone

In Figure 6-2 the dynamic compression modulus is shown as a function of the vertical normal strain for a value of the Poisson's ratio of 0.34. The curves shown are "virgin" curves, with no simultaneously applied shear loading. The value selected for the Poisson's ratio is near the center of the normal range of from approximately 0.2 to 0.5. Variation of the Poisson's ratio within that range will have little effect upon these curves, since the calculated value of the compression modulus is not very sensitive to the Poisson's ratio.

Superimposed upon Figure 6-2 are contours of equal values of cyclic vertical normal stress,  $\Delta\sigma_z$ . The range of  $\Delta\sigma_z$  in this testing series was

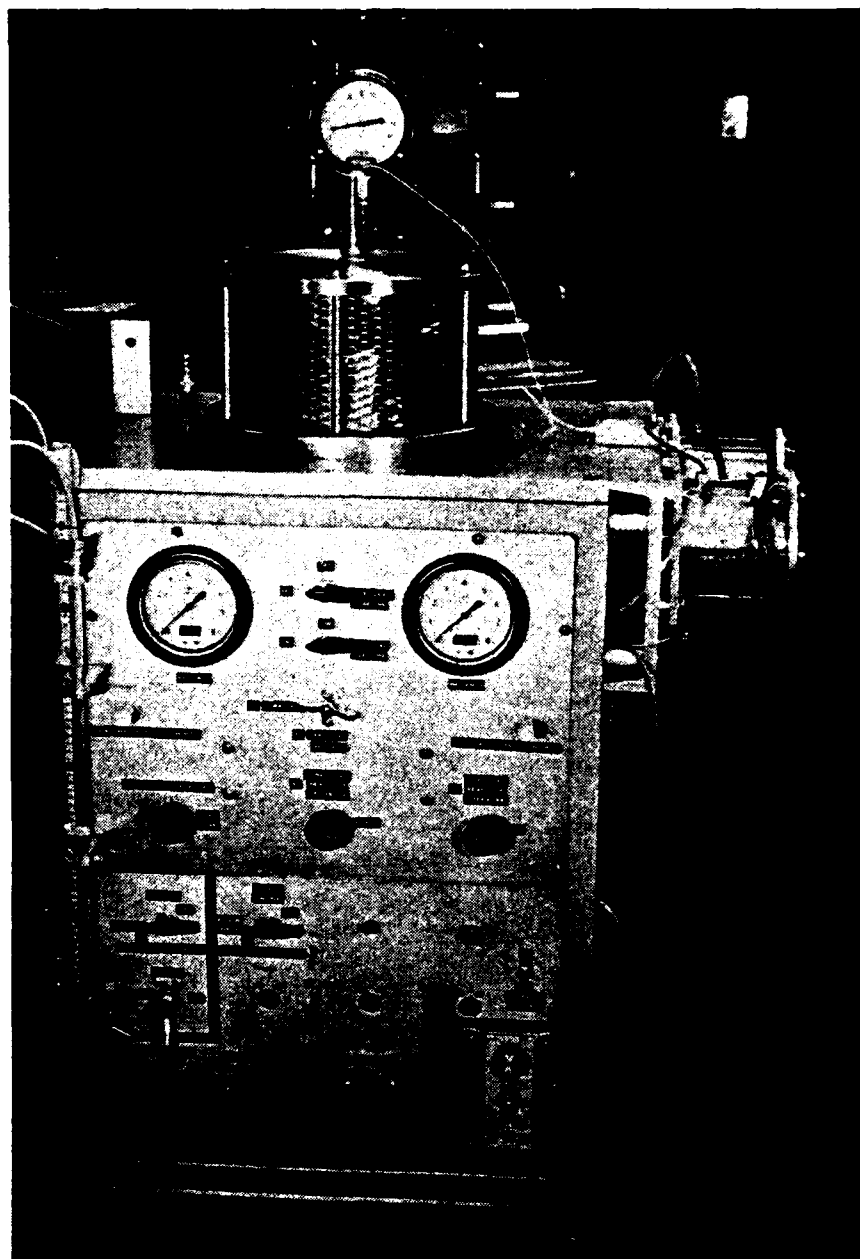


FIGURE 6-1 HOLLOW CYLINDER TESTING APPARATUS  
AND CONTROL PANEL

TABLE 6-1

## Summary of Hollow Cylinder Tests

TEST NO.	$\gamma_d$ (g/cc)	$D_R$ (%)	$\sigma_{3c}$ (KSC)	MODE V-VERTICAL C-COMBINED
B10-1	1.68	91.8	0.5	C
B11-1	1.67	88.8	0.5	C
B12-2	1.69	94.9	2.0	C
B13-3	1.69	94.9	3.5	C
AB15-2	1.71	100.0	2.0	V & C
B16-2	1.69	94.9	2.0	C
B17-3	1.69	94.9	3.5	C
B18-1	1.70	97.9	0.5	C
B19-2	1.68	91.8	2.0	C
B20-3	1.67	88.8	3.5	C
B21-1	1.67	88.8	0.5	C
B22L-1	1.58	59.3	0.5	C
B23L-2	1.58	59.3	2.0	C
B24L-3	1.55	48.7	3.5	C
A25L-1	1.59	62.7	0.5	V
A26L-2	1.56	52.3	2.0	V
A27L-3	1.55	48.7	3.5	V
A28-3	1.69	94.9	3.5	V
B29-3	1.68	91.8	3.5	C
B30L-3	1.58	59.3	3.5	C
B31-1	1.68	91.8	0.5	C

$\gamma_d$  = dry density of soil

$D_R$  = relative density

$\sigma_{3c}$  = lateral confining pressure

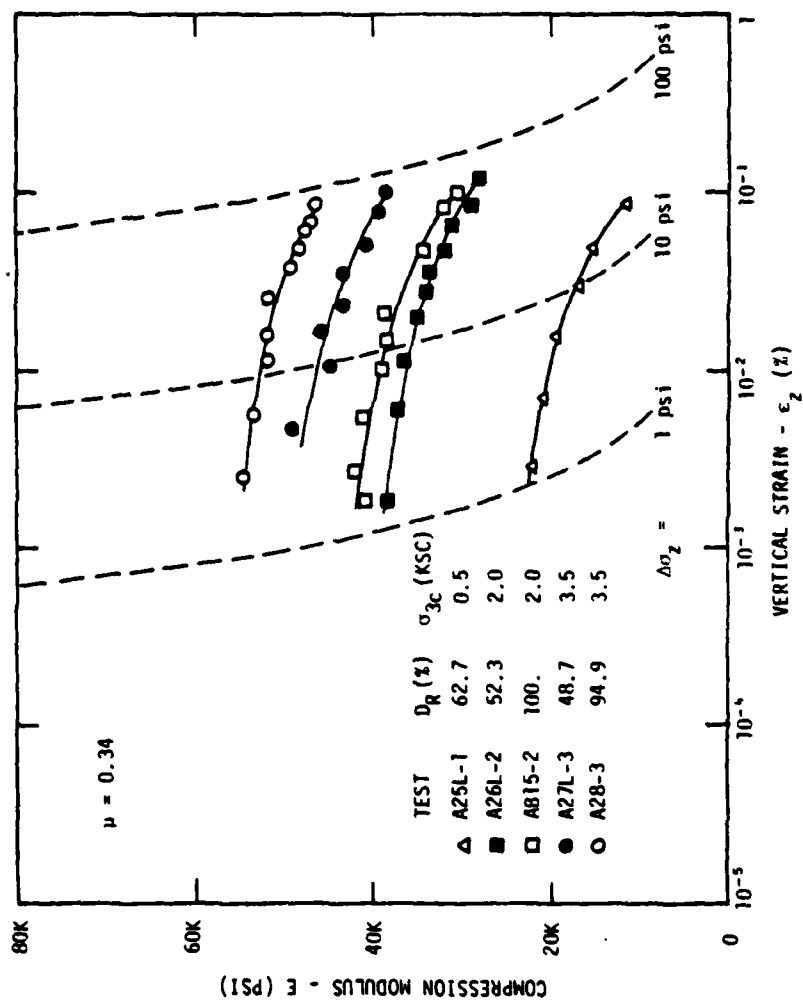


FIGURE 6-2 DEGRADATION OF COMPRESSION MODULUS WITH VERTICAL STRAIN FOR SEVERAL TESTS UNDER CONDITIONS OF VERTICAL LOADING ALONE

from approximately 1 psi to 100 psi. For low confining pressure tests particularly, these values of  $\Delta\sigma_z$  led to significant principal stress ratios during cyclic loading. These principal stress ratios are summarized in Table 6-2. Not all of the values in Table 6-2 were actually reached in the test specimens. Figure 6-2 shows the combinations of  $\sigma_{3c}$  and  $\Delta\sigma_z$  actually attained during testing.

Vertical strain amplitudes achieved during this testing series were in the range of from approximately  $2 \times 10^{-3}\%$  to  $2 \times 10^{-1}\%$ .

The compression moduli shown in Figure 6-2 were normalized against the moduli at a vertical normal strain of  $5 \times 10^{-3}\%$ , as shown in Figure 6-3. As with the low strain resonant column testing program, the variation of relative compression modulus with strain amplitude appears to be primarily a function of the confining pressure, with a lower confining pressure corresponding to a greater rate of degradation.

#### Combined Loading

As with the low strain resonant column testing program, cyclic loading tests under conditions of simultaneous vertical and torsional loading were performed on a number of hollow cylinder samples. The specimens tested represented two different densities and three different confining pressures.

#### Strain Measurements

In this testing series the value of the relative rotational displacement of the top of the specimen (and thus the shear strain) was measured directly with an LVDT mounted on the side of the specimen. Although the

TABLE 6-2

MAXIMUM PRINCIPAL STRESS RATIOS DURING CYCLIC LOADING -  $(\sigma_1/\sigma_3)_{\max.}$

$\Delta\sigma_z$ (psi) \ $\sigma_{3c}$ (KSC)	0.5	2.0	3.5
0. (Consolidation)	1.85	1.85	1.85
20.	3.21	2.19	2.04
40.	4.57	2.53	2.24
60.	5.93	2.87	2.43
80.	7.29	3.21	2.63
100.	8.65	3.55	2.82

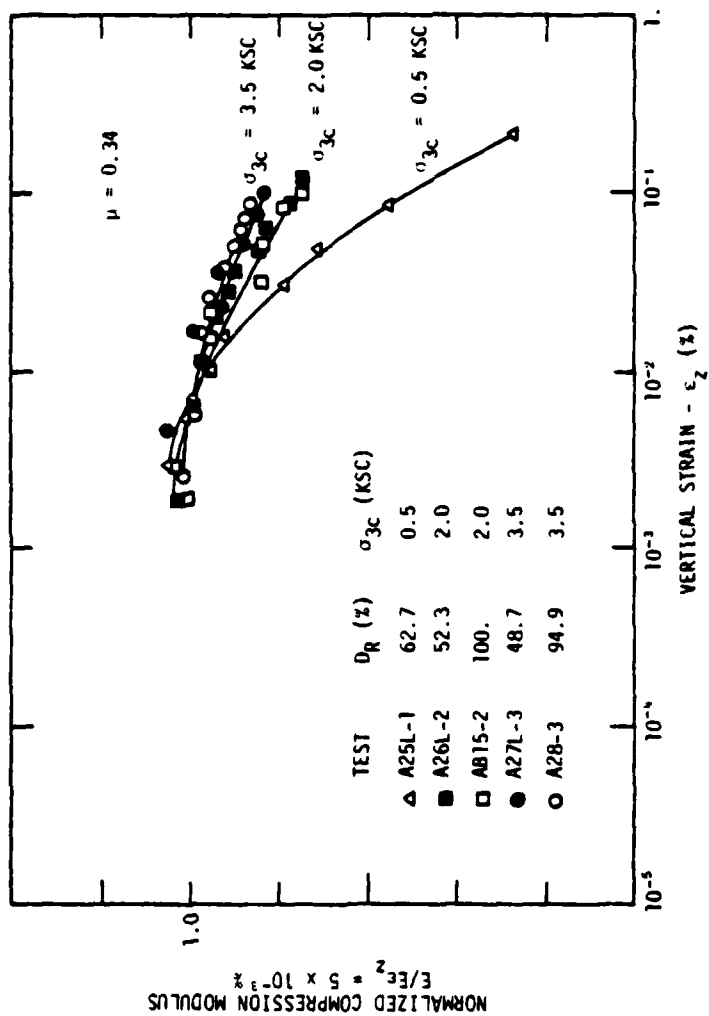


FIGURE 6-3 DEGRADATION OF NORMALIZED COMPRESSION MODULUS WITH VERTICAL STRAIN FOR SEVERAL TESTS UNDER CONDITIONS OF VERTICAL LOADING ALONE

relatively larger measurements were consistent, the relatively smaller shear strain measurements were somewhat erratic. This was found to be primarily due to the LVDT core friction, which was significant at very small displacements, causing the LVDT to "hang-up" and under-measure the true shear strain. This difficulty was not overcome by great care in setting up the LVDT to avoid core contact, because consolidation and dynamic straining quickly re-created the core friction problem.

The problem was further complicated by the fact that the calculated shear modulus values were extremely sensitive to the very small shear strains. A relatively minor variation in the measured shear strain could result in a large error in the calculated modulus, and would result in unreasonable predicted values for Poisson's ratio.

It was concluded that a more accurate estimate of the actual shear strain could be obtained using the measured stresses and vertical strain together with the elastic theory formulations developed in Chapters 2, 3, and 4.

The measured values of strain and stress provided a redundancy of data from which a Poisson's ratio could be computed. Because the shear strain is relatively insensitive to the value of the Poisson's ratio, the computed values of the Poisson's ratio are extremely sensitive to small errors in shear strain. By back-calculating values of the shear strain for various values of Poisson's ratio, a much more accurate evaluation of the shear strain may be made.

The measured values of the vertical and shear stress were obtained with calibrated differential pressure transducers attached to the loading cylinders, and are relatively accurate and consistent in determining those stress values. The vertical strain was measured with a proximeter

device, which accurately measures displacements without physical contact, avoiding the core friction problem. These data measurement devices are discussed in more detail in Appendix A-2.

When values of the shear strain were calculated from the measured stresses and vertical strain values, and for various values of Poisson's ratio, as described above, they were found to be in the same relative range as the measured values, but were generally slightly larger.

In the example of test results, presented in Appendices B-4 through B-6, both the measured and the calculated values of the shear strain are presented. The calculated values of the shear strain were used in developing the values of the shear modulus,  $G$ , and the strain ratios and octahedral shearing strains used in this chapter. The complete test results are reported elsewhere (Griffin, 1980).

#### Strain Ratio Effects

Normalized plots showing the degradation from the "virgin" modulus as a function of the ratio of shear strain to vertical normal strain were prepared for three different confining pressures. The resulting plots are shown in Figures 6-4, 6-5, and 6-6 for lateral confining pressures of 0.5, 2.0, and 3.5 KSC, respectively.

The plotted modulus reduction curves shown in Figures 6-4 through 6-6 are combined and summarized in Figure 6-7 for two values of vertical normal strain:  $10^{-1}\%$  and  $10^{-2}\%$ .

The effect of varying the Poisson's ratio is to vary the strain ratio slightly. This effect is shown in Figure 6-8.

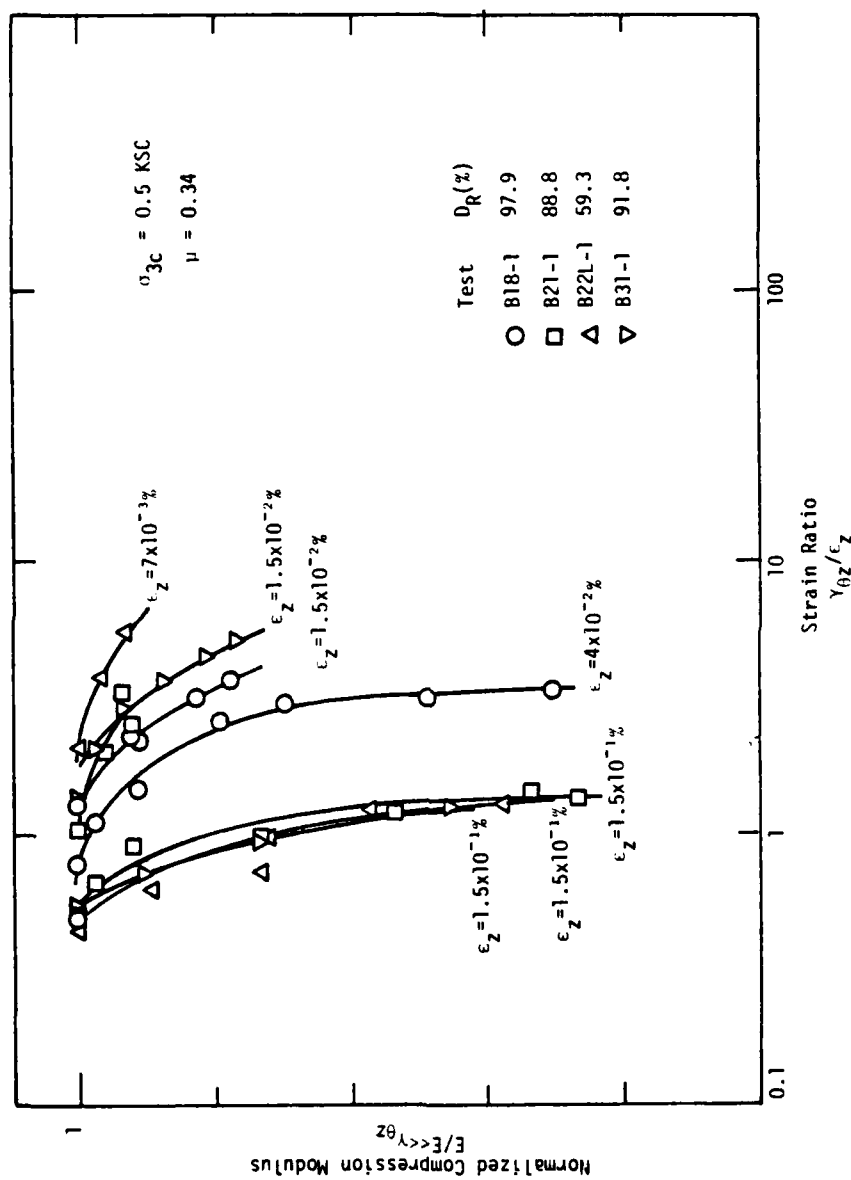


FIGURE 6-4 DEGRADATION OF NORMALIZED COMPRESSION MODULUS WITH RATIO OF SHEAR STRAIN TO VERTICAL STRAIN AT  $\sigma_{3c} = 0.5 \text{ KSC}$  FOR SEVERAL COMBINED LOADING TESTS

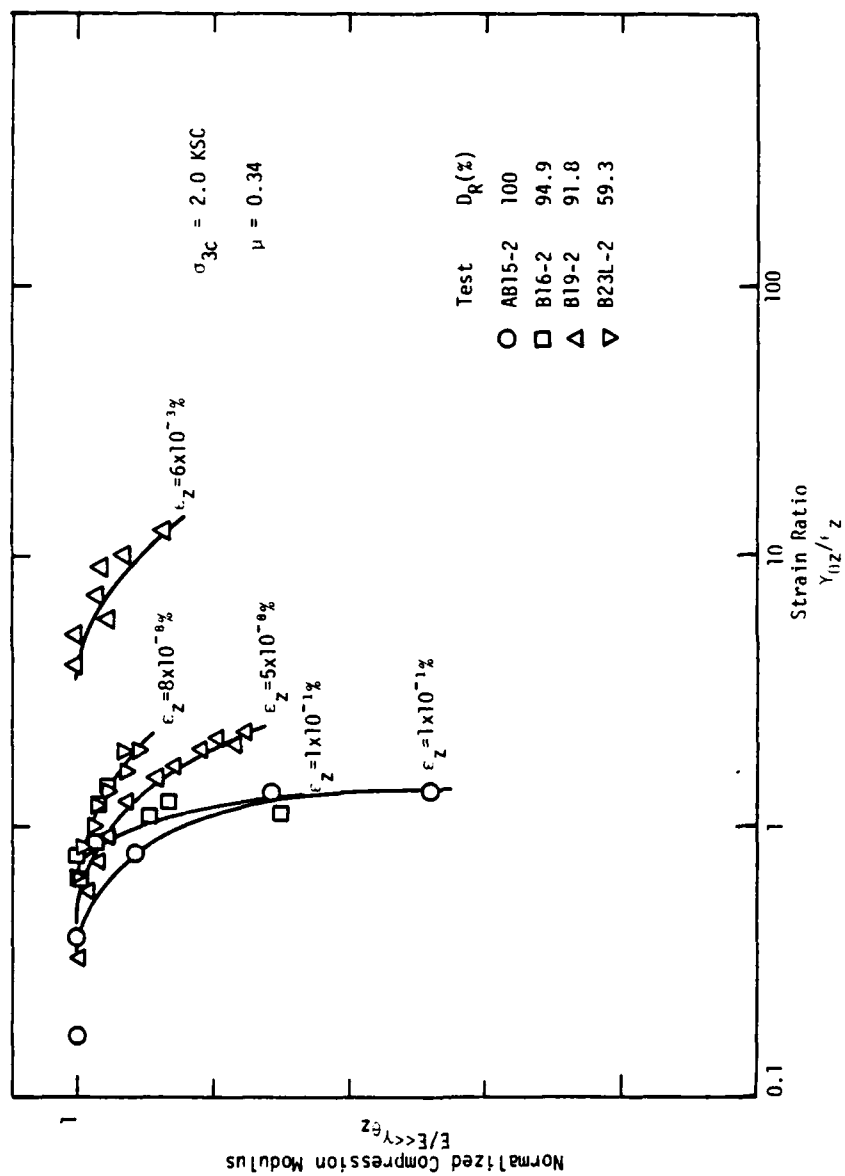


FIGURE 6-5 DEGRADATION OF NORMALIZED COMPRESSION MODULUS WITH RATIO OF SHEAR STRAIN TO VERTICAL STRAIN AT  $\sigma_{3c} = 2.0 \text{ KSC}$  FOR SEVERAL COMBINED LOADING TESTS

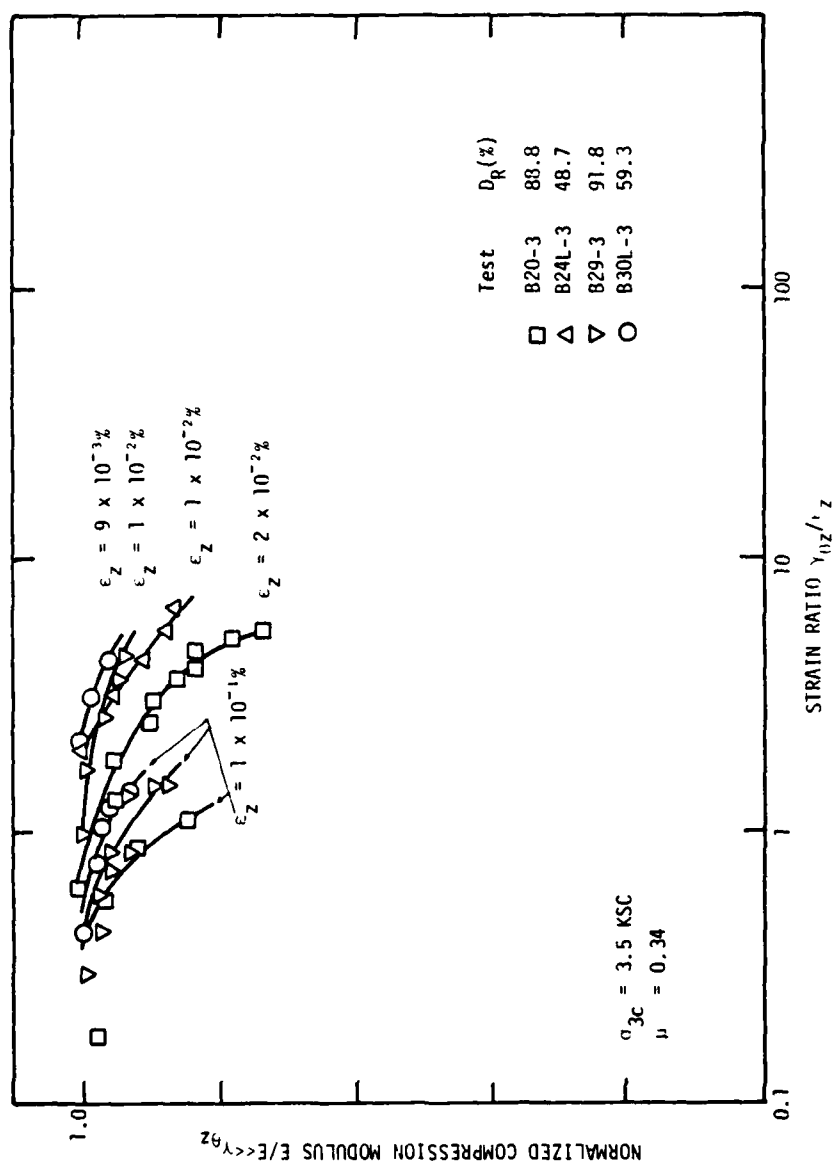


FIGURE 6-6 DEGRADATION OF NORMALIZED COMPRESSION MODULUS WITH RATIO OF SHEAR STRAIN TO VERTICAL STRAIN AT  $\sigma_{3c} = 3.5 \text{ KSC}$  FOR SEVERAL COMBINED LOADING TESTS

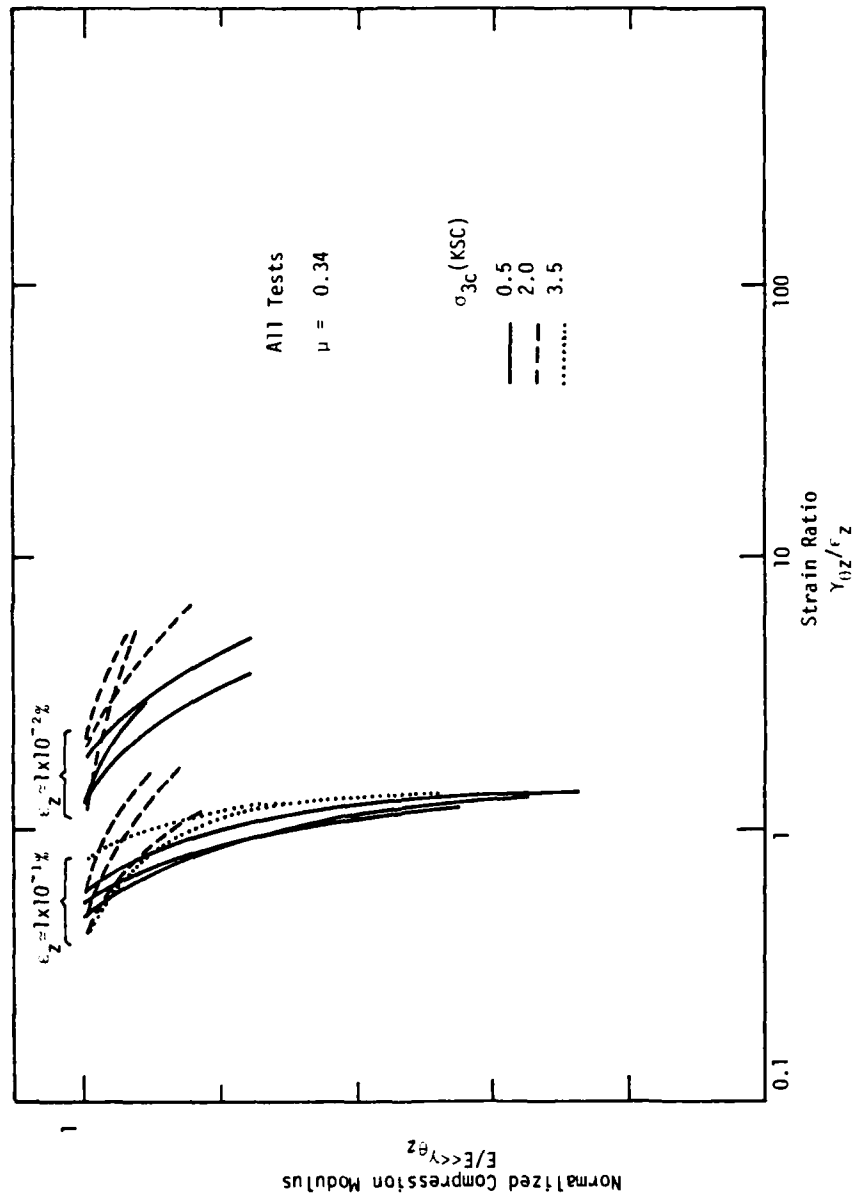


FIGURE 6-7 SUMMARY OF DEGRADATION OF NORMALIZED COMPRESSION MODULUS WITH RATIO OF SHEAR STRAIN TO VERTICAL STRAIN FOR ALL COMBINED LOADING TESTS

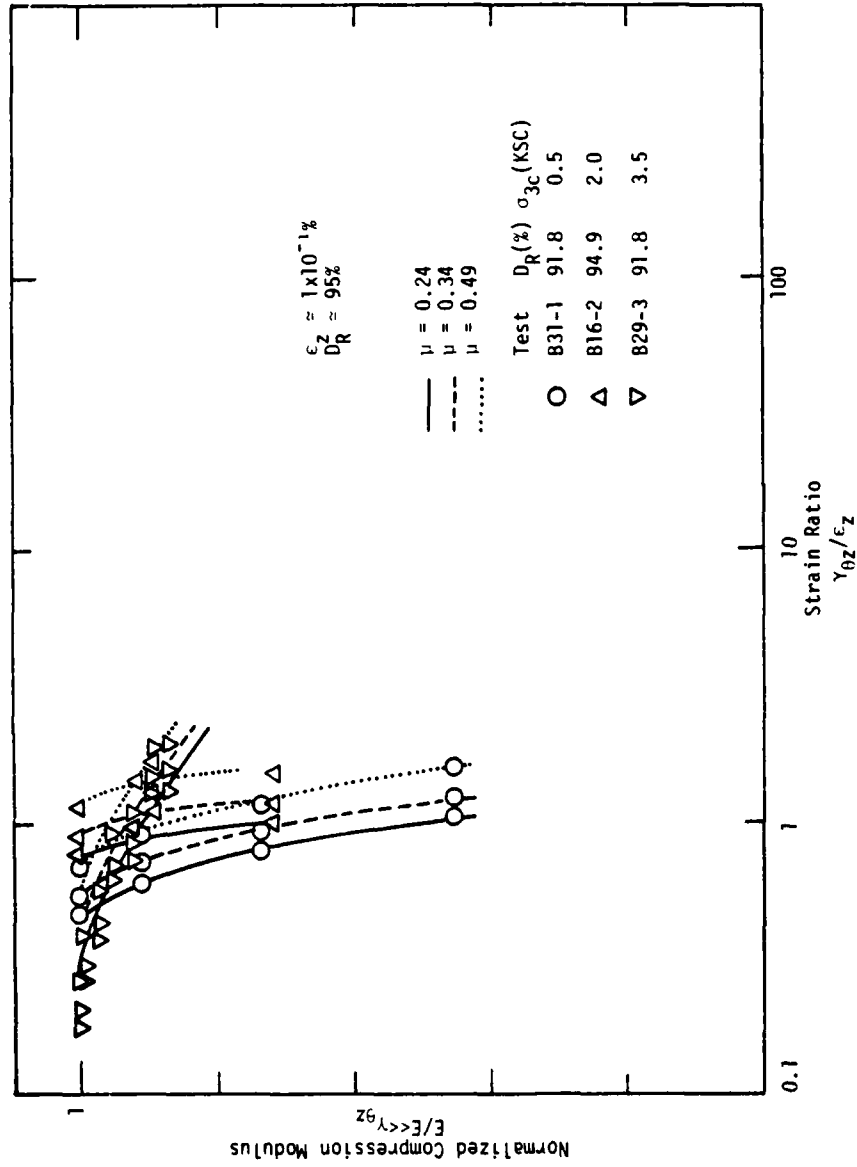


FIGURE 6-8 EFFECT OF POISSON'S RATIO,  $\mu$ , ON THE DEGRADATION OF THE NORMALIZED COMPRESSION MODULUS WITH THE RATIO OF SHEAR STRAIN TO VERTICAL STRAIN FOR SEVERAL TESTS

## Octahedral Shearing Strain Effects

As with the presentation in Chapter 5, the usefulness of the octahedral shearing strain in predicting compression-shear interaction was evaluated.

In Figure 6-9, the "virgin" normalized compression moduli curves are shown plotted against the octahedral shearing strain. For the data in these curves the principal strain directions are coincident with the vertical, radial, and tangential directions, and do not rotate during loading.

In the combined loading tests, the principal strain axes in the  $\theta z$  "plane" rotate continuously during loading, and the octahedral shearing strain arises from the combination of normal and shear strains in the vertical, radial, and tangential directions. The variation of the normalized compression modulus with octahedral shearing strain under combined loading conditions for a vertical normal strain amplitude,  $\epsilon_z$ , of 0.1%, are presented in Figures 6-10 through 6-12 for lateral confining pressures of 0.5, 2.0, and 3.5 KSC, respectively. These data are combined for comparison purposes in Figure 6-13.

It is apparent from the data presented in Figure 6-12 that the modulus degradation curve for a vertical normal strain of 0.1% is influenced primarily by the octahedral shearing strain amplitude, and is essentially independent of the confining pressure. It is therefore possible to draw one best-fit curve through the data as shown in Figure 6-13.

Similarly, a best-fit curve was drawn through the data for a vertical normal strain of approximately  $2 \times 10^{-2}\%$  as shown in Figure 6-14.

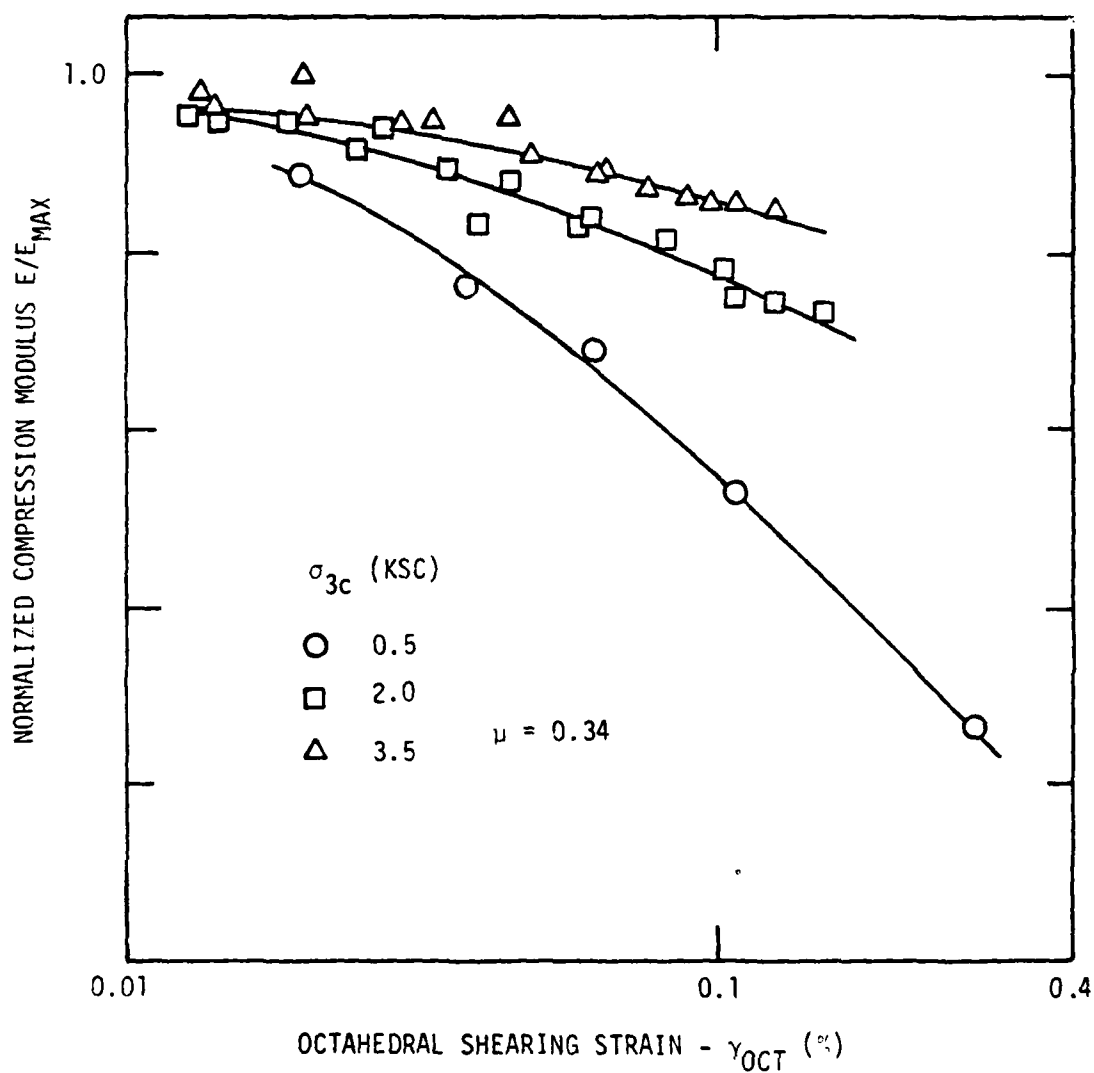


FIGURE 6-9 DEGRADATION OF NORMALIZED COMPRESSION MODULUS WITH OCTAHEDRAL SHEARING STRAIN FOR CONDITION OF VERTICAL LOADING ALONE

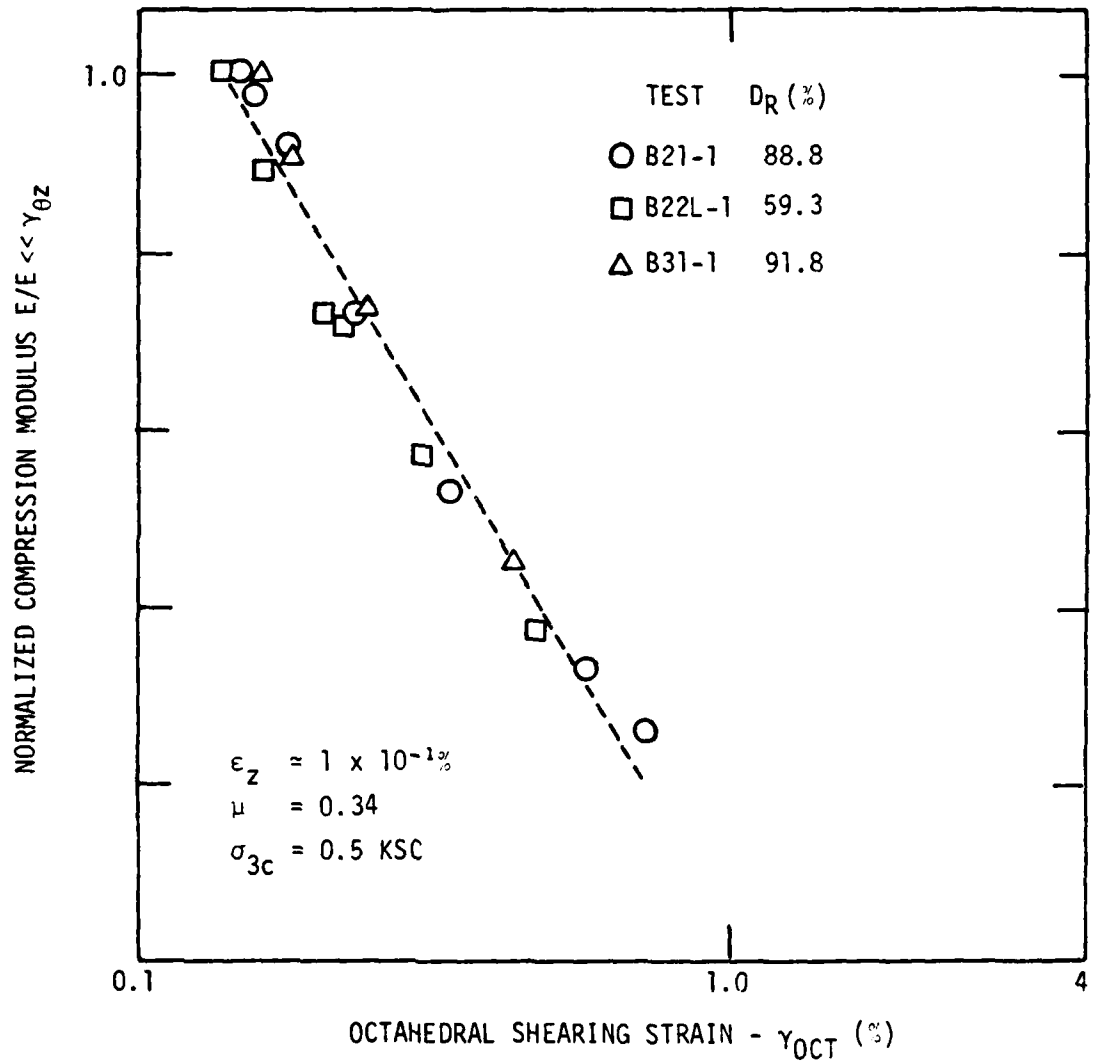


FIGURE 6-10 DEGRADATION OF NORMALIZED COMPRESSION MODULUS WITH OCTAHEDRAL SHEARING STRAIN AT  $\sigma_{3c} = 0.5 \text{ KSC}$  FOR SEVERAL COMBINED LOADING TESTS WITH A CONSTANT VERTICAL STRAIN OF  $10^{-1}\%$

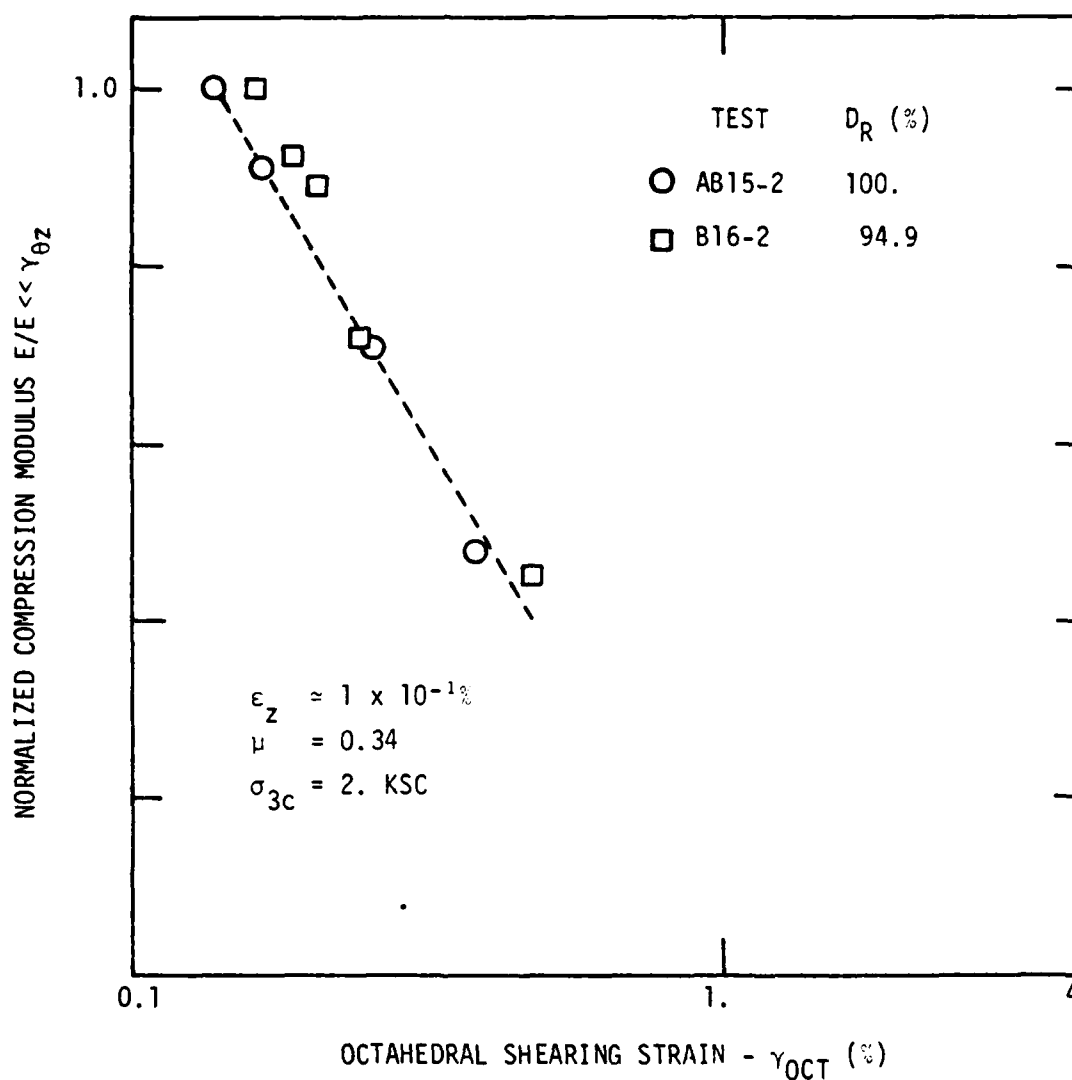


FIGURE 6-11 DEGRADATION OF NORMALIZED COMPRESSION MODULUS WITH OCTAHEDRAL SHEARING STRAIN AT  $\sigma_{3c} = 2.0$  KSC FOR SEVERAL COMBINED LOADING TESTS WITH A CONSTANT VERTICAL STRAIN OF  $10^{-1}\%$

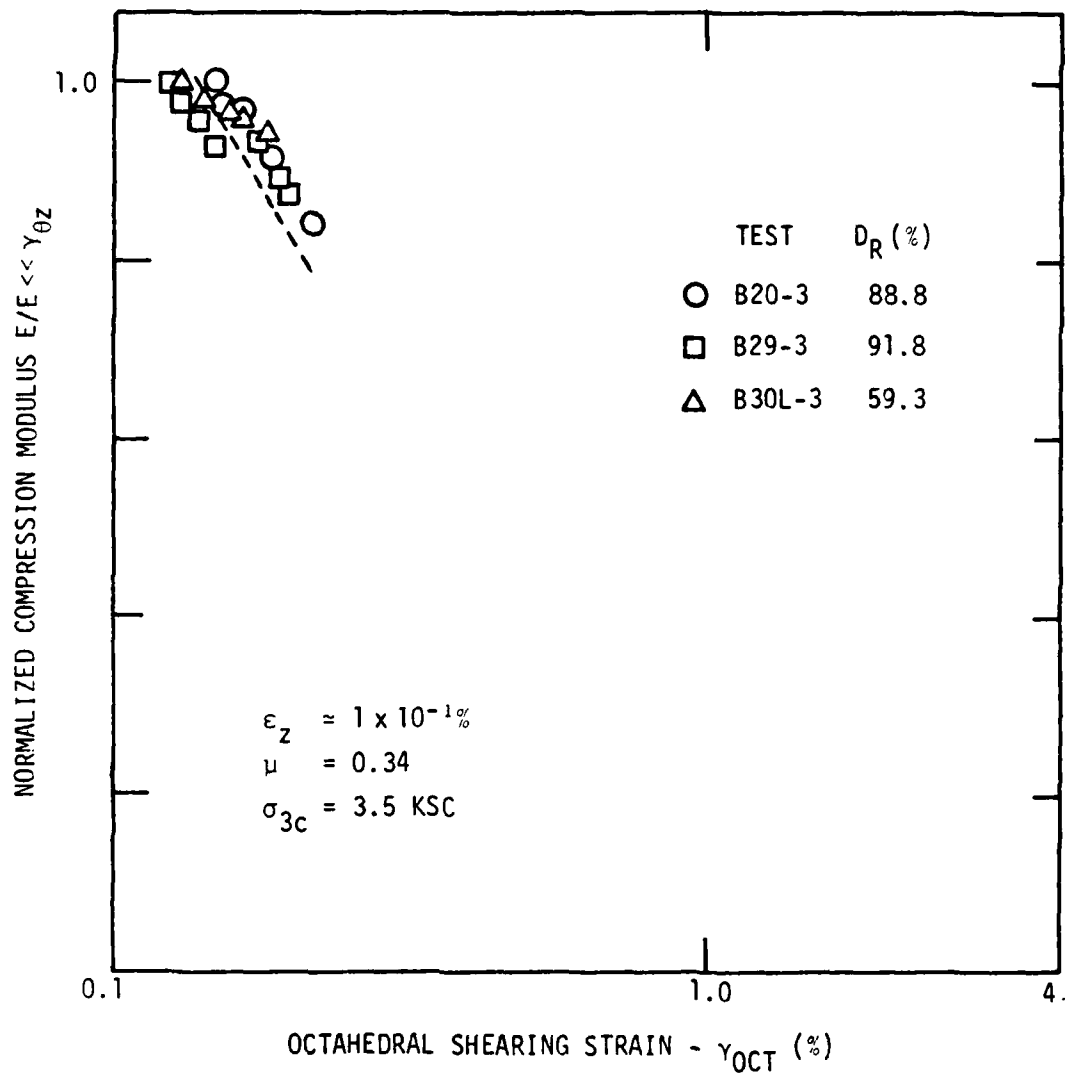


FIGURE 6-12 DEGRADATION OF NORMALIZED COMPRESSION MODULUS WITH OCTAHEDRAL SHEARING STRAIN AT  $\sigma_{3c} = 3.5 \text{ KSC}$  FOR SEVERAL COMBINED LOADING TESTS WITH A CONSTANT VERTICAL STRAIN OF  $10^{-1}\%$

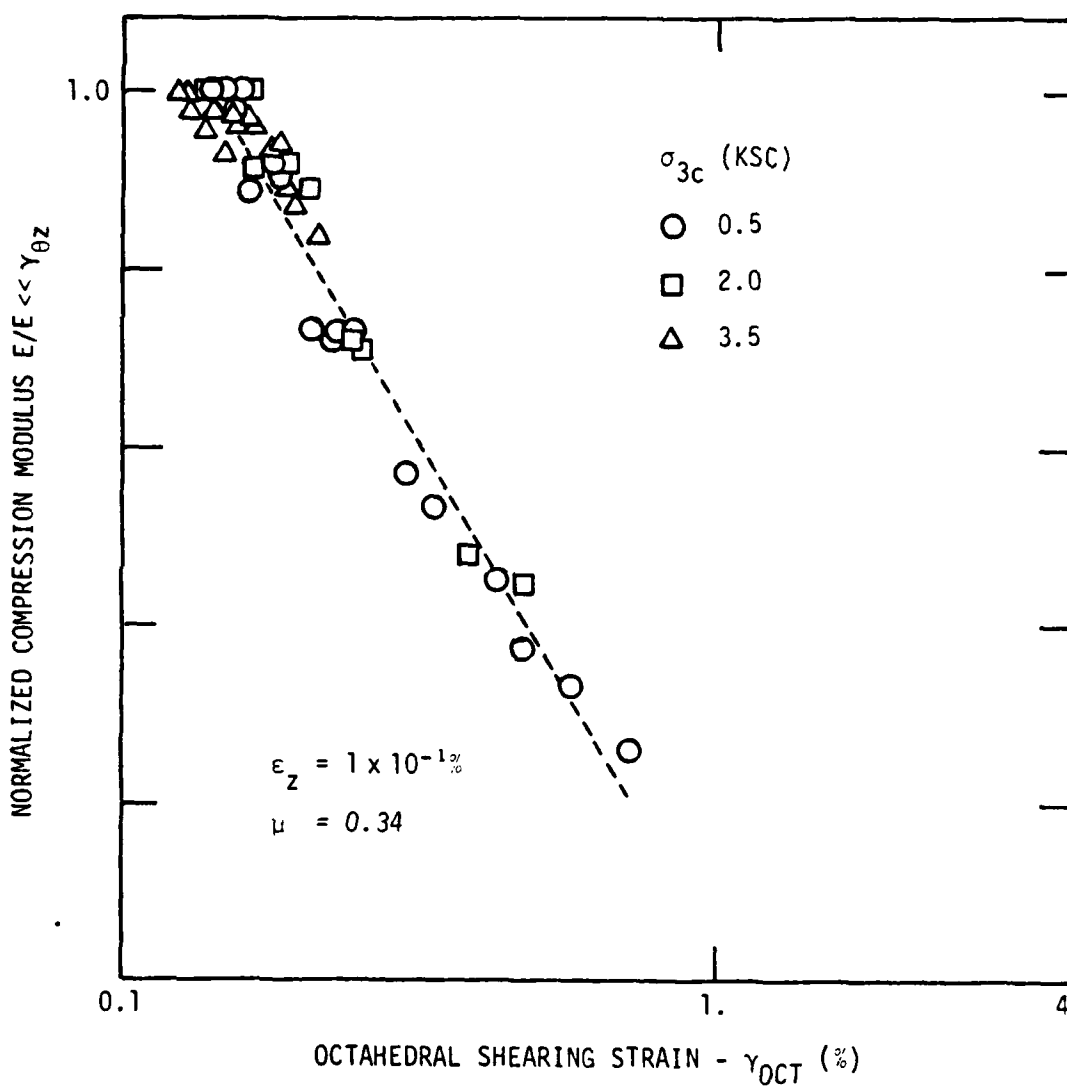


FIGURE 6-13 SUMMARY OF DEGRADATION OF NORMALIZED COMPRESSION MODULUS WITH OCTAHEDRAL SHEARING STRAIN FOR ALL COMBINED LOADING TESTS AT A CONSTANT VERTICAL STRAIN OF  $10^{-1\%}$

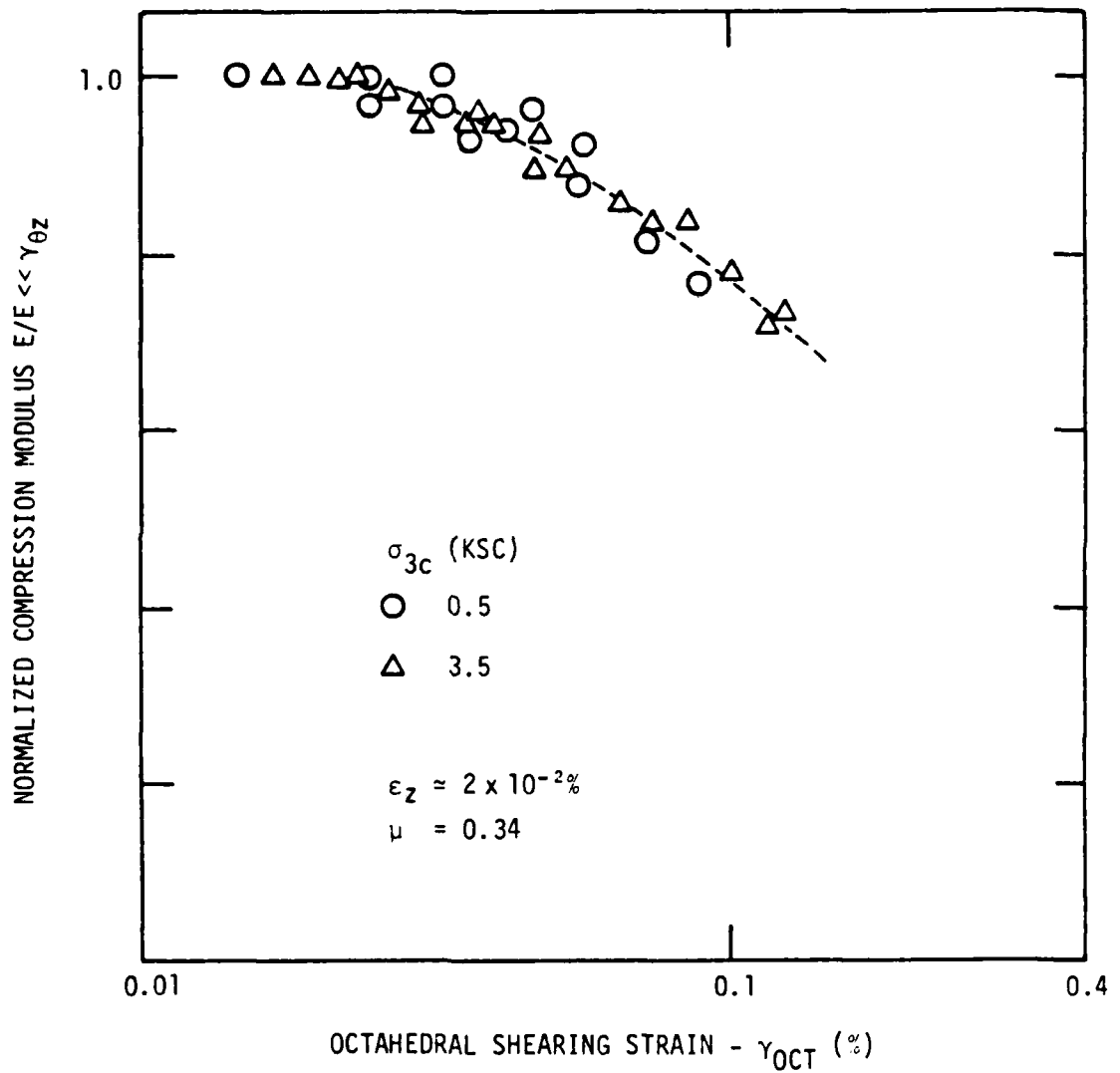


FIGURE 6-14 SUMMARY OF DEGRADATION OF NORMALIZED COMPRESSION MODULUS WITH OCTAHEDRAL SHEARING STRAIN FOR ALL COMBINED LOADING TESTS AT A CONSTANT VERTICAL STRAIN OF  $2 \times 10^{-2}\%$

These relative moduli-octahedral shearing strain curves were then combined with the virgin curves presented in Figure 6-9 to obtain the curves presented in Figures 6-15 through 6-17 using the procedure described for Figures 5-16 through 5-18. These plots were then combined for comparison purposes in Figure 6-18.

Unlike the results of the low strain resonant column presentation in Figures 5-16, 5-17, and 5-18, the curves summarized in Figure 6-18 show a distinct variation depending on how  $\gamma_{OCT}$  was developed; e.i., from vertical compression or from shear straining. Of course part of the variation shown in Figure 6-18 is due to variations in confining pressure, which was illustrated in Figures 6-15 through 6-17. For low confining pressures, the modulus appears to degrade more rapidly as a result of dynamic normal vertical straining than shear straining. For higher confining pressures, the reverse appears true. Superimposed upon Figure 6-18 is an interpolated curve where it appears that the degradation of modulus is independent of the source of  $\gamma_{OCT}$ . This curve has been labeled the "no interaction line," and appears at a lateral confining pressure of approximately 1.0 KSC.

To further summarize the results of this testing series, a set of best-fit curves have been presented in Figure 6-19 to show the degradation of normalized compression modulus with  $\gamma_{OCT}$  irrespective of the strain path. It is noted that the data varies from these curves to a greater degree than the comparable curves in Figure 5-19.

#### High Shear Strain Effects

Several combined loading tests were performed under conditions of

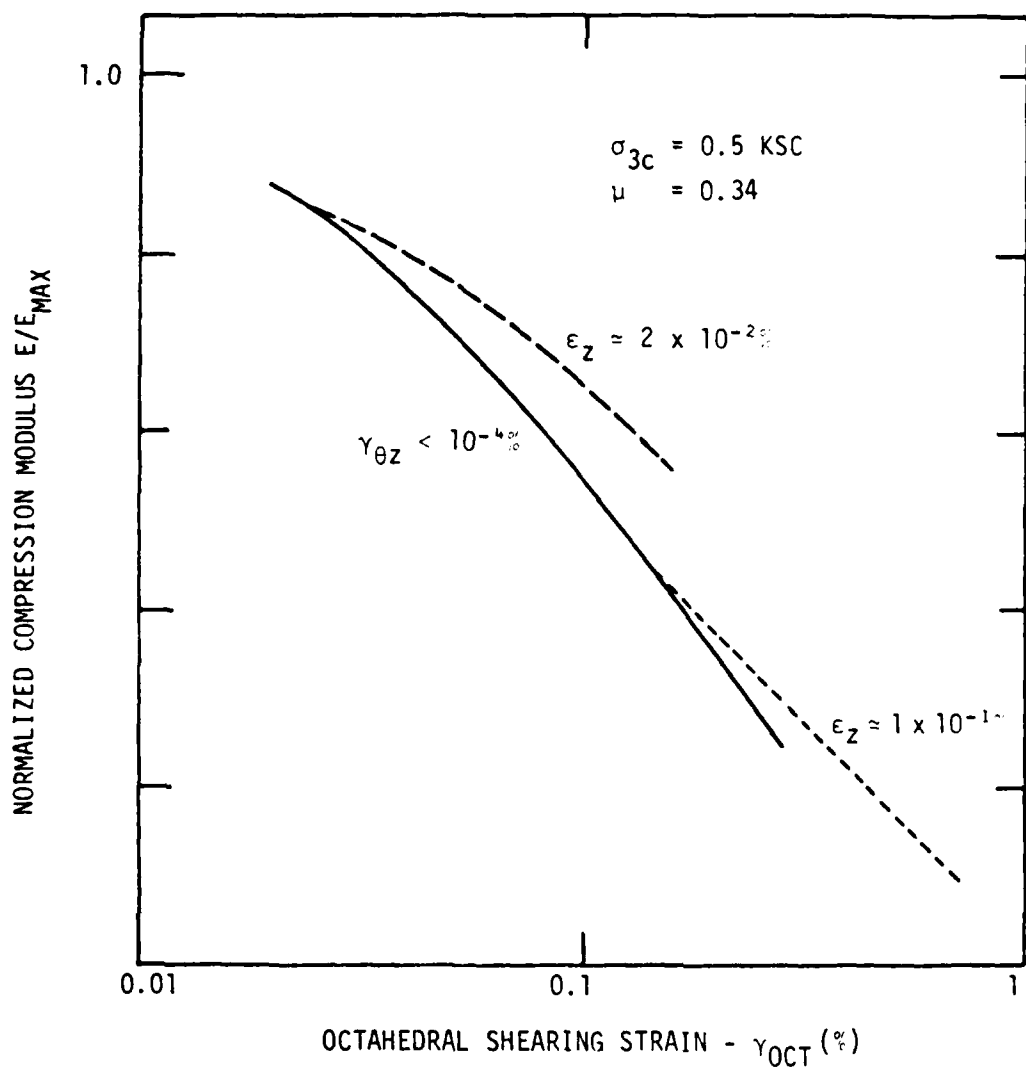


FIGURE 6-15 DEGRADATION OF NORMALIZED COMPRESSION MODULUS WITH OCTAHEDRAL SHEARING STRAIN AT  $\sigma_{3c} = 0.5 \text{ KSC}$  FOR BOTH VERTICAL AND COMBINED LOADING TESTS

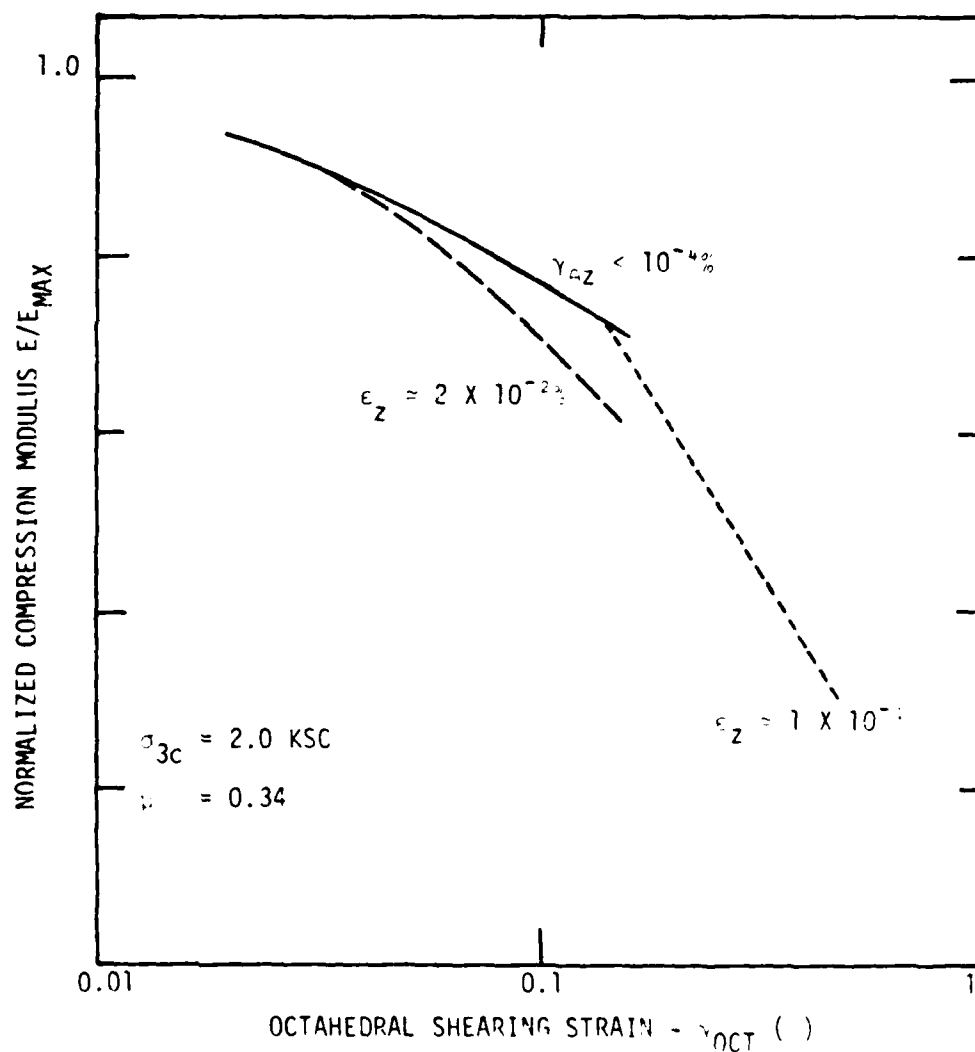


FIGURE 6-16 DEGRADATION OF NORMALIZED COMPRESSION MODULUS WITH OCTAHEDRAL SHEARING STRAIN AT  $\sigma_{3c} = 2.0 \text{ KSC}$  FOR BOTH VERTICAL AND COMBINED LOADING TESTS

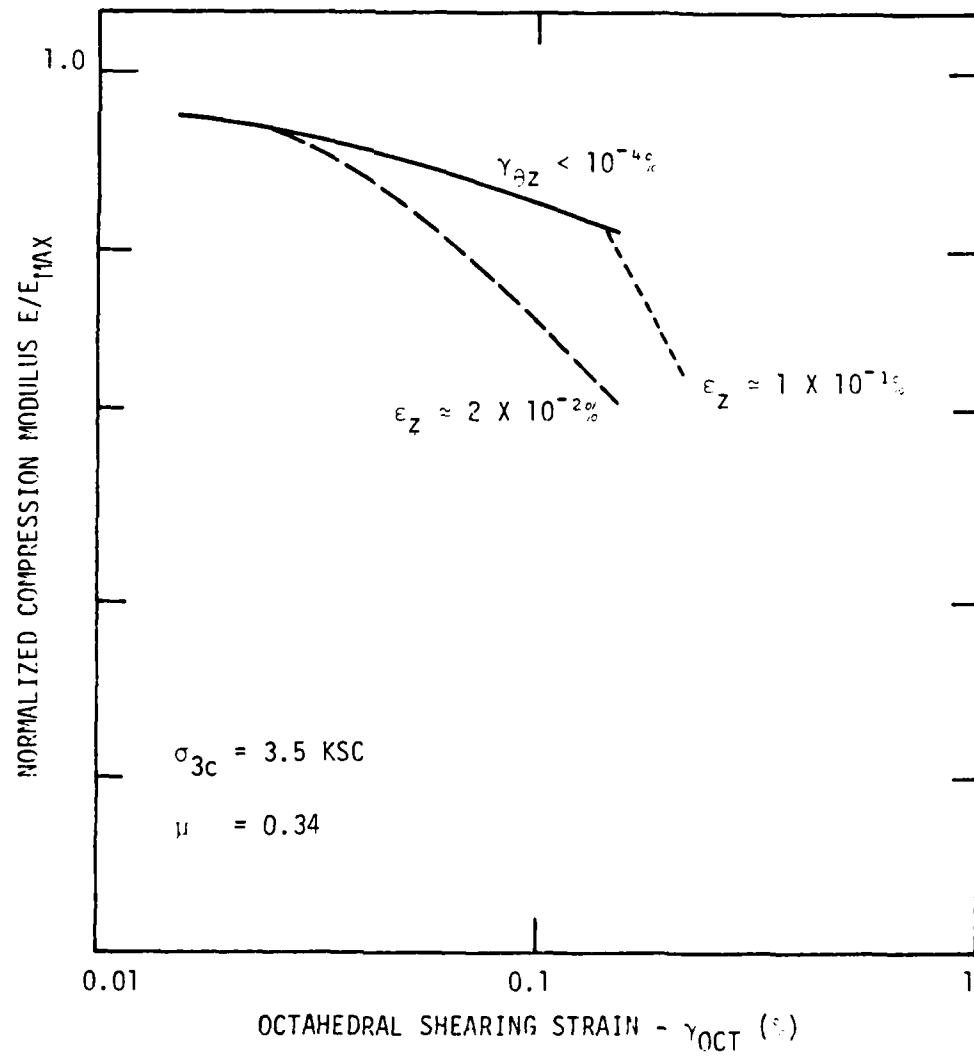


FIGURE 6-17 DEGRADATION OF NORMALIZED COMPRESSION MODULUS WITH OCTAHEDRAL SHEARING STRAIN AT  $\sigma_{3c} = 3.5 \text{ KSC}$  FOR BOTH VERTICAL AND COMBINED LOADING TESTS

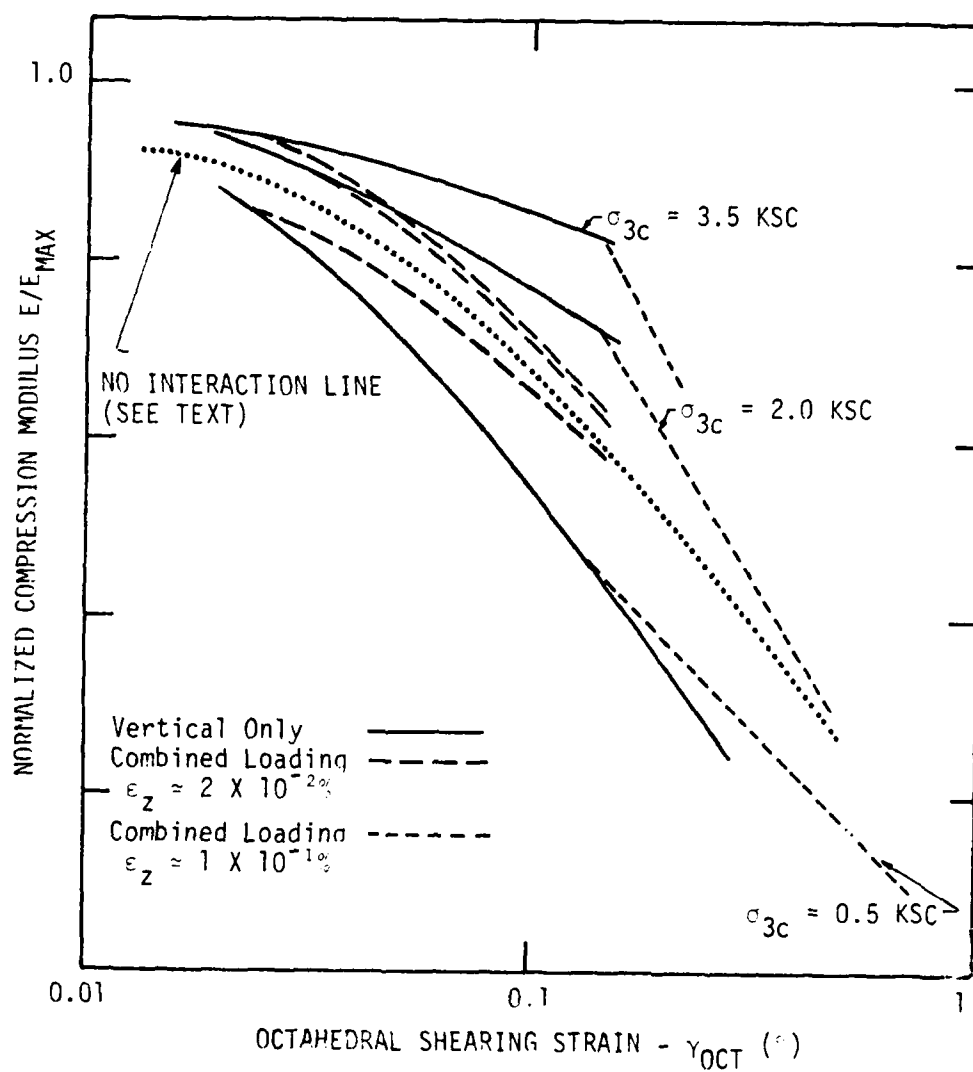


FIGURE 6-18 DEGRADATION OF NORMALIZED COMPRESSION MODULUS WITH OCTAHEDRAL SHEARING STRAIN FOR ALL VERTICAL AND COMBINED LOADING TESTS

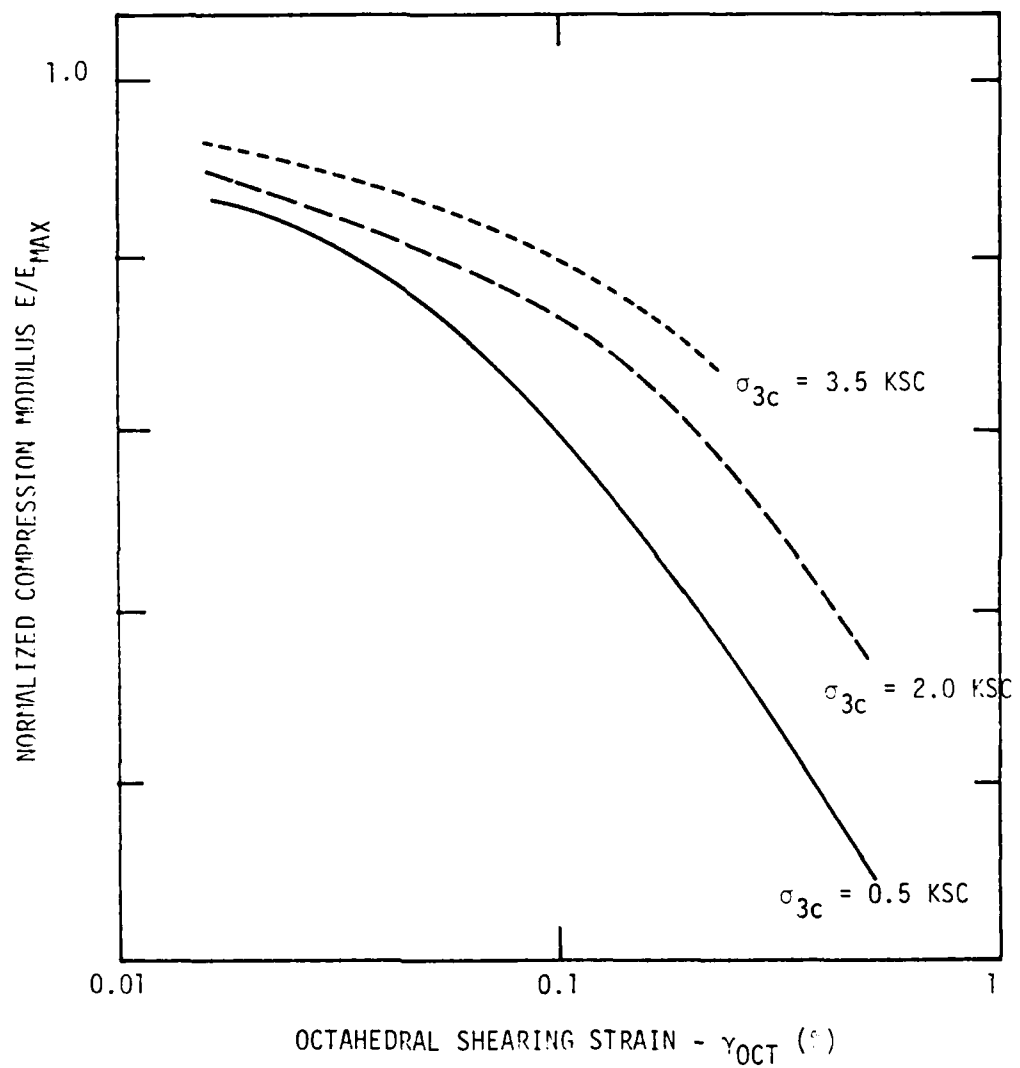


FIGURE 6-19 SUMMARY OF DEGRADATION OF NORMALIZED COMPRESSION MODULUS WITH OCTAHEDRAL SHEARING STRAIN

relatively very high shear strains, but it was very difficult, if not impossible, to determine accurate modulus values from these test results because of the shape of the hysteretical stress-strain plots. Several typical plots are shown in Figure 6-20.

The odd shapes of these hysteretic stress-strain plots provide a clue to the behavior of soils under these loading conditions. It is noted, for example, that several plots closely approximate a "Figure-8" shape, having two distinct loops. A Lissajous-figure analysis of a standing "Figure-8" would indicate an out-of-phase relationship, with the vertical axis at half the frequency of the horizontal axis. In the case of the hollow cylinder specimens it indicates that the soil sample is displaying two cycles of vertical strain for each cycle of vertical stress.

If we consider the case of a uniformly graded granular material with a relatively dense packing, the matrix of grains might look something like that shown in Figure 6-21(a). As large shear stresses are applied to the material in one direction, one grain would tend to "ride-over" another, resulting in a vertical displacement. As the shear stress reversed its direction in time, the grain would return essentially to its original packing position, then "ride-up" again upon another grain as shown in Figure 6-21(b). This effect would evidence as two cycles of vertical straining for each shear stress cycle, as shown in Figure 6-21(c).

In the case of relatively very high shear stress loading, the vertical straining resulting from this process might be large in comparison with the vertical strain induced by vertical loading. If this is the case, then a "Figure-8" stress-strain plot will result, as was observed in several tests. The other observed odd-shaped plots may be explained

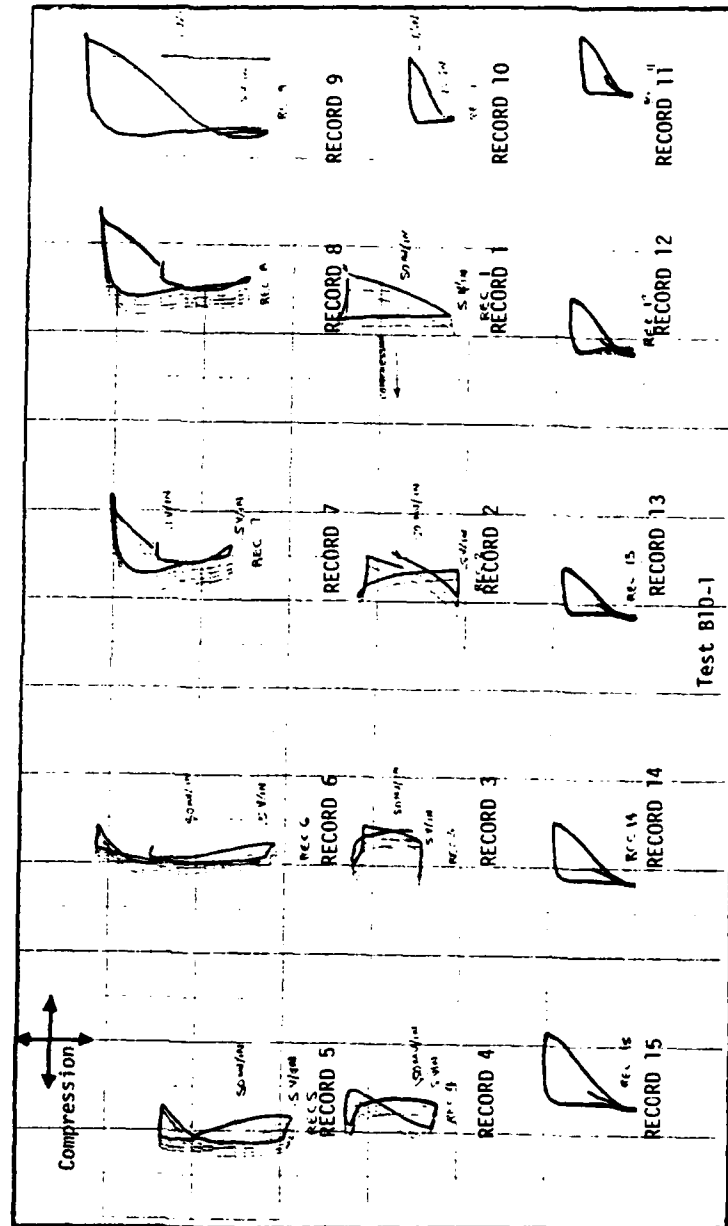


FIGURE 6-20 TYPICAL STRESS VS. STRAIN CURVES IN VERTICAL COMPRESSION UNDER CONDITION OF SIMULTANEOUS VERY HIGH RELATIVE SHEAR STRAIN

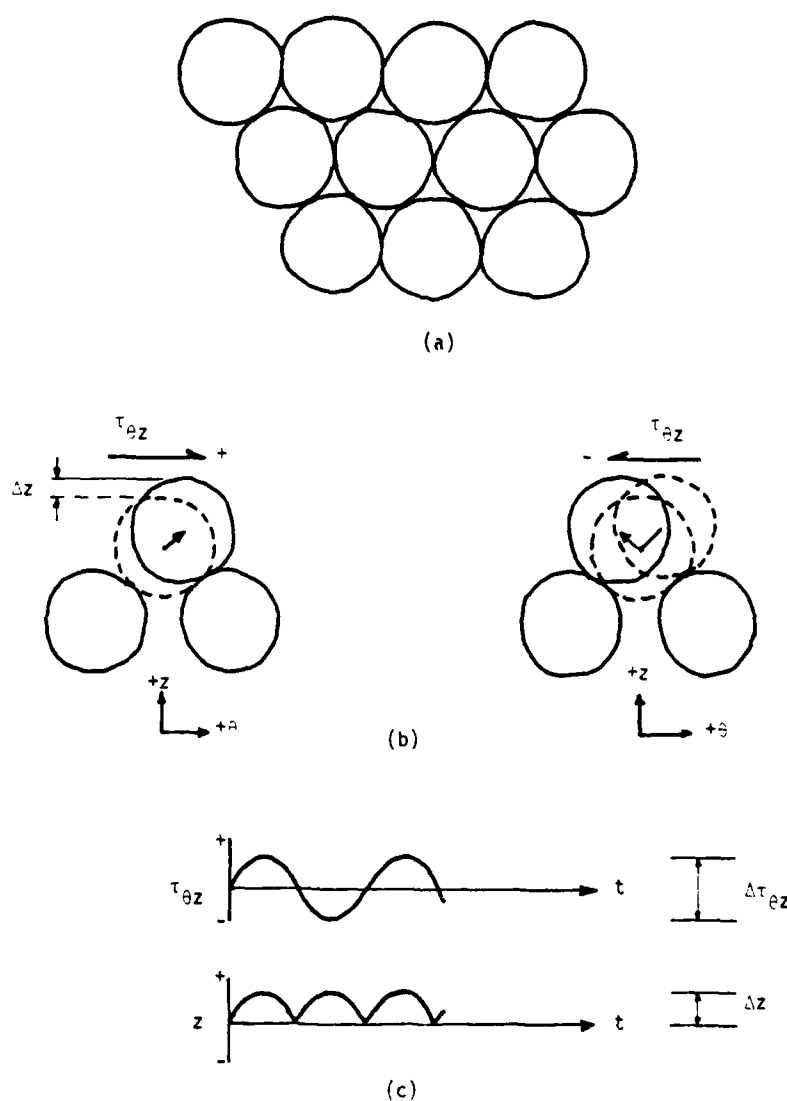


FIGURE 6-21 MATRIX OF A UNIFORMLY GRADED GRANULAR MATERIAL (a) AND DETAIL OF VERTICAL NORMAL STRAIN RESULTING FROM APPLICATION OF SHEAR STRESS (b) INCLUDING TIME HISTORIES (c)

by similar reasoning, considering phase effects and various combinations of vertical strain induced by vertical loading and shear loading.

It should be noted at this point that the consideration of a shear stress producing a normal strain is a coupling effect and is thus contrary to the assumptions of the applicability of elastic theory and Hooke's Law to this study.

This postulated theory of behavior is introduced only to aid in the understanding of soil behavior under conditions of very high shear straining, where inelastic, non-linear effects are apparent.

### Conclusions

As in Chapter 5, the test results from this testing series were presented in different ways. The degradation of modulus was presented both as a function of the strain ratio,  $\gamma_{\theta z}/\epsilon_z$ , and as a function of the octahedral shearing strain,  $\gamma_{OCT}$ . High shear strain effects were also explored.

### Strain Ratio Effects

The result of the first presentation, summarized in Figure 6-6, indicates that there exists a relatively consistent threshold strain ratio below which interaction effects are negligible. In the case of the high vertical normal strain tests, where  $\epsilon_z \approx 0.1\%$ , the threshold strain ratio fell to as low as 0.5, indicating that shear strains below 0.05% would have negligible effect in further degradation of modulus.

As with the low strain resonant column testing series, the normalized modulus curves were found to be relatively independent of relative density

within the range tested but were moderately dependent upon confining pressure. The magnitude of the interaction effects appears to be greater at lower confining pressures. This effect may be explained by the fact that the principal stress ratios,  $(\sigma_1/\sigma_3)_{MAX}$ , during cyclic loading increase very rapidly at lower confining pressures as shown in Table 6-2; so that the soil material more closely approaches a failure condition in these tests. If the incremental modulus degrades more rapidly with higher stress increments, which was observed in the hysteretic stress-strain plots for these tests, then greater straining (and greater interaction) is to be expected.

#### Octahedral Shearing Strain Effects

The second presentation was of the degradation of modulus with the octahedral shearing strain,  $\gamma_{OCT}$ , summarized in Figures 6-18 and 6-19. Unlike the low strain resonant column testing series results, there was some variation in the degradation curves depending upon how the  $\gamma_{OCT}$  was developed.

This variation is proportional to the interaction effect not accounted for by using  $\gamma_{OCT}$ . However, it was possible to select best-fit curves of normalized modulus vs.  $\gamma_{OCT}$  (Figure 6-19) for which the variations from the best-fit curves is quite acceptably small, except where  $\gamma_{OCT}$  becomes very large. When  $\gamma_{OCT}$  becomes very large and the confining pressure is relatively low, the assumptions on which the various derivations were made become invalid as discussed earlier.

Thus the accuracy of the normalized curves presented in Figure 6-19 decreases progressively with increasing  $\gamma_{OCT}$ , as can be judged by com-

paring them with the curves of Figure 6-18 from which they were derived.

The highest octahedral shearing strain used in this testing series was approximately 0.5%.

#### High Shear Strain Effects

An analysis of soil behavior involving the modeling of uniformly graded granular soil as a collection of discrete particles was presented to help explain the observed soil response to high cyclic shear strains imposed simultaneously with relatively low amplitude vertical loading. The test data presented in Figure 6-20 indicated inelastic, non-linear response of the soil material; specifically, significant vertical normal strains were observed to result from the application of high horizontal shear stresses. When such coupling response is significant, elastic theory and Hooke's Law would not apply.

## Chapter 7

### Comparison of Laboratory Test Results

#### Introduction

In both the triaxial resonant column testing series and the thin-walled hollow cylinder testing series, the effects of combined compression and shear loading were explored. The two testing series were conducted differently, producing different stress histories and different ranges of strain amplitudes. It is the purpose of this chapter to further develop the data presented from these two testing series in Chapters 5 and 6, and to develop a set of curves showing the loading effects over the full range of strains observed during testing.

#### Vertical Loading Alone

The compression modulus was plotted against the vertical strain under conditions of vertical compression loading alone in Figures 5-2 and 6-2. These figures were then normalized to the value of compression modulus at a vertical strain of  $\epsilon_z = 5 \times 10^{-3}\%$ , with the resulting curves shown in Figures 5-3 and 6-3. The value of  $\epsilon_z$  selected for normalization was chosen to maximize the amount of overlap in the data and to provide a simple means of combining the two sets of results.

The data from Figures 5-3 and 6-3 were combined and presented in Figure 7-1. These curves were then replotted in Figure 7-2 normalized to the maximum compression modulus at a vertical strain of  $\epsilon_z = 10^{-5}\%$ .

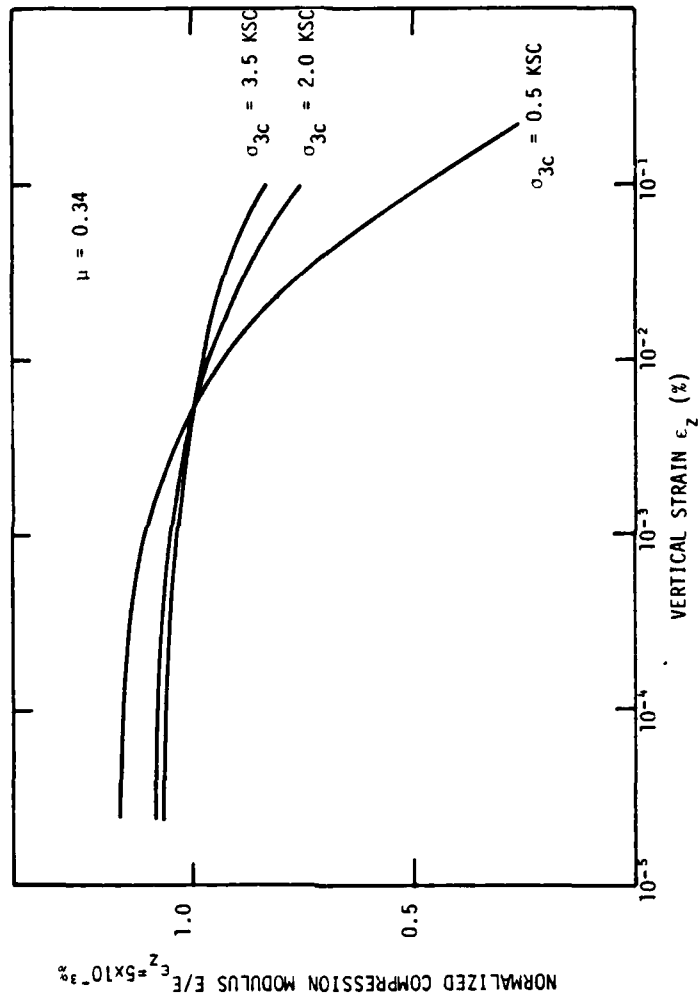


FIGURE 7-1 SUMMARY OF DEGRADATION OF NORMALIZED COMPRESSION MODULUS WITH VERTICAL STRAIN FOR RESONANT COLUMN AND HOLLOW CYLINDER TESTS UNDER CONDITION OF VERTICAL LOADING ALONE

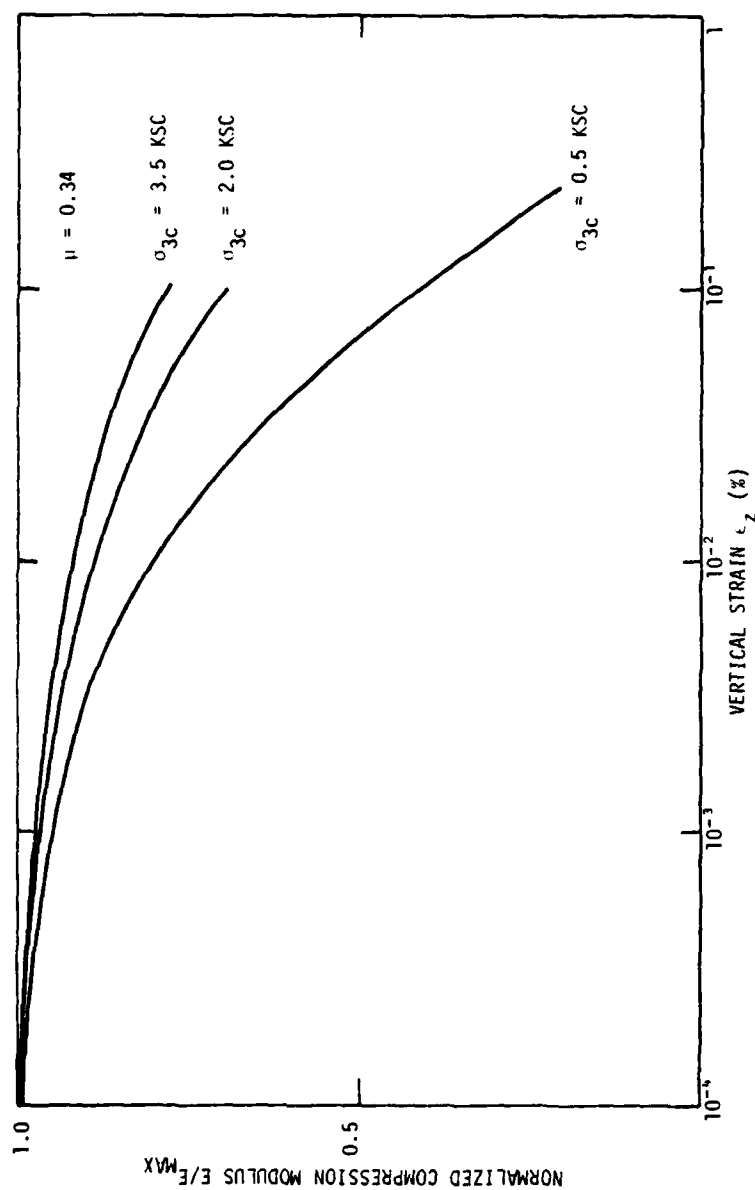


FIGURE 7-2 DEGRADATION OF NORMALIZED COMPRESSION MODULUS WITH VERTICAL STRAIN UNDER CONDITION OF VERTICAL LOADING ALONE AT LATERAL CONFINING PRESSURES,  $\sigma_{3c}$ , OF 0.5, 2.0, AND 3.5 KSC

## Mean Confining Stress

As indicated in these figures, the combined results were plotted for different values of lateral confining pressure,  $\sigma_{3c}$ . During the triaxial resonant column testing series, samples were consolidated in such a way that normal stresses in every direction were equal to  $\sigma_{3c}$ ; so that the mean confining stress during consolidation,  $\sigma_m$ , may be written:

$$\sigma_m = \frac{\sigma_{1c} + \sigma_{2c} + \sigma_{3c}}{3} = \sigma_{3c} \quad (7.1)$$

With the thin-walled hollow cylinder test specimens, however, the principal stresses are not all equal during consolidation, but are as follows:

$$\sigma_{1c} = 1.85 \cdot \sigma_{3c} \quad , \quad (7.2)$$

$$\sigma_{2c} = \mu \cdot (\sigma_{1c} + \sigma_{3c}), \quad (7.3)$$

and  $\sigma_{3c} = \sigma_{3c} \quad (7.4)$

The mean confining stress during consolidation becomes:

$$\sigma_m = \frac{\sigma_{1c} + \sigma_{2c} + \sigma_{3c}}{3} = \frac{(1 + \mu) \cdot 2.85 \cdot \sigma_{3c}}{3} \quad (7.5)$$

And where  $\mu = 0.34$ ,  $\sigma_m$  may be written:

$$\sigma_m = 1.273 \cdot \sigma_{3c} \quad (7.6)$$

Because the degradation of modulus with vertical strain for the two testing series may be better represented as a function of the mean confining stress than the lateral confining stress alone, it is desirable to replot the data from Figure 6-3 for values of  $\sigma_m$  of 0.5, 2.0, and 3.5 KSC.

In order to accomplish this replot, the variation of the normalized compression modulus was first plotted against the mean confining pressure,  $\sigma_m$ , for a constant range of strain. This plot is shown in Figure 7-3, with the vertical strain range of from  $\epsilon_z = 5 \times 10^{-3}$  to  $\epsilon_z = 10^{-1}$ . The circled data points in this figure come directly from the data in Figure 6-3, where  $\sigma_m$  is related to  $\sigma_{3c}$  by Equation 7.6. The triangles represent interpolated data points for  $\sigma_m$  values of 0.5, 2.0, and 3.5 KSC.

With the data represented by the triangles in Figure 7-3, it was possible to replot Figure 6-3 to reflect the desired values of  $\sigma_m$ . This plot is shown in Figure 7-4.

From Figures 7-4 and 5-2 it was possible to replot the normalized compression modulus-vertical strain curves in Figure 7-2 in terms of the mean confining stress,  $\sigma_m$ . This new plot is shown in Figure 7-5. It is noteworthy that the difference between this figure and Figure 7-2 is small. There is a somewhat more rapid degradation of modulus with increasing strain for the  $\sigma_m$  curves than for the comparable  $\sigma_{3c}$  curves.

#### Octahedral Shearing Strain

In Chapter 5 it was noted that the normalized compression modulus degraded with the octohedral shearing strain relatively independently of how that strain was developed: e.i., whether from vertical loading alone or from combined vertical and torsional loading. It was concluded therefore, that for the resonant column data, compression-shear interaction could be completely accounted for by using the octahedral shearing strains.

In Chapter 6 some compression-shear interaction effects (for hollow cylinder specimens) were noted which were not completely accounted for by

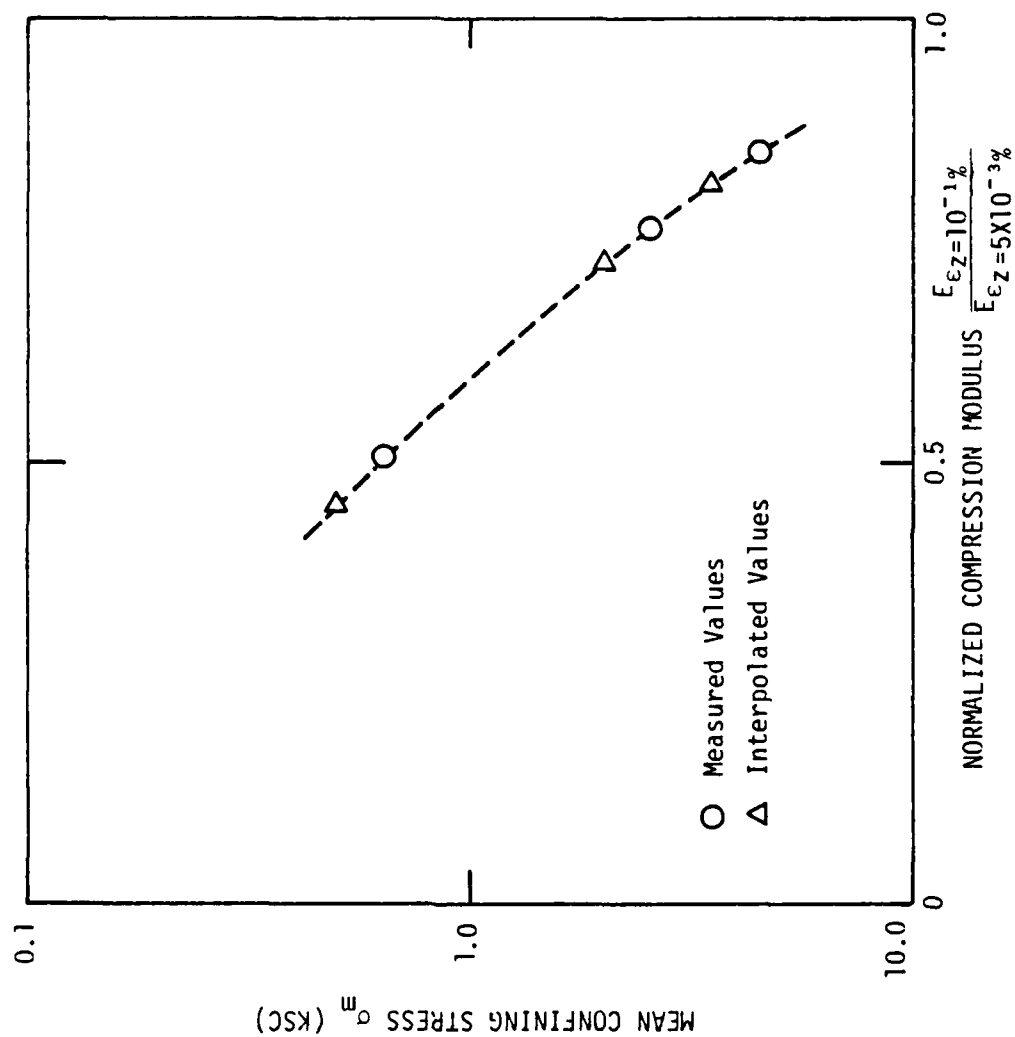


FIGURE 7-3 INTERPOLATION OF NORMALIZED COMPRESSION MODULUS VALUES FOR MEAN CONFINING PRESSURES,  $\sigma_m$ , OF 0.5, 2.0, AND 3.5 KSC

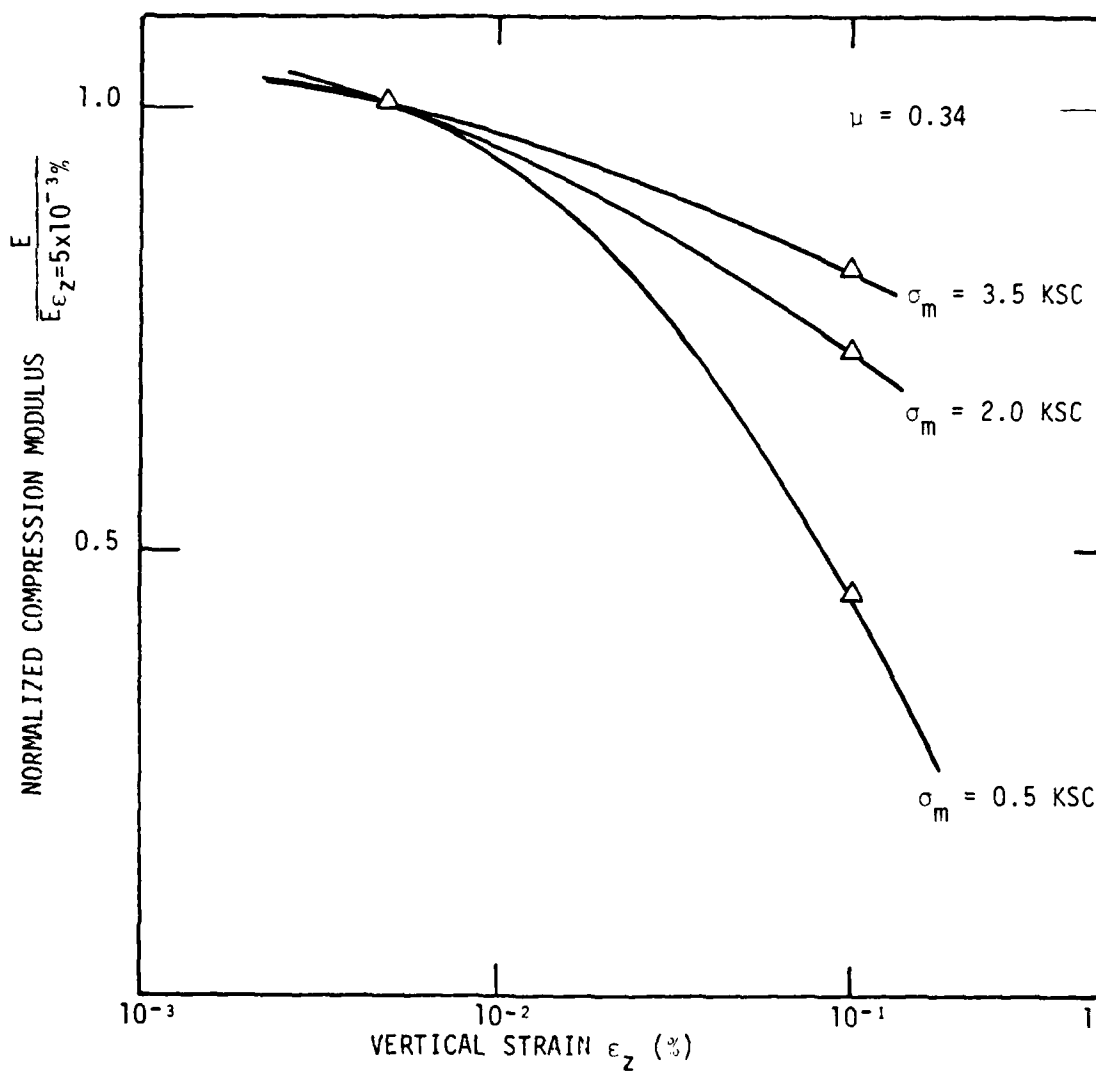


FIGURE 7-4 DEGRADATION OF NORMALIZED COMPRESSION MODULUS WITH VERTICAL STRAIN FOR HOLLOW CYLINDER TESTS UNDER CONDITION OF VERTICAL LOADING ALONE FOR MEAN CONFINING PRESSURE,  $\sigma_m$ , OF 0.5, 2.0, AND 3.5 KSC

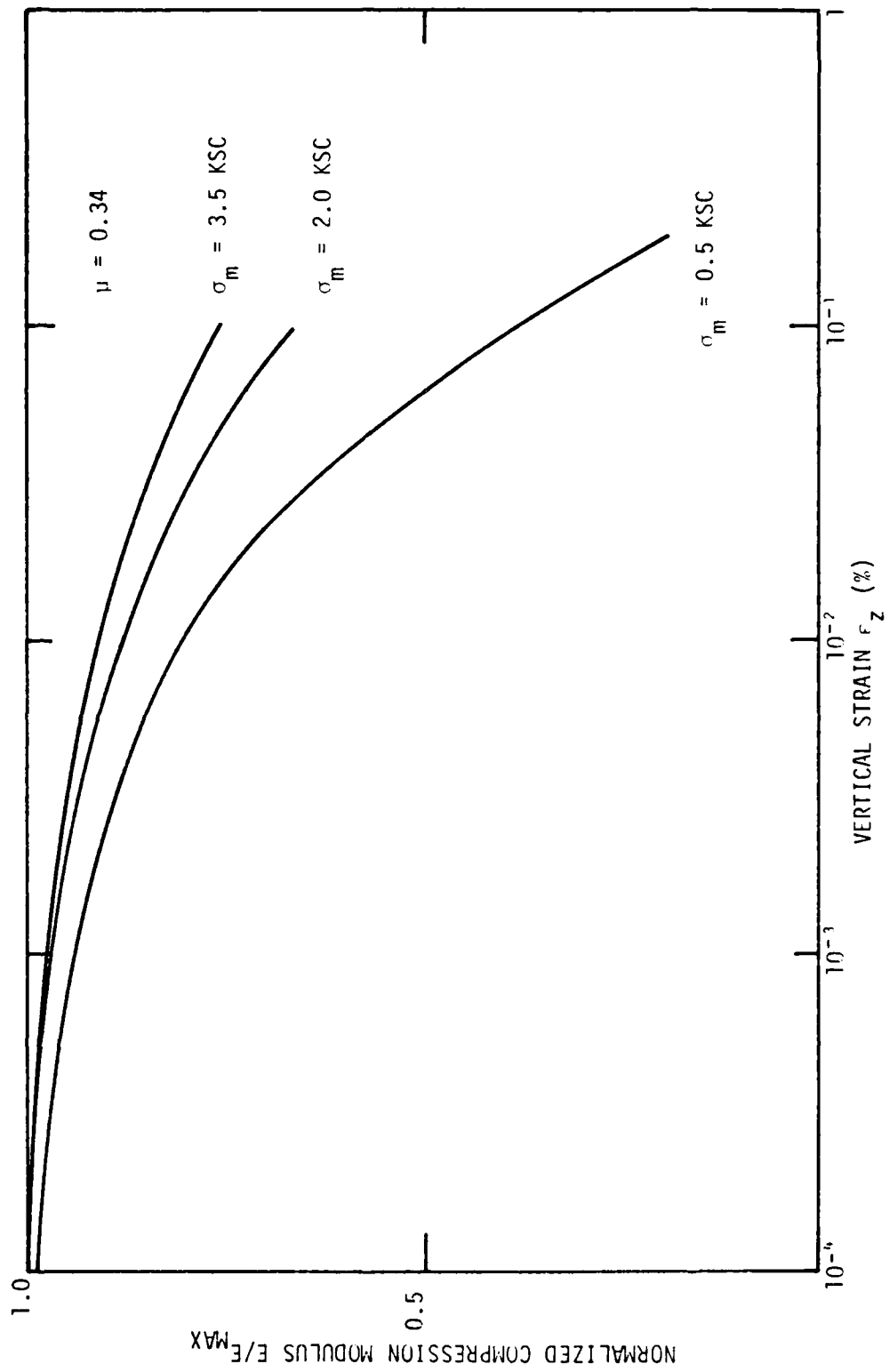


FIGURE 7-5 DEGRADATION OF NORMALIZED COMPRESSION MODULUS WITH VERTICAL STRAIN UNDER CONDITION OF VERTICAL LOADING ALONE AT MEAN CONFINING PRESSURES,  $\sigma_m$ , OF 0.5, 2.0, AND 3.5 KSC

the use of the octahedral strain. Nevertheless, it was possible to develop a family of "best fit" octahedral strain curves which represent an excellent approximation of the variation of normalized compression modulus with octahedral shearing strain under a wide range of combined loading conditions.

The octahedral shearing strain curves were presented in Figures 5-19 and 6-19 for the two testing series. Using the technique described above to develop a series of curves for values of  $\sigma_m$  of 0.5, 2.0, and 3.5 KSC, these two figures were combined as shown in Figure 7-6. This figure may be used with reasonable accuracy to predict the degradation of modulus with octahedral shearing strain for Monterey No. 0 sand or a similar sand.

#### Strain Ratio Effects

Another way of evaluating the compression-shear interaction effects upon the degradation of modulus with strain was discussed in Chapters 5 and 6, and was referred to as the strain ratio effect. Simply stated, the method involved the use of the strain ratio degradation curves presented in Figures 5-10 and 6-7, where the degree of degradation was shown as a function of the ratio of shear strain to vertical normal strain for specific values of vertical normal strain. To predict the degradation of compression modulus under any straining condition, one would first determine the degradation resulting from the vertical straining alone; then that degradation would be further reduced by the reduction factor determined from the strain ratio figures.

The initial degradation of modulus resulting from vertical straining alone may now be obtained directly from Figure 7-5. To provide a summary

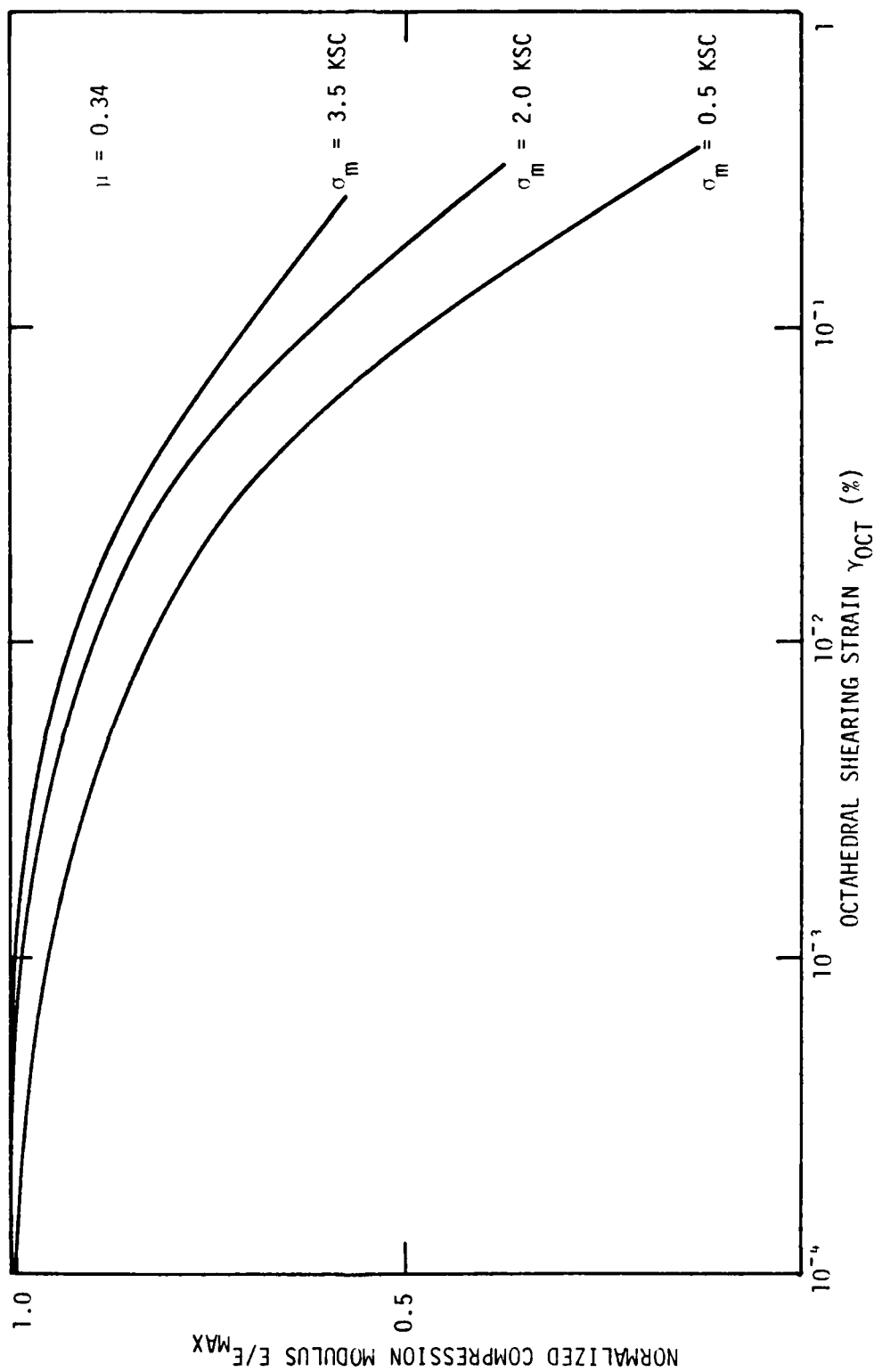


FIGURE 7-6 DEGRADATION OF NORMALIZED COMPRESSION MODULUS WITH OCTAHEDRAL SHEARING STRAIN AT MEAN CONFINING PRESSURES,  $\sigma_m$ , OF 0.5, 2.0, AND 3.5 KSC

figure for obtaining the additional degradation resulting from the existence of simultaneous shear straining, a set of strain ratio curves were plotted for values of vertical strain of  $10^{-1}$ ,  $10^{-2}$ ,  $10^{-3}$ , and  $10^{-4}$ %. These curves appear in Figure 7-7.

### Conclusions

The presentations made in Chapters 5 and 6 regarding the degradation of modulus with strain under combined compression-shear loading conditions were further developed to provide data curves over the entire strain range observed during the two testing series. These curves may be used to predict degradation of modulus under conditions of simultaneous compression-shear loading with reasonable accuracy.

### Octahedral Shearing Strain Effects

The degree of degradation of modulus may be predicted by calculating the octahedral shear strain from the complete strain state, and interpolating from the curves in Figure 7-6. This degradation may then be applied to an estimate of the maximum, low-strain modulus to determine the modulus corresponding to a given state of strain. The maximum modulus value may be obtained either from a laboratory or field test, such as a seismic survey to obtain P-wave velocity, or from published data showing typical values of low-strain compression moduli at various mean confining stresses. The values of low-strain moduli observed in these testing series are shown in Figures 5-2 and 6-2, and are available in more detail elsewhere (Griffin, 1980).

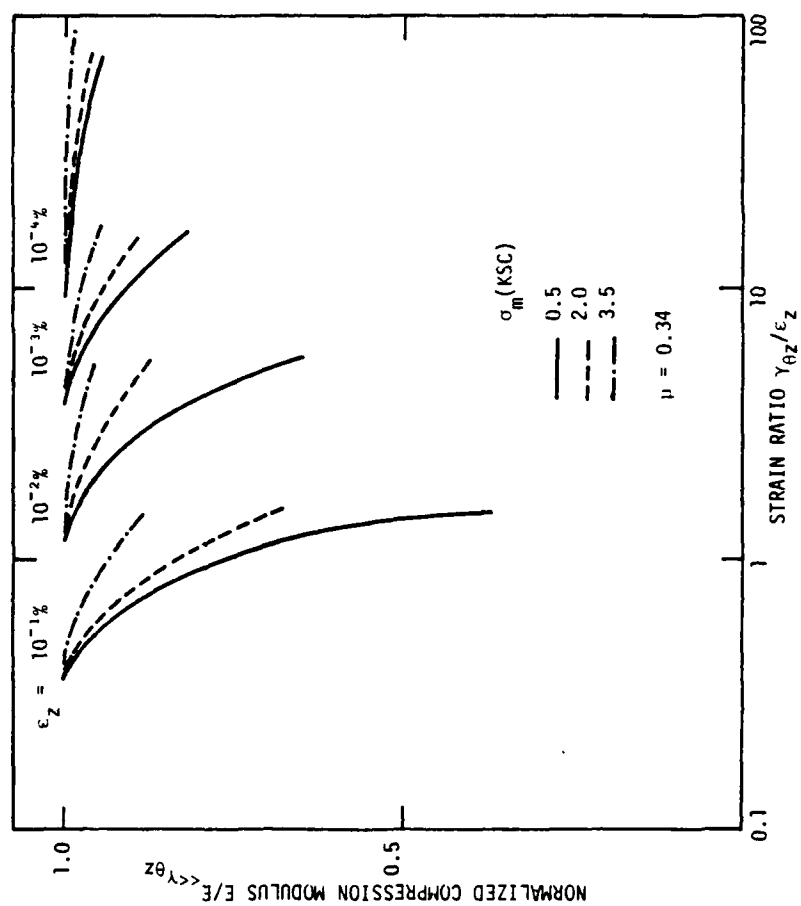


FIGURE 7-7 SUMMARY OF DEGRADATION OF NORMALIZED COMPRESSION MODULUS WITH RATIO OF SHEAR STRAIN TO NORMAL STRAIN

### Strain Ratio Effects

The degree of degradation of modulus may also be estimated if the vertical normal strain and the horizontal-vertical shear strain are known. The degradation resulting from vertical straining alone is first determined from Figure 7-5, then the additional degradation resulting from shear straining is obtained by interpolating from the curves in Figure 7-7. Because of the difficulty in making the logarithmic interpolations in Figure 7-7 the octahedral shearing strain technique described earlier appears more promising for estimating compression modulus values for analysis purposes.

## Chapter 8

### Large Scale Model Studies

#### Introduction

It is the purpose of this chapter to present the observed soil response for a series of large scale dynamic model studies on slopes of sand. Because the significant response is primarily due to yielding within the soil slope, which is beyond the elastic range of loading for the soil material, conventional elastic response analysis techniques are of little value. An attempt will be made to predict the point at which yielding begins using an analysis technique proposed by Seed and Goodman (1964).

In earlier chapters, compression-shear interaction effects were studied under a variety of combined loading conditions on laboratory samples of sand. Interaction effects were presented in such a manner as to show their influence upon the dynamic moduli of the sands under various conditions of density, confining pressure, and strain amplitude. One major advantage of this form of presentation was that there exist a large number of elastic analysis techniques which employ the dynamic moduli to predict soil response, thus allowing for relatively simple application of these research findings in conventional elastic analysis methods.

In order to evaluate any interaction effects occurring beyond the elastic loading range of the soils, it was necessary to perform a soil loading test in which yielding occurs with simultaneous shear-compression dynamic excitation, and for which an accurate analysis technique has been developed. These slope model studies appeared to meet those criteria.

### Test Set-up

The model studies were conducted on the 20 ft x 20 ft shaking table located at the Earthquake Simulator Laboratory at the Richmond Field Station, Earthquake Engineering Research Center, University of California, Berkeley, California. This table can move in one horizontal direction and the vertical direction. It was designed to exactly reproduce dynamic accelerations, velocities, and displacements, within certain limits, from analog records stored on either magnetic tape or disk. A detailed description of this shaking table has been provided by Rea (1972) and by Rea and Penzien (1972).

The cross-section of a typical soil slope specimen is shown in Figure 8-1. In this figure, four accelerometers and four DC linear variable displacement transformers (labeled DCDT) are shown. In addition to these, the table itself is heavily instrumented with accelerometers and displacement transducers.

### Test Box

The inside dimensions of the test box in which the soil slope specimens are formed are approximately 84.2 in x 42.5 in x 21.7 in, with a triangular spacer in one corner approximately 15.8 in on each side, placed at an angle of approximately 45° with the horizontal. The test box was bolted securely to the shaking table, and a layer of high-strength "hydrostone" cement mortar was placed between the box and the table, and in the base of the box to assure rigid, solid contact between the two.

The test box is shown in Figure 8-2(a), and the bracing behind the

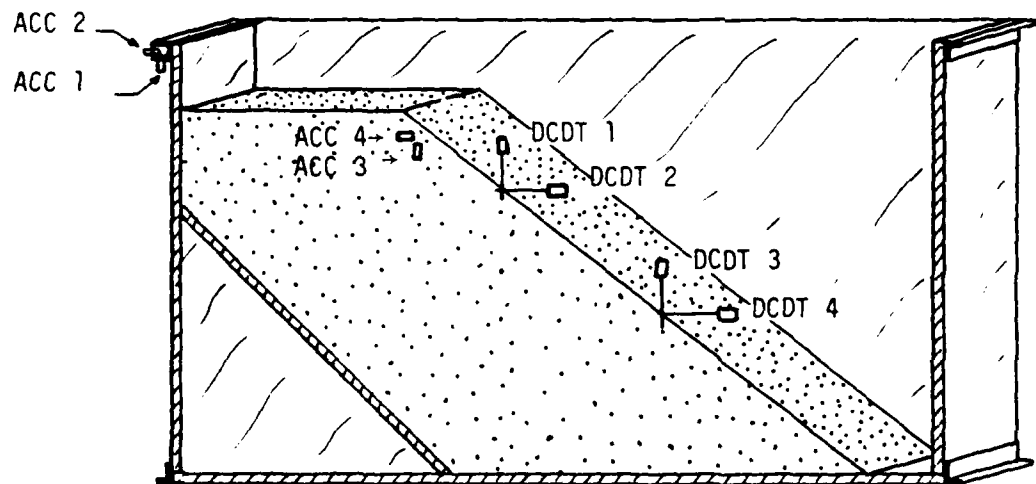
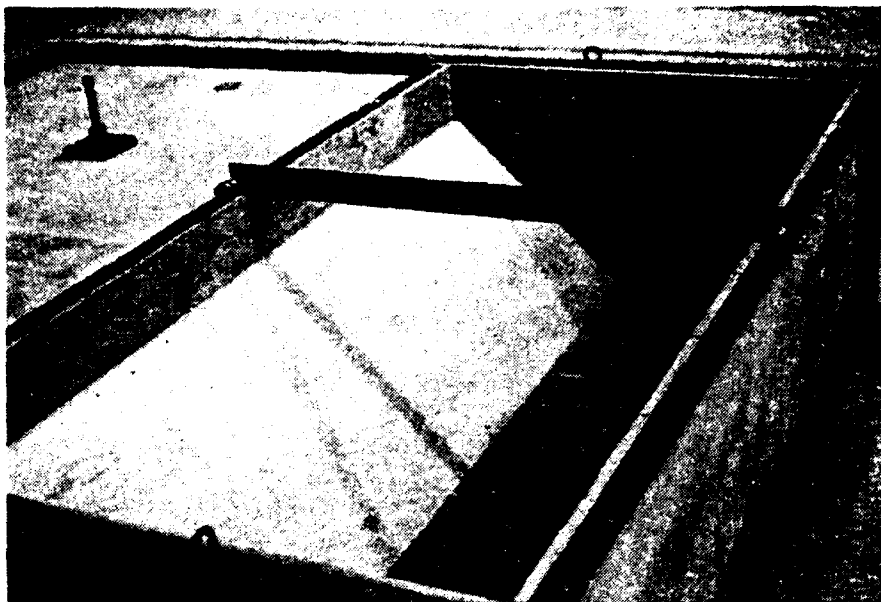
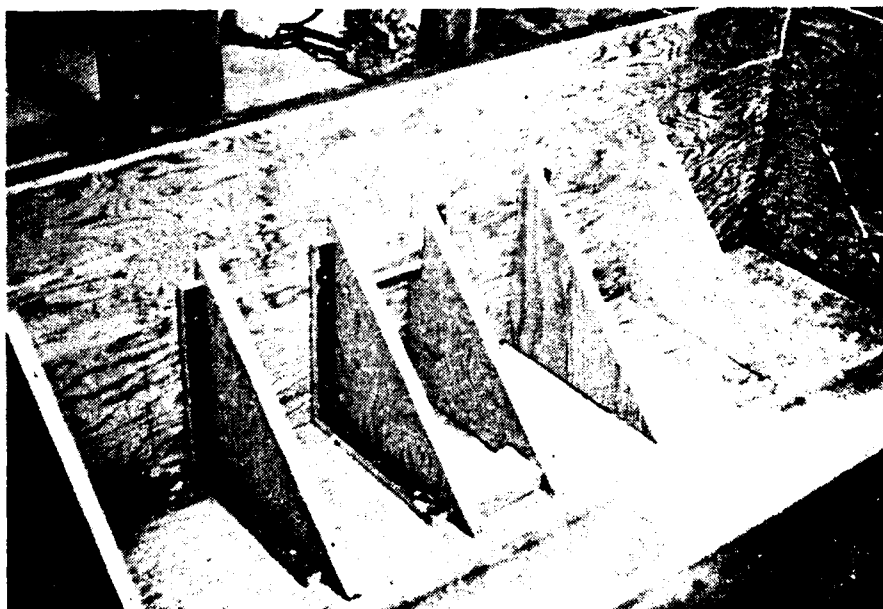


FIGURE 8-1 CUT-AWAY VIEW OF TYPICAL SLOPE SPECIMEN  
SHOWING LOCATION OF INSTRUMENTATION



(a)



(b)

FIGURE 8-2 DETAIL OF TEST BOX (a) AND BRACING  
BEHIND SPACER BOARD (b)

spacer board is shown in Figure 8-2(b). The bracing was installed to insure a stiff response of the spacer board during loading, so that its deflection during loading would be very small when compared with the displacements of the soil slope.

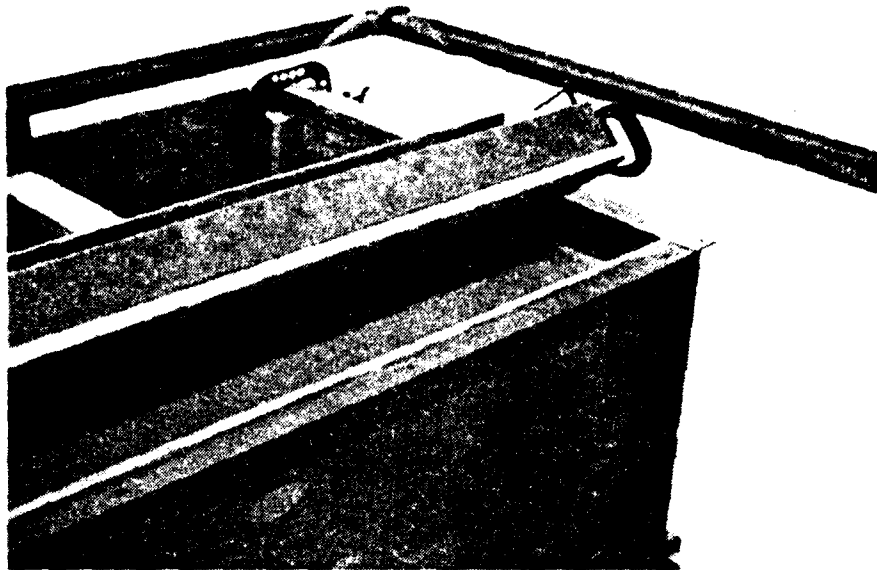
Before the test box was used for this testing series, a thin film of high-strength epoxy was sprayed upon the back, spacer board, and bottom, and a thin layer of the test sand placed upon those surfaces.

The sand used in this testing series was the same Monterey No. 0 sand used in the hollow cylinder and resonant column testing series.

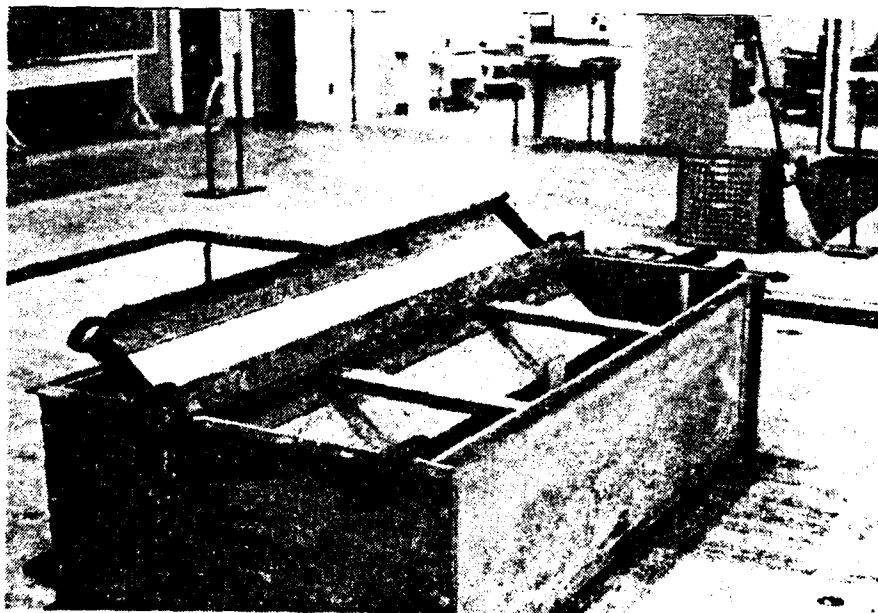
#### Forming Test Specimens

Slope specimens were formed by placing sand into a "mold" formed within the test box, and vibrating the sand, one lift at a time, until the desired slope height was obtained. Vibration was done by the shaking table. The forming "mold" assembly is shown in Figures 8-3(a) and (b).

A typical completed soil specimen is shown in Figures 8-4(a) and (b), with instrumentation in place. A closeup of the placement of the DCDT's on the soil slope surface is shown in Figure 8-5(a). As placed, the core of the DCDT's have a very thin (.01 in diameter), stiff 2 in length of piano wire protruding from them. This piano wire is coated with a very thin film of epoxy, and carefully inserted into the soil slope surface. The DCDT's are then zeroed by adjusting their position relative to their cores in the mounting bracket. Once the epoxy film hardens, the sand immediately surrounding the piano wire protrusion is cemented to the wire, but its fabric remains relatively undisturbed. A closeup of this wire, epoxy, sand cementation is shown in Figure 8-5(b).

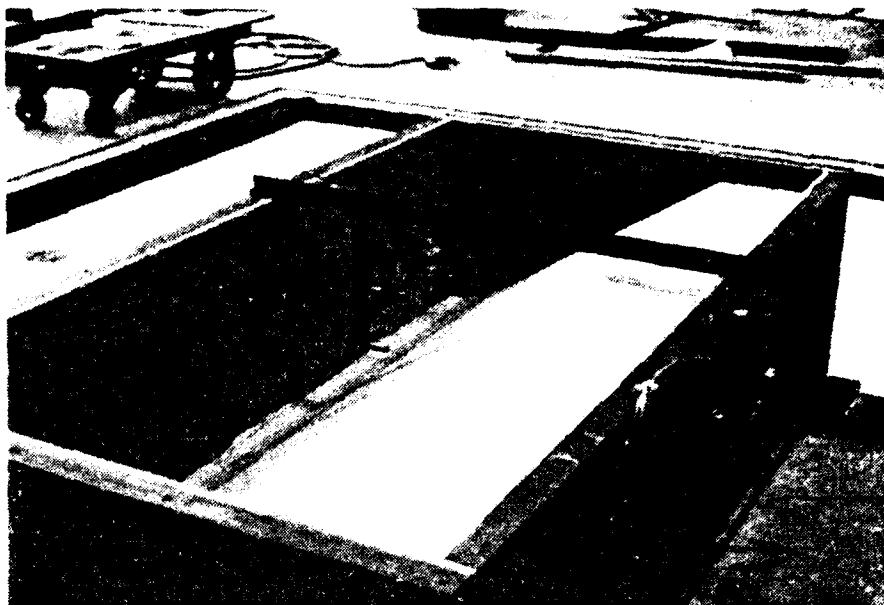


(a)

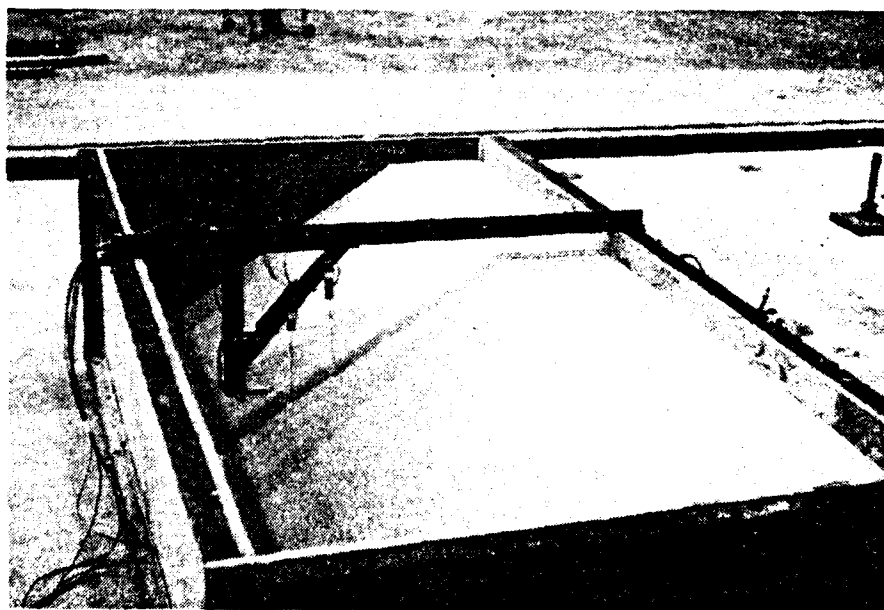


(b)

FIGURE 8-3 TWO VIEWS OF FORMING MOLD ASSEMBLY  
USED WHEN CONSTRUCTING SLOPE SPECIMENS



(a)



(b)

FIGURE 8-4 TWO VIEWS OF A COMPLETED, INSTRUMENTED  
SLOPE SPECIMEN READY TO BE TESTED



(a)



(b)

FIGURE 8-5 DETAIL OF PLACEMENT OF DCDT CORE PROBES  
ON THE SURFACE OF A SLOPE SPECIMEN (a),  
AND OF SAND-EPOXY BOND ON WIRE PERTUSION

### Summary of Tests

The tests performed in this testing series are summarized in Table 8-1.

### Soil Strength Characteristics

Because the yielding which occurs along the outer surface of the soil slopes is of primary importance to this study, it is important to know accurately the shear strength characteristics of the outermost soil slope materials.

The soil slopes were formed by vibrating soils within a forming mold, which was later removed. It is highly probable that passive pressures and other stress concentrations developed during sample formation resulted in non-uniform distribution of densities within the slopes. It is therefore necessary to determine the shear strength characteristics of the outermost soil materials by methods other than conventional shear-strength vs density correlations.

### Static Slope Failure

In Test No. 9, shown in Table 8-1, a marginal static slope failure occurred soon after the slope was formed. This observed failure, which was a shallow sloughing failure, provides a probable upper bound for the angle of internal friction,  $\phi$ , of:

$$\phi_{MAX} \approx \alpha_{failure} = 37.6^{\circ} \quad (8-1)$$

TABLE 8-1

## Summary of Soil Slope Model Tests

Test No.	Test Code No.	$\alpha(^{\circ})$	$D_R(\%)$	$a_v/a_h$	$\omega(^{\circ})$	Record	Mode (Horizontal or Combined)
1	291075.1	33.6	80	--	--	A	H
2	301075.1	33.6	80	.67	33.7	A	C
3	311075.1	33.6	95	--	--	A	H
4	101175.3	33.6	95	.67	33.7	A	C
4B	120576.1	33.6	95	.67	33.7	A	C
5	041175.1	35.3	95	--	--	A	H
5A	100576.1	35.3	95	--	--	A	H
6	051175.1	35.3	95	.67	33.7	A	C
6A	110576.1	35.3	95	.67	33.7	A	C
7	061176.1	35.3	80	--	--	A	H
8	101175.2	35.3	80	.67	33.7	A	C
7X	140576.1	35.3	80	--	--	B	H
8X	170576.1	35.3	80	.67	33.7	B	C
8Y	190576.1	35.3	80	.75	36.9	B	C
8Z	250576.1	35.3	80	.60	31.0	B	C
9	021175.*	37.6	95	(Static Slope Failure)			

where  $\alpha$  is the angle of the slope,

$D_R$  is the relative density of the soil,

$a_v$  is the peak vertical acceleration,

$a_h$  is the peak horizontal acceleration, and

$\omega$  is the angle of application of the resultant acceleration.

## Direct Shear Tests

During the testing series, two groups of special direct-shear tests were performed on the outermost soils of the slopes after they had been formed and were ready for testing. These direct-shear tests were performed by placing a lightweight block, specially prepared with a thin layer of sand epoxied to it, upon the surface of the slope. The block was then pulled upslope with a string until yielding occurred. As shown in Figure 8-6, if the weight of the block and the string tension are known, the normal and shear stresses on the failure surface at yielding are easily calculated.

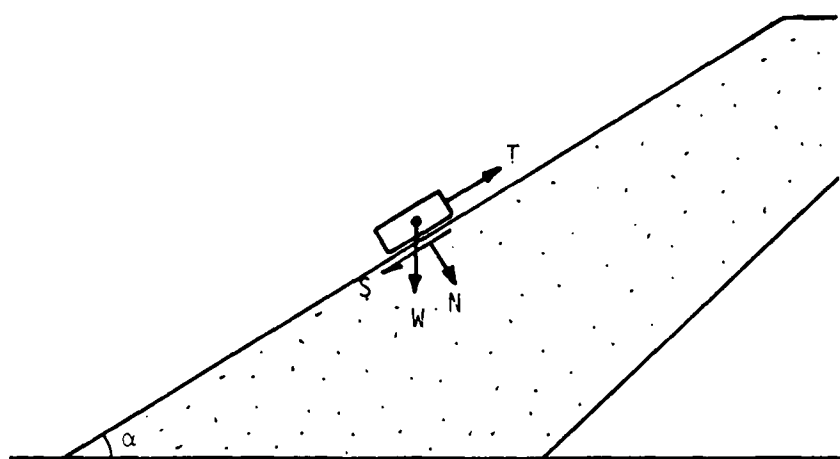
In Tables 8-2 and 8-3 the calculated values of  $N$  and  $S$  and the normal and shear stresses on the failure surface at yielding are shown for average relative densities of 95% and 80% respectively. From these tables, the shear strength plots shown in Figures 8-7 and 8-8 have been developed. From these figures it appears that the shear strength characteristics of the outermost slope materials are approximately the same even when the average soil densities are not, and are defined by the following equation:

$$S = s_i \cdot l + N \cdot \tan \phi \quad (8.2)$$

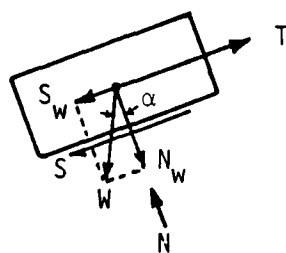
where  $s_i$  is the shear strength intercept,  $l$  is the length, and  $\phi$  is the angle of internal friction. Equation 8.2 may be rewritten as follows:

$$S = 0.029 \cdot l + N \cdot \tan(35.4^\circ) \quad (8.3)$$

It is interesting to note at this point that the value of  $s_i$  is very small, and that the values of  $s_i$  and  $\phi$  are much smaller than those used by Seed and Goodman in their studies involving Monterey sand. There are



(a)



(b)

$$S = T - S_w$$

$$N = N_w$$

$$S_w = W \sin \alpha$$

$$N_w = W \cos \alpha$$

FIGURE 8-6 DIAGRAM OF FORCES ACTING ON THE SLIDING BLOCK USED IN SURFACE DIRECT SHEAR TESTS PERFORMED ON SLOPE SPECIMENS

TABLE 8-2

N and S for  $D_R \approx 95\%$ 

Test	$\alpha(^{\circ})$	W(lb.)	$\frac{W \cos \alpha}{A}$	$\frac{W \sin \alpha}{A}$		
			N(psi)	-S <sub>w</sub> (psi)	+ T(psi)	= S(psi)
060576.0	33.5	0.1552	.0032	.0021	.0040	.0019
		0.5847	.012	.008	.0164	.0084
		1.2339	.0254	.0168	.0333	.0165
		0.3849	.0079	.0052	.0098	.0046
		0.1552	.0032	.0021	.0047	.0026
		0.5847	.012	.008	.0166	.0086
		0.1552	.0032	.0021	.0041	.002
		0.5847	.012	.008	.0151	.0071
100576.1	35.3	0.1552	.0031	.0022	.0047	.0025
		0.3849	.0078	.0055	.0121	.0066
		0.5847	.0118	.0083	.018	.0097
		0.8144	.0164	.0116	.0249	.0133
		0.1552	.0031	.0022	.0046	.0024
		0.3849	.0078	.0055	.0112	.0057
		0.5847	.0118	.0083	.0179	.0096
		0.8144	.0164	.0116	.0257	.0141
		0.1552	.0031	.0022	.0044	.0022
		0.3849	.0078	.0055	.0105	.005
		0.5847	.0118	.0083	.0163	.008
		0.8144	.0164	.0116	.0238	.0122
		0.1552	.0031	.0022	.0043	.0021
		0.3849	.0078	.0055	.0106	.0051
110576.1	35.7	0.5847	.0118	.0083	.0156	.0073
		0.8144	.0164	.0116	.0216	.01
		0.3849	.0078	.0055	.011	.0055
		0.8144	.0164	.0116	.0238	.0122
		0.1552	.0031	.0022	.0047	.0025
		1.2339	.0247	.0178	.0339	.0161
		0.1552	.0031	.0022	.0043	.0021
		0.5847	.0117	.0084	.017	.0086
		1.2339	.0247	.0178	.0339	.0161
		2.7893	.0559	.0402	.0741	.0339
		1.2339	.0247	.0178	.0336	.0158

 $\alpha$  = angle of slope

A = cross-sectional area of block

W = weight

T = tension in string

TABLE 8-3

N and S for  $D_R \approx 80\%$ 

Test	$\alpha(^{\circ})$	W(lb.)	$\frac{W \cos \alpha}{A}$	$\frac{W \sin \alpha}{A}$		
			N(psi)	$-S_w$ (psi)	+ T (psi)	= S (psi)
140576.1	35.2	.1552	.0031	.0022	.0044	.0022
		.5847	.0118	.0083	.0164	.0081
		.8045	.0162	.0115	.0226	.0111
		1.234	.0249	.0176	.0345	.0169
		2.789	.0563	.0397	.0774	.0377
		.5847	.0118	.0083	.0162	.0079
		1.234	.0249	.0176	.0351	.0175
		2.789	.0563	.0397	.0765	.0368
		.1522	.0031	.0022	.0044	.0022
		.5847	.0118	.0083	.0173	.0090
		.8045	.0162	.0115	.0234	.0119
		1.234	.0249	.0176	.0360	.0184
		2.789	.0563	.0397	.0785	.0388
170576.1	35.4	.1552	.0031	.0022	.0045	.0023
		.5847	.0118	.0083	.0163	.0080
		1.234	.0248	.0177	.0347	.0170
		2.789	.0561	.0399	.0761	.0362
		.8045	.0162	.0115	.0226	.0111
		.5847	.0118	.0083	.0166	.0083
		1.234	.0248	.0177	.0348	.0171
		2.789	.0561	.0399	.0812	.0413
		.1552	.0031	.0022	.0044	.0022
		.5847	.0118	.0083	.0170	.0087
		.8045	.0162	.0115	.0241	.0126
		1.234	.0248	.0177	.0351	.0174
		2.789	.0561	.0399	.0797	.0398
		.5847	.0118	.0083	.0170	.0087
		1.234	.0248	.0177	.0358	.0181
190576.1	35.3	.1552	.0031	.0022	.0045	.0023
		.5847	.0118	.0083	.0163	.0080
		.8045	.0162	.0115	.0239	.0124
		1.234	.0249	.0176	.0352	.0176
		2.789	.0562	.0398	.0812	.0414
		1.234	.0249	.0176	.0345	.0169
		2.789	.0562	.0398	.0788	.0390
		.1552	.0031	.0022	.0045	.0023
		.5847	.0118	.0083	.0164	.0081
		.8045	.0162	.0115	.0222	.0107
		1.234	.0249	.0176	.0344	.0168
		2.789	.0562	.0398	.0752	.0354
		3.439	.0693	.0491	.0910	.0419

continued

TABLE 8-3 continued

N and S for  $D_R \approx 80\%$ 

Test	$\alpha(^{\circ})$	W(lb.)	$\frac{W \cos \alpha}{A}$	$\frac{W \sin \alpha}{A}$		
			N(psi)	$-S_w$ (psi)	+ T(psi)	= S(psi)
250576.1	35.4	.1552	.0031	.0022	.0045	.0023
		.5847	.0118	.0083	.0170	.0087
		1.234	.0248	.0177	.0370	.0193
		2.789	.0561	.0399	.0811	.0412
		.1552	.0031	.0022	.0049	.0027
		.5847	.0118	.0083	.0170	.0087
		1.234	.0248	.0177	.0360	.0183
		.1552	.0031	.0022	.0045	.0023
		.5847	.0118	.0083	.0173	.0090
		1.234	.0248	.0177	.0345	.0168
		2.789	.0561	.0399	.0810	.0411

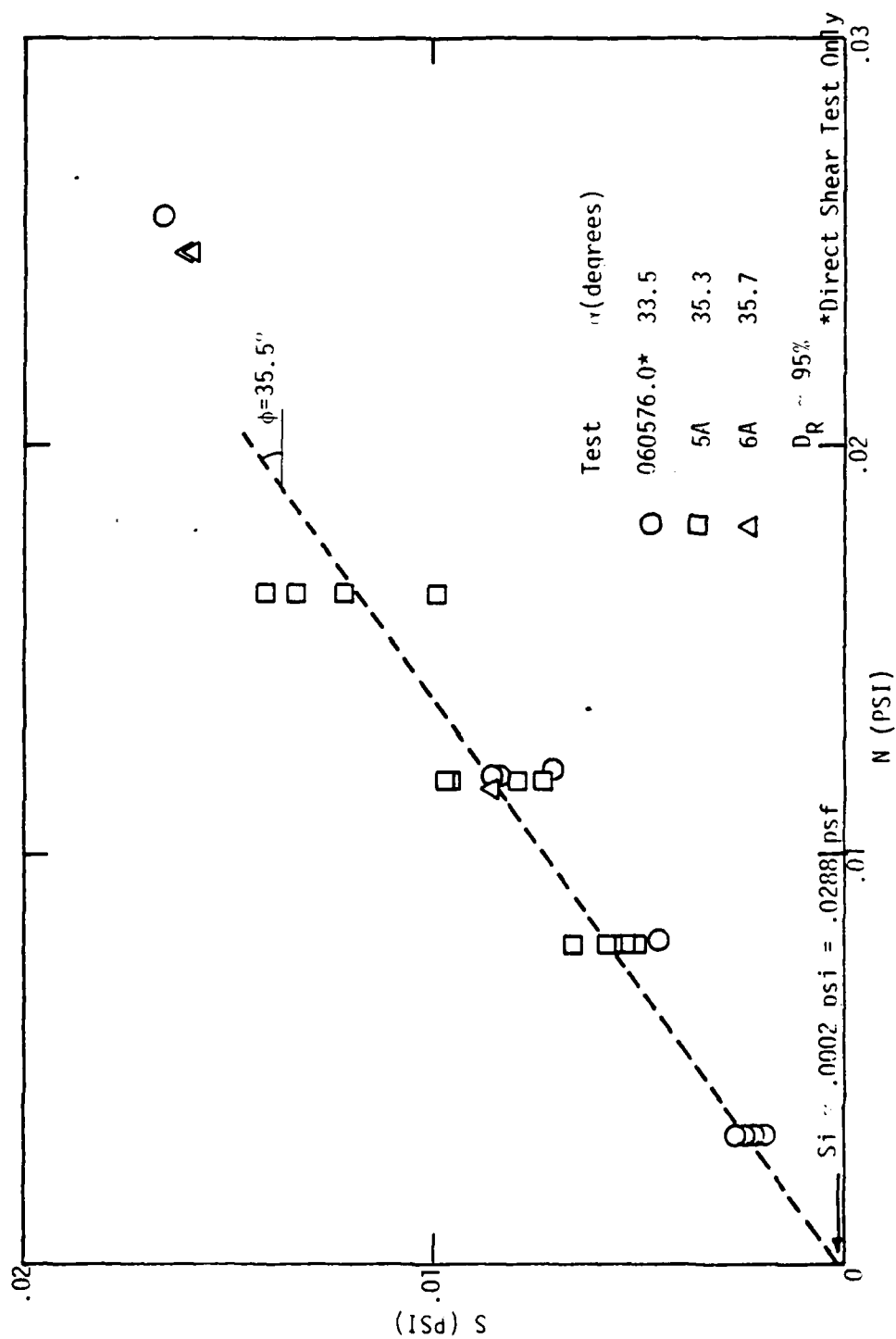


FIGURE 3-7 VARIATION OF  $N$  AND  $S$  FOR SLOPE SPECIMEN SANDS WITH AN AVERAGE RELATIVE DENSITY,  $D_R = 95\%$ .

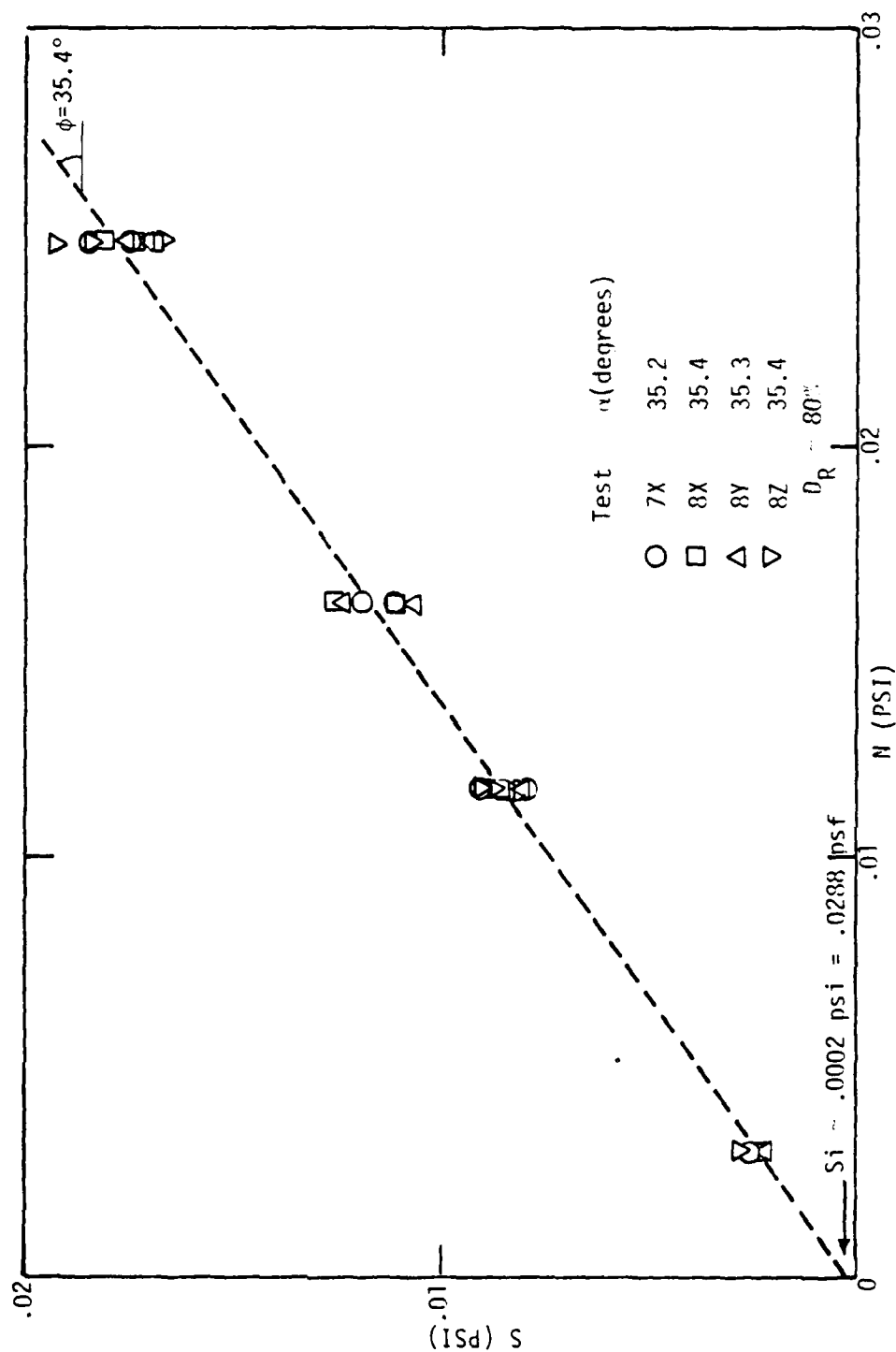


FIGURE 8-8 VARIATION OF  $N$  AND  $S$  FOR SLOPE SPECIMEN SANDS WITH AN AVERAGE RELATIVE DENSITY,  $D_R = 80\%$ .

several reasons for this difference, one of which is the fact that different gradations of Monterey sand were used in the Seed and Goodman study than were used in this testing program. A gradation analysis of the Monterey No. 20 sand used by Seed and Goodman is shown alongside that for the Monterey No. 0 sand used in this study in Figure 8-9.

The low value of the shear strength intercept,  $s_i$ , is expected both because of the low mean grain size of the sand, and because the outer slope material is probably at lower density than the average slope material density because of arching and stress concentration effects during the sample formation process. The effect of mean grain size on the value of  $s_i$  is shown in Figure 8-10, as developed by Seed and Goodman. The mean grain size of Monterey No. 0 sand (.015 millimeters) would correspond to a very low value for  $s_i$ .

The larger degree of uniformity of the gradation analysis curve for Monterey No. 0 sand would support a lower friction angle,  $\phi$ , for that sand.

#### Shaking Table Tests

As described earlier, slope specimens were subjected to sinusoidal dynamic loading in either the horizontal direction only, or in combined horizontal and vertical excitation. Combined horizontal and vertical loading was accomplished in phase, as illustrated in Figure 8-11. The resultant excitation which the samples experience is as shown in Figure 8-11(c), inclined at an angle  $\omega$  with the horizontal plane. The two loading conditions are further illustrated in Figure 8-12. The horizontal component of loading was held constant for the different testing series, so that the resultant acceleration amplitude in the combined loading

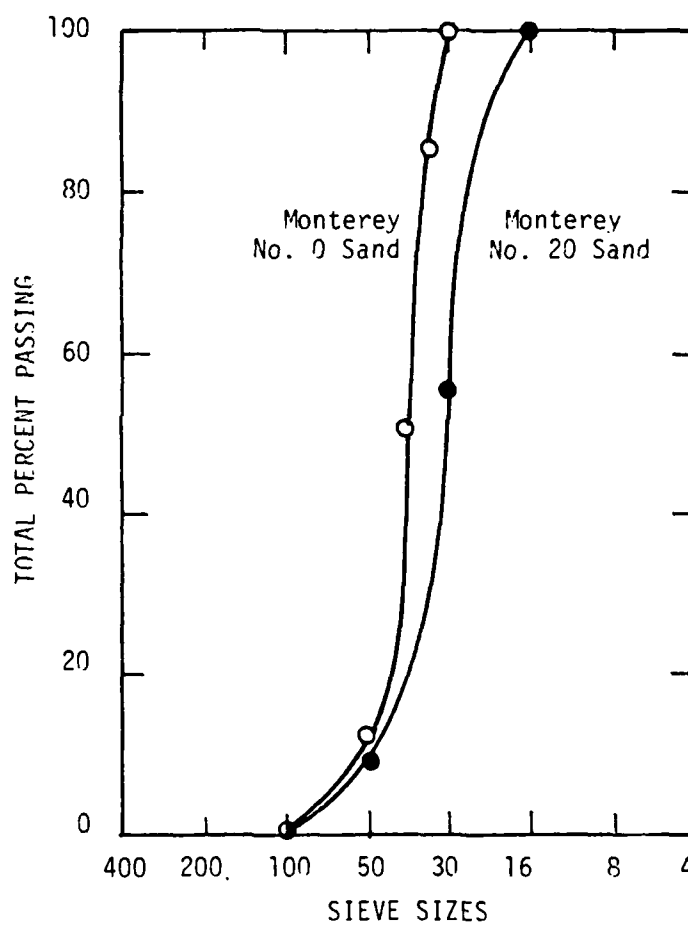


FIGURE 8-9 COMPARISON OF GRADATION ANALYSES FOR  
MONTEREY NO. 20 AND MONTEREY NO. 0 SANDS

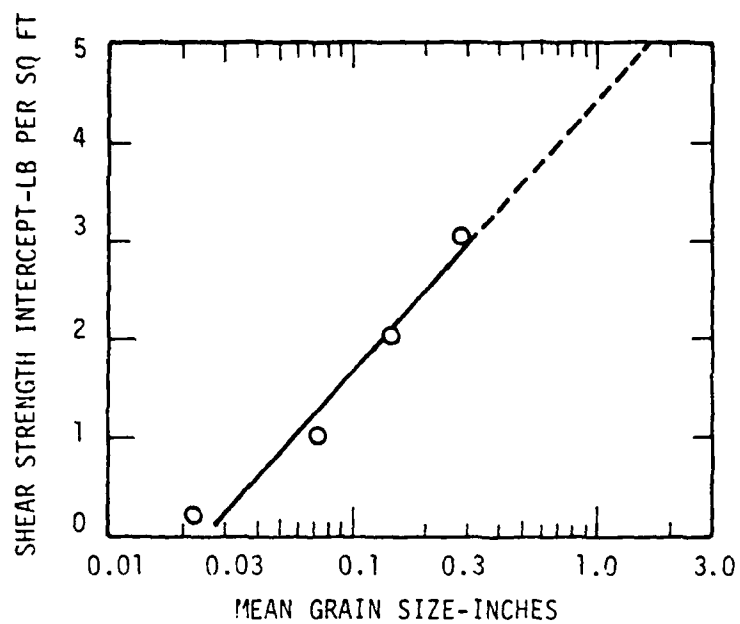
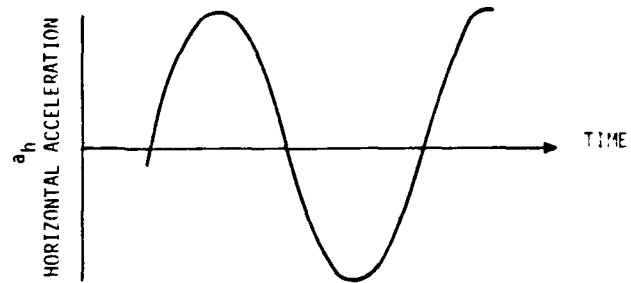
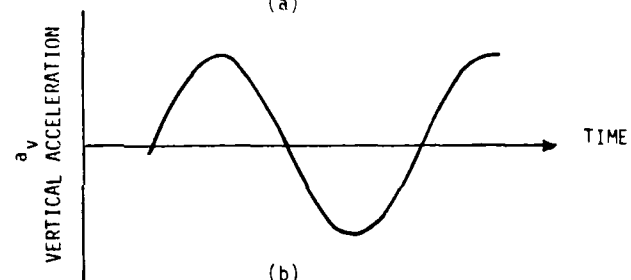


FIGURE 8-10 RELATIONSHIP BETWEEN SHEAR STRENGTH INTERCEPT  
AND MEAN GRAIN SIZE FOR UNIFORMLY GRADED SANDS

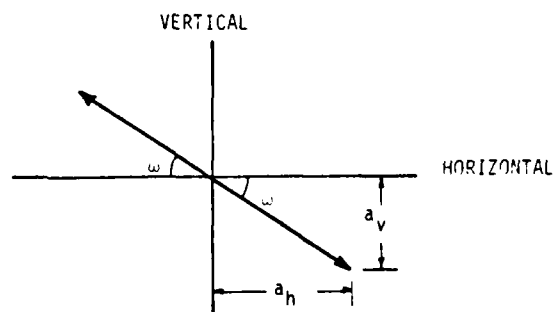
(AFTER SEED AND GOODMAN)



(a)

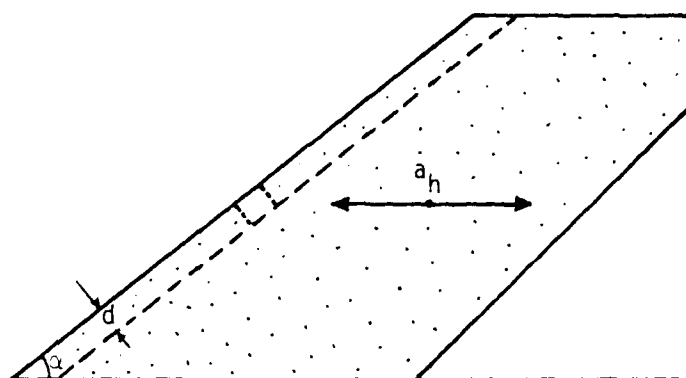


(b)

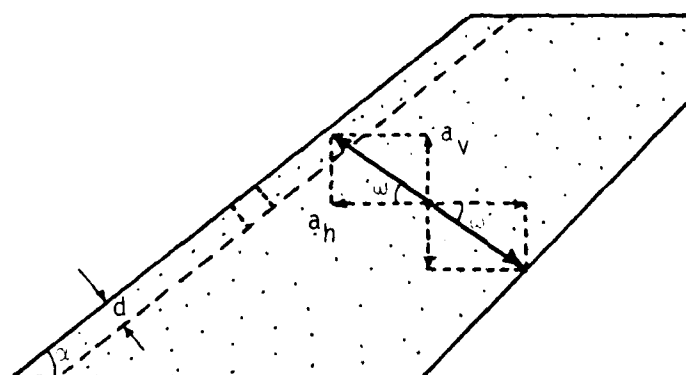


(c)

FIGURE 8-11 ILLUSTRATION OF IN-PHASE COMBINED HORIZONTAL AND VERTICAL LOADING USED IN SLOPE TESTS



(a)

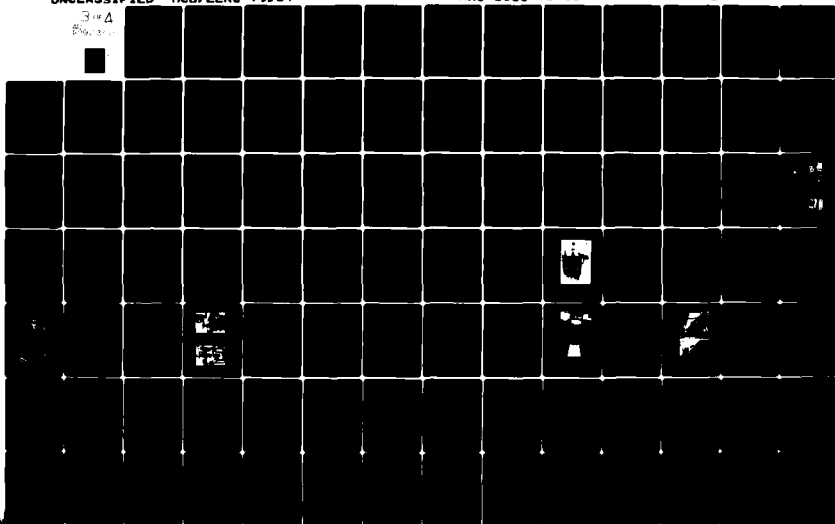


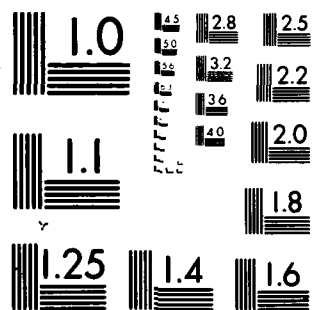
(b)

FIGURE 8-12 GRAPHICAL ILLUSTRATION OF APPLICATION OF HORIZONTAL ACCELERATION ALONE (a) AND COMBINED HORIZONTAL AND VERTICAL ACCELERATION (b) ON SLOPE SPECIMENS

AD-A092 352 CALIFORNIA UNIV BERKELEY EARTHQUAKE ENGINEERING RES--ETC F/G 8/13  
INTERACTION EFFECTS OF SIMULTANEOUS TORSIONAL AND COMPRESSIONAL--ETC(U)  
DEC 79 P M GRIFFIN, W N HOUSTON DAAG29-76-8-0257  
UNCLASSIFIED ICB/EERC-79/34 ARO-13838.1-85 NL

3 of 4  
ENCLOSURE





MICROCOPY RESOLUTION TEST CHART  
NATIONAL BUREAU OF STANDARDS-1963-A

tests was necessarily higher than in the horizontal loading tests.

#### Test Records

The two basic testing records utilized in this testing series were records A and B as shown in Figure 8-13. Record A consists of four acceleration amplitude steps of ten cycles each increasing in equal increments to a maximum acceleration amplitude of 0.35 g. Record B contains fifteen acceleration amplitude steps of five cycles each increasing in equal increments to a maximum acceleration amplitude of 0.175 g.

#### Analysis

In accordance with the analysis technique proposed by Seed and Goodman (1964), the sliding surface at which limiting equilibrium exists when the critical yield acceleration is applied is approximated as shown with the dashed line in Figure 8-12, at a depth  $d$  below the surface of the slope. The forces acting upon an element of soil along this sliding surface are illustrated in Figure 8-14(a). To satisfy equilibrium,  $F_u$  must equal  $F_d$  in this figure, and the remaining forces may be evaluated as follows:

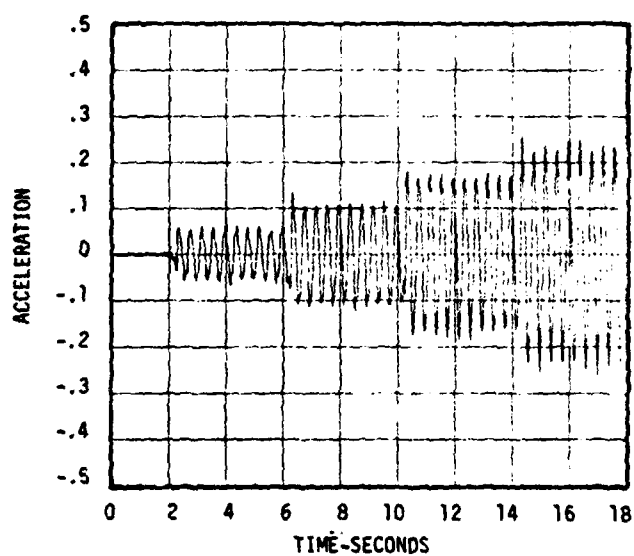
$$N = W \cdot \cos \alpha - k_y \cdot W \cdot \sin(\alpha + \omega), \text{ and} \quad (8.4)$$

$$S = W \cdot \sin \alpha + k_y \cdot W \cdot \cos(\alpha + \omega) \quad (8.5)$$

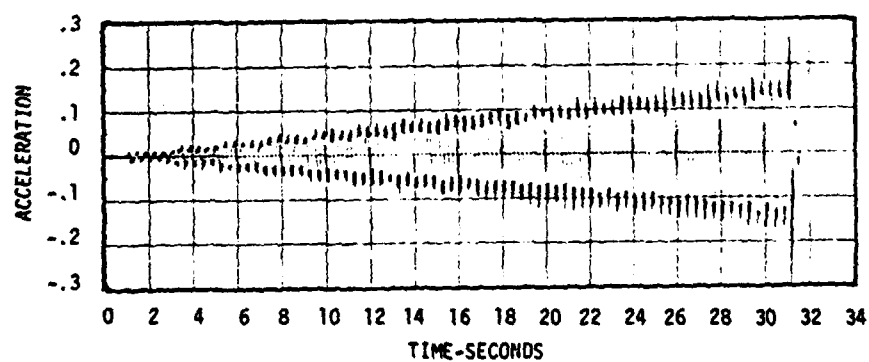
But, from Equation 8.2 we know that:

$$S = s_i \cdot l + N \cdot \tan \phi \quad (8.2)$$

Equations 8.4 and 8.5 may now be written:



(a) RECORD A



(b) RECORD B

FIGURE 8-13 EXAMPLES OF TWO ACCELERATION RECORDS  
USED IN SLOPE TESTS

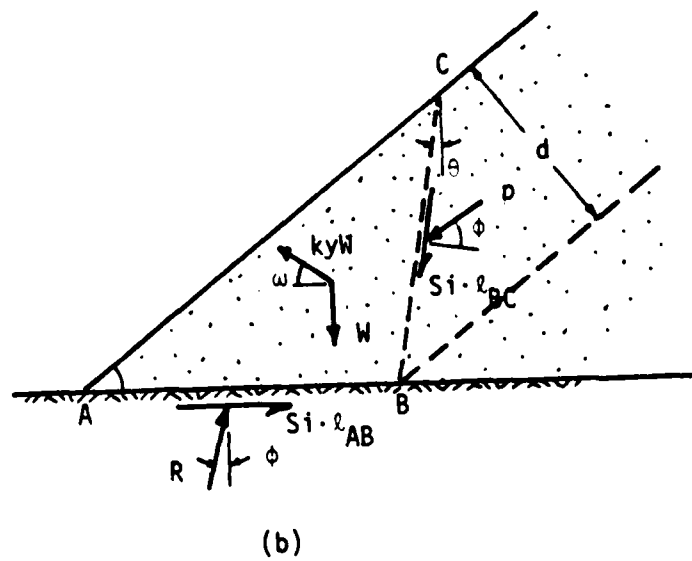
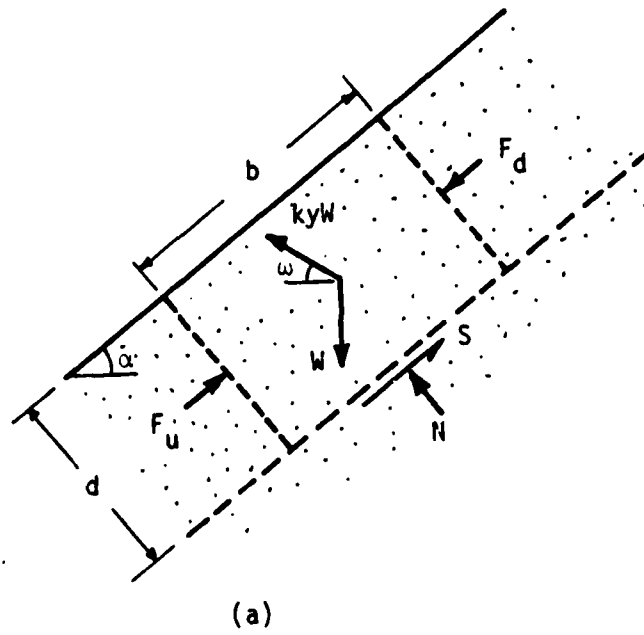


FIGURE 8-14 DIAGRAM OF FORCES ALONG SLIDING SURFACE AT LIMITING EQUILIBRIUM FOR SLOPE SPECIMENS

$$\begin{aligned}
 S &= s_i \cdot b + [W \cdot \cos \alpha - ky \cdot W \cdot \sin(\alpha + \omega)] \cdot \tan \phi \\
 &= W \cdot \sin \alpha + [ky \cdot W \cdot \cos(\alpha + \omega)]
 \end{aligned} \quad (8.6)$$

Collecting terms and writing:

$$W = b \cdot d \cdot \gamma_d \quad (8.7)$$

it is found that:

$$ky = \frac{\frac{s_i}{d \cdot \gamma_d} + \cos \alpha \cdot \tan \phi - \sin \alpha}{\cos(\alpha + \omega) + \sin(\alpha + \omega) \cdot \tan \phi} \quad (8.8)$$

$$\text{or: } ky = \frac{\sin(\phi - \alpha)}{\cos(\phi - \alpha - \omega)} + \frac{s_i}{d \cdot \gamma_d \cdot [\cos(\alpha + \omega) + \sin(\alpha + \omega) \cdot \tan \phi]} \quad (8.9)$$

For the slope of finite length used in this testing series, a passive wedge will form at the toe of the slope as shown in Figure 8-14(b). The primary effect of this passive wedge is to resist sliding not only by the shear resistance along the base of the sliding mass,  $S$ , but also by the force,  $P$ , at the toe of the slope.

Summing the forces perpendicular to the resultant force,  $R$ , gives the following expression:

$$\begin{aligned}
 [P \cdot \cos(2\phi - \theta)] + [ky \cdot W \cdot \cos(\phi - \omega)] &= \\
 W \cdot \sin \phi + [s_i \cdot l_{AB} \cdot \cos \phi] + [s_i \cdot l_{BC} \cdot \sin(\phi - \theta)] & \quad (8.10)
 \end{aligned}$$

Noting that,

$$l_{AB} = \frac{d}{\sin \alpha}, \text{ and} \quad (8.11)$$

$$l_{BC} = \frac{d}{\cos(\alpha + \theta)}, \quad (8.12)$$

and solving for  $P$  leads to the following:

$$P = \frac{W \cdot [\sin\phi - ky \cdot \cos(\phi - \omega)] + s_i \cdot d \cdot \left[ \frac{\cos\phi}{\sin\alpha} + \frac{\sin(\phi - \theta)}{\cos(\alpha + \theta)} \right]}{\cos(2\phi - \theta)} \quad (8.13)$$

$$\text{Writing} \quad W = \frac{\gamma_d \cdot d \cdot l_{AC}}{2} \quad (8.14)$$

$$\text{where} \quad l_{AC} = d \cdot [\tan\alpha + \tan(\alpha + \theta)] \quad (8.15)$$

and combining and rewriting Equation 8.13, the following is obtained:

$$P = \frac{d^2 \cdot \gamma_d}{2 \cos(2\phi - \theta)} \cdot \left[ \left\{ \tan\alpha + \tan(\alpha + \theta) \right\} \cdot \left\{ \sin\phi - ky \cdot \cos(\phi - \omega) \right\} + \frac{2s_i}{d \cdot \gamma_d} \cdot \cos\phi \cdot \left\{ \frac{1}{\sin\alpha} + \frac{\sin(\phi - \theta)}{\cos(\alpha + \theta) \cdot \cos\phi} \right\} \right] \quad (8.16)$$

As pointed out by Seed and Goodman, it is simply necessary to substitute the appropriate values of  $\alpha$ ,  $s_i$ ,  $\phi$  and  $\gamma_d$ , and a close approximation for  $ky$ , to obtain a relationship for  $P$  in terms of  $d$  and  $\theta$ . By means of several trials, the values of  $\theta$  giving the minimum value of  $P$  for different values of  $d$  can then be determined.

The influence of the force,  $P$ , can then be represented approximately by an equivalent shear resistance,  $s_e$ , as follows:

$$s_e = P/L \quad (8.17)$$

where  $L$  is the length of the slope. This is analogous to increasing the shear strength intercept,  $s_i$ , to a value of  $s_i + s_e$ , so that the corresponding value of  $ky$  is given by:

$$ky = \frac{\sin(\phi - \alpha)}{\cos(\phi - \alpha - \omega)} + \frac{s_i + s_e}{d \cdot \gamma_d \cdot [\cos(\alpha + \omega) + \sin(\alpha + \omega) \cdot \tan\phi]} \quad (8.18)$$

By means of several trials, the value of  $d$  corresponding to the minimum  $k_y$  may be determined.

The equations presented by Seed and Goodman differ from those above only in that their presentation dealt with the condition of horizontal accelerations only, whereas these equations were developed for combined vertical and horizontal accelerations. The vertical component of acceleration appears in Equations 8.16 and 8.18 in the form of the angle  $\omega$ .

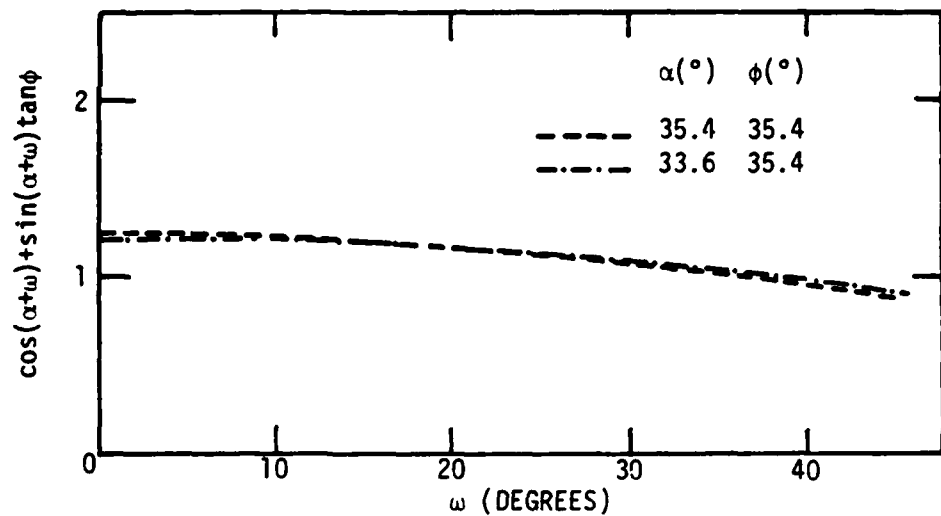
The influence of the angle,  $\omega$ , may be seen in its effect upon the value of  $k_y$  in Equation 8.18. The influence of the angle,  $\omega$ , upon the first term of that equation, and upon the denominator of the second term is illustrated graphically in Figure 8-15. It is apparent from this figure that  $k_y$  does not vary greatly as a function of the angle,  $\omega$ , for the soil and slope characteristics of the current testing program.

For these slope specimens,  $k_y$  at a value of  $\omega = 33.7^\circ$  will be approximately 1.2 times the value at  $\omega = 0$ . This fact is of value to this analysis, as it allows the use of the simplified analysis technique formulated by Seed and Goodman to predict yield accelerations for the current testing program. This eliminates the need to perform the trials and iterations as described earlier.

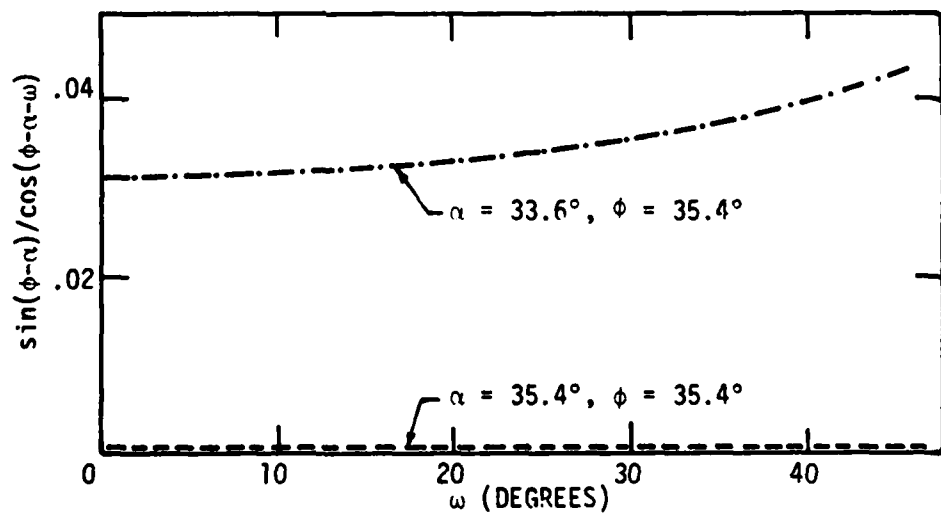
#### Simplified Analysis

In the simplified analysis proposed by Seed and Goodman, the yield acceleration is calculated as:

$$k_y = \tan(\phi - \alpha + \phi_{SL}) \quad (8.19)$$



(a)



(b)

FIGURE 8-15 VARIATION OF COMPONENTS OF EQUATION 8.18 WITH THE ANGLE,  $\omega$ , OF APPLICATION OF YIELD ACCELERATION,  $k_y$

where  $\phi_{SL}$  is a function only of the shear strength intercept,  $s_i$ , and the slope length,  $l$ . The values suggested for  $\phi_{SL}$  are presented in Figure 8-16. For the current testing program,  $s_i$  is approximately equal to 0.029 psf (from Figures 8-7 and 8-8), and the slopes are approximately 3 ft long.

As an example of how this simplified procedure may be used, consider the case of a slope with  $\alpha = 33.6^\circ$  and  $\omega = 36.9^\circ$ . From Figure 8-16, with  $s_i \approx 0.03$  and  $l \approx 3$  ft,  $\phi_{SL} \approx 0.8^\circ$ . Now, from Equation 8.19,

$$\begin{aligned} k_y &= \tan(35.4^\circ - 33.6^\circ + 0.8^\circ) \\ &= \tan(2.6^\circ) = 0.045 \end{aligned} \quad (8.20)$$

This value of  $k_y$  is that for  $\omega = 0$ . To obtain the value of  $k_y$  when  $\omega = 36.9^\circ$ , reference is made to Figure 8-15. The value of the first term in Equation 8.18, illustrated in Figure 8-15(b), is approximately 1.22 times the value when  $\omega = 0$ . Similarly, the value of the second term in Equation 8.18, whose denominator is illustrated in Figure 8-15(a), is also approximately 1.22 times the value when  $\omega = 0$ . The value of  $k_y$  from Equation 8-30 must therefore be multiplied by 1.22 to obtain the value when  $\omega = 36.9^\circ$ . This new value is as follows:

$$k_{y(\omega=36.9^\circ)} = (.045) \cdot (1.22) = .055 \quad (8.21)$$

#### Predicted Yield Accelerations

This computation was performed for the various test conditions encountered during this testing series, and a summary of the predicted yield acceleration values are presented in Table 8-4.

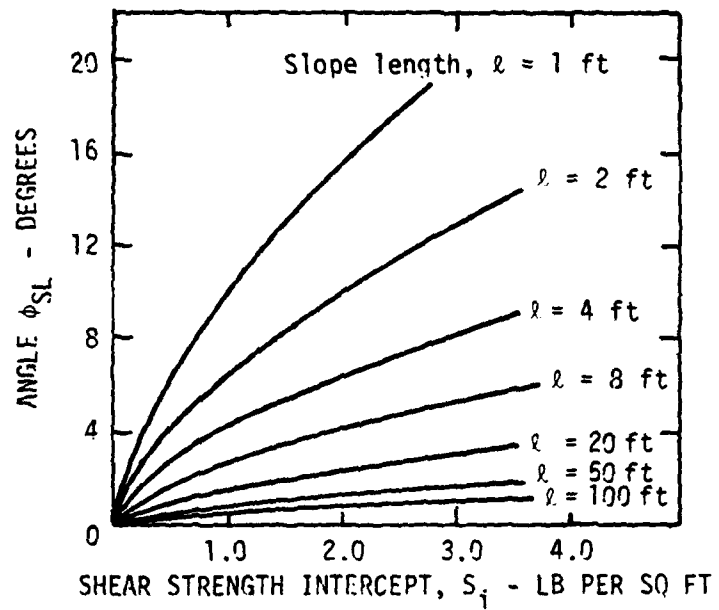


FIGURE 8-16 RELATIONSHIP BETWEEN SLOPE LENGTH,  
SHEAR STRENGTH INTERCEPT, AND ANGLE  $\phi_{SL}$   
(AFTER SEED AND GOODMAN)

TABLE 8-4

Predicted Values of Yield Acceleration,  
 $k_y$ , for Various Test Conditions

Angle $\omega$	Slope Angle, $\alpha$	
	33.6°	35.4°
0°	.045	.016
33.7°	.054	.019
36.9°	.055	.020
31°	.052	.018

(TEST 8Y)

(TEST 8Z)

### Test Results

As discussed earlier, test results consisted of digitized records of accelerations and displacements measured during the course of dynamic loading. For each test, four accelerometers and four DCDT's measured the response of the slope specimen and test box to the base excitation, and numerous accelerometers mounted upon the table measured the average horizontal and vertical table acceleration during loading. These digitized records are stored on magnetic tape, and are easily processed with the aid of a computer.

Presented in Figures 8-17 and 8-18 are several typical acceleration time histories which have been plotted from these digitized test results. In Figure 8-17 are several A records showing both table and top of slope accelerations in both the horizontal and vertical directions. Note how closely the top of slope acceleration records mirror the average table acceleration records. Similarly, Figure 8-18 includes several B records showing table and top of slope accelerograms for horizontal and vertical loading. Some high-frequency noise appears to have been "picked-up" in the top of slope response shown in these results.

The plotted time histories shown in these and the following figures were drawn by the CALCOMP plotter at the University of California Computing Center, Berkeley. A complete set of CALCOMP plots of results of this testing program are on file along with the digitized records at the Geotechnical Engineering Office at Berkeley.

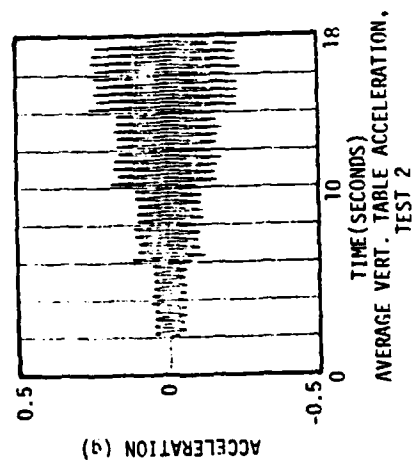
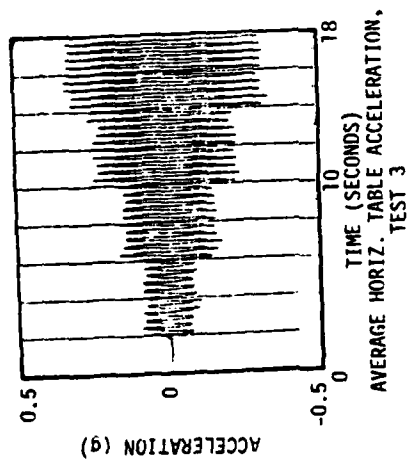
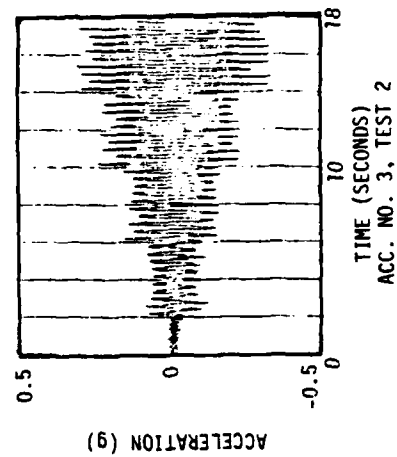
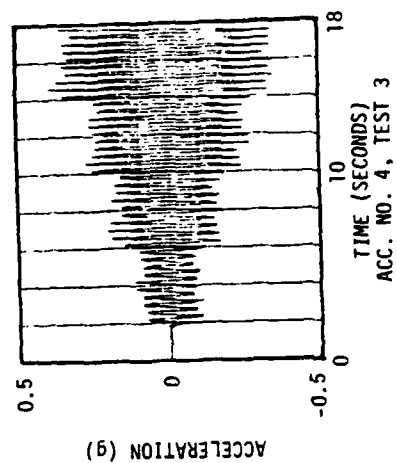


FIGURE 8-17 ACCELERATION TEST RECORDS FOR TESTS 2 AND 3

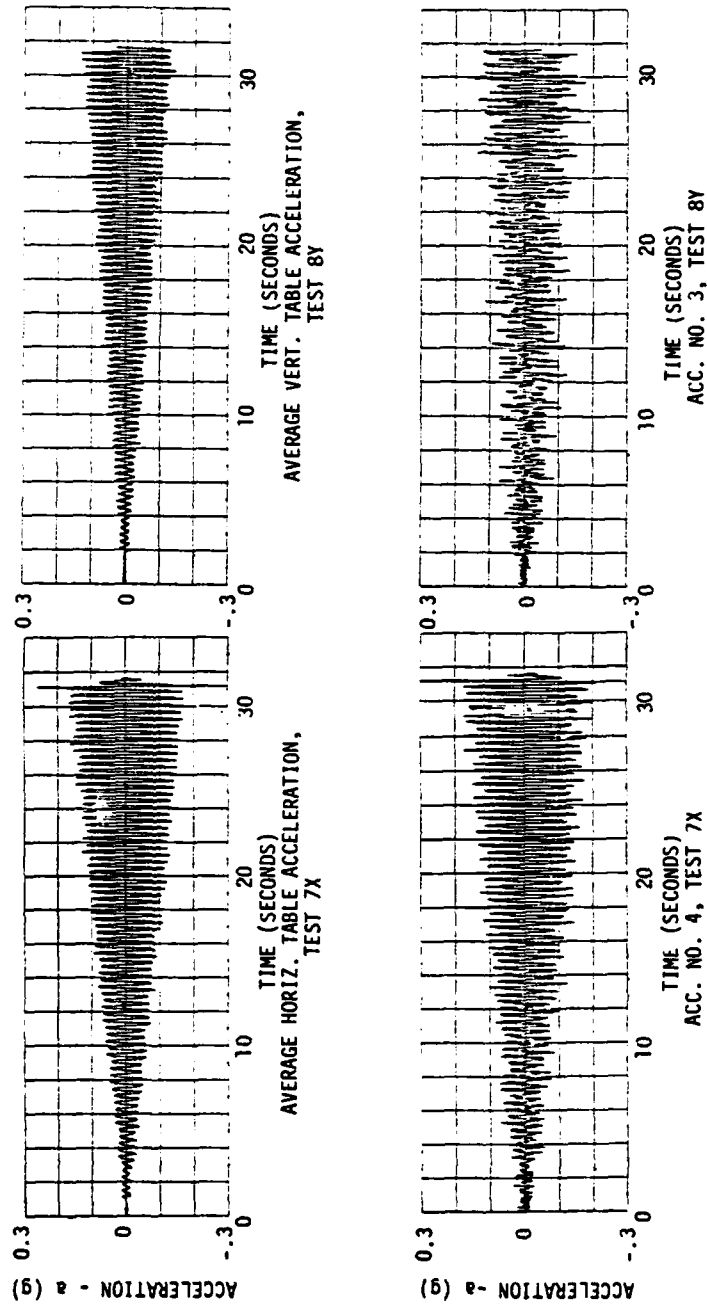


FIGURE 8-18 ACCELERATION TEST RECORDS FOR TESTS 7X AND 8Y

### Data Reduction

To obtain estimated values of the yield acceleration from the acceleration and displacement records, it is necessary to carefully study the displacement records to determine the time in the record when yielding first began.

Figures 8-19 and 8-20 include several typical acceleration and displacement records for tests 1 and 4 respectively. In Figure 8-19 yielding appears to begin at approximately 2 seconds into DCDT record No. 2, near the top of the slope, and some time later in DCDT record No. 3, near the bottom of the slope. At 2 seconds, the average horizontal table acceleration is changing from 0 g to approximately .085 g, and accelerometer No. 4 at the top of the slope is changing from .015 g to approximately 0.1 g. Although the .015 g acceleration before 2 seconds is essentially all high frequency noise, it is being applied upon the sample and is therefore a lower bound on the yield acceleration. Because yielding was first observed at 2 seconds, the yield acceleration for this slope must fall somewhere between these acceleration values.

In Figure 8-20, yielding may be seen at 2 seconds into DCDT records 1 and 4, at both the top and bottom of the slope. At this time the lower bound values of the yield acceleration are 0 g and .018 g, and the upper bound values are .106 g and .118 g for the table acceleration and top of slope acceleration respectively. These accelerations are obtained by noting the vertical ( $a_v$ ) and horizontal ( $a_h$ ) peak acceleration values and, because they are in phase, calculating the resultant acceleration,  $a'$ , as follows:

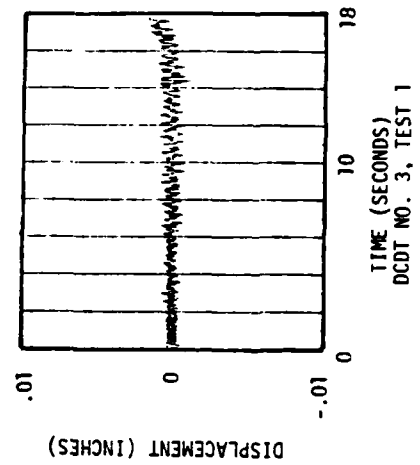
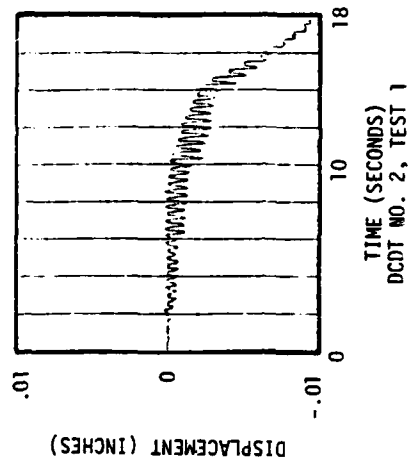
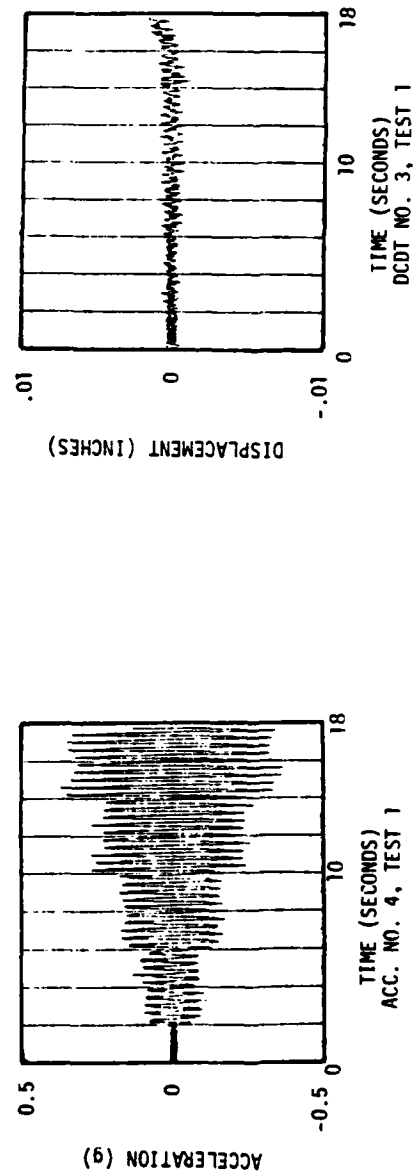
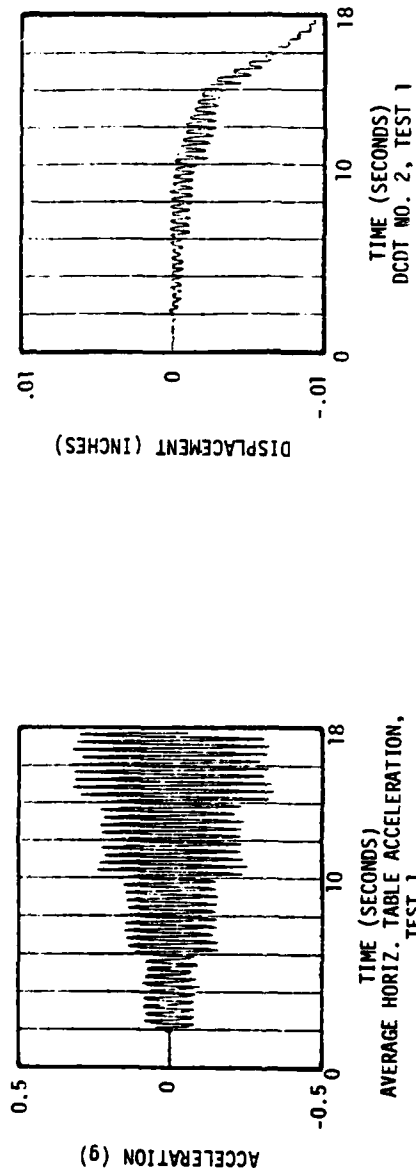


FIGURE 8-19 ACCELERATION AND DCDT TEST RECORDS FOR TEST NO. 1

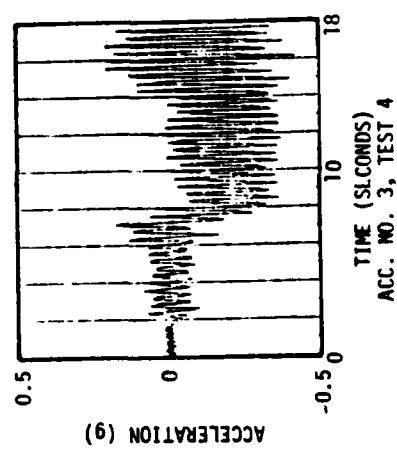
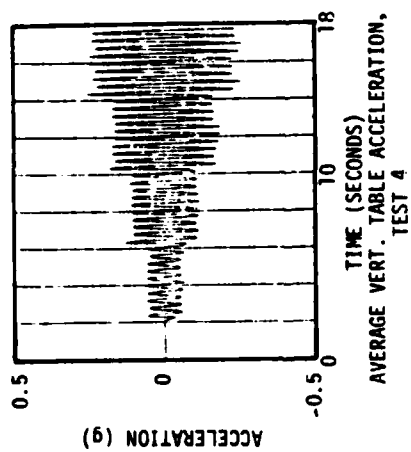
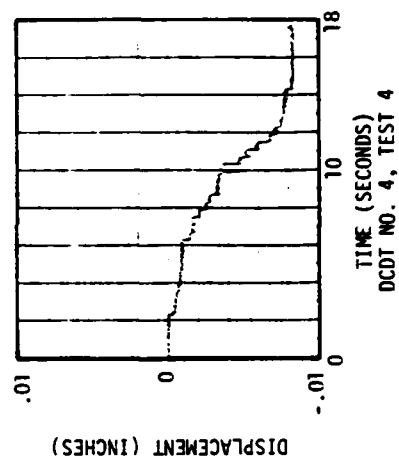
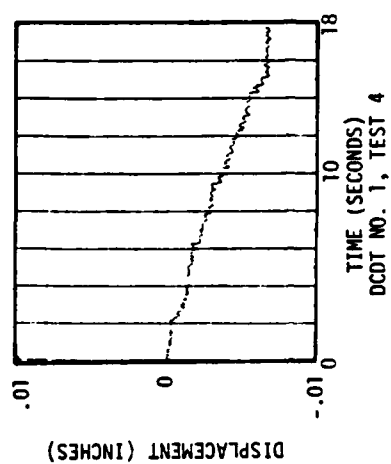


FIGURE 8-20 ACCELERATION AND DCDT TEST RECORDS FOR TEST NO. 4

$$a' = \sqrt{a_h^2 + a_v^2} \quad (8.22)$$

This value of  $a'$  is then the lower or upper bound on  $k_y$  for the slope.

In the example shown in Figure 8-20, the peak vertical table acceleration shown after 2 seconds is approximately 0.056 g. The peak horizontal table acceleration occurring at the same time, which is not shown in the figure, is approximately 0.09 g. The resultant acceleration is:

$$a' = \sqrt{(0.056)^2 + (0.09)^2} = 0.106 \quad (8.23)$$

This acceleration is an upper bound on the yield acceleration measured from the bottom of the slope.

It is interesting to note in Figure 8-20 that acceleration record No. 3 shows a marked shifting of center acceleration beginning at approximately seven seconds into the record. This occurred because the soil around this accelerometer began to move significantly at this time and the "plane" of the accelerometer rotated. The accelerometer was originally oriented vertically, so that the center axis was at a value of 1 g. If the center axis moves by .2 g, as it appears to at eight seconds, then the new center axis becomes 0.8 g. The accelerometer has been reoriented by the angle  $\theta$  from the vertical, where  $\theta$  is defined by the following expression

$$\theta = \arccos(0.8) = 36.9^\circ \quad (8.24)$$

#### Yield Accelerations

The computations described above for determining the upper and lower bounds on the yield acceleration,  $k_y$ , were performed for all tests in this testing series. The results are tabulated and compared with the

predicted values of  $k_y$  in Table 8-5. It is noteworthy that the predicted values of  $k_y$  generally fall within the bounds presented in that table. It should also be noted that for all but two of the tests, yielding was observed within 2 to 3 seconds into the record, as the first increment of acceleration was applied.

The observed values of  $k_y$  show two things:

1. There is often a significant difference between the amplitude of the accelerations at the bottom of the slope (the table) and the top of the slope, due primarily to amplification of the accelerations; and
2. There is usually a significant difference between the observed upper bound and observed lower bound, due primarily to the fact that the increments by which the acceleration amplitudes were increased were relatively large: typically larger than  $k_y$  itself.

This latter effect was minimized somewhat in the B record tests because a smaller increment of increased acceleration amplitude was used.

Due to these facts and the general technical difficulties of making accurate measurements of accelerations, it is difficult to obtain highly precise values of the observed  $k_y$  values. However, the comparisons shown in Table 8-5 serve at least to support the conclusion that no gross errors were made in computing the predicted  $k_y$  values. Furthermore, as a corollary, it may be reasonable to conclude that  $k_y$  can be computed as accurately as it can be directly measured.

One of the objectives of this research was to investigate the validity of direct vectorial superposition of the horizontal and vertical acceleration in arriving at the yield acceleration. Because of the

TABLE 8-5  
Summary of Yield Accelerations

Test No.	Time* (sec)	ky Lower Bound (g)		Predicted ky (g)	ky Upper Bound (g)	
		Top	Bottom		Top	Bottom
1	2	.015	0	.045	.1	.085
2	2	.038	0	.054	.119	.101
3	3	0	0	.045	.095	.08
4	2	.018	0	.054	.118	.106
4B	6	.129	.1	.054	.222	.198
5	2	0	0	.016	.085	.085
5A	2	.05	0	.016	.1	.09
6	2	.016	.014	.019	.122	.103
6A	1	.052	0	.019	.148	.104
7	2	0	0	.016	.095	.085
8	2	.018	0	.019	.127	.097
7X	8	.06	.035	.016	.07	.047
8X	2	.037	0	.019	.058	.019
8Y	2	.023	0	.020	.055	.021
8Z	2	.043	0	.018	.056	.018

\*"Time" refers to the time in a test record where yielding was first observed.

difficulty in pinpointing precise values of the observed  $k_y$  values, the validity of this superposition cannot be verified conclusively. However, the experimental evidence is at least consistent with the validity of this superposition.

It should also be noted that the calculated (predicted) value of  $k_y$  is quite sensitive to the near-surface  $\phi$  value, which is not easily measured with great accuracy. In view of this fact, it appears in retrospect that any error introduced by assuming validity of vectorial addition of the accelerations is much smaller than the error introduced by using imprecise  $\phi$  values in the computations. Furthermore, it appears that any error incurred by direct vectorial superposition is smaller than that which can be detected using an experimental program similar to that described herein.

In view of these conclusions it is recommended that direct superposition of simultaneous horizontal and vertical accelerations be made as outlined in this chapter if practical cases should arise where yield accelerations must be predicted.

#### Qualitative Observations

In addition to the quantitative tabulations presented in Table 8-5, it is of value to study the test records and qualitatively evaluate the performance of the slopes during dynamic loading.

The four DCDT test records for Test No. 3 are presented in Figure 8-21. Referring to the positioning of these instruments upon the slope which was shown in Figure 8-1; it is seen that DCDT's 1 and 2 are located in the upper portion of the slope, and DCDT's 3 and 4 are in the

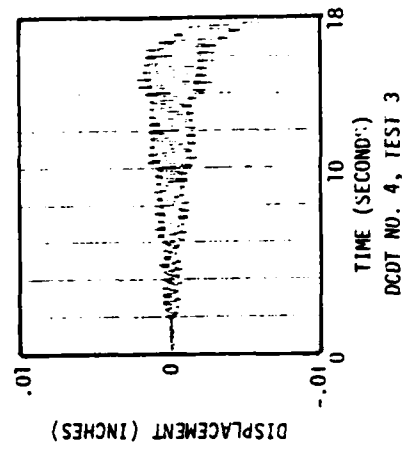
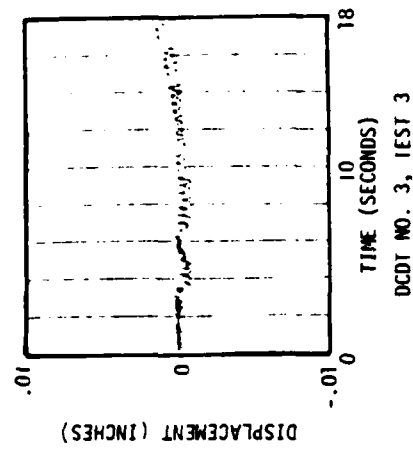
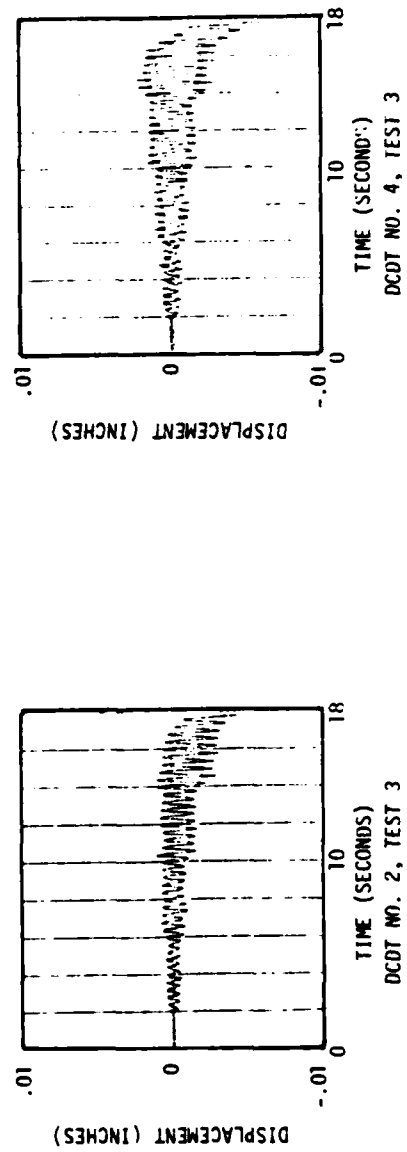
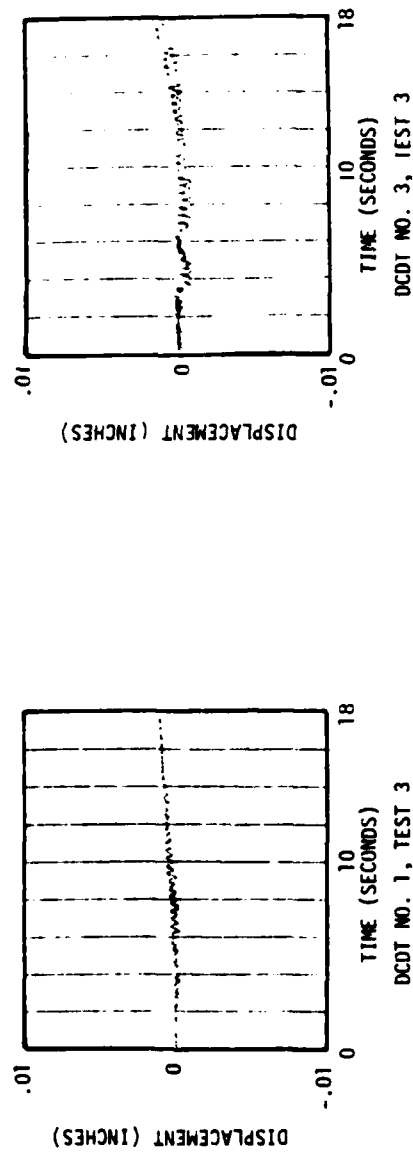


FIGURE 8-21 DCDT TEST RECORDS FOR TEST NO. 3

lower half. DCDT's 1 and 3 are vertically oriented, and DCDT's 2 and 4 are horizontal.

The two horizontal DCDT's reflect the acceleration record for Test No. 3 which was shown in Figure 8-17. Although yielding may be seen from the very beginning of these records, large permanent displacements are not seen until late in the record. This is because yielding may occur during only a small portion of each cycle of loading, and displacements do not accumulate to significant values until the larger accelerations occur.

Shown in Figures 8-22 through 8-25 are the DCDT test records for the four B record tests: 7X, 8X, 8Y, and 8Z. As was shown in Table 8-1, the only differences between these tests was in the value of the vertical component of acceleration. The vertical acceleration was zero for Test 7X, was 0.67 of the horizontal for Test 8X, etc. Because the horizontal component remained unchanged, the resultant acceleration amplitude steps were different for the different tests.

The DCDT test records for Test 7X shown in Figure 8-22 show considerably less permanent displacement than the other three tests, as would be expected. The DCDT test records for Tests 8X, 8Y, and 8Z show remarkable similarity, both in their shapes and in the amplitudes of the displacements. Theoretically, the displacements should be slightly greater for Test 8Y, and less for Test 8Z, since the vertical accelerations are slightly higher and lower for those tests. It is difficult to distinguish significant variation for these records, however.

#### Additional Observations

It should be emphasized that the placement of DCDT's on the face of

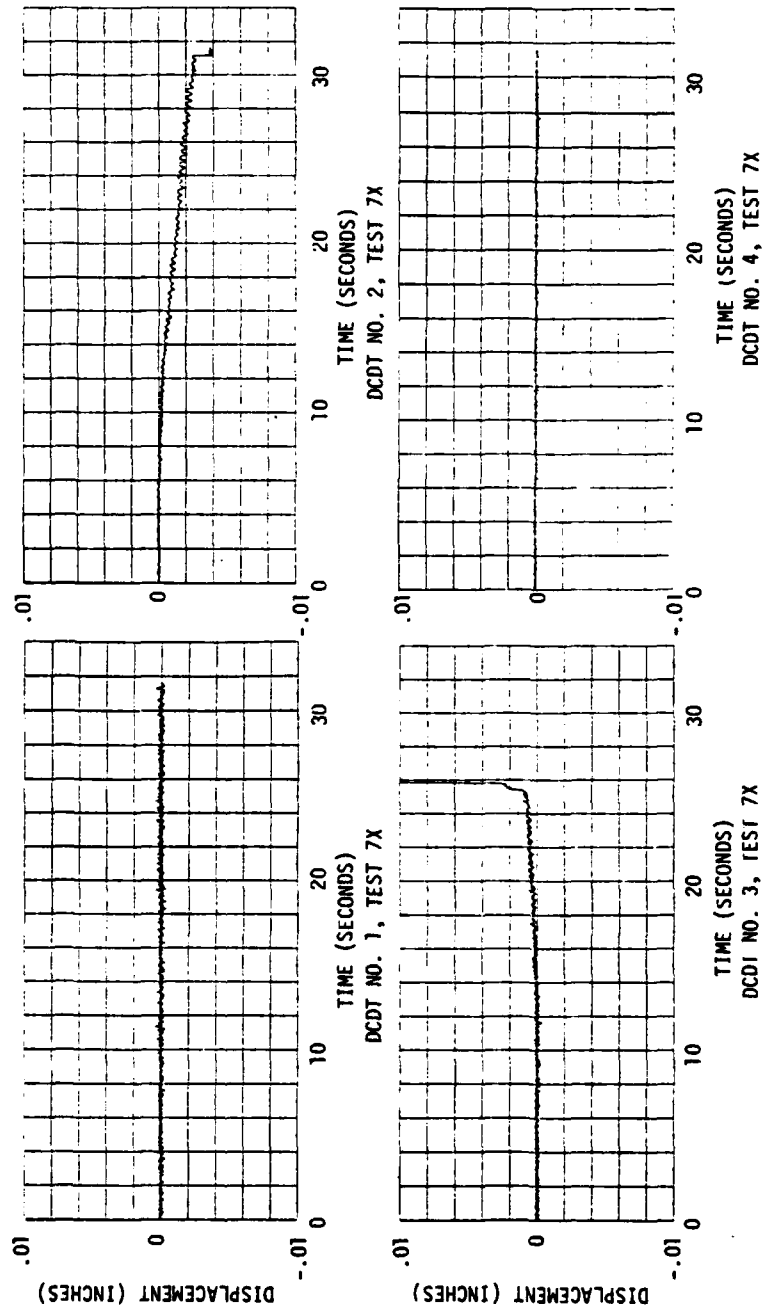


FIGURE 8-22 DCOT TEST RECORDS FOR TEST NO. 7X

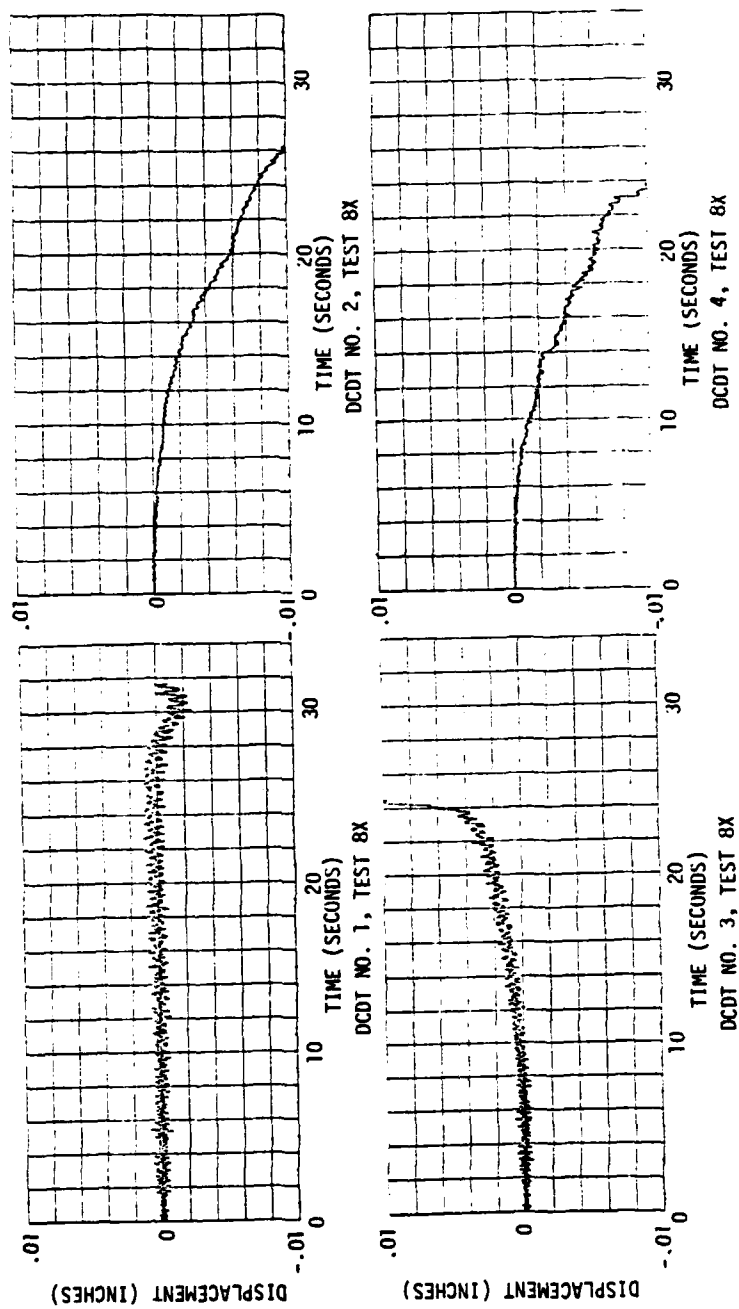


FIGURE 8-23 DCDT TEST RECORDS FOR TEST NO. 8X

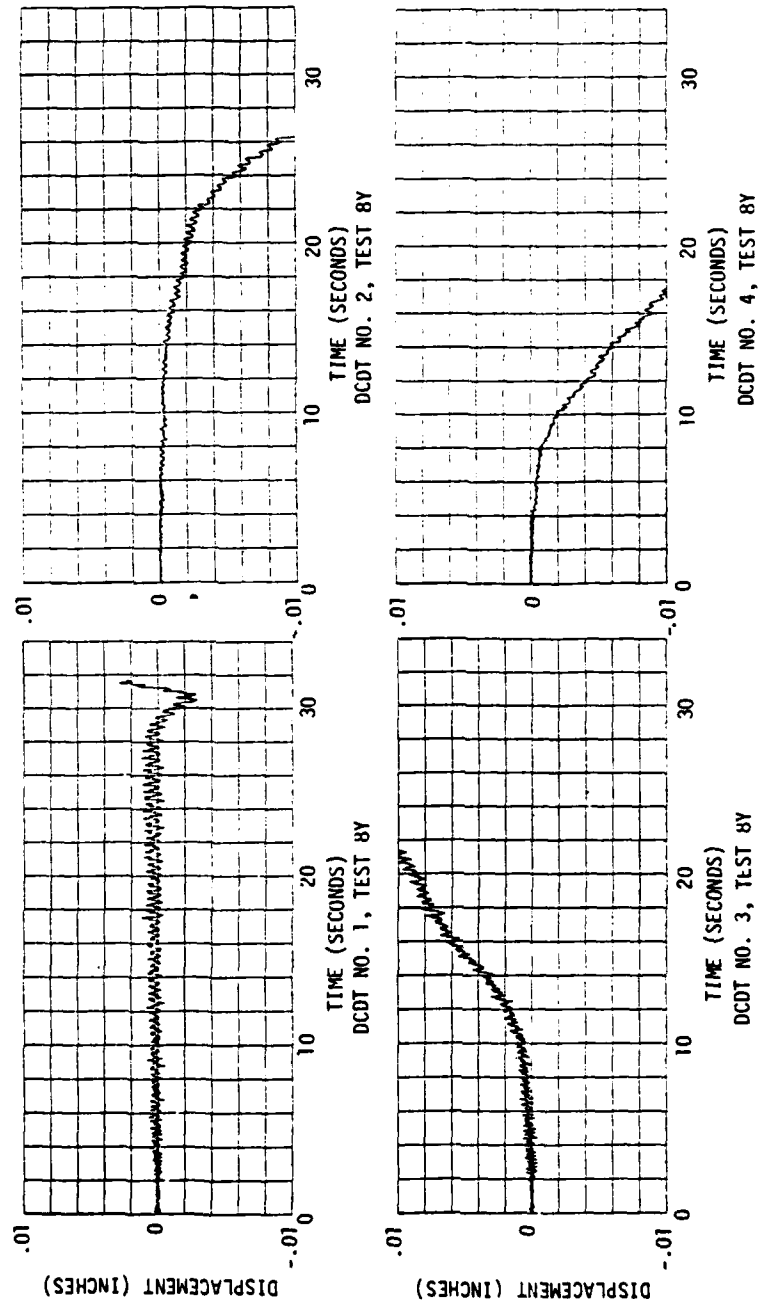


FIGURE 8-24 DCOT TEST RECORDS FOR TEST NO. 8Y

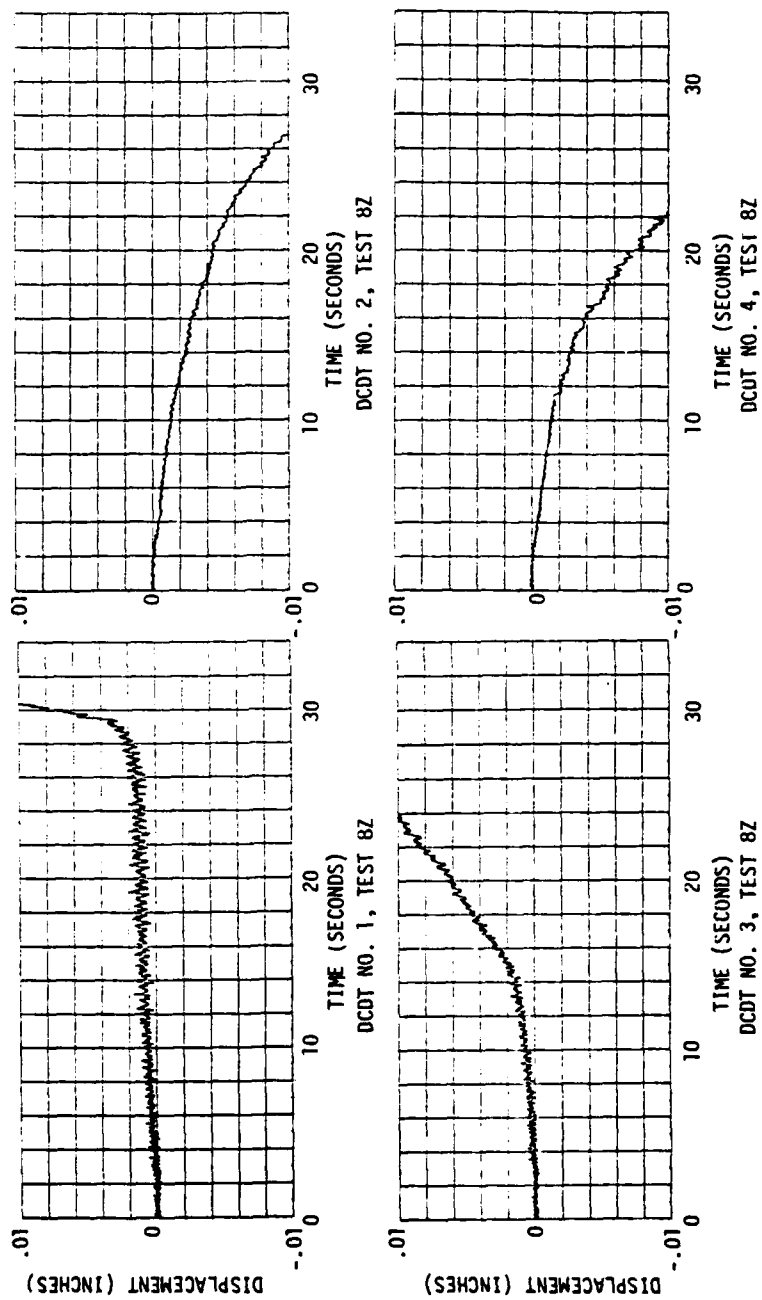


FIGURE 8-25 DCDT TEST RECORDS FOR TEST NO. 8Z

the test slopes was intended to assist in determining the point at which yielding began, and not to accurately measure displacements or strains. Because of the manner in which the DCDT core probes were carefully inserted into the soil, minimizing the disturbance to the soil structure, they are only capable of accurately measuring the very smallest displacements. As the sand grains become mobilized, they quickly flow around the core probes, thus preventing accurate measurements.

As an additional tool in this testing series, several tests were filmed with a high-speed data camera on 16 millimeter film. These films were synchronized to the base acceleration record and contained a minimum of 40 frames per cycle of loading. Thin horizontal lines were highlighted along the sides of those slopes which were photographed to provide a clear view of any large soil displacements and sand flows during dynamic loading. Additionally, a triangular "window" was cut out of one side of the test box to provide a better wide-angle view of the slope samples. These films are on file along with the other test results at the Geotechnical Engineering Office at the University of California, Berkeley.

#### Analysis of Real Slopes

The analyses of real slopes of cohesionless materials in the field, both natural and man-made, are somewhat more complex than for the carefully controlled laboratory test slopes of standard sand analyzed in this study. As discussed earlier, the predicted yield accelerations of slopes are extremely sensitive to the shear strength characteristics of the outermost slope material. The in-situ outer surface shear strengths may vary significantly in real slopes, and will be very difficult to accurately

measure. Nevertheless, it is believed that the analysis techniques described herein may be used with appropriate precautions and careful judgment to predict the yielding response of real slopes to real earthquakes.

When selecting the shear strength characteristics of the outer slope materials for analysis of a real slope, care should be taken to use the in-situ strengths. The shear strength intercept,  $s_i$ , will tend to be higher in-situ, particularly for older slopes or those with surface vegetation. The primary effect of a higher value of  $s_i$  is to move the critical sliding surface down into the slope, thus increasing the yield acceleration.

For some slopes, special direct shear tests, similar to those performed in this study, may be performed. In other slopes some other special field test may be devised to ascertain the in-situ shear strength characteristics. In either case, careful judgment should be exercised in selecting the values of  $s_i$  and  $\phi$  from the field tests to insure that the lowest measured values (and thus the most critical zones) are given maximum consideration in selecting weighted average values for analysis purposes.

#### Displacements

Seed and Goodman (1964) have also proposed a procedure for estimating total permanent displacements in slopes from yield acceleration values and dynamic acceleration records. This procedure is based on suggestions by Newmark (1963). It has been utilized and further refined by Makdisi and Seed (1977) and others. The procedure, simply stated, provides for the double integration of dynamic accelerations in excess of the yield accel-

eration to obtain values of dynamic displacement. Because displacement usually occurs during only one half of each dynamic cycle of loading, total residual displacement may be estimated by summing the incremental dynamic displacements accumulated for a particular earthquake record.

When this method is applied to real slopes, special precautions should be taken to consider the possibility that the predicted yield acceleration may decrease with progressively increasing displacements. Because the calculated yield acceleration is highly sensitive to the value used for the shear strength intercept,  $s_i$ ; the fact that the true value of  $s_i$  may change with straining should be taken into account. The variation of  $s_i$  with strain may also be evaluated from a field testing program.

It should also be noted that for the tests herein the horizontal and vertical accelerations were in phase and at the same frequency. Thus " $\omega$ " was constant for a given test. By contrast, in real slopes during an actual earthquake, the horizontal and vertical accelerations would be expected to have different and variable frequencies. Thus a numerical procedure using a computer program must be used to perform the double integration of the accelerations in excess of the yield acceleration. This integration must be performed over very small time steps, and the yield acceleration must be recomputed for each time step, as a function of  $\omega$ .

The double integration process should be repeated for various relative "starting points" for the horizontal and vertical acceleration records in order to obtain the range of residual displacement values which corresponds to these records.

### Conclusions

A large scale slope model testing program was developed to explore the effects of combined vertical and horizontal dynamic loading on the yield acceleration of sand slopes. The equipment, sample formation and instrumentation used was discussed in the first part of this chapter and in Appendix A-3.

The strength characteristics of the Monterey No. 0 sand were evaluated with special direct shear tests performed on the test slopes. The results of this evaluation are summarized in Figures 8-7 and 8-8.

The yield accelerations for the various dynamic test conditions were predicted by using an extension of an analysis method originally proposed by Seed and Goodman (1964). Equations 8.16 and 8.18 were derived to include the angle,  $\omega$ , which permits a vertical component of acceleration to be included in the analysis. By modifying the simplified technique proposed by Goodman and Seed, a simplified technique which includes vertical as well as horizontal accelerations was developed. From those equations the yield accelerations in Table 8-4 were predicted.

Using a procedure described in this chapter, the range of yield accelerations observed during the various model tests were determined, and were compared with the predicted values in Table 8-5. It was difficult to draw definitive conclusions concerning these comparisons both because of the variation in acceleration amplitude from top to bottom of the slopes, and because of the relatively large increments by which the table accelerations were increased.

It was concluded from this study that, because of these limitations and the general technical difficulties of making accurate measurements of

accelerations, it is difficult to obtain highly precise values of observed yield accelerations. Nevertheless, it appears that the yield acceleration may be predicted by the method outlined in this chapter, at least as accurately as it may be directly measured. The results summarized in Table 8-5 appear to support the conclusion that the predicted values of yield acceleration are reasonable estimates of the true values.

It is recommended that direct superposition of simultaneous horizontal and vertical accelerations be made, as outlined in this chapter, if practical cases should arise where yield accelerations must be predicted.

## Chapter 9

### Summary and Conclusions

#### Introduction

The objective of this research was to study the interaction effects of combined compression and shear loading on the response of sands to dynamic loading. Various experimental studies were performed to evaluate the response of Monterey No. 0 sand to various types of combined compression and shear cyclic loading. The behavior observed in these tests was then used to evaluate postulated theories of soil response under these combined loading conditions. The results of these studies and the main conclusions are summarized in this Chapter.

#### Effects of Combined Dynamic Loading

During the course of this research significant effects were observed during combined compression and shear cyclic loading. The primary observed effect of combined loading was the more rapid degradation of modulus with strain than would otherwise occur.

Because the effect of primary practical interest is the influence of simultaneous shear straining on the degradation of the compression modulus, it was this effect that was evaluated in detail in this study.

#### Strain Ratio Method

Two methods were developed and presented for calculating the degra-

dation of compression modulus with strain under combined loading conditions. The first of these, called the Strain Ratio Method, requires the computation of either the instantaneous or an overall average ratio of shear strain amplitude to compression (normal) strain amplitude. By entering the sets of curves presented in Figure 7-7, the additional degradation in compression modulus due to the presence of shear strain may be determined. This method requires logarithmic interpolation among the curves, depending on the value of normal compression strain amplitude and mean confining pressure.

#### Octahedral Shearing Strain Method

A simpler method, called the Octahedral Shearing Strain Method, requires that either the instantaneous or an average value of octahedral shearing strain be calculated from Equation 2-42. If the principal strains are known, the simpler Equation 2-44 may be used for this calculation. Once the octahedral shearing strain is known, the total degradation in compression modulus may be determined directly from Figure 7-6, interpolating only for the mean confining stress. This total degradation in modulus includes both the component due to normal compressive straining and that due to the presence of shear strains.

Using either of these methods a reasonable estimate of the degradation of modulus with the total straining may be obtained. This is a significant improvement over the current state of engineering practice. However, analysis of Figure 7-7 shows that the degradation in modulus due to interaction is of importance only when the shear strain is significant compared to the normal strain. In other cases the use of this technique

provides no advantage over current practice.

### Combined Loading Effects on Slope Stability

A series of large-scale shaking table tests were conducted upon slope models constructed of sand. These samples were subjected to purely horizontal or combined horizontal and vertical cyclic accelerations in an effort to determine the point at which yielding in the slopes began. The results of these tests were summarized in Table 8-5.

### Analysis Method

A method of analysis was proposed for use in practical cases where yield accelerations for slopes under combined horizontal and vertical accelerations are needed. This method is an extension of a method originally developed by Seed and Goodman (1964) for horizontal excitation alone.

The analysis method requires the calculation of a yield acceleration,  $k_y$ , from Equation 8-18 for the values of plane strain friction angle,  $\phi$ ; slope angle,  $\alpha$ ; angle of acceleration,  $\omega$ ; shear strength intercept,  $s_i$ ; the length of the slope,  $L$ ; and the density of the soil,  $\gamma_d$ . This value of  $k_y$  is calculated for several values of the depth of sliding surface,  $d$ ; and for the minimum value of the internal force,  $P$ , for those values of  $d$ . The minimum  $k_y$  is determined by an iterative process, utilizing Equations 8-16 and 8-18.

A modified, simplified approach was also presented. This simplified method requires the determination of the factor,  $\phi_{SL}$ , from Figure 8-16, and the calculation of the horizontal  $k_y$  using Equation 8-19. This value is then modified to account for the acceleration angle,  $\omega$ , by use of

Equation 8-18. An example of this latter process was presented using the shaking table strength characteristics and slope geometry, with the effect of variation of the angle,  $\omega$ , shown in Figure 8-15.

This latter, simplified method was used for the slopes and strength characteristics of this testing program, with the results presented in Tables 8-4 and 8-5.

It was concluded from this study that, because of the limitations of the testing program and the general technical difficulties of making accurate measurements of accelerations, it is difficult to obtain highly precise values of experimentally determined yield accelerations. Nevertheless, it appears that the yield acceleration may be predicted by the analytical method outlined at least as accurately as it may be directly measured. The results of this testing program, summarized in Table 8.5, support the conclusion that the analysis method proposed provides reasonable estimates of the true yield acceleration values.

It is therefore recommended that direct superposition of simultaneous horizontal and vertical accelerations be made, as outlined in Chapter 8, should practical cases arise where yield accelerations for slopes must be predicted.

## REFERENCES

- Boresi, A. P. and Lynn, P. P. (1974) "Elasticity in Engineering Mechanics," Prentice Hall, New York.
- Drnevich, V. P. (1975) "Operating Manual: Drnevich Resonant Column Apparatus," Soil Dynamics Instruments, Inc., Lexington, Kentucky.
- Goodman, R. E. (1963) "The Stability of Slopes in Cohesionless Materials During Earthquakes," Dissertation submitted in partial satisfaction of the requirements for the degree of Doctor of Philosophy, University of California, Berkeley.
- Griffin, P. M. (1980) "Influence of Shear and Compression Interaction of the Response of Sand to Dynamic Loading," Dissertation submitted in partial satisfaction of the requirements for the degree of Doctor of Philosophy, University of California, Berkeley.
- Lade, P. V. (1972) "The Stress-Strain and Strength Characteristics of Cohesionless Soils," Dissertation submitted in partial satisfaction of the requirements for the degree of Doctor of Philosophy, University of California, Berkeley.
- Makdisi, F. I. (1976) "Performance and Analysis of Earth Dams During Strong Earthquakes," Dissertation submitted in partial satisfaction of the requirements for the degree of Doctor of Philosophy, University of California, Berkeley.
- Makdisi, F. I. and Seed, H. B. (1977) "A Simplified Procedure for Estimating Earthquake-Induced Deformations in Dams and Embankments," Report No. EERC-77/19, Earthquake Engineering Research Center, University of California, Berkeley.
- Marachi, N. D. (1969) "Strength and Deformation Characteristics of Rockfill Materials," Dissertation submitted in partial satisfaction of the requirements for the degree of Doctor of Philosophy, University of California, Berkeley.
- Marachi, N. D., Chan, C. K., Seed, H. B. and Duncan, J. M. (1969) "Strength and Deformation Characteristics of Rockfill Materials," Report No. TE 69-5, Office of Research Services, University of California, Berkeley.
- Newmark, N. M. (1965) "Effects of Earthquakes on Dams and Embankments," Geotechnique, Vol. 15, No. 2.
- Rea, D. (1972) "Design and Construction of a 20 Ft. x 20 Ft. Prestressed Concrete Shaking Table," Proceedings of the FIP Symposium on Prestressed Concrete in Seismic Structures, Tbilisi, Georgia, USSR.

Rea, D. and Penzien, J. (1972) "Structural Research on Earthquake Simulation," Proceedings 41st Annual Convention of the Structural Engineers Association of California, pp. 15-22.

Seed, H. B. and Goodman, R. E. (1964) "Earthquake Stability of Slopes of Cohesionless Soils," Journal of the Soil Mechanics and Foundations Division, ASCE, Vol. 90, No. SM6, Proc. Paper 4128, November, pp. 43-73.

Appendix A  
Testing Apparatus

The following testing apparatus were utilized in this study:

- A-1      Resonant Column-Torsional Shear Apparatus
- A-2      Hollow Cylinder Test Apparatus
- A-3      Test Box for Slope Model Studies

Appendix A-1Resonant Column-Torsional Shear Apparatus

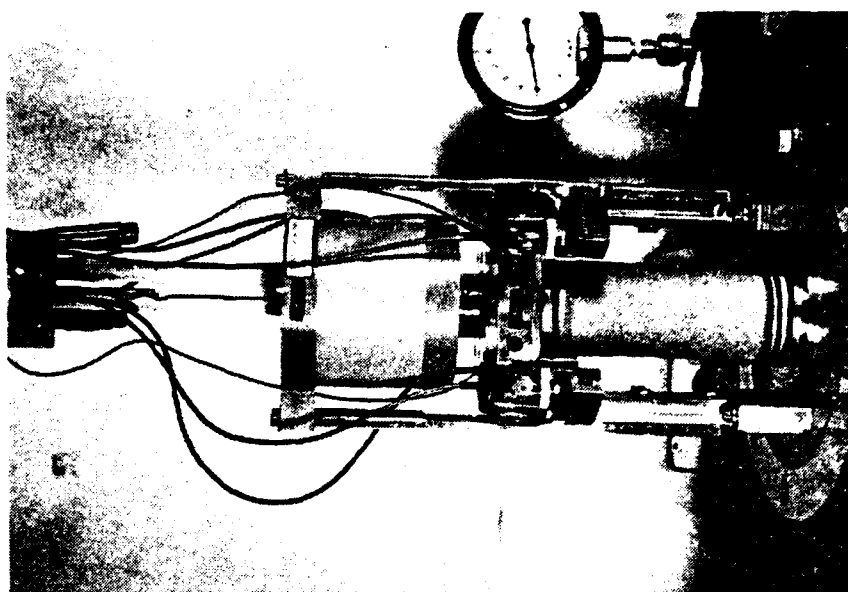
## Introduction

The Resonant Column-Torsional Shear testing apparatus used in this study was developed by Professor Vincent P. Drnevich of the University of Kentucky. The apparatus is capable of exciting cylindrical specimens either vertically or torsionally, or in both modes simultaneously. The testing set-up and a close-up of a sample prepared for testing are shown in Figure A1-1.

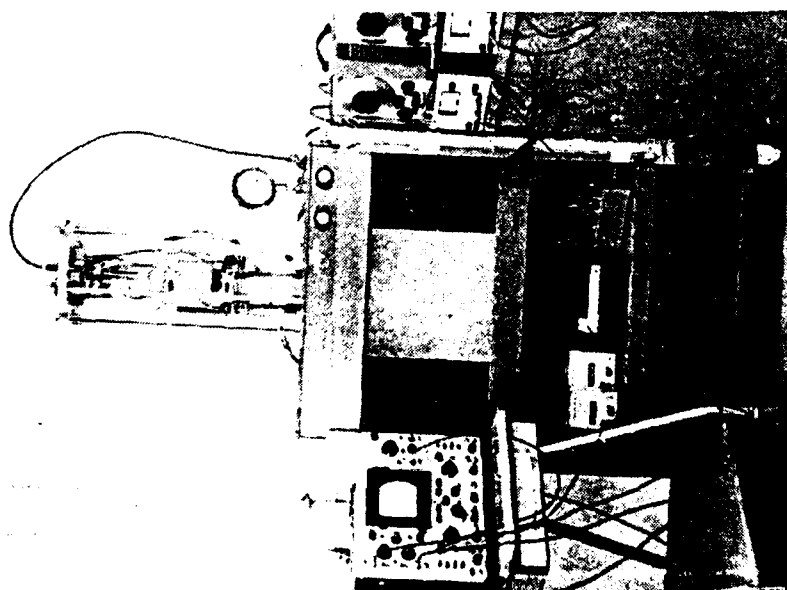
As seen in Figure A1-1(b), vertical excitation is obtained by applying an A.C. voltage across the large vertical coil mounted atop the specimen. The application of this voltage creates a sinusoidally varying magnetic field which interacts with the field of the large permanent magnet mounted to the counterbalanced framework, resulting in a sinusoidally varying vertical force being applied upon the specimen.

By varying the frequency and amplitude of the A.C. voltage, the cyclic stress applied upon the specimen can be controlled. A vertically oriented accelerometer is mounted within the cap assembly of the specimen, which measures the acceleration response to the applied cyclic stress.

Similarly, torsional stress is applied to the specimen by applying an A.C. voltage across the four torsionally oriented coils which are wired in series and mounted upon the counterbalanced framework alongside the specimen. The resulting electromagnetic field reacts with the magnetic field of the four torsionally oriented permanent magnets affixed to the cap assembly of the specimen, creating a cyclic torsional stress.



(b)



(a)

FIGURE A1-1 RESONANT COLUMN TESTING APPARATUS AND SETUP (a) AND  
CLOSE-UP OF SAMPLE PREPARED FOR TESTING (b)

A torsionally oriented accelerometer is mounted in the cap assembly for measuring the acceleration response to the applied torsional cyclic stress. Because the two loading systems are mechanically independent, it is possible to simultaneously excite the specimen vertically and torsionally without mechanical interaction of the loading.

#### Test Set-up

The complete test set-up is shown in Figure A1-1(a). Just below the testing apparatus on the first shelf of the cabinet is a 1 ft cube concrete block. This block acts as a counter balance for the applied cyclic loads, and is securely bolted to the steel framed cabinet. The base of the testing apparatus, including the framework alongside the specimen and the large vertical permanent magnet are securely attached to this counterbalancing concrete block.

The testing apparatus is completely enclosed within an airtight lucite cell. This enclosure allows for the application of cell confining pressures up to approximately 7 KSC. Additionally, the specimen may be confined with intercell vacuum of less than 1 KSC. Although the equipment is designed to allow both sample saturation and the use of water or other fluid for applying the external cell confining pressure, these options were not utilized in this testing series.

The A.C. voltages used to excite the specimens in both the vertical and torsional directions were produced by a low-frequency sine wave generator and power amplifier combination. The two generator/amplifier combinations are shown in the right side of Figure A1-1(a), above the utility cabinet. The sine wave generators used in this testing series

were Hewlett-Packard Model 202C, and the power amplifiers were Hewlett-Packard Model 6824A.

The output of these power amplifiers is wired to a control box which allows the operator to quickly switch the voltage to the coils when desired. This control box, which is located on the right hand side of the second shelf below the testing apparatus in Figure A1-1(a), also provides a sampling point for precise measurement of the amplitude and frequency of the voltages applied to the coils.

Located just to the left of the control box in the center of the second shelf is a Fluke Model 1900a frequency counter used for precise frequency measurements. The applied A.C. voltage is displayed on the vertical plates of an oscilloscope; in this study a Tectronics Model 565 Dual Beam Oscilloscope was used, and is shown on the left side in Figure A1-1(a). A dual beam oscilloscope was helpful in this testing program because it allowed for simultaneous monitoring of the vertical and torsional response during combined loading.

The two accelerometers mounted in the cap assembly are Colombia electrolytic devices, Model 200-1-H, and require a charge amplifier or cathode follower to condition their outputs before they can be read by conventional high impedance measuring equipment. Two charge amplifiers were used to supply an acceleration response signal to the oscilloscope. These charge amplifiers, which are shown on the left side of the second shelf in Figure A1-1(a), are Colombia Model 4102.

The output of the charge amplifiers are applied to the horizontal plates of the oscilloscope to produce Lissajous figures with the voltages applied to the driving coils. The acceleration amplitude may also be

measured using the oscilloscope display.

Cylindrically shaped samples are formed with a rubber membrane and conventional forming molds. The vertical weight of the cap assembly is offset with a constant-force spring shown in the top of Figure A1-1(b).

Determination of the strain amplitudes and damping factors from the raw test data is described in Chapter 4; and the determination of dynamic compression and shear moduli is discussed in Appendix C-3. Several typical data sheets are shown in Figures A1-2 through A1-4, and the test results from this raw data are presented in Appendices B1 through B3.

UNIVERSITY OF CALIFORNIA  
 RESONANT COLUMN - TORSIONAL SHEAR  
 DATA SHEET

Date 5/1/79Operator P. GRIFFIN Test No. 1A-1,2,3 Page 1 of 1Wb1 1015.57Wb2 345.00Spill 0Wal 226.97Wa2 210.90

Ws = W1 + W2 - Spill

W1 788.60W2 134.10Ws = 922.70Diameter = 2.795  
2.805Length = 5.398Confining = 3.6  
Pressure

Rec #	Mode	Coil	Accel	Reson	Rec #	Mode	Coil	Accel	Reson	DCF
	LoRT	Volt	Volt	Freq		LoRT	Volt	Volt	Freq	
1A-1	$\sigma_c = 0.5$									
1	L	2.7	52	324.4	3	L	20	205	446.2	
(48 hrs)										
1(a)	L	3.3	58	331.9	4	L	40	395	446.6	
				DCF 16%						
D	L	100	64	469.4	5	L	80	760	446.4	
1(b)	L	3.2	58	332.5	6	L	200	1700	445.3	
rupture hardware										
1(c)	L	3.2	63	327.9	D	L	1000	1020	629.7	25.5%
1A-2	$\sigma_c = 2.0$									
1	L	2.8	41	406.7	(60)	L	200	1880	445.6	
				DCF 148%						
D	L	100	59	575.2	7	L	400	3770	443.3	
1(a)	L	3.2	43	406.6	8	L	800	7.2K	439.5	
1A-3	$\sigma_c = 3.5$									
1	L	3.2	39	443.6	9	L	2K	16.75K	434.4	
				DCF 252%						
D	L	100	103	627.3	10	L	4K	31K	421.7	
1(a)	L	3.3	37	444.1	11	L	8K	49.5K	414.5	
2	L	7.8	82	466.1						

FIGURE A1-2 DATA SHEET FOR RESONANT COLUMN  
 TEST NO. 1A-3

UNIVERSITY OF CALIFORNIA  
 RESONANT COLUMN - TORSIONAL SHEAR  
 DATA SHEET

Date 6/25/77Operator PMGTest No. 12B-2Page 1 of 3Wb1 1039.98Wb2 815.90Spill 0.64Wal 286.82Waz 618.32

Ws = W1 + W2 - Spill

W1 753.16W2 197.58Ws = 950.10Diameter = 2.785"Length = 5.62'Confining = 2.0  
Pressure

Rec #	Mode LorT	Coil Volt	Accel Volt	Reson Freq	Rec #	Mode LorT	Coil Volt	Accel Volt	Reson Freq	DCF
1	L	4	31	298.9	1	L	4	61	392.3	
2	T	4	36	107.4	2	L	8	120	391.5	
9	L	8.4	120	391.2	D	L	100	68	554.8	17%
10	T	20	176	146.4	2a	L	8	120	391.6	
11	L	8.2	120	391.2	3	T	4	30	146.4	
12	T	40	345	146.3	4	T	8	64	146.3	
13	L	8.2	120	391.2	D	T	100	21	207.0	5.25%
14	T	80	650	145.9	4a	T	8	65	146.3	
15	L	8.4	120	390.3	S	L	8	120	392.0	
16	T	200	1.37K	144.8	6	T	4	33	146.4	
17	L	8.6	120	389.8	7	L	8.4	120	391.8	
18	T	400	2.35K	143.5	8	T	8.8	68	146.3	

FIGURE A1-3(a) DATA SHEET FOR RESONANT COLUMN  
 TEST NO. 12B-2

UNIVERSITY OF CALIFORNIA  
 RESONANT COLUMN - TORSIONAL SHEAR  
 DATA SHEET

Date 6/26/79Operator PMG Test No. 12B-2 Page 2 of 3

Wb1 \_\_\_\_\_

Wb2 \_\_\_\_\_

Spill \_\_\_\_\_

Wal \_\_\_\_\_

Wa2 \_\_\_\_\_

Ws = W1 + W2 - Spill

W1 \_\_\_\_\_

W2 \_\_\_\_\_

Ws = \_\_\_\_\_

Diameter = \_\_\_\_\_

Length = \_\_\_\_\_

Confining =  
Pressure

Rec #	Mode LorT	Coil Volt	Accel Volt	Reson Freq	Rec #	Mode LorT	Coil Volt	Accel Volt	Reson Freq	DCF
19	L	8.6	120	388.5	31	L	200	2.6K	386.8	
20	T	800	8.9K	141.5	32	T	200	1.3K	141.9	
21	L	9.6	120	386.7	33	L	215	2.6K	386.1	
22	T	2K	7.2K	137.2	34	T	400	2.25K	140.5	
NO TORS 23	L	NO TORS 8	NO TORS 120	NO TORS 389.7	35	L	225	2.6K	384.8	
24	L	20	305	389.7	36	T	800	4K	138.9	
25	L	40	620	389.2	37	L	250	2.6K	383.4	
26	L	80	1.23K	388.6	38	T	2K	8K	135.6 <del>134.1</del>	
27	L	200	2.53K	387.0	39	L	310	2.6K	379.1	
28	T	40	320	143.3	40	T	4K	11.5K	134.0	
29	L	200	2.6K	387.0	41	L	300	2.6K	372.9	
30	T	80	590	143.0	42	T	8K	17K	126.3	

FIGURE A1-3(b) DATA SHEET FOR RESONANT COLUMN  
 TEST NO. 12B-2 (continued)

UNIVERSITY OF CALIFORNIA  
RESONANT COLUMN - TORSIONAL SHEAR  
DATA SHEET

Date 6/26/79

Operator PMG

Test No. 128-2

Page 3 of 3

Wb1 \_\_\_\_\_

Wb2 \_\_\_\_\_

Sp111 \_\_\_\_\_

Wal \_\_\_\_\_

Wa2 \_\_\_\_\_

$$W_s = W_1 + W_2 - Spill$$

w1 \_\_\_\_\_

W2 \_\_\_\_\_

WS =

Diameter =

Length =

Confining =  
Pressure

[illegible]

FIGURE A1-3(c) DATA SHEET FOR RESONANT COLUMN  
TEST NO. 12B-2 (continued)

UNIVERSITY OF CALIFORNIA  
 RESONANT COLUMN - TORSIONAL SHEAR  
 DATA SHEET

Date 7/30/77Operator F.M.S. Test No. 18CD-3 Page 1 of 1Wb1 1271.32Wb2 103.43Spill 1.30Wal 344.30Wa2 816.03

Ws = W1 + W2 - Spill

W1 727.60W2 215.40Ws = 941.04

Wb1 - 5649  
 Wb2 - 1037

Diameter = 2 TIGLength = 5615Confining = 5.5 KSI  
 Pressure

Rec #	Mode LorT	Coil Volt	Accel Volt	Reson Freq	Rec #	Mode LorT	Coil Volt	Accel Volt	Reson Freq	DCF %
7	T	400	3K	158.2	TEST 1	18CD-1 T	4	56	104.7	
8	T	800	4.8K	156.2	D	T	100	22	148.1	5.5%
9	T	2K	9K	153.0	1a	T	4	<del>56</del> 52	105.0	
10	T	4K	13K	150.4	TEST 1	18CD-2 T	4	26	142.5	
11	T	8K	19K	146.2	D	T	100	22	201.5	5.5%
12	T	11K	23K	144.0	TEST 1	18CD-3 T	4	44	159.8	
					2	T	8	90	160.0	
					3	T	20	220	160.2	
					D	T	100	23	226.7	5.75%
					4	T	40	435	160.2	
					5	T	80	800	159.9	
					6	T	200	1.8K	159.0	

FIGURE A1-4 DATA SHEET FOR RESONANT COLUMN  
 TEST NO. 18C-3

Appendix A-2Hollow Cylinder Test Apparatus

The thin-walled hollow cylinder testing apparatus used in this testing program was a modification of a static loading device originally developed by Professor Poul V. Lade of the University of California at Los Angeles and Professor J. M. Duncan of the University of California at Berkeley (Lade, 1972). A front view of the testing apparatus showing the control panel is shown in Figure A2-1, and a diagram of the main loading chain is shown in Figure A2-2. The various numbered components from the load chain diagram are listed in Table A2-1.

This testing apparatus is capable of cyclic, stress-controlled loading in both the vertical and torsional directions, both separately and simultaneously. When vertical and torsional loading are applied simultaneously, both cyclic excitations are at the same frequency, but may be out of phase. The apparatus is capable of operating at any frequency between approximately 0.2 Hertz and 20 Hertz. All tests in this testing series were performed at a frequency of approximately 0.3 Hertz.

This apparatus is capable of loading hollow cylinder specimens cyclically at a peak-to-peak stress of up to 100 psi vertically and torsionally, simultaneously.

Loading System

Simply stated, dynamic load is applied to the test specimen as follows:

1. A variable speed motor, controlled on the front panel, operates at the desired frequency of loading (i.e. at 0.3 Hertz).
2. Two offset cam assemblies which are attached to the shaft of

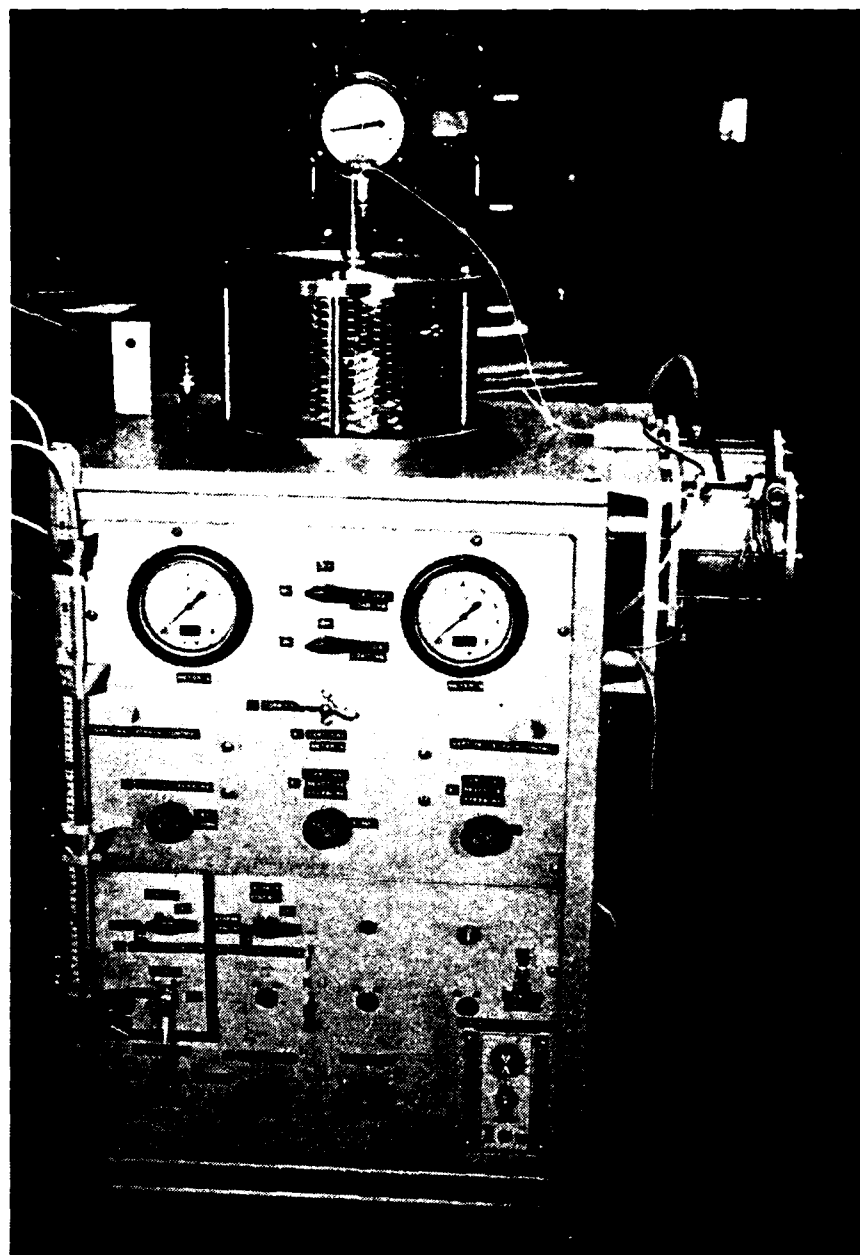


FIGURE A2-1 HOLLOW CYLINDER TESTING APPARATUS  
AND CONTROL PANEL

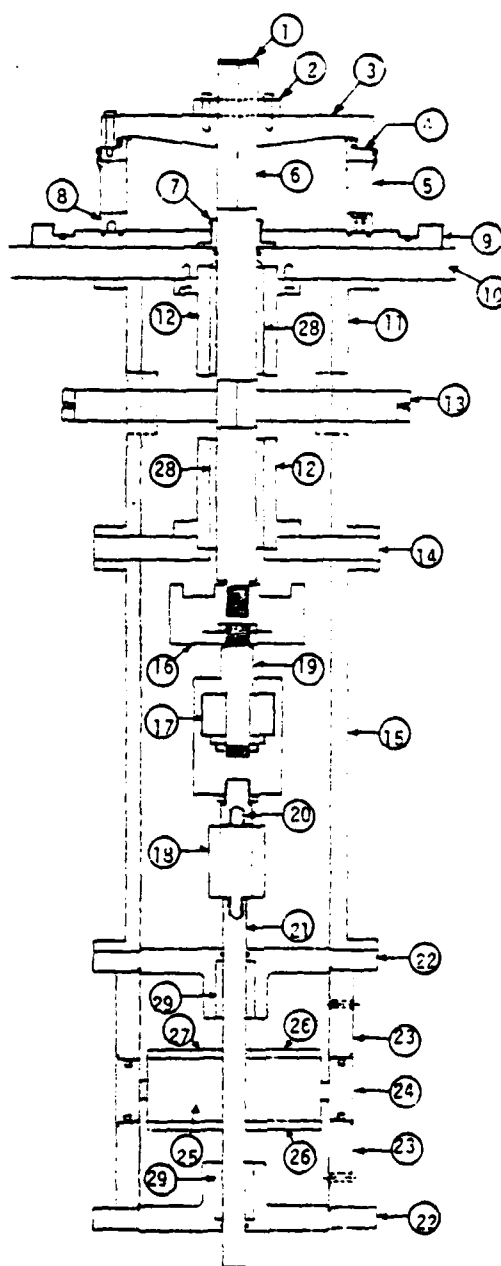


FIGURE A2-2 DETAIL OF LOAD CHAIN OF HOLLOW CYLINDER TESTING APPARATUS

TABLE A2-1

## Components of Hollow Cylinder Testing Apparatus

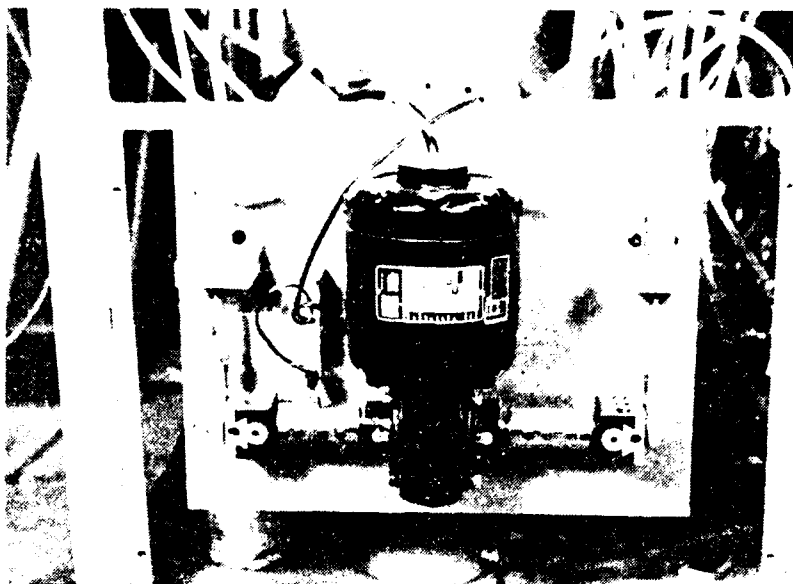
1. Proximeter Target
2. Center Shaft - Sample Top Clamping Assembly
3. Sample Top Piece
4. Sample Cap
5. Sample In Rubber Membrane
6. Center Shaft
7. Bellofram Rubber Cell Seal
8. Sample Base
9. Sample Bottom Plate
10. Top of Cabinet
11. Upper Standard Framework
12. Center Shaft Bearing Holders (2)
13. Torsional Moment Arms
14. Center Standard Plate
15. Lower Standard Framework
16. Vertical Load Cell
17. Thrust-Tension Joint
18. Double Ball Joint
19. Spacer Shaft
20. Spacer Shaft
21. Center Shaft of Double Acting Cylinder (Thompson Ball Shaft)
22. Top and Bottom Plates of Double Acting Cylinder (2)
23. Top and Bottom Walls of Double Acting Cylinder (2)

- 24. Center Wall of Double Acting Cylinder
- 25. Piston of Double Acting Cylinder
- 26. Piston Face Plates of Double Acting Cylinder (2)
- 27. Bellofram Rubber Membranes of Double Acting Cylinder (2)
- 28. Rotolin Center Shaft Bearings (2)
- 29. Thompson Ball Bearings (2)

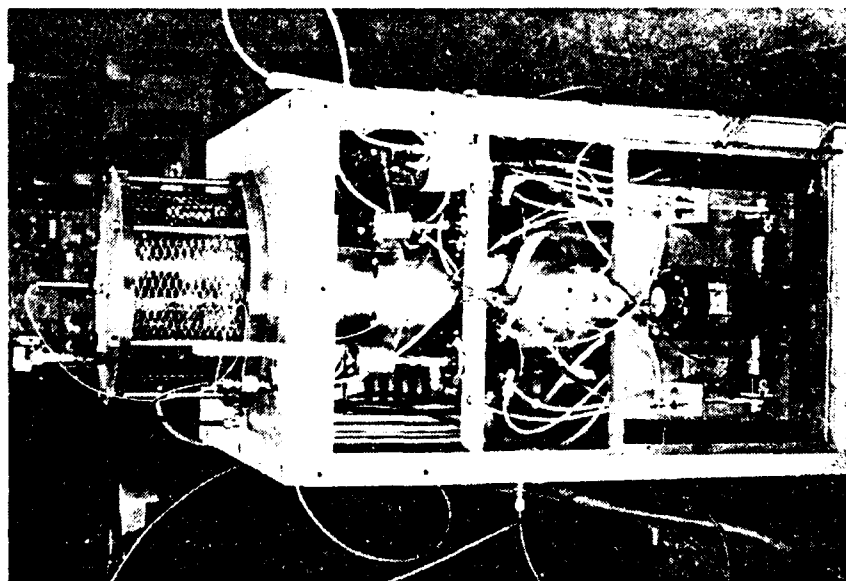
the variable speed motor cause two pistons to traverse into and out of two small pressure regulators in a cyclic manner, at the same frequency as the motor.

3. The output of the two small pressure regulators are fed to the control of two large pneumatic volume booster relays which are fed with 100 psi air pressure and 1/2-inch supply lines.
4. The output of these pneumatic volume booster relays are fed into two large reservoir cylinders which contain an air-oil interface and a supply of low-viscosity loading oil.
5. The output of one of the two large cylinders is then fed directly to the lower half of the vertical double acting cylinder, while the output of the other cylinder is fed directly to one of two torsionally balanced torsional loading cylinders.
6. The cyclic pressure in the lower half of the vertical double acting cylinder reacts with the constant pressure in the upper half of that cylinder, resulting in a sinusoidally varying force which is transmitted through the center shaft to the sample top piece, and thus to the sample.
7. The cyclic pressure in one of the two torsional loading cylinders reacts with the constant pressure in the other cylinder, resulting in a torsional, sinusoidally varying stress which is transmitted through the torsional moment arms and the center shaft to the sample top piece, and thus to the sample.

A photograph of the left side of the testing apparatus showing the variable speed motor, offset cams, small pressure regulators, and the large pneumatic volume booster relays is shown in Figure A2-3. The speed



(b)



(a)

FIGURE A2-3 VIEW OF LEFT SIDE OF HOLLOW CYLINDER TESTING APPARATUS (a)  
AND CLOSE-UP OF DYNAMIC LOAD CONTROL SYSTEM (b)

control for the variable speed motor is visible in the lower right corner of the front control panel in Figure A2-1.

Careful examination of Figure A2-3(a) shows that the two pneumatic volume booster relays, which are mounted on the cross-brace in the center of the photograph are vented at the control port at their tops by muffled, pin type vent valves. This is done because the small pressure regulators are not very efficient at venting air pressure when their regulated pressure is dropped, and they need additional externally provided venting to keep their time constants low during that portion of the loading cycle.

There are several details of interest in Figure A2-3(b). Close examination of the shaft couplers used between the center shaft of the variable speed motor and the offset cams reveals a small micro-switch mounted on the upper coupling. This microswitch was installed to provide a simple means of insuring that cyclic loading begins and ends at the same place in the loading cycle for each test. The switch is normally adjusted so that loading begins and ends at the balance point at the center of the sine wave of loading.

The phase lag between vertical and torsional loading is easily adjusted by adjusting the relative rotation of the offset cams with the shaft couplings. The offset cams are shown precisely in phase in the photograph.

The balance pressure at the center of the sine wave of loading is adjusted by positioning of the shaft between the offset cam and the piston of the small pressure regulator. Lengthening the shaft will result in a higher balance pressure. Care must be used when this adjustment is made that the selected balance pressure will allow sufficient "range" of peak-

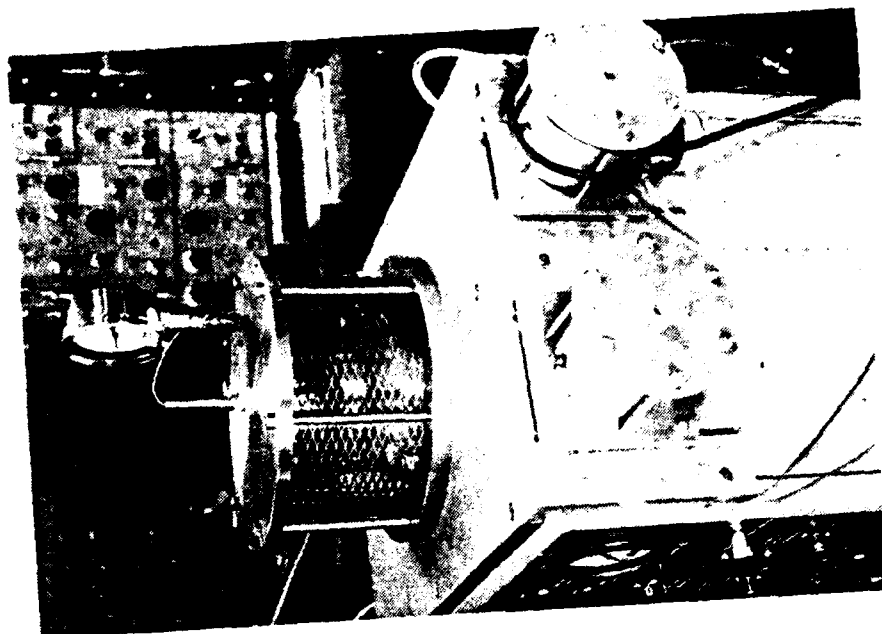
to-peak pressure to accommodate the range of load anticipated in each test.

A photograph showing the rear of the testing apparatus is provided in Figure A2-4(a); and a photograph showing the right side and the two torsional loading cylinders is presented as Figure A2-4(b). A 3/4-inch pressure hose may be seen at the rear of the test cabinet. This hose provides air pressure for the loading system in this apparatus.

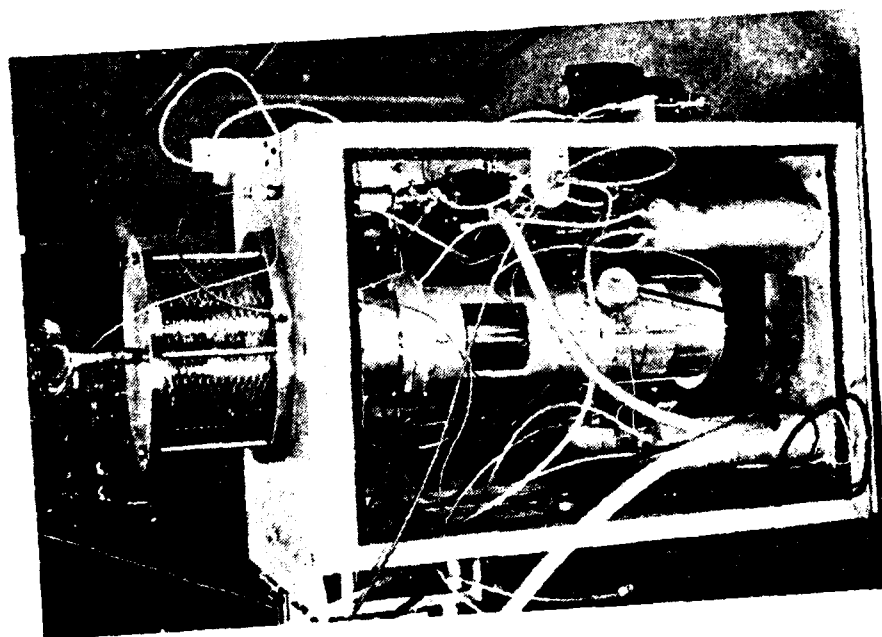
The two large reservoir cylinders, containing the air-oil interface, are in the bottom of the cabinet, out of the view of the photographs. Each cylinder is approximately seven inches in diameter and approximately fourteen inches high. It should be noted at this time that the use of air-oil cylinders and oil in the loading cylinders was provided in this testing apparatus so that it could also be used for strain-controlled static testing. If the apparatus was intended for use only for stress-controlled testing, it would have been quite possible (and desirable) to feed the output of the pneumatic volume booster relays directly into the loading cylinders, using air only.

The vertical double acting cylinder is visible in the center of Figure A2-4(a) near the bottom. A small differential pressure transducer is visible at the top of this cylinder. An identical differential pressure transducer is visible on the under-side of the right torsional loading cylinder in Figure A2-4(b). It is these two transducers which are calibrated to provide a measure of the vertical and torsional stress applied upon the specimens during testing.

Torsional strain is measured with a small LVDT mounted with long hose-clamps directly upon the sample (not visible in photographs). The vertical strain is measured with a proximeter device, which may be seen



(b)



(a)

FIGURE A2-4 VIEW OF REAR (a) AND RIGHT SIDE OF HOLLOW CYLINDER TESTING APPARATUS SHOWING TORSIONAL LOADING CYLINDERS (b)

on the top of the outer pressure cell in Figure A2-4(b).

External cell pressure is measured with the pressure gage mounted directly behind the proximeter on the top of the pressure cell.

The levels of constant pressure are maintained in the upper half of the vertical double acting cylinder and in one of the torsional loading cylinders by means of pressure regulators controlled on the front control panel. To ensure that constant pressure is maintained during loading, two reservoir cylinders are provided in series with the pressure lines. These cylinders are visible at the bottom of the cabinet in Figure A2-4(a) on the two sides of the cabinet. It should be noted that two pneumatic volume booster relays would have served equally well in this position.

The vertical load cell shown in Figure A2-2 is used primarily for calibration purposes, for adjustment purposes and to estimate the magnitude of mechanical friction developed in the load chain. The thrust-tension joint and the double ball joint, which are also shown in that figure, are designed to de-couple the vertical and torsional loading applied to the center shaft. The double ball joint corrects any small misalignment between the vertical double acting cylinder and the center shaft, and the thrust-tension joint allows transfer of vertical normal stresses to the center shaft, but rotates freely, preventing any torsional stresses from transmitting to the vertical cylinder.

The two torsional loading cylinders transfer their load to the torsional moment arms by means of 1/4-inch cables 18-inches long. Resultant lateral forces from these cables are balanced out by the two large Rotolin bearings through which the center shaft passes.

Recording of vertical stress and strain during this testing program

was done on a Hewlett-Packard Model 7046A xy-recorder. Torsional stress and strain and vertical load cell stress were recorded on a Sanborn Model 150 strip chart recorder. Examples of several tests results are presented in Figure A2-5.

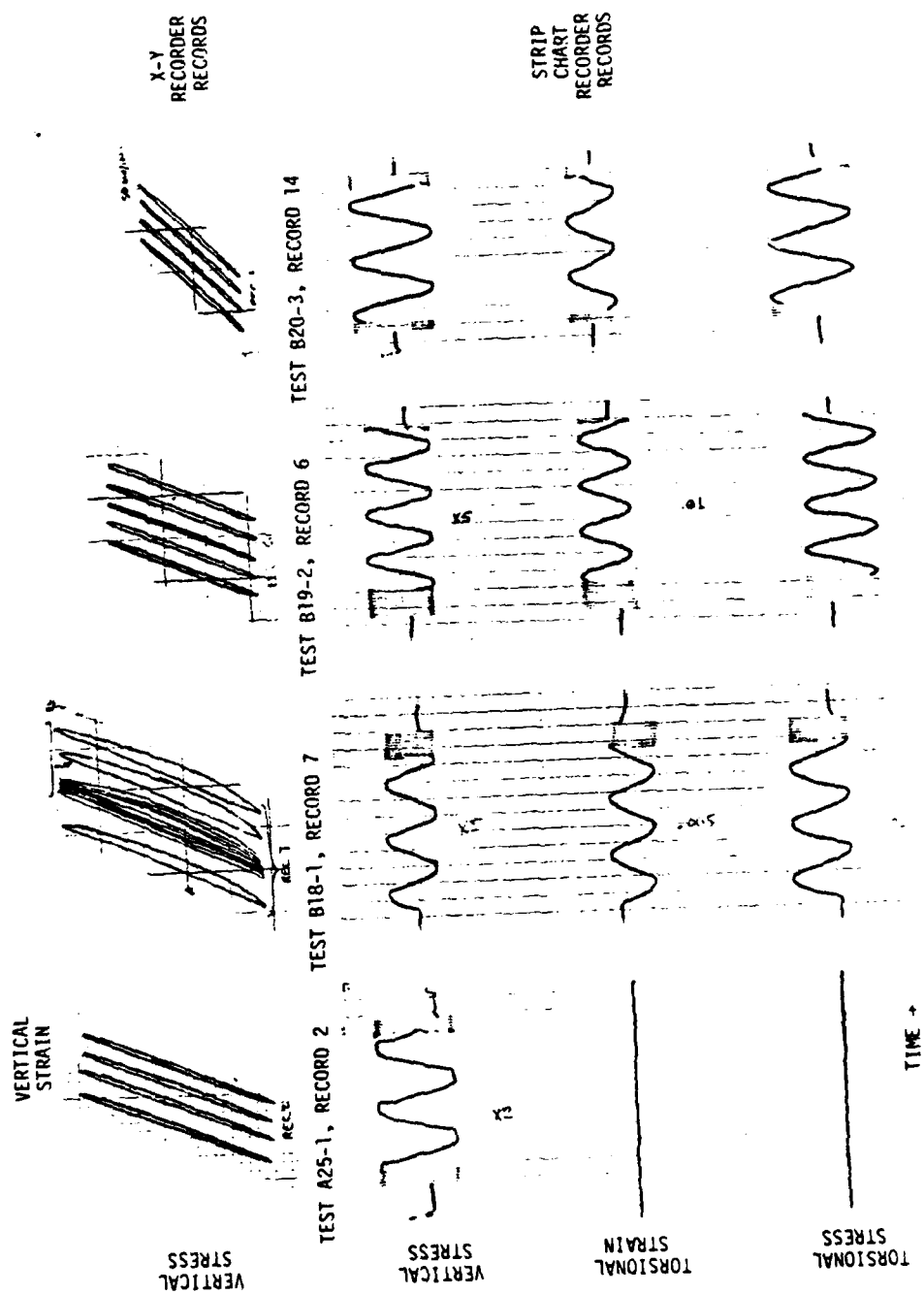


FIGURE A2-5 TEST RECORDS FOR 4 TYPICAL HOLLOW CYLINDER TESTS

### APPENDIX A3

#### Test Box for Slope Model Studies

The slope model studies were performed in a wooden test box affixed to the 20 ft x 20 ft shaking table at the Earthquake Simulator Laboratory, Earthquake Engineering Research Center, University of California, Berkeley, California. The shaking table is capable of reproducing with excellent accuracy dynamic accelerations, velocities, or displacements stored on magnetic tape or disk. The test box was designed both to contain the sand test slopes and to efficiently transfer the dynamic table motions to the slope models.

A schematic diagram of a typical slope specimen is shown in Figure A3-1. The inner dimensions of the test box, as illustrated in this figure, are approximately 84.2 in long x 42.5 in wide x 21.7 in high. A spacer board has been added as shown in the figure to reduce the total volume of sand needed for the construction of a test specimen. This spacer board, which is positioned at an angle of approximately 45° with the horizontal, is approximately 15.8 in on a side. Also visible in Figure A3-1 is a 2 in steel angle reinforcing system on the outer edges of the test box. This reinforcing system provides rigidity to the outer walls of the test box.

A view of the test box affixed to the shaking table is shown in Figure A3-2(a). As the box was placed upon the table, a layer of high-strength "hydrostone" cement mortar was placed between the box and the table. The box was then firmly bolted down to the table by seven 1-1/2 in diameter steel bolts. Three of these bolts were tightened against a 1/4 in thick steel plate which was placed in the bottom of the box, and

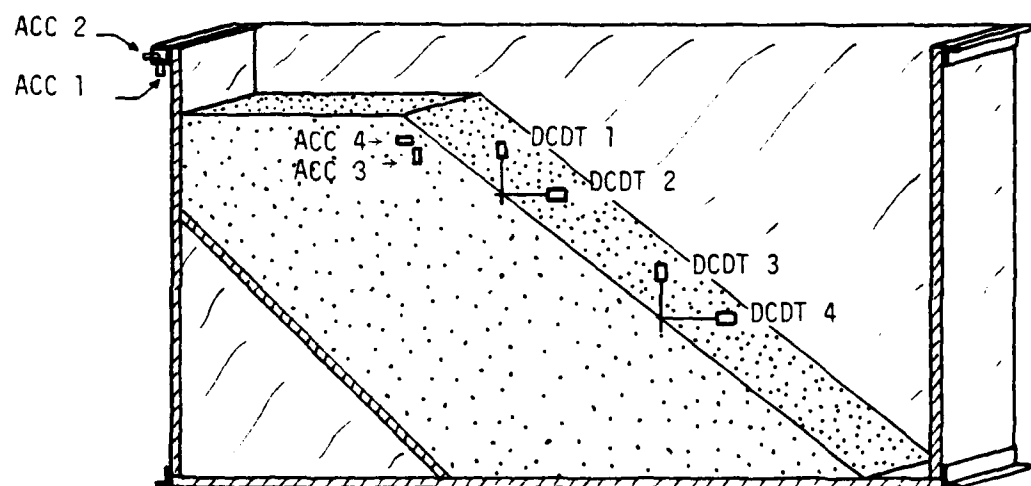
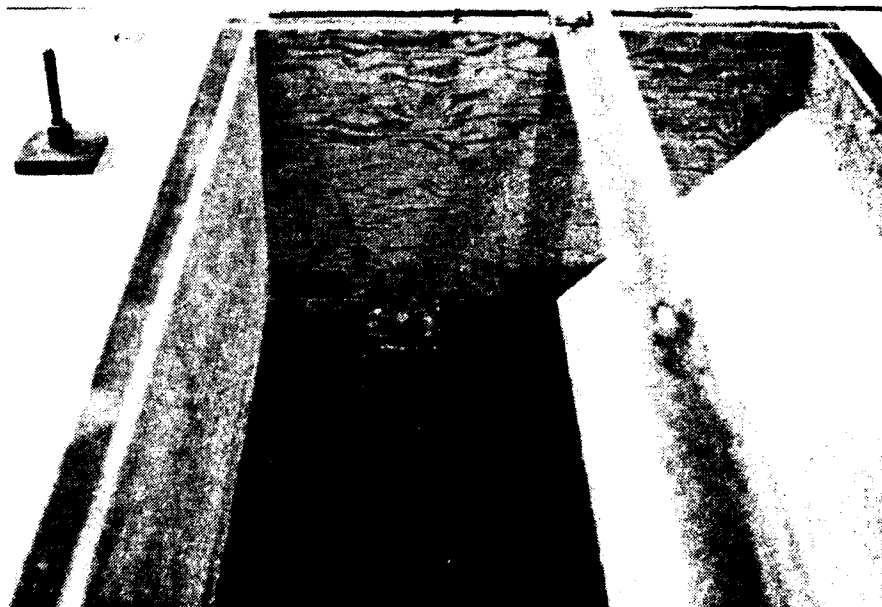


FIGURE A3-1 CUT-AWAY VIEW OF TYPICAL SLOPE SPECIMEN  
SHOWING LOCATION OF INSTRUMENTATION



(a)



(b)

FIGURE A3-2 VIEW OF TEST BOX ON SHAKING TABLE (a) AND CLOSE-UP OF STEEL PLATE AND SPACER BOARD IN TEST BOX (b)

the remaining four bolts were tightened against the reinforcing steel angles on the outer corners of the test box. Two of these outside bolts are visible on the outer edge of the test box in Figure A3-2(a), and the steel plate and bolts in the bottom of the test box may be seen in Figure A3-2(b).

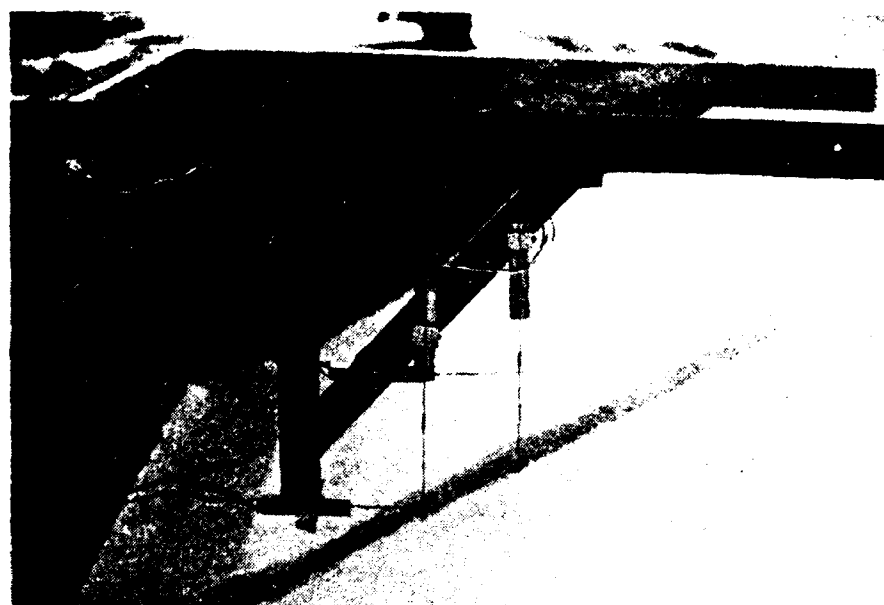
Behind the spacer board a stiff bracing system has been constructed to ensure that the deflection of the board during loading would be very small compared with the displacements of the soil slope. This bracing system consisted of six triangular 1-1/2 in thick plywood wedges, cut to exactly fit between the board and the inside corner of the test box.

Before slope specimens were constructed in the test box, a 2 in thick layer of high-strength "hydrostone" cement mortar was placed in the bottom of the box on top of the steel plate. The "hydrostone" was carefully leveled and a thin layer of the Monterey No. 0 test sand was cemented to the top of it. Also, a thin layer of the test sand was epoxyed with a high strength resin epoxy to the spacer board and the back wall of the test box. This treatment insured a level bottom and good soil-box contact between soil slope specimens and the test box.

A photograph showing the specimen forming "mold" in position within the test box is shown in Figure A3-3(a). The mold assembly consists of a 7 ft x 4 ft plywood panel, 1 in thick, which is reinforced with three longitudinal 3 in steel angles on the back side, and associated mounting hardware. The plywood panel is positioned to the desired specimen slope angle, and rigidly secured in place as shown in Figure A3-3(a). After the specimens are formed within the mold by table vibration, the plywood panel is carefully removed with an overhead crane, leaving a smooth slope



(a)



(b)

FIGURE A3-3 VIEW OF SPECIMEN FORMING MOLD IN PLACE WITHIN TEST BOX (a) AND VIEW OF DCDT'S ON MOUNTING FRAME AND FAILED SLOPE AFTER TESTING (b)

face on the specimen.

The mounting hardware which secures the plywood panel was designed to provide rigid support without distorting the smooth "plane" inner surface of the plywood. Two steel channels along the sides of the test box, covered with strips of compressible foam rubber, provide upward support at the edges for the plywood panel, while a longitudinal steel angle and two 2 in x 4 in lengths of lumber provide the securing downward force. A 7 ft long lumber 2x4 provides the toe footing support at the bottom of the plywood panel.

Instrumentation is mounted both within the test slopes and on the test box in preparation for each test. As the slope specimens are formed, two very small accelerometers, one vertical and one horizontal, are carefully positioned within the sand near the top face of the slope. The accelerometers are mounted on 1/32 in thick perforated aluminum wafers, approximately 7/8 in on a side. This allows for relatively accurate orientation with respect to the horizontal and vertical directions. Also, two accelerometers are mounted on the back side of the test box, behind the top of the slope on the steel reinforcing angle. These two accelerometers are also oriented for the vertical and horizontal directions, and may be observed in Figure A3-1.

A cross-brace is placed across the center of the test box after the test specimen is formed, and four DCDT's are affixed to it on a mounting framework as shown in Figure A3-3(b). The slope pictured in this figure has already failed, and characteristic sloughing of the sand downslope may be observed. Note that the rod extensions of the DCDT cores are bent slightly as a result of the soil mobility. This effect could result in

inaccurate readings at significant strains, as discussed in this report.

One additional modification performed on the test box during this testing series was the cutting of a triangular shaped "window" on one side of the box. This was to permit the photographing of the slope face with a high speed data camera during testing. The opening was approximately 10 in x 10 in with a diagonal at  $45^\circ$  with the horizontal. This modification was necessary for low angle photography, nearly parallel with the slope.

Appendix BExample Test Results

The following examples are included of test results from computer analysis of the raw test data:

## Resonant Column Test Results

B-1     Test No. 1A-3

B-2     Test No. 12B-2

B-3     Test No. 18C-3

## Hollow Cylinder Test Results

B-4     Test No. A26L-2

B-5     Test No. B29-3

B-6     Test No. B31-1

The complete test results are available in Griffin (1980).

## APPENDIX B-1

## Resonant Column Test No. 1A-3

TEST NO. 1A-3, PAY STIFFING 3/1/79

## TEST RESULTS FOR SAMPLE NO. 3

SIG JC KSC	WT GRAMS	DIAM CM	HEIGHT CM	NP	
3.50	922.70	7.10	13.71	11	
TCW GRAMS	ACPV	DCPV	ACFT	DCFT	PNI
1576.60	2500.00	25.80	2500.00	0.	31.45
VOL CC	Wt G/CC	SPH	SWR	SPWR	
542.73	1.70	5.93	1.71	5.31	
COILY MV-PP	ACCEV MV-PP	FREQ HERTZ	COILY MV-PP	ACCEV MV-PP	FREQ HERTZ
1.20	19.20	443.00	-0.	-0.	-0.
9.80	82.00	446.10	-0.	-0.	-0.
20.00	225.00	446.20	-0.	-0.	-0.
40.00	395.00	446.60	-0.	-0.	-0.
80.00	709.00	446.90	-0.	-0.	-0.
203.00	1730.00	447.30	-0.	-0.	-0.
400.00	3770.00	447.90	-0.	-0.	-0.
800.00	7200.00	449.50	-0.	-0.	-0.
2000.00	16200.00	449.80	-0.	-0.	-0.
4000.00	31200.00	424.70	-0.	-0.	-0.
8000.00	49000.00	414.50	-0.	-0.	-0.

CALCULATED STRESS STATE AND ELASTIC CONSTANTS, DATA SET NO. 1

MOOV	DEPSV	DAMPV	MOOT	DCANT	DAMPT	NUC	STRAT
PSI	PERCENT	PERCENT	PSI	PERCENT	PERCENT		
74934.28	.7170E-05		1.72				
NU	SIG1	SIG2	SIG3	BETA	EPS1	EPS2	EPS3
PSI	PSI	PSI	PSI	DEGREES	PERCENT	PERCENT	PERCENT
24	62.80	51.45	51.45	0	.7175E-05	.1722E-05	.1722E-05
29	64.35	51.45	51.45	0	.7175E-05	.2081E-05	0
34	66.05	51.45	51.45	0	.7175E-05	.2440E-05	0
39	67.52	51.45	51.45	0	.7175E-05	.2700E-05	0
44	68.97	51.45	51.45	0	.7175E-05	.3157E-05	0
49	70.27	51.45	51.45	0	.7175E-05	.3516E-05	0

## CALCULATED STRESS STATE AND ELASTIC CONSTANTS, DATA SET NO. 2

MOOV	DEPSV	DAMPV	MOOT	DCANT	DAMPT	NUC	STRAT
PSI	PERCENT	PERCENT	PSI	PERCENT	PERCENT		
78708.32	.1402E-04		2.65				
NU	SIG1	SIG2	SIG3	BETA	EPS1	EPS2	EPS3
PSI	PSI	PSI	PSI	DEGREES	PERCENT	PERCENT	PERCENT
24	63.81	51.45	51.45	0	.1402E-04	.3580E-05	.3580E-05
29	65.38	51.45	51.45	0	.1402E-04	.4375E-05	0
34	66.95	51.45	51.45	0	.1402E-04	.5072E-05	0
39	68.53	51.45	51.45	0	.1402E-04	.5818E-05	0
44	70.10	51.45	51.45	0	.1402E-04	.6564E-05	0
49	71.67	51.45	51.45	0	.1402E-04	.7310E-05	0

## CALCULATED STRESS STATE AND ELASTIC CONSTANTS, DATA SET NO. 3

MOOV	DEPSV	DAMPV	MOOT	DCANT	DAMPT	NUC	STRAT
PSI	PERCENT	PERCENT	PSI	PERCENT	PERCENT		
75819.30	.3728E-04		2.18				
NU	SIG1	SIG2	SIG3	BETA	EPS1	EPS2	EPS3
PSI	PSI	PSI	PSI	DEGREES	PERCENT	PERCENT	PERCENT
24	63.83	51.45	51.45	0	.3728E-04	.8947E-05	.8947E-05

29	66.40	51.45	51.45	0	.3728E-04	.1081E-04	.1081E-04
34	68.97	51.45	51.45	0	.3728E-04	.1207E-04	.1207E-04
39	71.54	51.45	51.45	0	.3728E-04	.1354E-04	.1354E-04
44	74.12	51.45	51.45	0	.3728E-04	.1443E-04	.1443E-04
49	76.69	51.45	51.45	0	.3728E-04	.1627E-04	.1627E-04

## CALCULATED STRESS STATE AND ELASTIC CONSTANTS, DATA SET NO. 4

MOOV	DEPSV	DAMPV	MOOT	DCANT	DAMPT	NUC	STRAT
PSI	PERCENT	PERCENT	PSI	PERCENT	PERCENT		
75956.30	.7170E-04		2.18				
NU	SIG1	SIG2	SIG3	BETA	EPS1	EPS2	EPS3
PSI	PSI	PSI	PSI	DEGREES	PERCENT	PERCENT	PERCENT
24	63.85	51.45	51.45	0	.7170E-04	.1721E-04	.1721E-04
29	66.42	51.45	51.45	0	.7170E-04	.2079E-04	.2079E-04
34	69.00	51.45	51.45	0	.7170E-04	.2438E-04	.2438E-04
39	71.57	51.45	51.45	0	.7170E-04	.2796E-04	.2796E-04
44	74.14	51.45	51.45	0	.7170E-04	.3155E-04	.3155E-04
49	76.71	51.45	51.45	0	.7170E-04	.3513E-04	.3513E-04

## CALCULATED STRESS STATE AND ELASTIC CONSTANTS, DATA SET NO. 5

MOOV	DEPSV	DAMPV	MOOT	DCANT	DAMPT	NUC	STRAT
PSI	PERCENT	PERCENT	PSI	PERCENT	PERCENT		
75997.28	.1381E-03		2.29				
NU	SIG1	SIG2	SIG3	BETA	EPS1	EPS2	EPS3
PSI	PSI	PSI	PSI	DEGREES	PERCENT	PERCENT	PERCENT
24	63.88	51.45	51.45	0	.1381E-03	.3316E-04	.3316E-04
29	66.45	51.45	51.45	0	.1381E-03	.4004E-04	.4004E-04
34	69.02	51.45	51.45	0	.1381E-03	.4695E-04	.4695E-04
39	71.59	51.45	51.45	0	.1381E-03	.5386E-04	.5386E-04
44	74.16	51.45	51.45	0	.1381E-03	.6077E-04	.6077E-04
49	76.73	51.45	51.45	0	.1381E-03	.6768E-04	.6768E-04

## CALCULATED STRESS STATE AND ELASTIC CONSTANTS, DATA SET NO. 6

	MODV PSI	DEPSV PERCENT	DAMPV PERCENT	MODT PSI	OGANT PERCENT	DAMPT PERCENT	NUC	STRAT		
	75513.75	.3104E-03	2.53							
NU	SIG1 PSI	SIG2 PSI	SIG3 PSI	BETA DEGREES	EPS1 PERCENT	EPS2 PERCENT	EPS3 PERCENT	EATA DEGREES	EPSOC PERCENT	GAMOC PERCENT
.24	66.03	51.45	51.45	0.	.3104E-03	.7449E-04	.7449E-04	0.	.5380E-04	.3629E-03
.29	66.60	51.45	51.45	0.	.3104E-03	.9001E-04	.9001E-04	0.	.6382E-04	.3775E-03
.34	69.18	51.45	51.45	0.	.3104E-03	.1055E-03	.1055E-03	0.	.8311E-04	.3921E-03
.39	71.75	51.45	51.45	0.	.3104E-03	.1211E-03	.1211E-03	0.	.8270E-04	.4066E-03
.44	74.32	51.45	51.45	0.	.3104E-03	.1366E-03	.1366E-03	0.	.1242E-04	.4214E-03
.49	76.89	51.45	51.45	0.	.3104E-03	.1521E-03	.1521E-03	0.	.2042E-04	.4362E-03

## CALCULATED STRESS STATE AND ELASTIC CONSTANTS, DATA SET NO. 7

	MODV PSI	DEPSV PERCENT	DAMPV PERCENT	MODT PSI	OGANT PERCENT	DAMPT PERCENT	NUC	STRAT		
	74908.99	.0933E-03	2.29							
NU	SIG1 PSI	SIG2 PSI	SIG3 PSI	BETA DEGREES	EPS1 PERCENT	EPS2 PERCENT	EPS3 PERCENT	EATA DEGREES	EPSOC PERCENT	GAMOC PERCENT
.24	44.32	51.45	51.45	0.	.0933E-03	.1665E-03	.1665E-03	0.	.1203E-03	.8113E-03
.29	60.89	51.45	51.45	0.	.0933E-03	.2012E-03	.2012E-03	0.	.9715E-04	.8440E-03
.34	69.60	51.45	51.45	0.	.0933E-03	.2359E-03	.2359E-03	0.	.7402E-04	.8767E-03
.39	72.04	51.45	51.45	0.	.0933E-03	.2706E-03	.2706E-03	0.	.5089E-04	.9094E-03
.44	74.81	51.45	51.45	0.	.0933E-03	.3053E-03	.3053E-03	0.	.2770E-04	.9421E-03
.49	77.18	51.45	51.45	0.	.0933E-03	.3400E-03	.3400E-03	0.	.4426E-05	.9748E-03

## CALCULATED STRESS STATE AND ELASTIC CONSTANTS, DATA SET NO. 8

	MODV PSI	DEPSV PERCENT	DAMPV PERCENT	MODT PSI	OGANT PERCENT	DAMPT PERCENT	NUC	STRAT		
	73357.43	.1357E-02	2.39							
NU	SIG1	SIG2	SIG3	BETA	EPS1	EPS2	EPS3	EATA	EPSOC	GAMOC
.24	54.70	51.45	51.45	0.	.1357E-02	.3239E-03	.3239E-03	0.	.2376E-03	.1979E-02
.29	67.10	51.45	51.45	0.	.1357E-02	.3914E-03	.3914E-03	0.	.1489E-03	.1561E-02
.34	69.84	51.45	51.45	0.	.1357E-02	.4544E-03	.4544E-03	0.	.1439E-03	.1709E-02
.39	72.03	51.45	51.45	0.	.1357E-02	.5203E-03	.5203E-03	0.	.1499E-03	.1757E-02
.44	75.38	51.45	51.45	0.	.1357E-02	.5938E-03	.5938E-03	0.	.5308E-04	.1632E-02
.49	77.65	51.45	51.45	0.	.1357E-02	.6613E-03	.6613E-03	0.	.5197E-05	.1846E-02

## CALCULATED STRESS STATE AND ELASTIC CONSTANTS, DATA SET NO. 9

	MODV PSI	DEPSV PERCENT	DAMPV PERCENT	MODT PSI	OGANT PERCENT	DAMPT PERCENT	NUC	STRAT		
	71462.16	.3118E-02	2.65							
NU	SIG1 PSI	SIG2 PSI	SIG3 PSI	BETA DEGREES	EPS1 PERCENT	EPS2 PERCENT	EPS3 PERCENT	EATA DEGREES	EPSOC PERCENT	GAMOC PERCENT
.24	69.00	51.45	51.45	0.	.3118E-02	.7483E-03	.7483E-03	0.	.5308E-03	.1645E-02
.29	69.61	51.45	51.45	0.	.3118E-02	.9041E-03	.9041E-03	0.	.4345E-03	.1745E-02
.34	71.18	51.45	51.45	0.	.3118E-02	.1200E-02	.1200E-02	0.	.3326E-03	.1746E-02
.39	73.76	51.45	51.45	0.	.3118E-02	.1210E-02	.1210E-02	0.	.2286E-03	.1406E-02
.44	76.33	51.45	51.45	0.	.3118E-02	.1472E-02	.1472E-02	0.	.1287E-03	.1233E-02
.49	78.90	51.45	51.45	0.	.3118E-02	.1734E-02	.1734E-02	0.	.2078E-04	.1530E-02

## CALCULATED STRESS STATE AND ELASTIC CONSTANTS, DATA SET NO. 10

	MODV PSI	DEPSV PERCENT	DAMPV PERCENT	MODT PSI	OGANT PERCENT	DAMPT PERCENT	NUC	STRAT		
	64608.68	.6222E-02	2.75							
NU	SIG1 PSI	SIG2 PSI	SIG3 PSI	BETA DEGREES	EPS1 PERCENT	EPS2 PERCENT	EPS3 PERCENT	EATA DEGREES	EPSOC PERCENT	GAMOC PERCENT
.24	66.07	51.45	51.45	0.	.6222E-02	.1493E-02	.1493E-02	0.	.1079E-02	.7275E-02
.29	79.94	51.45	51.45	0.	.6222E-02	.1803E-02	.1803E-02	0.	.4711E-03	.7588E-02
.34	73.22	51.45	51.45	0.	.6222E-02	.2116E-02	.2116E-02	0.	.6637E-03	.7861E-02
.39	75.78	51.45	51.45	0.	.6222E-02	.2427E-02	.2427E-02	0.	.4563E-03	.8153E-02
.44	79.38	51.45	51.45	0.	.6222E-02	.2738E-02	.2738E-02	0.	.2499E-03	.8449E-02
.49	82.93	51.45	51.45	0.	.6222E-02	.3049E-02	.3049E-02	0.	.5148E-04	.8741E-02

## CALCULATED STRESS STATE AND ELASTIC CONSTANTS, DATA SET NO. 11

	MODV PSI	DESV PERCENT	DAMPV PERCENT	MODY PSI	OGANT PERCENT	DAMPY PERCENT	MUC	STRAT		
	66*28.91	.1033E-01	3.52							
NU	SIG1 PSI	SIG2 PSI	SIG3 PSI	BETA DEGREES	EPS1 PERCENT	EPS2 PERCENT	EPS3 PERCENT	EATA DEGREES	EPSOC PERCENT	GANOC PERCENT
.24	70.55	51.45	51.45	0.	.1033E-01	.2478E-02	.2478E-02	0.	.1790E-02	.1207E-01
.29	73.13	51.45	51.45	0.	.1033E-01	.2994E-02	.2994E-02	0.	.1646E-02	.1294E-01
.34	75.70	51.45	51.45	0.	.1033E-01	.3511E-02	.3511E-02	0.	.1501E-02	.1309E-01
.39	78.27	51.45	51.45	0.	.1033E-01	.4027E-02	.4027E-02	0.	.1357E-02	.1457E-01
.44	80.84	51.45	51.45	0.	.1033E-01	.4543E-02	.4543E-02	0.	.1213E-02	.1605E-01
.49	83.42	51.45	51.45	0.	.1033E-01	.5060E-02	.5060E-02	0.	.1069E-02	.1753E-01



200.00	2400.00	347.30	40.00	370.00	147.30
200.00	2400.00	346.40	40.00	360.00	143.00
215.30	2620.30	346.10	700.00	1700.00	141.90
225.00	2600.00	346.40	400.00	750.00	140.50
231.00	2600.00	343.40	800.00	4000.00	139.80
310.00	2600.00	370.10	2300.00	4300.00	136.60
330.63	2600.00	372.40	4070.00	11500.00	134.00
700.00	2600.00	366.70	4090.00	17000.00	129.30
100.00	2600.00	366.70	11000.00	21000.00	129.00
245.00	2600.00	342.00	-0.00	-0.00	0.00

## CALCULATED STRESS STATE AND ELASTIC CONSTANTS, DATA SET NO. 1

WQWV PSI	DEPSV PERCENT	DAMPV PERCENT	WQWV PSI	DEGANT PERCENT	DAMPV PERCENT	MUC	STRAT			
41777.44	1174E-04	.493								
WQWV PSI	DEPSV PERCENT	DAMPV PERCENT	WQWV PSI	DEGANT PERCENT	DAMPV PERCENT	MUC	STRAT			
40	SIG1 PSI	SIG2 PSI	SIG3 PSI	BETA DEGREES	EPS1 PERCENT	EPS2 PERCENT	EPS3 PERCENT	FATA DEGREES	EPSOC PERCENT	GAMOC PERCENT
.76	16.44	20.40	20.40	0.	1374E-04	3308E-05	3304E-05	0.	2300E-05	1611E-04
.70	17.43	20.40	20.40	0.	1374E-04	1087E-05	3007E-05	2.	1010E-05	1674E-04
.36	39.40	20.40	20.40	0.	1374E-04	4684E-05	4684E-05	0.	1470E-05	1741E-04
.10	40.47	20.40	20.40	0.	1374E-04	5760E-05	4374E-05	2.	1011E-05	1804E-04
.44	12.34	20.40	20.40	0.	1374E-04	0.00E-05	0.00E-05	0.	1413E-05	1874E-04
.40	43.61	20.40	20.40	0.	1374E-04	6754E-05	6754E-05	2.	0140E-07	1934E-04

## CALCULATED STRESS STATE AND ELASTIC CONSTANTS, DATA SET NO. 2

WQWV PSI	DEPSV PERCENT	DAMPV PERCENT	WQWV PSI	DEGANT PERCENT	DAMPV PERCENT	MUC	STRAT			
61526.25	2723E-04	.94								
WQWV PSI	SIG1 PSI	SIG2 PSI	SIG3 PSI	BETA DEGREES	EPS1 PERCENT	EPS2 PERCENT	EPS3 PERCENT	FATA DEGREES	EPSOC PERCENT	GAMOC PERCENT
.76	16.47	20.40	20.40	0.	2723E-04	4534E-05	4534E-05	0.	4710E-05	3147E-04
.70	37.44	20.40	20.40	0.	2723E-04	7494E-05	7494E-05	0.	3417E-05	3311E-04
.16	10.41	20.40	20.40	0.	2723E-04	4257E-05	4257E-05	0.	7004E-05	3440E-04
.10	40.40	20.40	20.40	0.	2723E-04	1.00E-05	1.00E-05	2.	1087E-05	3708E-04
.44	42.35	20.40	20.40	0.	2723E-04	1108E-04	1108E-04	0.	1084E-05	3404E-04
.40	43.47	20.40	20.40	0.	2723E-04	1334E-04	1334E-04	0.	1415E-04	3875E-04

## CALCULATED STRESS STATE AND ELASTIC CONSTANTS, DATA SET NO. 3

WQWV PSI	DEPSV PERCENT	DAMPV PERCENT	WQWV PSI	DEGANT PERCENT	DAMPV PERCENT	MUC	STRAT
			23727.70	3618E-04	.66		
WQWV PSI	DEPSV PERCENT	DAMPV PERCENT	WQWV PSI	DEGANT PERCENT	DAMPV PERCENT	MUC	STRAT
.76	20.41	20.40	20.30	45.00	1465E-04	1465E-04	45.000
.70	20.41	20.40	20.30	45.00	1465E-04	1465E-04	45.000
.36	20.41	20.40	20.30	45.00	1465E-04	1465E-04	45.000
.10	20.41	20.40	20.30	45.00	1465E-04	1465E-04	45.000
.44	20.41	20.40	20.30	45.00	1465E-04	1465E-04	45.000
.40	20.41	20.40	20.30	45.00	1465E-04	1465E-04	45.000

## CALCULATED STRESS STATE AND ELASTIC CONSTANTS, DATA SET NO. 4

WQWV PSI	DEPSV PERCENT	DAMPV PERCENT	WQWV PSI	DEGANT PERCENT	DAMPV PERCENT	MUC	STRAT			
23689.81 7728E-04 .62										
WQWV PSI	SIG1 PSI	SIG2 PSI	SIG3 PSI	BETA DEGREES	EPS1 PERCENT	EPS2 PERCENT	EPS3 PERCENT	FATA DEGREES	EPSOC PERCENT	GAMOC PERCENT
.76	20.42	20.40	20.30	45.00	3120E-04	-	3120E-04	45.000	5110E-04	5110E-04
.70	20.42	20.40	20.30	45.00	3120E-04	-	3120E-04	45.000	5110E-04	5110E-04
.36	20.42	20.40	20.30	45.00	3120E-04	-	3120E-04	45.000	5110E-04	5110E-04
.10	20.42	20.40	20.30	45.00	3120E-04	-	3120E-04	45.000	5110E-04	5110E-04
.44	20.42	20.40	20.30	45.00	3120E-04	-	3120E-04	45.000	5110E-04	5110E-04
.40	20.42	20.40	20.30	45.00	3120E-04	-	3120E-04	45.000	5110E-04	5110E-04

## CALCULATED STRESS STATE AND ELASTIC CONSTANTS, DATA SET NO. 5

WQWV PSI	DEPSV PERCENT	DAMPV PERCENT	WQWV PSI	DEGANT PERCENT	DAMPV PERCENT	MUC	STRAT
-------------	------------------	------------------	-------------	-------------------	------------------	-----	-------

61603.50 .2716F-04									
NU	SIG1 PSI	SIG2 PSI	SIG3 PSI	DATA DEGREE	EPS1 PERCENT	EPS2 PERCENT	EPS3 PERCENT	DATA DEGREE	EPS1 PERCENT
.24	70.47	20.40	20.40	0	.2716F-04-.4518F-05-.4418F-05			1	.4707F-04-.3178F-04
.20	37.04	20.40	20.40	0	.2716F-04-.7474F-05-.7474F-05			2	.1402F-05-.7107F-04
.36	30.43	20.40	20.40	0	.2716F-04-.9213F-05-.9213F-05			3	.7407F-05-.7471F-04
.10	43.04	20.40	20.40	0	.2716F-04-.1184F-04-.1184F-04			4	.1081F-05-.7468F-04
.44	47.35	20.40	20.40	0	.2716F-04-.1104F-04-.1104F-04			5	.1244F-05-.7467F-04
.40	41.87	20.40	20.40	0	.2716F-04-.1331F-04-.1331F-04			6	.1813F-05-.7414F-04

## CALCULATED STRESS STATE AND ELASTIC CONSTANTS, DATA SET NO. 6

NU	MOBY PSI	DEPSV PERCENT	DANDV PERCENT	MOBY PSI	DEPSV PERCENT	DANDV PERCENT	MUC	STREY	
	61620.54	.2716F-04	.00	23722.20	.3470E-04	.5946	.7948	.7310	
NU	SIG1 PSI	SIG2 PSI	SIG3 PSI	DATA DEGREE	EPS1 PERCENT	EPS2 PERCENT	EPS3 PERCENT	DATA DEGREE	
.24	70.47	20.40	20.40	.00	.2940E-04-.6424F-05-.6961E-05			.27	.4712F-04-.7468F-04
.20	37.04	20.40	20.40	.05	.2942E-04-.6743E-05-.1174F-04			.25	.2030F-04-.7770F-04
.36	30.43	20.40	20.40	.08	.2942E-04-.1060F-04-.1306F-04			.26	.1301F-05-.7814F-04
.10	40.48	20.40	20.40	.04	.2897E-04-.1100F-04-.1434F-04			.24	.1047F-05-.8070F-04
.44	42.35	20.40	20.40	.04	.2940E-04-.1372F-04-.1563E-04			.27	.1812F-05-.8140F-04
.60	29.40	20.40	20.40	.00	.2940E-04-.1372F-04-.1563E-04			.27	.1812F-05-.8140F-04

## CALCULATED STRESS STATE AND ELASTIC CONSTANTS, DATA SET NO. 7

NU	MOBY PSI	DEPSV PERCENT	DANDV PERCENT	MOBY PSI	DEPSV PERCENT	DANDV PERCENT	MUC	STREY	
	61411.00	.2727F-04	.00	23685.81	.4711F-04	.5810	.7966	1.4047	
NU	SIG1 PSI	SIG2 PSI	SIG3 PSI	DATA DEGREE	EPS1 PERCENT	EPS2 PERCENT	EPS3 PERCENT	DATA DEGREE	
.24	70.47	20.40	20.40	.16	.3606E-04-.6546E-05-.1623E-04			.46	.4774F-05-.8674F-04
.20	37.04	20.40	20.40	.17	.3471F-04-.7004E-05-.1775F-04			.47	.7417F-05-.8674F-04
.36	30.43	20.40	20.40	.11	.2840F-04-.6771E-05-.1448E-04			.47	.7030F-05-.8607F-04

.24	40.89	20.40	20.40	.10	.7674F-04-.1063E-04-.1047F-04			.41	.7082F-05-.8909F-04
.20	47.34	20.40	20.40	.09	.7404F-04-.1200F-04-.2070F-04			.47	.1701F-04-.8604F-04
.36	47.42	20.40	20.40	.08	.7463F-04-.1236E-04-.2192F-04			.40	.1414F-04-.8530F-04

## CALCULATED STRESS STATE AND ELASTIC CONSTANTS, DATA SET NO. 8

NU	MOBY PSI	DEPSV PERCENT	DANDV PERCENT	MOBY PSI	DEPSV PERCENT	DANDV PERCENT	MUC	STREY	
	61431.00	.2727E-04	.06	23722.20	.2122E-03	.5812	.7948	7.4417	
NU	SIG1 PSI	SIG2 PSI	SIG3 PSI	DATA DEGREE	EPS1 PERCENT	EPS2 PERCENT	EPS3 PERCENT	DATA DEGREE	
.24	70.47	20.40	20.40	.41	.7405F-04-.6546E-05-.6973F-04			.43	.4774F-05-.8673F-04
.20	37.04	20.40	20.40	.39	.6554F-04-.7408E-05-.6622E-04			.41	.4817E-05-.8673F-04
.36	30.43	20.40	20.40	.29	.6411F-04-.6771E-05-.6712F-04			.42	.2308F-05-.8674F-04
.10	40.48	20.40	20.40	.24	.6466F-04-.1063E-04-.6402F-04			.41	.7333F-05-.8674F-04
.44	42.35	20.40	20.40	.22	.6471E-04-.1200F-04-.6884F-04			.41	.1301F-05-.8674F-04
.40	43.04	20.40	20.40	.20	.6377F-04-.1334E-04-.6884E-04			.40	.1813F-05-.8674F-04

## CALCULATED STRESS STATE AND ELASTIC CONSTANTS, DATA SET NO. 9

MOBY PSI	DEPSV PERCENT	DANDV PERCENT	MOBY PSI	DEPSV PERCENT	DANDV PERCENT	MUC	STREY			
61431.00	.2727F-04	.06	23685.81	.4166E-03	.6786	.8064	7.6301			
NU	SIG1 PSI	SIG2 PSI	SIG3 PSI	DATA DEGREE	EPS1 PERCENT	EPS2 PERCENT	EPS3 PERCENT	DATA DEGREE	EPS4C PERCENT	DANDV PERCENT
.24	36.47	20.40	20.40	.60	.1150F-01-.6546F-04-.6915F-04			.70	.4724F-04	.1770F-03
.20	37.94	20.40	20.40	.60	.1152E-03-.7408E-05-.6946E-04			.70	.5817E-05	.1735F-03
.36	30.43	20.40	20.40	.60	.1142F-03-.6771E-05-.6876E-04			.70	.7000E-05	.1770E-03
.10	40.48	20.40	20.40	.60	.1142F-03-.1067E-04-.6754E-04			.70	.2330F-05	.1770E-03
.44	42.35	20.40	20.40	.60	.1134F-03-.1200E-04-.6835E-04			.68	.1061F-05	.1741F-03
.40	43.02	20.40	20.40	.59	.1131E-03-.1336E-04-.6918E-04			.68	.1813F-05	.1743E-03

## CALCULATED STRESS STATE AND ELASTIC CONSTANTS, DATA SET NO. 10

MODV PSI	DEPSV PERCENT	DAMPV PERCENT	MODT PSI	OGAMT PERCENT	DAMPT PERCENT	MUC	STRAT			
61149.65	.2730E-04	.99	23560.44	.7092E-03	.6076	.2977	14.4058			
NU	SIG1 PSI	SIG2 PSI	SIG3 PSI	BETA DEGREES	EPS1 PERCENT	EPS2 PERCENT	EPS3 PERCENT	EATA DEGREES	EPSOC PERCENT	GAMOC PERCENT
.74	36.48	29.40	29.40	1.50	.2084E-03	.6574E-05	.1870E-03	.74	.4746E-06	.3230E-03
.70	37.95	29.40	29.40	1.25	.2074E-03	.7944E-05	.1884E-03	.74	.3835E-06	.3230E-03
.76	39.42	29.40	29.40	1.00	.2072E-03	.9314E-05	.1891E-03	.76	.2922E-06	.3240E-03
.70	40.89	29.40	29.40	.83	.2066E-03	.1068E-04	.1899E-03	.76	.2009E-06	.3242E-03
.74	42.36	29.40	29.40	.62	.2060E-03	.1205E-04	.1906E-03	.74	.1046E-06	.3243E-03
.70	43.83	29.40	29.40	.74	.2053E-03	.1342E-04	.1914E-03	.73	.1870E-06	.3245E-03

## CALCULATED STRESS STATE AND ELASTIC CONSTANTS, DATA SET NO. 11

MODV PSI	DEPSV PERCENT	DAMPV PERCENT	MODT PSI	OGAMT PERCENT	DAMPT PERCENT	MUC	STRAT			
40836.71	.2753E-04	1.01	23206.52	.1089E-02	.7209	.3109	30.6066			
NU	SIG1 PSI	SIG2 PSI	SIG3 PSI	BETA DEGREES	EPS1 PERCENT	EPS2 PERCENT	EPS3 PERCENT	EATA DEGREES	EPSOC PERCENT	GAMOC PERCENT
.74	36.48	29.40	29.38	3.16	.4330E-03	.6608E-05	.4121E-03	.73	.4173E-06	.6803E-03
.70	37.96	29.40	29.38	2.62	.4323E-03	.7985E-05	.4124E-03	.76	.3455E-06	.6802E-03
.76	39.43	29.40	29.38	2.24	.4317E-03	.9362E-05	.4135E-03	.76	.2437E-06	.6803E-03
.70	40.90	29.40	29.39	1.95	.4310E-03	.1070E-04	.4142E-03	.76	.2019E-06	.6804E-03
.74	42.36	29.40	29.39	1.73	.4304E-03	.1212E-04	.4149E-03	.76	.1101E-06	.6804E-03
.70	43.83	29.40	29.39	1.56	.4297E-03	.1349E-04	.4157E-03	.76	.1836E-06	.6804E-03

## CALCULATED STRESS STATE AND ELASTIC CONSTANTS, DATA SET NO. 12

MODV PSI	DEPSV PERCENT	DAMPV PERCENT	MODT PSI	OGAMT PERCENT	DAMPT PERCENT	MUC	STRAT			
62584.93	.2705E-04	1.01	22791.70	.2950E-02	.6406	.3291	57.3488			
NU	SIG1 PSI	SIG2 PSI	SIG3 PSI	BETA DEGREES	EPS1 PERCENT	EPS2 PERCENT	EPS3 PERCENT	EATA DEGREES	EPSOC PERCENT	GAMOC PERCENT

.74	76.44	29.40	29.34	5.38	.7691E-03	.6035E-05	.7571E-03	.77	.4792E-06	.1205E-02
.70	78.00	29.40	29.38	4.67	.7676E-03	.8018E-05	.7578E-03	.72	.3871E-06	.1205E-02
.76	79.44	29.40	29.34	3.87	.7667E-03	.9403E-05	.7588E-03	.77	.2949E-06	.1205E-02
.70	80.92	29.40	29.36	3.16	.7661E-03	.1079E-04	.7592E-03	.77	.2024E-06	.1204E-02
.74	82.36	29.40	29.37	2.46	.7644E-03	.1217E-04	.7599E-03	.77	.1109E-06	.1205E-02
.70	83.84	29.40	29.37	2.66	.7647E-03	.1358E-04	.7606E-03	.77	.1843E-06	.1205E-02

## CALCULATED STRESS STATE AND ELASTIC CONSTANTS, DATA SET NO. 13

MODV PSI	DEPSV PERCENT	DAMPV PERCENT	MODT PSI	OGAMT PERCENT	DAMPT PERCENT	MUC	STRAT			
40024.80	.2761E-04	1.13	22166.82	.5034E-02	1.6136	.3543	98.7018			
NU	SIG1 PSI	SIG2 PSI	SIG3 PSI	BETA DEGREES	EPS1 PERCENT	EPS2 PERCENT	EPS3 PERCENT	EATA DEGREES	EPSOC PERCENT	GAMOC PERCENT
.74	76.44	29.40	29.23	9.75	.1240E-02	.6647E-05	.1248E-02	.78	.4837E-06	.2046E-02
.70	78.00	29.40	29.26	7.32	.1238E-02	.8094E-05	.1240E-02	.78	.3907E-06	.2046E-02
.76	79.44	29.40	29.28	6.28	.1234E-02	.9444E-05	.1240E-02	.78	.2977E-06	.2046E-02
.70	80.90	29.40	29.29	5.40	.1237E-02	.1089E-04	.1250E-02	.78	.2044E-06	.2046E-02
.74	82.36	29.40	29.30	4.80	.1247E-02	.1220E-04	.1251E-02	.78	.1110E-06	.2046E-02
.70	83.80	29.40	29.31	4.40	.1260E-02	.1367E-04	.1252E-02	.78	.1840E-06	.2046E-02

## CALCULATED STRESS STATE AND ELASTIC CONSTANTS, DATA SET NO. 14

MODV PSI	DEPSV PERCENT	DAMPV PERCENT	MODT PSI	OGAMT PERCENT	DAMPT PERCENT	MUC	STRAT			
				20834.41	.4986E-02	1.17				
NU	SIG1 PSI	SIG2 PSI	SIG3 PSI	BETA DEGREES	EPS1 PERCENT	EPS2 PERCENT	EPS3 PERCENT	EATA DEGREES	EPSOC PERCENT	GAMOC PERCENT
.74	31.46	29.40	27.34	45.00	.4003E-02		.4003E-02	45.000		.6937E-02
.70	31.46	29.40	27.34	45.00	.4003E-02		.4003E-02	45.000		.6937E-02
.76	31.46	29.40	27.34	45.00	.4003E-02		.4003E-02	45.000		.6937E-02
.70	31.46	29.40	27.34	45.00	.4003E-02		.4003E-02	45.000		.6937E-02
.74	31.46	29.40	27.34	45.00	.4003E-02		.4003E-02	45.000		.6937E-02
.70	31.46	29.40	27.34	45.00	.4003E-02		.4003E-02	45.000		.6937E-02

## CALCULATED STRESS STATE AND ELASTIC CONSTANTS, DATA SET NO. 15

MODV PSI	DEPSV PERCENT	DAMPV PERCENT	MODT PSI	OGANT PERCENT	DAMPOT PERCENT	MUC	SYBAT			
12941.79	.2748E-04	.74								
NU	SIG1 PSI	SIG2 PSI	SIG3 PSI	ETA DEGREES	EPS1 PERCENT	EPS2 PERCENT	EPS3 PERCENT	ETA DEGREES	EPSOC PERCENT	GAMOC PERCENT
.74	16.47	20.40	20.40	0.	.2748E-04	.6505E-05	.6505E-05	0.	.4767E-06	.2212E-04
.72	17.04	20.40	20.40	0.	.2748E-04	.7040E-05	.7040E-05	0.	.5847E-05	.3342E-04
.74	10.41	20.40	20.40	0.	.2748E-04	.9342E-05	.9342E-05	0.	.2071E-05	.3671E-04
.70	40.43	20.40	20.40	0.	.2748E-04	.1072E-04	.1072E-04	0.	.2215E-05	.3601E-04
.64	40.34	20.40	20.40	0.	.2748E-04	.1200E-04	.1200E-04	0.	.1000E-05	.3751E-04
.61	43.47	20.40	20.40	0.	.2748E-04	.1346E-04	.1346E-04	0.	.1432E-06	.3900E-04

## CALCULATED STRESS STATE AND ELASTIC CONSTANTS, DATA SET NO. 16

MODV PSI	DEPSV PERCENT	DAMPV PERCENT	MODT PSI	OGANT PERCENT	DAMPOT PERCENT	MUC	SYBAT			
12641.79	.5044E-04	.97								
NU	SIG1 PSI	SIG2 PSI	SIG3 PSI	ETA DEGREES	EPS1 PERCENT	EPS2 PERCENT	EPS3 PERCENT	ETA DEGREES	EPSOC PERCENT	GAMOC PERCENT
.74	16.45	20.40	20.40	0.	.6084E-04	.1676E-04	.1676E-04	0.	.1211E-04	.1145E-04
.70	37.07	20.40	20.40	0.	.6084E-04	.2025E-04	.2025E-04	0.	.0778E-06	.4404E-04
.74	10.44	20.40	20.40	0.	.6084E-04	.2375E-04	.2375E-04	0.	.7490E-05	.4427E-04
.70	40.41	20.40	20.40	0.	.6084E-04	.2774E-04	.2774E-04	0.	.5175E-05	.4143E-04
.74	42.19	20.40	20.40	0.	.6084E-04	.3073E-04	.3073E-04	0.	.2794E-05	.4487E-04
.60	41.44	20.40	20.40	0.	.6084E-04	.3422E-04	.3422E-04	0.	.4444E-06	.4411E-04

## CALCULATED STRESS STATE AND ELASTIC CONSTANTS, DATA SET NO. 17

MODV PSI	DEPSV PERCENT	DAMPV PERCENT	MODT PSI	OGANT PERCENT	DAMPOT PERCENT	MUC	SYBAT			
13405.64	.1423E-03	.94								
NU	SIG1 PSI	SIG2 PSI	SIG3 PSI	ETA DEGREES	EPS1 PERCENT	EPS2 PERCENT	EPS3 PERCENT	ETA DEGREES	EPSOC PERCENT	GAMOC PERCENT
.74	36.54	20.40	20.40	0.	.1423E-03	.3410E-04	.3410E-04	0.	.2447E-04	.1404E-03
.70	37.31	20.40	20.40	0.	.1427E-03	.4124E-04	.4124E-04	0.	.1991E-04	.1741E-03
.74	30.40	20.40	20.40	0.	.1423E-03	.4430E-04	.4430E-04	0.	.1514E-04	.1708E-03
.70	40.40	20.40	20.40	0.	.1427E-03	.4411E-04	.4411E-04	0.	.1344E-04	.1604E-03
.64	42.42	20.40	20.40	0.	.1427E-03	.6763E-04	.6763E-04	0.	.5603E-05	.1637E-03
.60	43.40	20.40	20.40	0.	.1423E-03	.6974E-04	.6974E-04	0.	.9480E-06	.1690E-03

## CALCULATED STRESS STATE AND ELASTIC CONSTANTS, DATA SET NO. 18

MODV	DEPSV	DAMPV	MODT	OGANT	DAMPOT	MUC	SYBAT			
PSI	PERCENT	PERCENT	PSI	PERCENT	PERCENT					
12614.12	.7932E-03	.92								
NU	SIG1 PSI	SIG2 PSI	SIG3 PSI	ETA DEGREES	EPS1 PERCENT	EPS2 PERCENT	EPS3 PERCENT	ETA DEGREES	EPSOC PERCENT	GAMOC PERCENT
.74	36.43	20.40	20.40	0.	.2432E-03	.4708E-04	.4708E-04	0.	.4402E-04	.3711E-03
.70	38.10	20.40	20.40	0.	.2432E-03	.4214E-04	.4214E-04	0.	.7845E-04	.3404E-03
.74	30.47	20.40	20.40	0.	.2032E-03	.4630E-04	.4630E-04	0.	.3271E-04	.3474E-03
.70	41.44	20.40	20.40	0.	.2432E-03	.1105E-03	.1105E-03	0.	.2022E-04	.3712E-03
.64	42.51	20.40	20.40	0.	.2432E-03	.1246E-03	.1246E-03	0.	.1133E-04	.3445E-03
.60	43.40	20.40	20.40	0.	.2032E-03	.1588E-03	.1588E-03	0.	.1488E-05	.3497E-03

## CALCULATED STRESS STATE AND ELASTIC CONSTANTS, DATA SET NO. 19

MODV PSI	DEPSV PERCENT	DAMPV PERCENT	MODT PSI	OGANT PERCENT	DAMPOT PERCENT	MUC	SYBAT			
10110.04	.5874E-03	1.12								
NU	SIG1 PSI	SIG2 PSI	SIG3 PSI	ETA DEGREES	EPS1 PERCENT	EPS2 PERCENT	EPS3 PERCENT	ETA DEGREES	EPSOC PERCENT	GAMOC PERCENT
.74	36.45	20.40	20.40	0.	.5874E-03	.1410E-03	.1410E-03	0.	.1410E-03	.4804E-03
.70	38.20	20.40	20.40	0.	.5874E-03	.1704E-03	.1704E-03	0.	.4774E-04	.7147E-03
.74	34.75	20.40	20.40	0.	.5874E-03	.1947E-03	.1947E-03	0.	.6740E-04	.7451E-03
.70	41.22	20.40	20.40	0.	.5874E-03	.2211E-03	.2211E-03	0.	.4308E-04	.7091E-03
.64	42.44	20.40	20.40	0.	.5874E-03	.2585E-03	.2585E-03	0.	.2350E-04	.7073E-03
.60	44.16	20.40	20.40	0.	.5874E-03	.2878E-03	.2878E-03	0.	.3410E-05	.6227E-03

## CALCULATED STRESS STATE AND ELASTIC CONSTANTS, DATA SET NO. 20

	WDOV PSI	DEPSV PERCENT	DAMPV PERCENT	WDOY PSI	DEANT PERCENT	DAMPY PERCENT	MUC	STRAT		
	60119.99	.0037E-03	1.00	22728.21	.4628E-03	.6173	.3276	.3334		
NU	SIG1 PSI	SIG2 PSI	SIG3 PSI	BETA DEGREES	EPS1 PERCENT	EPS2 PERCENT	EPS3 PERCENT	DATA DEGREES	EPSOC PERCENT	GAMOC PERCENT
.74	34.97	29.40	29.40	.71	.6170E-03	.1440E-03	.1542E-03	.13	.1846E-03	.7247E-03
.76	36.24	29.40	29.40	.68	.6168E-03	.1251E-03	.1870E-03	.13	.2452E-04	.7424E-03
.78	39.74	29.40	29.40	.51	.6100E-03	.2053E-03	.2176E-03	.12	.6470E-04	.7607E-03
.79	41.21	29.43	29.40	.44	.6150E-03	.2354E-03	.2474E-03	.12	.6477E-04	.8040E-03
.80	42.70	29.40	29.40	.36	.6152E-03	.2650E-03	.2771E-03	.11	.2412E-04	.8350E-03
.81	44.17	29.40	29.40	.30	.6140E-03	.2650E-03	.2804E-03	.11	.4630E-06	.8634E-03

## CALCULATED STRESS STATE AND ELASTIC CONSTANTS, DATA SET NO. 21

	WDOV PSI	DEPSV PERCENT	DAMPV PERCENT	WDOY PSI	DEANT PERCENT	DAMPY PERCENT	MUC	STRAT		
	60647.04	.4643E-03	1.00	33633.18	.3487E-03	.6684	.3268	.3176		
NU	SIG1 PSI	SIG2 PSI	SIG3 PSI	BETA DEGREES	EPS1 PERCENT	EPS2 PERCENT	EPS3 PERCENT	DATA DEGREES	EPSOC PERCENT	GAMOC PERCENT
.74	36.42	29.40	29.40	1.30	.8481E-03	.1450E-03	.1890E-03	.23	.1047E-03	.7693E-03
.76	39.29	29.40	29.40	1.09	.8466E-03	.1753E-03	.2175E-03	.22	.6440E-04	.7955E-03
.78	39.74	29.40	29.40	.83	.8452E-03	.2055E-03	.2443E-03	.22	.6446E-04	.8210E-03
.79	41.23	29.40	29.40	.62	.8438E-03	.2357E-03	.2752E-03	.21	.6432E-04	.8465E-03
.80	42.73	29.40	29.40	.47	.8426E-03	.2659E-03	.3042E-03	.20	.6417E-04	.8751E-03
.81	44.17	29.40	29.40	.35	.8414E-03	.2961E-03	.3332E-03	.20	.6079E-05	.9019E-03

## CALCULATED STRESS STATE AND ELASTIC CONSTANTS, DATA SET NO. 22

WDOV PSI	DEPSV PERCENT	DAMPV PERCENT	WDOY PSI	DEANT PERCENT	DAMPY PERCENT	MUC	STRAT			
57440.49	.6005E-03	1.17	22286.28	.1069E-02	.7598	.3425	1.3756			
NU	SIG1 PSI	SIG2 PSI	SIG3 PSI	BETA DEGREES	EPS1 PERCENT	EPS2 PERCENT	EPS3 PERCENT	DATA DEGREES	EPSOC PERCENT	GAMOC PERCENT
.74	36.44	29.40	29.38	2.84	.7021E-03	.1456E-03	.3312E-03	.42	.1041E-03	.8933E-03
.76	38.33	29.40	29.38	2.30	.7877E-03	.1750E-03	.3544E-03	.41	.8491E-04	.1004E-02
.78	39.77	29.40	29.38	2.04	.7824E-03	.2052E-03	.3827E-03	.40	.6460E-04	.1024E-02
.79	41.24	29.40	29.39	1.80	.7740E-03	.2355E-03	.4081E-03	.39	.6444E-04	.1047E-02
.80	42.71	29.40	29.39	1.60	.7737E-03	.2660E-03	.4341E-03	.38	.2426E-04	.1069E-02
.81	44.14	29.40	29.39	1.44	.7690E-03	.2972E-03	.4603E-03	.37	.6043E-05	.1091E-02

## CALCULATED STRESS STATE AND ELASTIC CONSTANTS, DATA SET NO. 23

WDOV	DEPSV	DAMPV	WDOY	DEANT	DAMPY	MUC	STRAT			
PSI	PERCENT	PERCENT	PSI	PERCENT	PERCENT					
59435.39	.6106E-03	1.22	21849.70	.2946E-02	.8779	.3602	2.4122			
NU	SIG1	SIG2	SIG3	BETA	EPS1	EPS2	EPS3	DATA	EPSOC	GAMOC
	PSI	PSI	PSI	DEGREES	PERCENT	PERCENT	PERCENT	DEGREES	PERCENT	PERCENT
.74	36.99	29.40	29.36	4.40	.4060E-03	.1466E-03	.8966E-03	.55	.1060E-03	.1390E-02
.76	38.36	29.40	29.35	4.12	.1052E-02	.1771E-03	.6184E-03	.54	.0549E-04	.1413E-02
.78	39.80	29.40	29.36	3.54	.1844E-02	.2070E-03	.6410E-03	.53	.6513E-04	.1420E-02
.79	41.20	29.40	29.37	3.11	.1930E-02	.2381E-03	.6630E-03	.52	.6478E-04	.1444E-02
.80	42.70	29.40	29.37	2.74	.1829E-02	.2687E-03	.6832E-03	.50	.6442E-04	.1464E-02
.81	44.20	29.40	29.37	2.49	.1821E-02	.2992E-03	.7099E-03	.51	.6071E-05	.1477E-02

## CALCULATED STRESS STATE AND ELASTIC CONSTANTS, DATA SET NO. 24

	WDOV PSI	DEPSV PERCENT	DAMPV PERCENT	WDOY PSI	DEANT PERCENT	DAMPY PERCENT	MUC	STRAT		
	59006.67	.6151E-03	1.36	21353.91	.5358E-02	.9877	.3816	4.7059		
NU	SIG1 PSI	SIG2 PSI	SIG3 PSI	BETA DEGREES	EPS1 PERCENT	EPS2 PERCENT	EPS3 PERCENT	DATA DEGREES	EPSOC PERCENT	GAMOC PERCENT
.74	36.99	29.40	29.23	6.57	.1627E-02	.1476E-03	.1179E-02	.65	.1086E-03	.2703E-02
.76	38.99	29.40	29.24	5.83	.1618E-02	.1786E-03	.1170E-02	.64	.0541E-04	.2849E-02
.78	39.89	29.40	29.28	5.23	.1604E-02	.2091E-03	.1190E-02	.64	.6561E-04	.2752E-02
.79	41.34	29.40	29.29	5.47	.1594E-02	.2394E-03	.1210E-02	.63	.6511E-04	.2331E-02

.40 47.30 70.40 24.30 4.48 .154E-02-.270E-03-.173E-02 .43 .280E-04 .276E-02  
 .40 46.34 70.40 24.31 4.40 .157E-02-.261E-03-.174E-02 .43 .216E-04 .274E-02

# CALCULATED STRESS STATE AND ELASTIC CONSTANTS, DATA SET NO. 25

WAVE NO.	DEPTH PERCENT	DAMP PERCENT	WAVE NO.	DEPTH PERCENT	DAMP PERCENT	MUC	STRAT
57000.40	.420E-03	1.64	20341.31	.112E-01	1.2346	.4174	8.0372

WAVE NO.	SIG1 PSI	SIG2 PSI	SIG3 PSI	RETA DEGREES	POSI PERCENT	POSI PERCENT	POSI PERCENT	RETA DEGREES	POSI PERCENT	POSI PERCENT
.74	17.47	20.40	24.75	15.48	.3077E-02	.1510E-03	.2400E-02	.77	.1000E-03	.444E-02
.74	14.44	20.40	24.75	15.48	.3077E-02	.1510E-03	.2400E-02	.77	.1000E-03	.444E-02
.74	40.28	20.40	24.75	15.48	.3077E-02	.1510E-03	.2400E-02	.77	.1000E-03	.444E-02
.74	11.44	20.40	24.75	15.48	.3077E-02	.1510E-03	.2400E-02	.77	.1000E-03	.444E-02
.74	17.47	20.40	24.75	15.48	.3077E-02	.1510E-03	.2400E-02	.77	.1000E-03	.444E-02
.74	14.44	20.40	24.75	15.48	.3077E-02	.1510E-03	.2400E-02	.77	.1000E-03	.444E-02

# CALCULATED STRESS STATE AND ELASTIC CONSTANTS, DATA SET NO. 26

WAVE NO.	DEPTH PERCENT	DAMP PERCENT	WAVE NO.	DEPTH PERCENT	DAMP PERCENT	MUC	STRAT
57000.40	.420E-03	1.63	18273.47	.105E-01	1.2177	.4047	12.7290

WAVE NO.	SIG1 PSI	SIG2 PSI	SIG3 PSI	RETA DEGREES	POSI PERCENT	POSI PERCENT	POSI PERCENT	RETA DEGREES	POSI PERCENT	POSI PERCENT
.74	14.44	20.40	24.75	20.78	.440E-02	.1540E-03	.1911E-02	.74	.117E-01	.400E-02
.74	11.44	20.40	24.75	20.78	.440E-02	.1540E-03	.1911E-02	.74	.117E-01	.400E-02
.74	40.28	20.40	24.75	20.78	.440E-02	.1540E-03	.1911E-02	.74	.117E-01	.400E-02
.74	11.44	20.40	24.75	20.78	.440E-02	.1540E-03	.1911E-02	.74	.117E-01	.400E-02
.74	14.44	20.40	24.75	20.78	.440E-02	.1540E-03	.1911E-02	.74	.117E-01	.400E-02
.74	11.44	20.40	24.75	20.78	.440E-02	.1540E-03	.1911E-02	.74	.117E-01	.400E-02

# CALCULATED STRESS STATE AND ELASTIC CONSTANTS, DATA SET NO. 27

WAVE NO.	DEPTH PERCENT	DAMP PERCENT	WAVE NO.	DEPTH PERCENT	DAMP PERCENT	MUC	STRAT
57000.40	.444E-03	1.53	18210.37	.104E-01	2.3240	.4084	20.0770

WAVE NO.	SIG1 PSI	SIG2 PSI	SIG3 PSI	RETA DEGREES	POSI PERCENT	POSI PERCENT	POSI PERCENT	RETA DEGREES	POSI PERCENT	POSI PERCENT
.74	10.47	20.40	24.90	26.33	.603E-02	.159E-03	.4433E-02	.75	.115E-03	.109E-01
.74	11.44	20.40	24.90	26.33	.603E-02	.159E-03	.4433E-02	.75	.115E-03	.109E-01
.74	40.28	20.40	24.90	26.33	.603E-02	.159E-03	.4433E-02	.75	.115E-03	.109E-01
.74	11.44	20.40	24.90	26.33	.603E-02	.159E-03	.4433E-02	.75	.115E-03	.109E-01
.74	10.47	20.40	24.90	26.33	.603E-02	.159E-03	.4433E-02	.75	.115E-03	.109E-01
.74	11.44	20.40	24.90	26.33	.603E-02	.159E-03	.4433E-02	.75	.115E-03	.109E-01

# CALCULATED STRESS STATE AND ELASTIC CONSTANTS, DATA SET NO. 28

WAVE NO.	DEPTH PERCENT	DAMP PERCENT	WAVE NO.	DEPTH PERCENT	DAMP PERCENT	MUC	STRAT
57000.40	.677E-03	1.43	17447.41	.102E-01	2.5404	.5150	25.4070

WAVE NO.	SIG1 PSI	SIG2 PSI	SIG3 PSI	RETA DEGREES	POSI PERCENT	POSI PERCENT	POSI PERCENT	RETA DEGREES	POSI PERCENT	POSI PERCENT
.74	40.17	20.40	26.05	29.19	.402E-02	.161E-03	.431E-02	.76	.118E-03	.140E-01
.74	41.32	20.40	26.05	29.19	.402E-02	.161E-03	.431E-02	.76	.118E-03	.140E-01
.74	42.51	20.40	26.05	29.19	.402E-02	.161E-03	.431E-02	.76	.118E-03	.140E-01
.74	43.74	20.40	26.05	29.19	.402E-02	.161E-03	.431E-02	.76	.118E-03	.140E-01
.74	44.91	20.40	26.05	29.19	.402E-02	.161E-03	.431E-02	.76	.118E-03	.140E-01
.74	46.10	20.40	26.05	29.19	.402E-02	.161E-03	.431E-02	.76	.118E-03	.140E-01

# CALCULATED STRESS STATE AND ELASTIC CONSTANTS, DATA SET NO. 29

WAVE NO.	DEPTH PERCENT	DAMP PERCENT	WAVE NO.	DEPTH PERCENT	DAMP PERCENT	MUC	STRAT
57000.40	.104E-03	1.44					

WAVE NO.	SIG1 PSI	SIG2 PSI	SIG3 PSI	RETA DEGREES	POSI PERCENT	POSI PERCENT	POSI PERCENT	RETA DEGREES	POSI PERCENT	POSI PERCENT
.74	36.92	20.40	24.40	0.	.619E-03	.148E-03	.140E-03	0.	.107E-03	.744E-03

20	74.20	70.43	79.40	0.	.F19AF-03-.1707E-03-.1707E-03	0.	.A07AF-04	.703AF-03
30	13.74	30.40	30.40	0.	.A10AF-03-.2107E-03-.2107E-03	0.	.A07AF-04	.703AF-03
40	41.23	70.40	70.40	0.	.A10AF-03-.2416E-03-.2416E-03	0.	.A44AF-04	.A170F-03
50	42.77	79.40	79.40	0.	.A10AF-03-.2725E-03-.2725E-03	0.	.A44AF-04	.A170F-03
60	44.11	70.43	79.40	0.	.A10AF-03-.3036E-03-.3036E-03	0.	.A131E-03	.A70AF-03

## APPENDIX B-3

## Resonant Column Test No. 18C-3

TEST NO. 18C-3, DAT GRIFFIN, 7/13/79

TEST RESULTS FOR SAMPLE NO. 7

SIZE INCH	WT GRAMS	DIAM CM	HEIGHT CM	NR	
3.90	961.04	7.10	14.78	12	
TYPE GRADE	ACRV	DCRV	ACFT	DCFT	PMF
1476.40	2503.00	14.75	2500.00	5.75	31.45
VOL CC	UNIT %/CC	SPH	SHF	SPH/R	
5844.00	1.67	6.05	1.68	8.38	
GENL MV-DB	ACGEN MV-DB	BROW HERTZ	COLT MV-DB	ACCOLT MV-DB	PROT HERTZ
-0.	-0.	-0.	0.00	00.00	100.00
-0.	-0.	-0.	20.00	220.00	100.00
-0.	-0.	-0.	40.00	435.00	100.00
-0.	-0.	-0.	60.00	650.00	100.00
-0.	-0.	-0.	80.00	865.00	100.00
-0.	-0.	-0.	100.00	1080.00	100.00
-0.	-0.	-0.	120.00	1295.00	100.00
-0.	-0.	-0.	140.00	1510.00	100.00
-0.	-0.	-0.	160.00	1725.00	100.00
-0.	-0.	-0.	180.00	1940.00	100.00
-0.	-0.	-0.	200.00	2155.00	100.00
-0.	-0.	-0.	220.00	2370.00	100.00
-0.	-0.	-0.	240.00	2585.00	100.00
-0.	-0.	-0.	260.00	2800.00	100.00
-0.	-0.	-0.	280.00	3015.00	100.00
-0.	-0.	-0.	300.00	3230.00	100.00
-0.	-0.	-0.	320.00	3445.00	100.00
-0.	-0.	-0.	340.00	3660.00	100.00
-0.	-0.	-0.	360.00	3875.00	100.00
-0.	-0.	-0.	380.00	4090.00	100.00
-0.	-0.	-0.	400.00	4305.00	100.00
-0.	-0.	-0.	420.00	4520.00	100.00
-0.	-0.	-0.	440.00	4735.00	100.00
-0.	-0.	-0.	460.00	4950.00	100.00
-0.	-0.	-0.	480.00	5165.00	100.00
-0.	-0.	-0.	500.00	5380.00	100.00
-0.	-0.	-0.	520.00	5595.00	100.00
-0.	-0.	-0.	540.00	5810.00	100.00
-0.	-0.	-0.	560.00	6025.00	100.00
-0.	-0.	-0.	580.00	6240.00	100.00
-0.	-0.	-0.	600.00	6455.00	100.00
-0.	-0.	-0.	620.00	6670.00	100.00
-0.	-0.	-0.	640.00	6885.00	100.00
-0.	-0.	-0.	660.00	7100.00	100.00
-0.	-0.	-0.	680.00	7315.00	100.00
-0.	-0.	-0.	700.00	7530.00	100.00
-0.	-0.	-0.	720.00	7745.00	100.00
-0.	-0.	-0.	740.00	7960.00	100.00
-0.	-0.	-0.	760.00	8175.00	100.00
-0.	-0.	-0.	780.00	8390.00	100.00
-0.	-0.	-0.	800.00	8605.00	100.00
-0.	-0.	-0.	820.00	8820.00	100.00
-0.	-0.	-0.	840.00	9035.00	100.00
-0.	-0.	-0.	860.00	9250.00	100.00
-0.	-0.	-0.	880.00	9465.00	100.00
-0.	-0.	-0.	900.00	9680.00	100.00
-0.	-0.	-0.	920.00	9895.00	100.00
-0.	-0.	-0.	940.00	10110.00	100.00
-0.	-0.	-0.	960.00	10325.00	100.00
-0.	-0.	-0.	980.00	10540.00	100.00
-0.	-0.	-0.	1000.00	10755.00	100.00

CALCULATED STRESS STATE AND PLASTIC CONSTANTS, DATA SET NO. 1

WDOV PSI	DEPSV PERCENT	DAMPV PERCENT	WDOV PSI	OGAMT PERCENT	DAMPV PERCENT	MUC	STRAT			
			27794.40	.4475E-04	.49					
WDOV PSI	SIG1 PSI	SIG2 PSI	SIG3 PSI	BETA DEGREES	EPS1 PERCENT	EPS2 PERCENT	EPS3 PERCENT	BATA DEGREES	EPSOC PERCENT	GAMOC PERCENT
.74	51.45	51.45	51.44	45.00	.1812E-04		-.1812E-04	45.000		.2049E-04
.77	51.45	51.45	51.44	45.00	.1812E-04		-.1812E-04	45.000		.2049E-04
.78	51.45	51.45	51.44	45.00	.1812E-04		-.1812E-04	45.000		.2049E-04
.79	51.45	51.45	51.44	45.00	.1812E-04		-.1812E-04	45.000		.2049E-04
.80	51.45	51.45	51.44	45.00	.1812E-04		-.1812E-04	45.000		.2049E-04
.81	51.45	51.45	51.44	45.00	.1812E-04		-.1812E-04	45.000		.2049E-04

## CALCULATED STRESS STATE AND ELASTIC CONSTANTS, DATA SET NO. 2

WDOV PSI	DEPSV PERCENT	DAMPV PERCENT	WDOV PSI	OGAMT PERCENT	DAMPV PERCENT	MUC	STRAT			
			27844.01	.9130E-04	.48					
WDOV PSI	SIG1 PSI	SIG2 PSI	SIG3 PSI	BETA DEGREES	EPS1 PERCENT	EPS2 PERCENT	EPS3 PERCENT	BATA DEGREES	EPSOC PERCENT	GAMOC PERCENT
.74	51.45	51.45	51.42	45.00	.3697E-04		-.3697E-04	45.000		.6038E-04
.75	51.45	51.45	51.42	45.00	.3697E-04		-.3697E-04	45.000		.6038E-04
.76	51.45	51.45	51.42	45.00	.3697E-04		-.3697E-04	45.000		.6038E-04
.77	51.45	51.45	51.42	45.00	.3697E-04		-.3697E-04	45.000		.6038E-04
.78	51.45	51.45	51.42	45.00	.3697E-04		-.3697E-04	45.000		.6038E-04
.79	51.45	51.45	51.42	45.00	.3697E-04		-.3697E-04	45.000		.6038E-04
.80	51.45	51.45	51.42	45.00	.3697E-04		-.3697E-04	45.000		.6038E-04

## CALCULATED STRESS STATE AND ELASTIC CONSTANTS, DATA SET NO. 3

WDOV PSI	DEPSV PERCENT	DAMPV PERCENT	WDOV PSI	OGAMT PERCENT	DAMPV PERCENT	MUC	STRAT		
			27931.77	.2276E-01	.49				
WDOV PSI	SIG1 PSI	SIG2 PSI	BETA DEGREES	EPS1 PERCENT	EPS2 PERCENT	EPS3 PERCENT	BATA DEGREES	EPSOC PERCENT	GAMOC PERCENT
.74	51.45	51.45	51.39	45.00	.0015E-04	-.0015E-04	45.000		.1472E-03
.75	51.45	51.45	51.39	45.00	.0015E-04	-.0015E-04	45.000		.1472E-03
.76	51.45	51.45	51.39	45.00	.0015E-04	-.0015E-04	45.000		.1472E-03
.77	51.45	51.45	51.39	45.00	.0015E-04	-.0015E-04	45.000		.1472E-03
.78	51.45	51.45	51.39	45.00	.0015E-04	-.0015E-04	45.000		.1472E-03
.79	51.45	51.45	51.39	45.00	.0015E-04	-.0015E-04	45.000		.1472E-03
.80	51.45	51.45	51.39	45.00	.0015E-04	-.0015E-04	45.000		.1472E-03

## CALCULATED STRESS STATE AND ELASTIC CONSTANTS, DATA SET NO. 4

WDOV PSI	DEPSV PERCENT	DAMPV PERCENT	WDOV PSI	OGAMT PERCENT	DAMPV PERCENT	MUC	STRAT			
			27933.72	.4403E-03	.50					
WDOV PSI	SIG1 PSI	SIG2 PSI	SIG3 PSI	BETA DEGREES	EPS1 PERCENT	EPS2 PERCENT	EPS3 PERCENT	BATA DEGREES	EPSOC PERCENT	GAMOC PERCENT
.74	51.47	51.45	51.33	45.00	.1783E-03		-.1783E-03	45.000		.2911E-03
.75	51.47	51.45	51.33	45.00	.1783E-03		-.1783E-03	45.000		.2911E-03
.76	51.47	51.45	51.33	45.00	.1783E-03		-.1783E-03	45.000		.2911E-03
.77	51.47	51.45	51.33	45.00	.1783E-03		-.1783E-03	45.000		.2911E-03
.78	51.47	51.45	51.33	45.00	.1783E-03		-.1783E-03	45.000		.2911E-03
.79	51.47	51.45	51.33	45.00	.1783E-03		-.1783E-03	45.000		.2911E-03
.80	51.47	51.45	51.33	45.00	.1783E-03		-.1783E-03	45.000		.2911E-03

## CALCULATED STRESS STATE AND ELASTIC CONSTANTS, DATA SET NO. 5

WDOV PSI	DEPSV PERCENT	DAMPV PERCENT	WDOV PSI	OGAMT PERCENT	DAMPV PERCENT	MUC	STRAT			
27829.20				.9126E-03		.54				
WDOV PSI	SIG1 PSI	SIG2 PSI	SIG3 PSI	BETA DEGREES	EPS1 PERCENT	EPS2 PERCENT	EPS3 PERCENT	BATA DEGREES	EPSOC PERCENT	GAMOC PERCENT
.74	51.69	51.45	51.22	45.00	.3791E-03		-.3791E-03	45.000		.5376E-03
.75	51.69	51.45	51.22	45.00	.3791E-03		-.3791E-03	45.000		.5376E-03
.76	51.69	51.45	51.22	45.00	.3791E-03		-.3791E-03	45.000		.5376E-03
.77	51.69	51.45	51.22	45.00	.3791E-03		-.3791E-03	45.000		.5376E-03
.78	51.69	51.45	51.22	45.00	.3791E-03		-.3791E-03	45.000		.5376E-03
.79	51.69	51.45	51.22	45.00	.3791E-03		-.3791E-03	45.000		.5376E-03
.80	51.69	51.45	51.22	45.00	.3791E-03		-.3791E-03	45.000		.5376E-03

[illegible]

## CALCULATED STRESS STATE AND ELASTIC CONSTANTS, DATA SET NO. 7

[illegible]

## CALCULATED STRESS STATE AND ELASTIC CONSTANTS, DATA SET NO. A

NO	SIG1 DET	SIG2 DET	SIG3 DET	REF1 DEFECT	REF2 DEFECT	REF3 DEFECT	REF4 DEFECT	REF5 DEFECT	REF6 DEFECT
78	51.45	51.45	51.45	45.00	2060F-32=	-2060F-32	45.003	1370F-32	
79	51.45	51.45	51.45	45.00	2060F-32=	-2060F-32	45.003	1370F-32	
80	51.45	51.45	51.45	45.00	2060F-32=	-2060F-32	45.003	1370F-32	
81	51.45	51.45	51.45	45.00	2060F-32=	-2060F-32	45.003	1370F-32	
82	51.45	51.45	51.45	45.00	2060F-32=	-2060F-32	45.003	1370F-32	
83	51.45	51.45	51.45	45.00	2060F-32=	-2060F-32	45.003	1370F-32	
84	51.45	51.45	51.45	45.00	2060F-32=	-2060F-32	45.003	1370F-32	
85	51.45	51.45	51.45	45.00	2060F-32=	-2060F-32	45.003	1370F-32	
86	51.45	51.45	51.45	45.00	2060F-32=	-2060F-32	45.003	1370F-32	
87	51.45	51.45	51.45	45.00	2060F-32=	-2060F-32	45.003	1370F-32	
88	51.45	51.45	51.45	45.00	2060F-32=	-2060F-32	45.003	1370F-32	
89	51.45	51.45	51.45	45.00	2060F-32=	-2060F-32	45.003	1370F-32	
90	51.45	51.45	51.45	45.00	2060F-32=	-2060F-32	45.003	1370F-32	

## CALCULATED STRESS STATE AND ELASTIC CONSTANTS, DATA SET NO. 9

[illegible]

~~#01CUC-7E9-970F35-57-87F-AAD-E1A5T+6-CONSTANTS-DATA SET NO-10~~

WIND DIR	WIND SPEED	WIND DIRECTION	WIND SPEED	WIND DIRECTION	WIND SPEED	WIND DIRECTION	WIND SPEED	WIND DIRECTION
240	20.44	149	7.01	1.66				
WIND DIR	WIND SPEED	WIND DIRECTION	WIND SPEED	WIND DIRECTION	WIND SPEED	WIND DIRECTION	WIND SPEED	WIND DIRECTION
240	20.44	149	7.01	1.66				

## CALCULATED STRESS STATE AND ELASTIC CONSTANTS, DATA SET NO. 11

MODV PSI	DPDEV PERCENT	DAMPV PERCENT	MODT PSI	DCART PERCENT	DAMPY PERCENT	MUC	STRAT			
			21244.75	.2309E-01	2.28					
NU	SIG1 PSI	SIG2 PSI	SIG3 PSI	RTA DEGREES	EPS1 PERCENT	EPS2 PERCENT	EPS3 PERCENT	FATA DEGREES	FRQC PERCENT	GANC PERCENT
.74	44.87	51.45	44.08	45.00	.0148E-02		.0148E-02	45.000		.1527E-01
.79	46.87	51.45	46.08	45.00	.0148E-02		.0148E-02	45.000		.1527E-01
.74	44.87	51.45	46.08	45.00	.0148E-02		.0148E-02	45.000		.1527E-01
.79	46.87	51.45	46.08	45.00	.0148E-02		.0148E-02	45.000		.1527E-01
.74	44.87	51.45	46.08	45.00	.0148E-02		.0148E-02	45.000		.1527E-01
.79	46.87	51.45	46.08	45.00	.0148E-02		.0148E-02	45.000		.1527E-01

## CALCULATED STRESS STATE AND ELASTIC CONSTANTS, DATA SET NO. 12

MODV PSI	DPDEV PERCENT	DAMPV PERCENT	MODT PSI	DCART PERCENT	DAMPY PERCENT	MUC	STRAT			
			22569.85	.2881E-01	2.59					
NU	SIG1 PSI	SIG2 PSI	SIG3 PSI	RTA DEGREES	EPS1 PERCENT	EPS2 PERCENT	EPS3 PERCENT	FATA DEGREES	FRQC PERCENT	GANC PERCENT
.74	47.04	41.45	44.05	45.00	.1166E-01		.1166E-01	45.000		.1905E-01
.79	47.04	51.45	44.05	45.00	.1166E-01		.1166E-01	45.000		.1905E-01
.74	47.04	51.45	44.05	45.00	.1166E-01		.1166E-01	45.000		.1905E-01
.79	47.04	51.45	44.05	45.00	.1166E-01		.1166E-01	45.000		.1905E-01
.74	47.04	51.45	44.05	45.00	.1166E-01		.1166E-01	45.000		.1905E-01
.79	47.04	51.45	44.05	45.00	.1166E-01		.1166E-01	45.000		.1905E-01
.74	47.04	51.45	44.05	45.00	.1166E-01		.1166E-01	45.000		.1905E-01
.79	47.04	51.45	44.05	45.00	.1166E-01		.1166E-01	45.000		.1905E-01

## APPENDIX B-4

Hollow Cylinder Test No. A26L-2

GP 155 14, TEST 47, A76L-2, MARCH 10, 1975

TEST RESULTS FOR SAMPLE NO. 1A

SIG W	WT	HEIGHT	T	NR
KSC	GRAMS	INCHES	INCHES	
2.22	591.87	1.95	.77	10

VCL	INT
CC	GACC
610.20	1.5A

DESIG      YESX    STANT    OGANI    ALPHA

1.700J	.001A	-3.	-0.	-3.
4.1A30	.3300	-3.	-0.	-3.
4.320J	.2110	-3.	-0.	-3.
15.433J	.0110	-0.	-0.	-0.
21.333J	.0110	-7.	-0.	-7.
21.330J	.3330	-0.	-0.	-0.
13.133J	.3490	-0.	-0.	-0.
49.1300	.3630	-0.	-0.	-0.
45.7000	.0970	-0.	-0.	-0.
74.4390	.1100	-0.	-0.	-0.

STATE AND ELASTIC CONSTANTS, DATA SET NO. 1

44	NAME %1	DEATH PERCENT	HOUSE %1	DEATH PERCENT	HOOF. %1	DEATH PERCENT	CRIM. %1	CRIM. PERCENT	MUR	STR
24	4432-33	1846-02	1428-01	5618-00			1686-02			
29	3949-31	1940-02	1376-14	5121-00			1743-33			
29	39124-00	1940-02	1331-28	5119-30			16700-00			
16	39742-31	1840-02	1276-79	7461-00			1721-97			
29	39406-00	1940-02	1340-01	5618-00			1213-33			
49	32929-30	1940-02	1140-04	5618-00			11050-00			

NO	SIG1 PSI	SIG2 PSI	SIG3 PSI	BETA DEGREES	EPS1 PERCENT	EPS2 PERCENT	EPS3 PERCENT	EATA DEGREES	EPSOC PERCENT	GAMOC PERCENT
24	88.10	20.40	20.30	0.	1844E-03		5430E-03	0.	4311E-03	2071E-02
29	55.10	20.40	20.33	0.	1844E-03		7941E-03	0.	3640E-03	2149E-02
14	55.10	20.40	20.76	0.	1844E-03		4910E-03	0.	2984E-03	2311E-02
30	55.10	20.40	20.40	0.	1844E-03		1140E-02	0.	2710E-03	2491E-02
44	88.10	20.32	20.40	0.	1844E-03		1651E-02	0.	1310E-03	2698E-02
19	55.10	41.05	20.40	0.	1844E-03		1774E-02	0.	2413E-04	2906E-02

## STRESS STATE AND ELASTIC CONSTANTS, DATA SET NO. 2

NO	MOOT PSI	DEPSV PERCENT	MOOVS PSI	EPSV PERCENT	MOOT PSI	DEGANT PERCENT	CMOOT PSI	CGAMV PERCENT	MUC	STRAIT
24	37410.12	0.154E-02	14776.25	5662E+00			15931.50			
29	29105.11	0.154E-02	13472.50	5642E+00			14963.17			
14	37374.47	0.154E-02	13442.03	5662E+00			13915.25			
30	35444.24	0.154E-02	13446.36	5642E+00			12322.13			
44	37404.32	0.154E-02	13322.09	5662E+00			11739.00			
19	31454.91	0.154E-02	11592.71	5662E+00			10600.98			

NO	SIG1 PSI	SIG2 PSI	SIG3 PSI	BETA DEGREES	EPS1 PERCENT	EPS2 PERCENT	EPS3 PERCENT	EATA DEGREES	EPSOC PERCENT	GAMOC PERCENT
24	54.07	20.40	20.73	0.	0.154E-02		1443E-02	0.	1484E-02	0.903E-02
29	50.47	20.40	20.05	0.	0.154E-02		2410E-02	0.	1313E-02	0.727E-02
14	54.07	20.40	20.37	0.	0.154E-02		3170E-02	0.	0.944E-03	0.774E-02
30	54.07	20.40	20.40	0.	0.154E-02		2034E-02	0.	0.904E-03	0.530E-02
44	54.07	20.40	20.40	0.	0.154E-02		4435E-02	0.	0.430E-03	0.904E-02
19	54.07	42.32	20.40	0.	0.154E-02		5413E-02	0.	0.804E-04	0.981E-02

## STRESS STATE AND ELASTIC CONSTANTS, DATA SET NO. 3

NO	MOOT PSI	DEPSV PERCENT	MOOVS PSI	EPSV PERCENT	MOOT PSI	DEGANT PERCENT	CMOOT PSI	CGAMV PERCENT	MUC	STRAIT
24	14941.87	0.112E-01	14599.27	5713E+00			15662.05			
29	17740.44	0.112E-01	14179.02	5713E+00			14031.05			
14	14941.87	0.112E-01	13656.37	5713E+00			12717.33			
30	14340.97	0.112E-01	13122.31	5713E+00			12579.44			
44	13274.51	0.112E-01	12483.85	5713E+00			11548.45			

NO	SIG1 PSI	SIG2 PSI	SIG3 PSI	BETA DEGREES	EPS1 PERCENT	EPS2 PERCENT	EPS3 PERCENT	EATA DEGREES	EPSOC PERCENT	GAMOC PERCENT
24	40.34	20.40	21.23	0.	0.112E-01		3463E-02	0.	2573E-02	0.126E-01
29	40.34	20.40	20.40	0.	0.112E-01		4402E-02	0.	2222E-02	0.137E-01
14	40.34	20.40	20.40	0.	0.112E-01		5412E-02	0.	1.827E-02	0.241E-01
30	40.34	20.40	20.40	0.	0.112E-01		6444E-02	0.	1.717E-02	0.182E-01
44	40.34	20.40	20.40	0.	0.112E-01		7444E-02	0.	0.905E-03	0.164E-01
19	40.34	42.32	20.40	0.	0.112E-01		1.094E-01	0.	1.175E-03	0.180E-01

## STRESS STATE AND ELASTIC CONSTANTS, DATA SET NO. 4

NO	MOOT PSI	DEPSV PERCENT	MOOVS PSI	EPSV PERCENT	MOOT PSI	DEGANT PERCENT	CMOOT PSI	CGAMV PERCENT	MUC	STRAIT
24	37372.23	0.104E-01	14678.70	5795E+00			15015.00			
29	44140.10	0.104E-01	14440.32	5795E+00			14027.13			
14	37372.23	0.104E-01	14042.99	5795E+00			12070.34			
30	35503.21	0.104E-01	13322.73	5795E+00			12241.51			
44	31443.41	0.104E-01	12731.52	5795E+00			11043.49			
19	30000.00	0.104E-01	11443.30	5795E+00			10078.40			

NO	SIG1 PSI	SIG2 PSI	SIG3 PSI	BETA DEGREES	EPS1 PERCENT	EPS2 PERCENT	EPS3 PERCENT	EATA DEGREES	EPSOC PERCENT	GAMOC PERCENT
24	42.09	20.40	21.06	0.	0.104E-01		4154E-02	0.	4444E-02	0.218E-01
29	42.09	20.40	20.40	0.	0.104E-01		5440E-02	0.	4244E-02	0.230E-01
14	42.09	20.40	20.40	0.	0.104E-01		6440E-02	0.	4144E-02	0.247E-01
30	42.09	20.40	20.40	0.	0.104E-01		7440E-02	0.	4044E-02	0.267E-01
44	42.09	20.40	20.40	0.	0.104E-01		8440E-02	0.	3944E-02	0.284E-01
19	42.09	42.32	20.40	0.	0.104E-01		9440E-02	0.	3844E-02	0.304E-01

## STRESS STATE AND PLASTIC CONSTANTS, DATA SET NO. 4

NO	MOOT PSI	DEPSV PERCENT	MOOVS PSI	EPSV PERCENT	MOOT PSI	DEGANT PERCENT	CMOOT PSI	CGAMV PERCENT	MUC	STRAIT
24	56644.15	0.274E-01	14144.00	6432E+00			14441.12			
29	57315.18	0.274E-01	14118.18	6432E+00			13642.71			
14	56644.15	0.274E-01	14211.40	6432E+00			12401.24			

.19 37608.82 +2709E-01 13625.44 +3877E+00 11729.79  
 .20 24652.86 +3740E-01 13667.88 +2817E+00 10562.53  
 .19 29220.49 +2709E-01 12211.31 +3877E+00 9806.98

NU	SIG1 PSI	SIG2 PSI	SIG3 PSI	BETA DEGREES	EPS1 PERCENT	EPS2 PERCENT	EPS3 PERCENT	EATA DEGREES	EPSCC PERCENT	GAMCC PERCENT
.76	46.04	29.40	23.47	0.	+2709E-010.	-1131E-01	0.	+316E-02	+1106E-01	0.
.78	65.34	29.40	27.39	0.	+2709E-010.	-1131E-01	0.	+540E-02	+377E-01	0.
.76	64.34	27.11	29.40	0.	+2709E-010.	-1177E-01	0.	+847E-02	+384E-01	0.
.78	65.04	26.43	29.40	0.	+2709E-010.	-1770E-01	0.	+332E-02	+173E-01	0.
.76	65.34	21.56	29.40	0.	+2709E-010.	-2174E-01	0.	+107E-02	+2847E-01	0.
.78	65.34	20.28	29.40	0.	+2709E-010.	-2661E-01	0.	+342E-03	+616E-01	0.

## STRESS STATE AND ELASTIC CONSTANTS, DATA SET NO. 6

NU	MODVT PSI	DEPRV PERCENT	MODVS PSI	EPSV PERCENT	MODT PSI	DEMT PERCENT	MODT PSI	CGMT PERCENT	MUC	STRAT
.76	37371.53	+3500E-01	15402.04	+591E+00						
.78	34406.77	+3500E-01	14988.94	+599E+00						
.76	37507.13	+3500E-01	14454.12	+599E+00						
.78	34173.36	+3500E-01	13882.46	+599E+00						
.76	37551.04	+3500E-01	13174.33	+599E+00						
.78	28749.35	+3500E-01	12414.36	+599E+00						

NU	SIG1 PSI	SIG2 PSI	SIG3 PSI	BETA DEGREES	EPS1 PERCENT	EPS2 PERCENT	EPS3 PERCENT	EATA DEGREES	EPSCC PERCENT	GAMCC PERCENT
.76	67.99	29.40	23.37	0.	+3590E-010.	-1134E-01	0.	+819E-02	+4037E-01	0.
.78	67.99	29.40	28.24	0.	+3590E-010.	-1466E-01	0.	+707E-02	+424E-01	0.
.76	67.99	23.11	29.40	0.	+3590E-010.	-1949E-01	0.	+502E-02	+451E-01	0.
.78	67.99	27.08	29.40	0.	+3590E-010.	-250E-01	0.	+314E-02	+486E-01	0.
.76	67.99	27.45	29.40	0.	+3590E-010.	-2821E-01	0.	+25E-02	+524E-01	0.
.78	67.99	27.72	29.40	0.	+3590E-010.	-3449E-01	0.	+449E-03	+574E-01	0.

## STRESS STATE AND PLASTIC CONSTANTS, DATA SET NO. 7

NU	MODVT PSI	DEPRV PERCENT	MODVS PSI	EPSV PERCENT	MODT PSI	DEMT PERCENT	MODT PSI	CGMT PERCENT	MUC	STRAT
.76	33792.89	+4615E-01	15600.07	+6862E+00						

.78 77962.45 +4615E-01 15101.40 +6862E+00 12729.71  
 .76 31711.11 +4615E-01 14430.28 +6862E+00 11833.75  
 .78 32621.28 +4615E-01 14675.74 +6862E+00 12037.70  
 .76 29714.14 +4615E-01 13347.70 +6862E+00 12040.77  
 .78 27247.75 +4615E-01 12774.05 +6862E+00 9147.47

NU	SIG1 PSI	SIG2 PSI	SIG3 PSI	BETA DEGREES	EPS1 PERCENT	EPS2 PERCENT	EPS3 PERCENT	EATA DEGREES	EPSCC PERCENT	GAMCC PERCENT
.76	70.94	29.40	24.08	0.	+4615E-010.	-1497E-01	0.	+104E-02	+517E-01	0.
.78	73.94	29.40	29.10	0.	+4615E-010.	-1124E-01	0.	+912E-02	+441E-01	0.
.76	73.94	24.43	29.40	0.	+4615E-010.	-2374E-01	0.	+743E-02	+580E-01	0.
.78	70.94	29.13	29.40	0.	+4615E-010.	-1791E-01	0.	+446E-02	+522E-01	0.
.76	70.94	24.15	29.40	0.	+4615E-010.	-2024E-01	0.	+322E-02	+574E-01	0.
.78	70.94	20.17	29.40	0.	+4615E-010.	-2446E-01	0.	+637E-03	+710E-01	0.

## STRESS STATE AND ELASTIC CONSTANTS, DATA SET NO. 8

NU	MODVT PSI	DEPRV PERCENT	MODVS PSI	EPSV PERCENT	MODT PSI	DEMT PERCENT	MODT PSI	CGMT PERCENT	MUC	STRAT
.76	71074.49	+6442E-01	14059.33	+6246E+00						
.78	58109.57	+6442E-01	14602.78	+6246E+00						
.76	31301.39	+6442E-01	15070.96	+6246E+00						
.78	29771.92	+6442E-01	14448.97	+6246E+00						
.76	28247.20	+6442E-01	13741.77	+6246E+00						
.78	24637.31	+6442E-01	12848.37	+6246E+00						

NU	SIG1 PSI	SIG2 PSI	SIG3 PSI	BETA DEGREES	EPS1 PERCENT	EPS2 PERCENT	EPS3 PERCENT	EATA DEGREES	EPSCC PERCENT	GAMCC PERCENT
.76	77.04	29.40	25.95	0.	+6442E-010.	-1204E-01	0.	+147E-02	+726E-01	0.
.78	73.04	29.43	24.48	0.	+6442E-010.	-1318E-01	0.	+127E-02	+764E-01	0.
.76	77.04	26.19	29.40	0.	+6442E-010.	-2324E-01	0.	+136E-02	+517E-01	0.
.78	77.04	21.51	29.40	0.	+6442E-010.	-2171E-01	0.	+744E-02	+517E-01	0.
.76	77.04	20.83	29.40	0.	+6442E-010.	-2077E-01	0.	+601E-02	+444E-01	0.
.78	77.04	20.16	29.40	0.	+6442E-010.	-2420E-01	0.	+844E-03	+1035E-01	0.

## STRESS STATE AND ELASTIC CONSTANTS, DATA SET NO. 9

NU	MODVT PSI	DEPRV PERCENT	MODVS PSI	EPSV PERCENT	MODT PSI	DEMT PERCENT	MODT PSI	CGMT PERCENT	MUC	STRAT
----	--------------	------------------	--------------	-----------------	-------------	-----------------	-------------	-----------------	-----	-------

NO	SIG1 PSI	SIG2 PSI	SIG3 PSI	RETA DEGREES	EDS1 PERCENT	EDS2 PERCENT	EDS3 PERCENT	DATA DEGREES	EDS4 PERCENT	GAMMA PERCENT
28	30546.20	.4413E-01	14321.70	.6451E+00				13320.24		
29	21445.72	.4413E-01	15214.74	.6451E+00				11500.70		
30	24473.74	.4513E-01	15270.35	.6451E+00				12450.16		
31	27400.15	.4513E-01	16040.13	.6451E+00				0444.41		
32	24144.45	.4413E-01	13023.43	.6451E+00				0374.37		
33	24637.24	.4413E-01	13120.69	.6451E+00				0267.53		

## STRESS STATE AND ELASTIC CONSTANTS, DATA SET NO. 10

NO	WDMV PSI	EDS1 PERCENT	WDMV PSI	EDS2 PERCENT	WDMV PSI	EDS3 PERCENT	WDMV PSI	EDS4 PERCENT	MUR	STRAT
28	29427.37	.1210E+00	16494.76	.4810E+00				12024.44		
29	29284.74	.1210E+00	15419.89	.4810E+00				11274.40		
30	27387.40	.1210E+00	15254.57	.4810E+00				10443.24		
31	24433.40	.1210E+00	14700.42	.4810E+00				0452.30		
32	24414.44	.1210E+00	14455.67	.4810E+00				440.04		
33	24047.04	.1210E+00	13421.01	.4810E+00				404.74		

NO	SIG1 PSI	SIG2 PSI	SIG3 PSI	RETA DEGREES	EDS1 PERCENT	EDS2 PERCENT	EDS3 PERCENT	DATA DEGREES	EDS4 PERCENT	GAMMA PERCENT
28	07.40	20.40	20.30	0.	.1210E+000.		~.1472E-01	0.	.1740E-01	.1740E+00
29	07.40	20.41	20.40	0.	.1210E+000.		~.1473E-01	0.	.1740E-01	.1740E+00
30	07.40	21.41	20.40	0.	.1210E+000.		~.1473E-01	0.	.1740E-01	.1740E+00
31	07.40	21.42	20.40	0.	.1210E+000.		~.1473E-01	0.	.1740E-01	.1740E+00
32	07.40	21.72	20.40	0.	.1210E+000.		~.1473E-01	0.	.1740E-01	.1740E+00
33	07.40	21.72	20.40	0.	.1210E+000.		~.1473E-01	0.	.1740E-01	.1740E+00

## APPENDIX B-5

## Hollow Cylinder Test No. B29-3

RAY GRIPPER, TEST NO. B29-3, MARCH 27, 1976

## TEST RESULTS FOR SAMPLE NO. 19

SIGAC- KSC	WZ GRAMS	NETGAK INCHES	L INCHES	NR
3.50	1047.66	1.08	.78	29

VOL CC	WBT GACC
524.41	1.68

## DESIGN - DRESS - GRADE - GAST - ALPHA

1.7100	.0012	.0193	.0034	.0010
3.2100	.0034	.0158	.0032	.0000
6.9700	.0069	.0155	.0012	.0010
11.0300	.0113	.0048	.0001	.0010
15.1800	.0112	.0222	.0048	.0000
19.3600	.0113	.0403	.0048	.0048
23.4700	.0118	.0624	.0155	.0170
27.6800	.0122	.0878	.0188	.0490
31.8400	.0125	.1130	.0210	.0010
36.1300	.0145	.1463	.0061	.0000
40.5300	.0173	.0168	.0040	.0390
44.9100	.0240	.0171	.0030	.0370
49.2800	.0379	.0173	.0031	.0010
53.6400	.0430	.0233	.0033	.0430
57.9400	.0484	.0240	.0035	.0170
62.2300	.0433	.0249	.0033	.0370
66.5100	.0570	.0252	.0033	.0370
70.8300	.0660	.0304	.0048	.0010
75.1300	.0670	.0720	.0130	.0010
79.4000	.0870	.0904	.0188	.0078
83.6300	.0999	.1200	.0227	.0738
87.8300	.0860	.1860	.0300	.0810
92.0000	.1010	.1800	.0344	.1230
96.4200	.1040	.2320	.0408	.0730
100.8300	.1380	.2690	.0475	.0010
105.2300	.1430	.3130	.0558	.1000
109.6300	.0920	.0775	.0334	.0010
114.0000	.1030	.0780	.0040	.0010

STRESS STATE AND ELASTIC CONSTANTS, DATA SET NO. 4										
NU	WDMY PSI	WDSV PERCENT	WDMV PSI	WDSV PERCENT	WDMY PSI	WDSV PERCENT	WDMY PSI	WDSV PERCENT	WDMY PSI	WDSV PERCENT
.74	47156.37	1139E-02	14950.69	9317E+00	145944.05	7417E-03	19814.65	9557E-02	-.86	4.4962
.76	45810.39	1139E-02	14841.69	9317E+00	145944.05	7417E-03	17761.65	9557E-02	-.86	4.4962
.78	44754.39	1139E-02	13823.63	9317E+00	145944.05	7417E-03	14512.72	9557E-02	-.87	5.2029
.79	43627.44	1139E-02	13406.51	9317E+00	145944.05	7417E-03	14261.76	9557E-02	-.87	5.7544
.80	42151.24	1139E-02	12740.34	9317E+00	145944.05	7417E-03	14010.70	9557E-02	-.88	6.2374
.80	38374.70	1139E-02	12016.11	9317E+00	145944.05	7417E-03	12756.43	9557E-02	-.88	6.4462
NU	WDMY PSI	WDSV PERCENT	WDMV PSI	WDSV PERCENT	WDMY PSI	WDSV PERCENT	WDMY PSI	WDSV PERCENT	WDMY PSI	WDSV PERCENT
.74	94.41	91.45	35.32	1.03	1447E-02	1317E-03	1770E-02	14.46	1770E-03	1770E-02
.76	94.41	91.45	35.32	1.03	1447E-02	1317E-03	1770E-02	14.46	1770E-03	1770E-02
.78	94.41	91.45	35.32	1.03	1447E-02	1317E-03	1770E-02	14.46	1770E-03	1770E-02
.79	94.41	91.45	35.32	1.03	1447E-02	1317E-03	1770E-02	14.46	1770E-03	1770E-02
.80	94.41	91.45	35.32	1.03	1447E-02	1317E-03	1770E-02	14.46	1770E-03	1770E-02
.80	94.41	91.45	35.32	1.03	1447E-02	1317E-03	1770E-02	14.46	1770E-03	1770E-02
STRESS STATE AND ELASTIC CONSTANTS, DATA SET NO. 7										
NU	WDMY PSI	WDSV PERCENT	WDMV PSI	WDSV PERCENT	WDMY PSI	WDSV PERCENT	WDMY PSI	WDSV PERCENT	WDMY PSI	WDSV PERCENT
.74	44323.74	1139E-02	14472.41	9317E+00	174602.47	7389E-03	19444.30	1041E-02	-.86	4.6374
.76	47156.37	1139E-02	14950.69	9317E+00	174602.47	7389E-03	18155.65	1041E-02	-.86	4.6374
.78	45810.39	1139E-02	14841.69	9317E+00	174602.47	7389E-03	17761.65	1041E-02	-.86	4.6374
.79	44754.39	1139E-02	13823.63	9317E+00	174602.47	7389E-03	17461.65	1041E-02	-.86	4.6374
.80	43627.44	1139E-02	13406.51	9317E+00	174602.47	7389E-03	17161.65	1041E-02	-.86	4.6374
.80	42151.24	1139E-02	12740.34	9317E+00	174602.47	7389E-03	16861.65	1041E-02	-.86	4.6374
.80	38374.70	1139E-02	12016.11	9317E+00	174602.47	7389E-03	16561.65	1041E-02	-.86	4.6374
NU	WDMY PSI	WDSV PERCENT	WDMV PSI	WDSV PERCENT	WDMY PSI	WDSV PERCENT	WDMY PSI	WDSV PERCENT	WDMY PSI	WDSV PERCENT
.74	94.40	91.45	35.40	1.03	1447E-02	1317E-03	1770E-02	14.46	1770E-03	1770E-02
.76	94.40	91.45	35.40	1.03	1447E-02	1317E-03	1770E-02	14.46	1770E-03	1770E-02
.78	94.40	91.45	35.40	1.03	1447E-02	1317E-03	1770E-02	14.46	1770E-03	1770E-02
.79	94.40	91.45	35.40	1.03	1447E-02	1317E-03	1770E-02	14.46	1770E-03	1770E-02
.80	94.40	91.45	35.40	1.03	1447E-02	1317E-03	1770E-02	14.46	1770E-03	1770E-02
.80	94.40	91.45	35.40	1.03	1447E-02	1317E-03	1770E-02	14.46	1770E-03	1770E-02
STRESS STATE AND ELASTIC CONSTANTS, DATA SET NO. 3										
NU	WDMY PSI	WDSV PERCENT	WDMV PSI	WDSV PERCENT	WDMY PSI	WDSV PERCENT	WDMY PSI	WDSV PERCENT	WDMY PSI	WDSV PERCENT
.74	47241.34	1139E-02	14999.04	9370E+00	177651.58	7145E-03	19946.81	6199E-02	-.87	4.915
.76	45712.48	1139E-02	14674.45	9370E+00	177651.58	7145E-03	17744.63	6199E-02	-.87	4.915
.78	44131.50	1139E-02	14149.77	9370E+00	177651.58	7145E-03	16842.19	6199E-02	-.88	5.095
.79	42402.01	1139E-02	13584.67	9370E+00	177651.58	7145E-03	16289.17	6199E-02	-.88	5.1107
.80	41221.54	1139E-02	13020.04	9370E+00	177651.58	7145E-03	16035.96	6199E-02	-.88	5.2099
.80	38374.70	1139E-02	12175.04	9370E+00	177651.58	7145E-03	15742.75	6199E-02	-.88	5.3765
NU	WDMY PSI	WDSV PERCENT	WDMV PSI	WDSV PERCENT	WDMY PSI	WDSV PERCENT	WDMY PSI	WDSV PERCENT	WDMY PSI	WDSV PERCENT
.74	94.40	91.45	35.40	1.03	1447E-02	1317E-03	1770E-02	14.46	1770E-03	1770E-02
.76	94.40	91.45	35.40	1.03	1447E-02	1317E-03	1770E-02	14.46	1770E-03	1770E-02
.78	94.40	91.45	35.40	1.03	1447E-02	1317E-03	1770E-02	14.46	1770E-03	1770E-02
.79	94.40	91.45	35.40	1.03	1447E-02	1317E-03	1770E-02	14.46	1770E-03	1770E-02
.80	94.40	91.45	35.40	1.03	1447E-02	1317E-03	1770E-02	14.46	1770E-03	1770E-02
.80	94.40	91.45	35.40	1.03	1447E-02	1317E-03	1770E-02	14.46	1770E-03	1770E-02
STRESS STATE AND ELASTIC CONSTANTS, DATA SET NO. 6										
NU	WDMY PSI	WDSV PERCENT	WDMV PSI	WDSV PERCENT	WDMY PSI	WDSV PERCENT	WDMY PSI	WDSV PERCENT	WDMY PSI	WDSV PERCENT
.74	45590.45	1139E-01	15231.15	9414E+00	176046.82	2730E-04	18423.51	1084E-02	-.89	1.743
.76	44049.75	1139E-01	14800.35	9414E+00	176046.82	2730E-04	17211.53	1084E-02	-.89	1.866
.78	42478.42	1139E-01	14364.22	9414E+00	176046.82	2730E-04	15999.63	1084E-02	-.89	2.082
.79	41108.45	1139E-01	13704.26	9414E+00	176046.82	2730E-04	14787.37	1084E-02	-.89	2.172
.80	39996.64	1139E-01	13021.55	9414E+00	176046.82	2730E-04	13575.29	1084E-02	-.89	2.385
.80	36423.37	1139E-01	12241.97	9414E+00	176046.82	2730E-04	12363.21	1084E-02	-.89	2.597
NU	WDMY PSI	WDSV PERCENT	WDMV PSI	WDSV PERCENT	WDMY PSI	WDSV PERCENT	WDMY PSI	WDSV PERCENT	WDMY PSI	WDSV PERCENT
.74	100.70	91.45	36.51	1.03	1147E-01	8547E-04	1344E-02	4.84	1344E-02	1344E-01

[illegible]

NO	GEOM PSI	GEOM PERCENT	MOUSE PSI	MOUSE PERCENT	MOOT PSI	MOOT PERCENT	DEMT PSI	DEMT PERCENT	CMAT PSI	CMAT PERCENT	MIC	STAT
24	6442.47	1119E-01	18245.16	9414E+00	173890.54	1081E+02	18774.84	1762E-01			-.87	1.5473
25	6450.42	1119E-01	14813.58	9414E+00	173890.54	1081E+02	17444.82	1194E-01			-.87	1.6542
26	6442.15	1119E-01	14704.08	9414E+00	173890.54	1081E+02	16003.74	2020E-01			-.87	1.7811
29	61100.06	1119E-01	13713.74	9414E+00	173890.54	1081E+02	15006.48	2104E-01			-.86	1.9048
30	61003.93	1119E-01	12642.53	9414E+00	173890.54	1081E+02	12451.52	2391E-01			-.86	2.1000
40	37583.18	1119E-01	12700.45	9414E+00	173890.54	1081E+02	12006.18	2476E-01			-.86	2.1357
NO	GEOM PSI	GEOM PERCENT	MOUSE PSI	MOUSE PERCENT	MOOT PSI	MOOT PERCENT	DEMT PSI	DEMT PERCENT	CMAT PSI	CMAT PERCENT	MIC	STAT

W1	ADVP PS1	DEPRV PERCENT	MDVRS PS1	EMCV PERCENT	MDTV PS1	PRANT PERCENT	CANDT PERCENT	CGMVR PERCENT	WIC	STOBT
.74	47552.1A	1.140E-01	15242.51	1.041E+00	147559.31	1.3471E-02	12545.22	1.2733E-01	-.44	2.7007
.77	45047.80	1.119E-01	14913.90	1.041E+00	147672.31	1.3471E-02	12448.55	1.2075E-01	-.44	2.8151
.78	45247.3A	1.118E-01	14104.41	1.041E+00	147652.31	1.3471E-02	12464.88	1.2146E-01	-.44	2.8434
.80	45272.01	1.118E-01	13714.84	1.041E+00	147655.31	1.3471E-02	12464.88	1.2146E-01	-.44	2.8434
.81	45272.03	1.118E-01	13262.03	1.041E+00	147652.31	1.3471E-02	12464.88	1.2146E-01	-.44	2.8434
.89	451459.65	1.140E-01	12200.73	1.041E+00	147652.31	1.3471E-02	12246.46	1.0475E-01	-.44	3.4546
W1	SIG1 PS1	SIG2 PS1	SIG3 PS1	AFTA DEGREES	EMV1 PERCENT	EMV2 PERCENT	EMV3 PERCENT	PATA DEGREES	MDVRC PERCENT	CGMVC PERCENT
.74	101.28	51.65	36.18	5.41	1.2084E-01	1.3754E-02	1.0455E-02	31.24	1.7179E-02	1.9500E-01
.75	101.34	51.65	43.7	5.41	1.2084E-01	1.3754E-02	1.0455E-02	31.24	1.7179E-02	1.9500E-01
.76	101.30	51.65	41.30	5.41	1.2726E-01	1.6125E-02	1.1087E-01	34.65	1.9219E-02	2.0715E-01
.78	101.48	52.32	41.48	5.41	1.2307E-01	1.7601E-03	1.3204E-04	36.37	1.4500E-03	1.7001E-01
.80	101.49	60.73	51.45	5.41	1.2545E-01	1.9112E-02	1.5155E-01	36.11	1.4500E-03	1.7001E-01
.89	101.49	60.73	51.45	10.25	1.2715E-01	1.1192E-01	1.5247E-01	44.44	1.1584E-03	1.8191E-01

WU	WJ07 PST	DESV PERCENT	WJ05 PST	DESV PERCENT	WJ07 PST	DESV PERCENT	WJ07 PST	DESV PERCENT	WU	WT07 PST
26	44006.00	1270E-01	15231.99	0423E+00	200574.36	3583E-02	17744.60	3050F-31	00	31106
29	47761.19	1270E-01	14810.44	0421E+00	200574.36	3583E-02	16577.19	4131F-01	00	31607
30	61200.25	1270E-01	13764.11	0423E+00	200574.36	3583E-02	16409.74	0000E+01	00	30610
39	39478.00	1270E-01	13110.86	0423E+00	200574.36	3583E-02	13074.97	5234F-01	00	30609
49	74484.53	1270E-01	12287.09	0423E+00	200574.36	3583E-02	11407.54	5751F-31	00	40609
WU	SIG1	SIG2	SIG3	REV4	EP51	EP52	EP53	FATA	EP50C	GAMCQ

	PSI	PSI	PSI	DEGREE	PERCENT	PERCENT	PERCENT	DEGREE	PERCENT	PERCENT
.74	101.94	51.45	35.85	6.01	.7643E-01	-.3882E-02	-.1411E-01	14.17	.2807E-02	-.1440E-01
.76	101.74	41.44	43.17	6.79	.2770E-01	-.3021E-02	-.1460E-01	14.71	.2874E-02	-.1473E-01
.78	101.54	41.44	43.17	7.28	.1022E-01	-.6132E-03	-.1661E-01	17.23	.1047E-02	-.1644E-01
.80	101.34	41.44	43.17	9.13	.3066E-01	-.7859E-03	-.1887E-01	17.41	.1147E-02	-.1724E-01
.82	101.14	41.44	43.17	11.01	.1705E-01	-.9459E-03	-.2074E-01	18.43	.1782E-02	-.1814E-01
.84	100.94	41.44	43.17	13.77	.1555E-01	-.1181E-01	-.2324E-01	38.47	.1707E-02	-.1891E-01

## STRESS STATE AND ELASTIC CONSTANTS, DATA SET NO. 9

NU	MODV PSI	DEPSV PERCENT	MODVS PSI	EPSV PERCENT	MODT PSI	DEGNT PERCENT	MODT PSI	DEGNT PERCENT	NUC	STRT
.74	43546.47	.1240E-01	15742.60	.9420E+00	102114.76	.4702E-02	17575.19	.4747E-01	-.48	7.7801
.76	42443.43	.1240E-01	14813.50	.9426E+00	102114.76	.4702E-02	16418.02	.5103E-01	-.48	4.2417
.78	42003.94	.1240E-01	14104.50	.9426E+00	102114.76	.4702E-02	15267.44	.5490E-01	-.48	4.1444
.80	37515.40	.1240E-01	13714.14	.9426E+00	102114.76	.4702E-02	15106.60	.5930E-01	-.48	6.7146
.82	37208.40	.1240E-01	13045.91	.9426E+00	102114.76	.4702E-02	10701.14	.6470E-01	-.48	6.1144
.84	35144.74	.1240E-01	12290.41	.9436E+00	102114.76	.4702E-02	11793.88	.7104E-01	-.48	5.1404
NU	SIG1 PSI	SIG2 PSI	SIG3 PSI	DATA DEGREE	EPS1 PERCENT	EPS2 PERCENT	EPS3 PERCENT	DATA DEGREE	DEGNT PERCENT	DEGNT PERCENT
.74	102.94	41.44	75.52	7.29	.1009E-01	-.7077E-02	-.1416E-01	17.40	.2874E-02	-.1416E-01
.76	102.74	41.44	43.17	8.22	.1259E-01	-.3144E-02	-.190E-01	34.27	.2847E-02	-.1442E-01
.78	102.54	41.44	50.45	9.41	.1444E-01	-.4444E-02	-.2184E-01	34.44	.2074E-02	-.1744E-01
.80	102.34	41.44	51.44	10.44	.1444E-01	-.4052E-02	-.2404E-01	34.31	.1414E-02	-.1144E-01
.82	102.14	41.44	51.44	13.14	.1821E-01	-.9904E-03	-.2404E-01	34.40	.1404E-02	-.1404E-01
.84	101.94	41.44	51.44	16.25	.2237E-01	-.1210E-01	-.2974E-01	34.47	.1404E-02	-.1414E-01

## STRESS STATE AND ELASTIC CONSTANTS, DATA SET NO. 10

NU	MODV PSI	DEPSV PERCENT	MODVS PSI	EPSV PERCENT	MODT PSI	DEGNT PERCENT	MODT PSI	DEGNT PERCENT	NUC	STRT
.74	47191.74	.1104E-01	15239.55	.9411E+00	149389.46	.9181E-03	15028.93	.7207E-02	-.44	4.501
.76	44444.73	.1104E-01	14411.31	.9411E+00	149389.46	.9181E-03	14444.73	.7714E-02	-.44	4.444
.78	44244.73	.1104E-01	14101.63	.9411E+00	149389.46	.9181E-03	14244.73	.8704E-02	-.44	4.444
.80	42444.73	.1104E-01	13711.39	.9411E+00	149389.46	.9181E-03	13711.39	.9944E-02	-.44	4.137
.82	42444.73	.1104E-01	13044.20	.9411E+00	149389.46	.9181E-03	13221.32	.9714E-02	-.44	4.7876
.84	34244.73	.1104E-01	12738.34	.9411E+00	149389.46	.9181E-03	12744.01	.1074E-01	-.44	4.601

NU	SIG1 PSI	SIG2 PSI	SIG3 PSI	DATA DEGREE	EPS1 PERCENT	EPS2 PERCENT	EPS3 PERCENT	DATA DEGREE	DEGNT PERCENT	DEGNT PERCENT
.74	100.74	41.44	34.40	1.23	.1214E-01	-.1069E-02	-.1303E-02	14.57	.2524E-02	-.1374E-01
.76	100.77	41.44	44.10	1.39	.1224E-01	-.1710E-02	-.1427E-02	17.47	.2144E-02	-.1444E-01
.78	100.77	41.44	51.44	1.60	.1244E-01	-.130E-02	-.140E-02	17.47	.1904E-02	-.1404E-01
.80	100.76	41.44	51.44	1.90	.1244E-01	-.1591E-02	-.1404E-02	18.41	.1374E-02	-.1444E-01
.82	100.76	41.44	51.44	2.32	.1244E-01	-.1850E-02	-.1870E-02	20.77	.1414E-02	-.1404E-01
.84	100.70	41.44	51.44	2.90	.1376E-01	-.2175E-02	-.1669E-01	22.35	.1404E-02	-.1404E-01

## STRESS STATE AND ELASTIC CONSTANTS, DATA SET NO. 11

NU	MODV PSI	DEPSV PERCENT	MODVS PSI	EPSV PERCENT	MODT PSI	DEGNT PERCENT	MODT PSI	DEGNT PERCENT	NUC	STRT
.74	45144.64	.1743E-01	14419.50	.9474E+00	154041.11	.8057E-03	15007.48	.7044E-02	-.44	4.471
.76	43174.14	.1743E-01	14082.46	.9474E+00	154041.11	.8057E-03	14005.40	.7044E-02	-.44	4.471
.78	42444.64	.1743E-01	14447.18	.9474E+00	154041.11	.8057E-03	13804.29	.7573E-02	-.44	4.014
.80	42417.73	.1743E-01	14040.13	.9474E+00	154041.11	.8057E-03	13816.68	.8274E-02	-.44	5.325
.82	34444.64	.1743E-01	13101.24	.9474E+00	154041.11	.8057E-03	13617.30	.1010E-01	-.44	4.707
.84	34102.17	.1743E-01	12430.59	.9474E+00	154041.11	.8057E-03	12215.44	.1100E-01	-.44	4.065
NU	SIG1 PSI	SIG2 PSI	SIG3 PSI	DATA DEGREE	EPS1 PERCENT	EPS2 PERCENT	EPS3 PERCENT	DATA DEGREE	DEGNT PERCENT	DEGNT PERCENT
.74	102.94	41.44	37.17	1.17	.1414E-01	-.7817E-03	-.5904E-02	11.46	.3874E-02	-.7044E-01
.76	101.94	41.44	44.91	1.32	.1430E-01	-.8677E-03	-.7102E-02	12.24	.3437E-02	-.7144E-01
.78	101.94	41.44	51.44	1.53	.1444E-01	-.9471E-03	-.7447E-02	13.04	.2414E-02	-.7102E-01
.80	101.94	41.44	51.44	1.84	.1444E-01	-.1037E-02	-.1110E-01	14.01	.2884E-02	-.7471E-01
.82	101.94	41.44	51.44	2.19	.1474E-01	-.1358E-02	-.1370E-01	14.35	.1244E-02	-.7471E-01
.84	101.94	41.44	51.44	2.41	.1494E-01	-.1610E-02	-.1675E-01	16.24	.2774E-02	-.7471E-01

## STRESS STATE AND ELASTIC CONSTANTS, DATA SET NO. 12

NU	MODV PSI	DEPSV PERCENT	MODVS PSI	EPSV PERCENT	MODT PSI	DEGNT PERCENT	MODT PSI	DEGNT PERCENT	NUC	STRT
.74	44447.74	.2414E-01	15608.82	.9542E+00	16044.05	.8509E-03	17872.44	.7474E-02	-.47	3.153
.76	43197.90	.2414E-01	15169.71	.9542E+00	16044.05	.8509E-03	16743.37	.8174E-02	-.47	3.774
.78	43112.35	.2414E-01	14444.50	.9542E+00	16044.05	.8509E-03	15594.24	.8780E-02	-.47	3.631
.80	39040.72	.2414E-01	14043.45	.9542E+00	16044.05	.8509E-03	14344.15	.9402E-02	-.47	4.789
.82	38533.34	.2414E-01	13356.19	.9542E+00	16044.05	.8509E-03	13204.04	.1074E-01	-.47	4.274

CU	WFOVT PS1	DESV PERCENT	CPV4 PERCENT	DESV PERCENT	MODT PS1	DESV PERCENT	FMMVT PS1	DESV PERCENT	FCAMVT PERCENT	MUC	STRAT
24	6747.65	3.813E-01	15972.68	9642E+00	204678.28	6.941E-03	17775.76	7624E-07		-.00	1.007
25	61437.09	1.910E-01	15133.63	9642E+00	204678.28	6.941E-03	18139.73	8149E-02		-.00	0.218
26	62754.32	1.810E-01	14680.01	9642E+00	204678.28	6.941E-03	19022.73	8793E-02		-.00	0.230
27	61437.09	1.910E-01	15133.63	9642E+00	204678.28	6.941E-03	19022.73	8793E-02		-.00	0.230
28	74440.02	2.419E-01	13458.40	9642E+00	204678.28	6.941E-03	17279.14	1070E-02		-.01	0.271
29	74440.02	2.419E-01	12971.27	9642E+00	204678.28	6.941E-03	11542.61	1437E-01		-.07	0.297
W1	WFOVT PS1	SIG2 PERCENT	SIG3 PERCENT	RETA PERCENT	EDS1 PERCENT	EDS2 PERCENT	EDS3 PERCENT	RETA PERCENT	EDS4 PERCENT	EDS5 PERCENT	EDS6 PERCENT
24	112.57	51.45	39.33	1.03	18556E-01	3.779E-03	12067E-01	5.65	7509E-07	4437E-01	0.649E-01
25	112.57	51.45	42.63	1.44	18556E-01	4.314E-03	12067E-01	5.65	7509E-07	4437E-01	0.649E-01
26	112.57	51.45	1.33	1.03	18556E-01	4.314E-03	12067E-01	5.65	7509E-07	4437E-01	0.649E-01
27	112.57	51.45	1.33	1.03	18556E-01	4.314E-03	12067E-01	5.65	7509E-07	4437E-01	0.649E-01
28	112.57	51.45	1.33	1.03	18556E-01	4.314E-03	12067E-01	5.65	7509E-07	4437E-01	0.649E-01
29	112.57	51.45	1.33	1.03	18556E-01	4.314E-03	12067E-01	5.65	7509E-07	4437E-01	0.649E-01

NO.	47745 751	DEBENT PERCENT	MORTGAGE PCT	PERCENT	MORT PCT	DEBENT PERCENT	CMOS PERCENT	DEBENT PERCENT	MUT	STRT
20	41240.51	5.2100-31	14284.36	9624E+00	241243.02	7.380E-03	16640.00	10.020-31	0.02	0.023
20	40179.44	5.2100-31	15810.10	9.424E+00	247473.02	7.399E-03	15973.47	11.14E-01	0.02	0.023
15	34767.74	4.2700-01	157670.12	9.424E+00	247473.02	7.399E-03	14454.34	1.2121E-01	0.02	0.230

[illegible][illegible]

WU	WDOVT PSI	DEPSV PERCENT	WDOVS PSI	DEPSV PERCENT	WDOVT PSI	DEPSV PERCENT	WDOVT PSI	DEPSV PERCENT	WU	STRET
72	3800A.30	6393E-01	14775.00	1314E+01	77470.92	7394E-03	15325.96	1209E-01	703	11007

NO	SIG1 PSI	SIG2 PSI	SIG3 PSI	RPTA DEGREES	EPS1 PERCENT	EPS2 PERCENT	EPS3 PERCENT	EATA DEGREES	EPSOC PERCENT	GAMOC PERCENT
10	36370.00	-43076-01	16703.70	-1014F+01	276740-52	-7340E-03	14317.68	-1350F-01	-0.93	-1496
11	36440.18	-43076-01	16702.88	-1014F+01	276740-52	-7340E-03	14300.19	-1400E-01	-0.94	-1481
12	36197.04	-43076-01	16092.08	-1014F+01	276740-52	-7340E-03	12301.10	-1419E-01	-0.94	-1427
13	32253.31	-43076-01	14754.10	-1014F+01	276740-52	-7340E-03	11297.52	-1762F-01	-0.94	-2008
14	32267.90	-43076-01	13526.44	-1014F+01	276740-52	-7340E-03	12764.43	-1034F-01	-0.94	-2305

## STRESS STATE AND ELASTIC CONSTANTS, DATA SET NO. 12

NO	MOOVT PSI	DEPSV PERCENT	MOOVS PSI	EPSV PERCENT	MOOY PSI	DEGMY PERCENT	CMOYT PSI	CGAMY PERCENT	MUC	STRAE
14	37417.28	-0773F-01	17003.60	-1079E+01	240074.74	-7340E-03	14306.00	-1335F-01	-0.94	-1346
15	36741.25	-0773F-01	16426.44	-1029E+01	240074.74	-7340E-03	14303.50	-1420E-01	-0.94	-1442
16	36110.49	-0773F-01	15077.11	-1079E+01	240074.74	-7340E-03	17101.00	-1537E-01	-0.94	-1874
17	37411.43	-0773F-01	15204.85	-1079E+01	240074.74	-7340E-03	13377.47	-2000F-01	-0.92	-2098
18	37014.3F	-0773F-01	14540.77	-1028E+01	240074.74	-7340E-03	11114.00	-1812F-01	-0.94	-1404
19	36144.97	-0773F-01	13710.22	-1029E+01	240074.74	-7340E-03	10123.42	-1040E-01	-0.94	-2038

NO	SIG1 PSI	SIG2 PSI	SIG3 PSI	RPTA DEGREES	EPS1 PERCENT	EPS2 PERCENT	EPS3 PERCENT	EATA DEGREES	EPSOC PERCENT	GAMOC PERCENT
15	174.37	51.45	44.46	1.29	-0919F-01	-4517F-03	-3086F-01	3.40	-2290E-01	-1107E+00
16	134.03	49.42	44.46	1.44	-0827E-01	-5195F-03	-3062E-01	4.16	-1027E-01	-1142E+00
17	174.34	42.00	51.45	1.02	-0833F-01	-4000F-03	-4034F-01	4.47	-1480E-01	-1236E+00
18	174.32	77.78	51.45	1.07	-0746E-01	-7074E-03	-4300F-01	4.43	-1174F-01	-1224E+00
19	134.34	41.45	44.46	1.70	-0844F-01	-4122E-03	-3670F-01	5.26	-1401E-01	-1416E+00
20	134.34	40.72	44.46	1.67	-0824E-01	-4002F-03	-3300F-01	5.78	-1278E-01	-1573E+00

## STRESS STATE AND ELASTIC CONSTANTS, DATA SET NO. 14

NO	MOOVT PSI	DEPSV PERCENT	MOOVS PSI	EPSV PERCENT	MOOY PSI	DEGMY PERCENT	CMOYT PSI	CGAMY PERCENT	MUC	STRAE
14	37404.30	-0473F-01	17020.70	-1027E+01	217440.80	-1003E-02	15243.15	-2518F-01	-0.91	-2404
15	36770.05	-0473F-01	16561.68	-1027E+01	217440.80	-1003E-02	14740.71	-2609E-01	-0.92	-2747
16	36874.42	-0473F-01	15072.77	-1027E+01	217440.80	-1003E-02	13377.47	-2000F-01	-0.92	-2098
17	36317.27	-0473F-01	14213.46	-1027E+01	217440.80	-1003E-02	12274.57	-3178E-01	-0.92	-3244
18	32167.64	-0473F-01	14464.36	-1027E+01	217440.80	-1003E-02	14231.74	-3418E-01	-0.93	-1553
19	33449.24	-0473F-01	13774.23	-1027E+01	217440.80	-1003E-02	10728.95	-3743F-01	-0.93	-3760

NO	SIG1 PSI	SIG2 PSI	SIG3 PSI	RPTA DEGREES	EPS1 PERCENT	EPS2 PERCENT	EPS3 PERCENT	EATA DEGREES	EPSOC PERCENT	GAMOC PERCENT
16	174.15	51.45	44.46	2.48	-0834F-01	-4612E-02	-3044F-01	7.30	-2200E-01	-1100E+00
17	124.17	53.40	51.45	2.73	-0857F-01	-4463E-02	-3041F-01	7.70	-1907E-01	-1164E+00
18	174.10	52.44	51.45	3.00	-0855F-01	-4127E-02	-4044F-01	8.34	-1763F-01	-1240E+00
19	134.16	72.00	51.45	3.53	-0911F-01	-4246E-02	-4144F-01	8.00	-1637F-01	-1307E+00
20	134.16	41.44	44.46	4.12	-0844F-01	-4010E-02	-3400F-01	4.73	-6040E-02	-1441E+00
21	174.17	40.52	51.45	5.05	-1007E-00	-4751F-02	-0743F-01	10.60	-1204E-02	-1570E+00

## STRESS STATE AND ELASTIC CONSTANTS, DATA SET NO. 19

NO	MOOVT PSI	DEPSV PERCENT	MOOVS PSI	EPSV PERCENT	MOOY PSI	DEGMY PERCENT	CMOYT PSI	CGAMY PERCENT	MUC	STRAE
14	35370.3A	-0773E-01	16962.33	-1029E+01	203131.13	-2011E-02	14011.03	-3670E-01	-0.91	-3763
15	35370.41	-0773E-01	16845.36	-1029E+01	203131.13	-2011E-02	13900.34	-3737E-01	-0.91	-4028
16	24723.47	-0773E-01	15918.30	-1029E+01	203131.13	-2011E-02	12944.06	-4235E-01	-0.91	-4133
17	31727.20	-0773E-01	14244.42	-1029E+01	203131.13	-2011E-02	11048.53	-4880F-01	-0.93	-4646
18	31649.76	-0773E-01	14114.46	-1029E+01	203131.13	-2011E-02	10847.08	-4801E-01	-0.97	-5107
19	22414.14	-0773E-01	13677.50	-1029E+01	203131.13	-2011E-02	10000.04	-5481F-01	-0.93	-4408

## STRESS STATE AND ELASTIC CONSTANTS, DATA SET NO. 20

NO	MOOVT PSI	DEPSV PERCENT	MOOVS PSI	EPSV PERCENT	MOOY PSI	DEGMY PERCENT	CMOYT PSI	CGAMY PERCENT	MUC	STRAE
----	--------------	------------------	--------------	-----------------	-------------	------------------	--------------	------------------	-----	-------

	PSI	PERCENT	PSI	PERCENT	PSI	PERCENT	PSI	PERCENT		
.74	34970.36	.0773F-01	10962.33	.1029F+01	196626.55	.4031F-02	14911.33	.4911F-01	-.91	.4963
.70	35310.41	.0773F-01	10962.33	.1029F+01	196626.55	.4031F-02	14911.33	.4911F-01	-.91	.4913
.76	34703.42	.0773F-01	10962.33	.1029F+01	196626.55	.4031F-02	14911.33	.4911F-01	-.91	.4919
.70	33271.72	.0773F-01	10962.33	.1029F+01	196626.55	.4031F-02	14911.33	.4911F-01	-.91	.4914
.66	31547.78	.0773F-01	10962.33	.1029F+01	196626.55	.4031F-02	14911.33	.4911F-01	-.91	.4914
.60	29914.14	.0773F-01	10962.33	.1029F+01	196626.55	.4031F-02	14911.33	.4911F-01	-.91	.4914

	PSI	SIGZ	PSI	SIGY	DATA DIFFERS	PSI	PERCENT	PSI	PERCENT	DATA DIFFERS	PSI	PERCENT	DATA DIFFERS
.74	174.12	.51+.25	43.81	.4.81	1.04E+00	-56.88E-02	-1.00E-01	13.25	.779E-01	-.1168F+03			
.70	174.14	.51.33	41.84	.4.13	1.04E+00	-46.49E-02	-1.90E-01	13.49	.157E-01	-.1279F+03			
.76	174.27	.42.10	41.84	.5.79	1.02E+00	-7.81E-02	-5.01E-01	14.47	.1540F+01	.1715F+03			
.70	134.17	.71.10	51.84	.6.83	1.05E+00	-8.56E-02	-7.74E-01	15.47	.1174F+01	.1404F+03			
.66	114.21	.107E+00	7.79	.1.07E+00	-1.03E-01	-1.03E-01	-1.03E-01	16.48	.0846F+01	.1179E+03			
.60	113.72	.80.44	41.84	.4.32	1.09E+00	-1.11E-01	-1.93E-01	14.84	.1174F+02	.1672E+00			

## STRESS STATE AND ELASTIC CONSTANTS, DATA SET NO. 21

NU	MODUL	PERSV	MODVS	PERSV	MODT	OGAMT	CMODT	CGAMV	BUC	STRT
PSI	PERCENT	PSI	PERCENT	PSI	PERCENT	PERCENT	PERCENT	PERCENT	PERCENT	PERCENT
.74	30390.30	.0975F-01	14015.41	.1070F+01	197944.74	.5043F-02	14440.64	.6072F-01	-.91	.6047
.70	34374.71	.0975F-01	14015.41	.1070F+01	197944.74	.5043F-02	14440.64	.6072F-01	-.91	.6016
.76	31744.16	.0975F-01	14015.41	.1070F+01	197944.74	.5043F-02	14440.64	.6072F-01	-.91	.6012
.70	37471.47	.0975F-01	14015.41	.1070F+01	197944.74	.5043F-02	14440.64	.6072F-01	-.91	.6014
.66	33447.27	.0975F-01	14015.41	.1070F+01	197944.74	.5043F-02	14440.64	.6072F-01	-.91	.6014
.60	29114.44	.0975F-01	14015.41	.1070F+01	197944.74	.5043F-02	14440.64	.6072F-01	-.91	.6014

## STRESS STATE AND ELASTIC CONSTANTS, DATA SET NO. 22

NU	MODUL	PERSV	MODVS	PERSV	MODT	OGAMT	CMODT	CGAMV	BUC	STRT
PSI	PERCENT	PSI	PERCENT	PSI	PERCENT	PERCENT	PERCENT	PERCENT	PERCENT	PERCENT
.74	30370.31	.0975F-01	14015.41	.1070F+01	197944.74	.5043F-02	14440.64	.6072F-01	-.91	.6014
.70	34374.71	.0975F-01	14015.41	.1070F+01	197944.74	.5043F-02	14440.64	.6072F-01	-.91	.6014
.76	31744.16	.0975F-01	14015.41	.1070F+01	197944.74	.5043F-02	14440.64	.6072F-01	-.91	.6014
.70	37471.47	.0975F-01	14015.41	.1070F+01	197944.74	.5043F-02	14440.64	.6072F-01	-.91	.6014
.66	33447.27	.0975F-01	14015.41	.1070F+01	197944.74	.5043F-02	14440.64	.6072F-01	-.91	.6014
.60	29114.44	.0975F-01	14015.41	.1070F+01	197944.74	.5043F-02	14440.64	.6072F-01	-.91	.6014

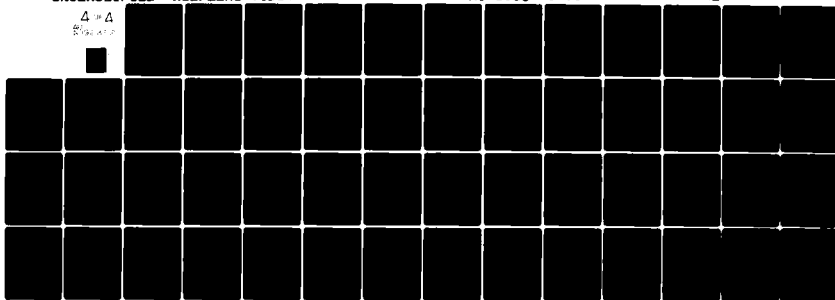
## STRESS STATE AND ELASTIC CONSTANTS, DATA SET NO. 23

NU	MODUL	PERSV	MODVS	PERSV	MODT	OGAMT	CMODT	CGAMV	BUC	STRT
PSI	PERCENT	PSI	PERCENT	PSI	PERCENT	PERCENT	PERCENT	PERCENT	PERCENT	PERCENT
.74	34374.71	.0975F-01	14015.41	.1070F+01	197944.74	.5043F-02	14440.64	.6072F-01	-.91	.6014
.70	37471.47	.0975F-01	14015.41	.1070F+01	197944.74	.5043F-02	14440.64	.6072F-01	-.91	.6014
.76	31744.16	.0975F-01	14015.41	.1070F+01	197944.74	.5043F-02	14440.64	.6072F-01	-.91	.6014
.70	34374.71	.0975F-01	14015.41	.1070F+01	197944.74	.5043F-02	14440.64	.6072F-01	-.91	.6014
.66	33447.27	.0975F-01	14015.41	.1070F+01	197944.74	.5043F-02	14440.64	.6072F-01	-.91	.6014
.60	29114.44	.0975F-01	14015.41	.1070F+01	197944.74	.5043F-02	14440.64	.6072F-01	-.91	.6014

AD-A092 352 CALIFORNIA UNIV BERKELEY EARTHQUAKE ENGINEERING RES--ETC F/G 8/13  
INTERACTION EFFECTS OF SIMULTANEOUS TORSIONAL AND COMPRESSIONAL--ETC(U)  
DEC 79 P M GRIFFIN; W N HOUSTON DAAG29-76-8-0257  
UNCLASSIFIED UCB/EERC-79/34 ARO-13838.1-05 NL

4 x 4

REGULATED

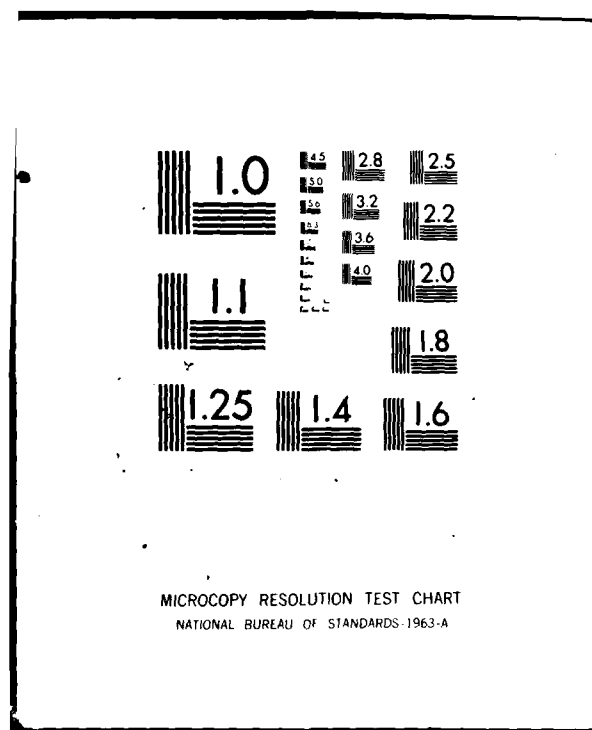


END

DATE

FILMED

DTIC



[illegible]

TUGG STATE AND FLORIDA—CONSTANT, DATA OF L. NO. 28

[illegible]

STRESS STATE AND PLASTIC CONSTANTS, DATA SET NO. 26

[illegible]

STRESS STATE AND ELASTIC CONSTANTS, DATA SET NO. 27

[illegible]

## STRESS STATE AND ELASTIC CONSTANTS, DATA SET NO. 28

NO	MODY PSI	DESV PERCENT	MODS PSI	DESV PERCENT	MODY PSI	DESV PERCENT	MODY PSI	DESV PERCENT	MUC	STREY
10	10037.25	+1332E+00	1724E+07	+1034E+01	256735.18	+8097E-03	15880.32	+1500E-01	-.02	1310
20	17537.87	+1332E+00	10781.04	+1078E+01	256735.18	+8097E-03	14555.28	+1400E-01	-.03	1412
30	10701.14	+1034E+00	14184.41	+1418E+01	256735.18	+8097E-03	13235.28	+1274E-01	-.03	1414
40	10701.14	+1034E+00	14514.66	+1451E+01	256735.18	+8097E-03	12705.26	+1204E-01	-.03	1414
50	11301.34	+1078E+00	14757.28	+1475E+01	256735.18	+8097E-03	11480.24	+1040E-01	-.04	1300
60	11144.44	+1078E+00	13004.24	+1078E+01	256735.18	+8097E-03	10455.27	+974E-01	-.04	1300
NO	SIG1 PSI	SIG2 PSI	SIG3 PSI	ETA PERCENT	EPS1 PERCENT	EPS2 PERCENT	EPS3 PERCENT	DATA PERCENT	EPSFC PERCENT	GAUFC PERCENT
10	137.74	41.45	49.34	1.32	+1042E+00	+4404E-03	+3977E-01	3.74	+2347E-01	+1104E+00
20	137.74	44.41	51.45	1.47	+1042E+00	+5144E-03	+3977E-01	4.02	+2464E-01	+1214E+00
30	137.74	44.41	51.45	1.44	+1042E+00	+5014E-03	+3977E-01	4.32	+1877E-01	+1114E+00
40	137.74	71.71	41.45	1.41	+1042E+00	+6044E-03	+6035E-01	4.67	+1447E-01	+1407E+00
50	137.74	47.16	51.45	2.24	+1042E+00	+8244E-03	+6144E-01	3.07	+7417E-01	+1594E+00
60	137.74	42.40	41.45	7.71	+1042E+00	+9044E-03	+6017E-01	5.44	+1357E-01	+1470E+00

## STRESS STATE AND ELASTIC CONSTANTS, DATA SET NO. 30

NO	MODY PSI	DESV PERCENT	MODS PSI	DESV PERCENT	MODY PSI	DESV PERCENT	MODY PSI	DESV PERCENT	MUC	STREY
10	17405.38	+1103E+00	17471.00	+1040E+01	263153.56	+8097E-03	15842.81	+1440E-01	-.03	1210
20	14441.08	+1103E+00	14037.28	+1040E+01	263153.56	+8097E-03	14282.52	+1441E-01	-.03	1300
30	15121.27	+1103E+00	14340.04	+1040E+01	263153.56	+8097E-03	17004.73	+1444E-01	-.04	1300
40	11650.17	+1103E+00	14778.08	+1040E+01	263153.56	+8097E-03	12111.64	+1400E-01	-.04	1214
50	12307.32	+1103E+00	14007.47	+1040E+01	263153.56	+8097E-03	11111.45	+1444E-01	-.04	1444
60	10141.06	+1103E+00	14046.23	+1040E+01	263153.56	+8097E-03	10121.34	+1400E-01	-.04	1210
NO	SIG1 PSI	SIG2 PSI	SIG3 PSI	ETA PERCENT	EPS1 PERCENT	EPS2 PERCENT	EPS3 PERCENT	DATA PERCENT	EPSFC PERCENT	GAUFC PERCENT
10	147.44	41.45	44.41	1.30	+1107E+00	+4304E-03	+1747E-01	3.44	+2747E-01	+1344E+00
20	147.44	44.41	44.41	1.44	+1107E+00	+5014E-03	+4747E-01	3.70	+2847E-01	+1414E+00
30	147.44	65.34	51.45	1.03	+1107E+00	+8004E-03	+2145E-01	4.04	+1474E-01	+1507E+00
40	147.44	71.71	51.45	1.47	+1200E+00	+8704E-03	+7627E-01	4.70	+1474E-01	+1410E+00

10	142.42	23.27	51.45	2.10	+1201E+00	+8024E-03	+9377E-01	4.44	+4021E-01	+1791E+00
20	142.42	42.44	51.45	2.10	+1201E+00	+8024E-03	+1104E-01	5.13	+1400E-01	+1414E+00

## APPENDIX B-6

Hollow Cylinder Test No. B31-1

DAI GIFFIN, 1957 WJ, P31-1, APRIL 23, 1970

1747 0851279 000 944050 42, 21

9151C	87	140000	1	140000
9151C	10000	140000	140000	140000
9151C	10000	10000	10000	10000

v7k	u87
CP	<del>CACC</del>
410,26	1,92

1971	1972	1973	1974	1975
1. 1971	3.325	0.140	0.000	-0.000
2. 1972	0.140	0.000	0.000	-0.000
3. 1973	0.140	0.000	0.000	-0.000
4. 1974	0.140	0.000	0.000	-0.000
5. 1975	0.140	0.000	0.000	-0.000
6. 1976	0.140	0.000	0.000	-0.000
7. 1977	0.140	0.000	0.000	-0.000
8. 1978	0.140	0.000	0.000	-0.000
9. 1979	0.140	0.000	0.000	-0.000
10. 1980	0.140	0.000	0.000	-0.000
11. 1981	0.140	0.000	0.000	-0.000
12. 1982	0.140	0.000	0.000	-0.000
13. 1983	0.140	0.000	0.000	-0.000
14. 1984	0.140	0.000	0.000	-0.000
15. 1985	0.140	0.000	0.000	-0.000
16. 1986	0.140	0.000	0.000	-0.000
17. 1987	0.140	0.000	0.000	-0.000
18. 1988	0.140	0.000	0.000	-0.000
19. 1989	0.140	0.000	0.000	-0.000
20. 1990	0.140	0.000	0.000	-0.000

STRESS STATE AND PLASTIC CONSTANTS, DATA SET NO. 1

№	УЗДУТ 041	УЗДУТ 080СМТ	УЗДУТ 041	УЗДУТ 080СМТ	УЗДУТ 041	УЗДУТ 080СМТ	УЗДУТ 041	УЗДУТ 080СМТ	УЗДУТ 041
20	2672.20	1980-02	13106.40	17000.00	10370.73	1170-02	10030.10	14000-01	0.00



[illegible]

YR	DATE	DEBIT		CREDIT		BAL	CARRY	BANK	STATE								
		AMT	PERCENT	AMT	PERCENT												
78	12/24/78	171.00	-01	136.72	-13	171.00	-00	67.00	-00	63.00	-02	80.00	-10	230.70	-01	-00	7.1113
78	12/24/78	171.00	-01	136.72	-13	171.00	-00	67.00	-00	63.00	-02	75.20	-03	374.90	-01	-00	3.3304
78	12/24/78	171.00	-01	136.72	-13	171.00	-00	67.00	-00	63.00	-02	69.00	-03	1.1570	-01	-00	1.4307
78	12/24/78	171.00	-01	136.72	-13	171.00	-00	67.00	-00	63.00	-02	64.00	-02	560.00	-01	-00	7.7700
78	12/24/78	171.00	-01	136.72	-13	171.00	-00	67.00	-00	63.00	-02	64.00	-02	560.00	-01	-00	7.7700
78	12/24/78	171.00	-01	136.72	-13	171.00	-00	67.00	-00	63.00	-02	64.00	-02	560.00	-01	-00	7.7700

Q1	SIG1 P1	SIG2 P1	SIG3 P1	PATA DEGREES	P01 PERCENT	P02 PERCENT	P03 PERCENT	PATA DEGREES	P04 PERCENT	P05 PERCENT
26	14.00	7.15	4.45	14.42	100.00-01	50.27E-02	1.190E-31	36.00	100.00-02	4.775E-31
24	14.00	1.20	9.44	20.22	130.87E-01	70.28E-02	1.120E-31	26.44	133.86-02	5.047E-01
16	14.00	7.15	6.41	71.07	6.024E-01	4.854E-02	6.737E-01	37.70	2.779E-02	4.013E-01
13	13.14	7.44	7.35	26.20	4.710E-01	1.1040E-01	1.750E-31	17.77	7.860E-02	5.017E-01
12	12.61	7.44	7.44	26.46	4.858E-01	1.1040E-01	1.750E-31	17.77	7.860E-02	5.017E-01
10	12.61	0.62	7.30	20.67	4.710E-01	1.1631E-01	1.751E-31	18.01	1.237E-01	7.084E-01

\_\_\_\_\_

	741	PERCENT	841	PERCENT	941	PERCENT	041	PERCENT	141	PERCENT
70	1404.75	14032-01	13264.44	14002-00	95621.82	90012-02	3454.04	77670-01	-00	3.0100
71	1404.75	14032-01	13264.44	14002-00	95621.82	90012-02	4464.27	77702-01	-05	4.0270
72	1404.75	14032-01	13264.44	14002-00	95621.82	90012-02	5474.51	77834-01	-05	4.1500
73	1404.75	14032-01	13264.44	14002-00	95621.82	90012-02	6484.75	77966-01	-05	4.2730
74	1404.75	14032-01	13264.44	14002-00	95621.82	90012-02	7494.99	78098-01	-07	4.3960
75	1404.75	14032-01	13264.44	14002-00	95621.82	90012-02	8505.23	78230-01	-07	4.5190

[illegible]

QU	WQVOT PST	NEWV PERCENT	DOVS PST	EPV PERCENT	MDT PST	DEMT PERCENT	CMDT PST	CEMT PERCENT	WAC	STRT
26	17676.66	2314F-61	13673.69	1700F-68	5466F-62	1164E-61	7827.49	9047E-61	-62	0.0687
29	17676.66	2314E-61	13704.69	1702E-68	5466E-62	1164F-61	6548.74	1049E-61	-65	0.7619
76	11514.01	2274F-61	12229.70	1704E-68	5466E-62	1164F-61	6182.99	1032F-60	-63	0.1227
79	14498.66	2014E-61	13408.68	1384E-66	5466E-63	1164E-61	8444.99	1124E-60	-66	0.0000
82	17676.66	2314E-61	13704.69	1702E-68	5466E-62	1164F-61	6548.74	1049E-61	-65	0.7619
85	2371.66	2234E-61	11023.71	1707E-68	5466E-62	1164E-61	4715.94	1250E-60	-67	0.6264

W	1121 01	1162 01	1163 01	DATA CENTERS	SPC PERCENT	SPC PERCENT	SPC PERCENT	DATA CENTERS	SPC PERCENT	SAVED PERCENT
70	20.50	7.30	3.00	24.00	10000-01	10000-02	16730-01	30.67	10000-02	77700-01
80	20.62	7.30	0.11	20.00	10710-01	10310-02	34750-01	30.07	10140-02	80740-01
10	20.67	7.30	0.10	77.63	10310-01	10000-02	10200-01	30.00	10200-02	80740-01
90	30.00	7.30	0.00	33.00	10470-01	10000-02	52110-01	00.30	10400-02	10070-00
40	21.07	7.40	7.30	33.70	10470-01	10500-02	50000-01	00.71	10010-02	11040-00

## STRESS STATE AND ELASTIC CONSTANTS, DATA SET NO. 9

NU	WTOVT PSI	DEPRV PERCENT	MOVS PSI	PRSV PERCENT	MOOT PSI	THANT PERCENT	CHOOT PSI	CHANY PERCENT	MUC	STRAT
.24	24790.10	.1341E-01	14120.27	.1030E+00	111140.77	.1470E-02	9940.43	.1579E-01	-.00	1.1904
.26	26340.04	.1341E-01	13730.00	.1030E+00	111140.77	.1470E-02	9740.04	.1579E-01	-.00	1.2011
.28	28120.07	.1341E-01	13040.30	.1030E+00	111140.77	.1470E-02	9440.06	.1579E-01	-.00	1.2161
.30	29700.04	.1341E-01	12711.50	.1030E+00	111140.77	.1470E-02	9074.05	.1579E-01	-.00	1.2445
.32	31717.72	.1341E-01	12080.30	.1030E+00	111140.77	.1470E-02	7367.20	.1579E-01	-.00	1.4735
.34	19000.73	.1341E-01	11702.27	.1030E+00	111140.77	.1470E-02	6700.07	.1579E-01	-.01	1.7774
NU	S121 PSI	S122 PSI	S123 PSI	ETA DEGREES	EPS1 PERCENT	EPS2 PERCENT	EPS3 PERCENT	DATA DEGREES	EPSOC PERCENT	GAMOC PERCENT
.24	17.10	7.34	5.67	7.00	.1722E-01	.3613E-02	.4707E-02	24.41	.3103E-02	.1047E-01
.26	17.67	7.35	6.07	6.70	.1700E-01	.4040E-02	.4547E-02	28.57	.2643E-02	.2120E-01
.28	17.00	6.07	7.30	0.00	.1610E-01	.4400E-02	.5000E-02	30.50	.2190E-02	.2264E-01
.30	17.00	6.07	7.30	11.20	.1070E-01	.5140E-02	.5800E-02	27.44	.1630E-02	.2470E-01
.32	17.00	10.42	7.30	13.15	.1040E-01	.5400E-02	.6100E-02	20.70	.0710E-02	.2600E-01
.34	17.67	11.57	7.30	15.70	.2030E-01	.6770E-02	.1407E-01	20.07	.1770E-02	.2403E-01

## STRESS STATE AND ELASTIC CONSTANTS, DATA SET NO. 10

NU	WTOVT PSI	DEPRV PERCENT	MOVS PSI	PRSV PERCENT	MOOT PSI	THANT PERCENT	CHOOT PSI	CHANY PERCENT	MUC	STRAT
.24	27557.01	.2137E-01	14921.75	.1711E+00	111140.77	.1470E-02	11071.77	.1604E-01	-.00	.7040
.26	26440.00	.2137E-01	14040.00	.1711E+00	111140.77	.1470E-02	10700.00	.1604E-01	-.00	.7030
.28	24767.17	.2137E-01	14033.30	.1711E+00	111140.77	.1470E-02	9410.01	.1700E-01	-.00	.6100
.30	24703.75	.2137E-01	13425.40	.1711E+00	111140.77	.1470E-02	9040.23	.1604E-01	-.00	.6771
.32	27000.00	.2137E-01	12740.30	.1711E+00	111140.77	.1470E-02	8157.00	.1604E-01	-.00	.6913
.34	29130.00	.2137E-01	10430.00	.1711E+00	111140.77	.1470E-02	7430.00	.1604E-01	-.00	1.0400
NU	S121 PSI	S122 PSI	S123 PSI	ETA DEGREES	EPS1 PERCENT	EPS2 PERCENT	EPS3 PERCENT	DATA DEGREES	EPSOC PERCENT	GAMOC PERCENT
.24	19.34	7.30	6.30	6.07	.2340E-01	.2740E-02	.4000E-02	17.57	.4000E-02	.7050E-01
.26	19.34	6.07	7.30	6.07	.2340E-01	.2740E-02	.4000E-02	17.57	.4000E-02	.7050E-01
.28	19.34	6.07	7.30	6.07	.2340E-01	.2740E-02	.4000E-02	17.57	.4000E-02	.7050E-01
.30	23.22	10.20	7.30	0.04	.2440E-01	.3470E-02	.1700E-01	20.63	.2530E-02	.1210E-01
.32	23.22	11.50	7.30	11.50	.2511E-01	.4070E-02	.1604E-01	21.45	.1500E-02	.2400E-01
.34	29.13	12.00	7.30	13.07	.2540E-01	.4730E-02	.2530E-01	27.13	.2700E-02	.1070E-01

## STRESS STATE AND ELASTIC CONSTANTS, DATA SET NO. 11

NU	WTOVT PSI	DEPRV PERCENT	MOVS PSI	PRSV PERCENT	MOOT PSI	THANT PERCENT	CHOOT PSI	CHANY PERCENT	MUC	STRAT
.24	10300.00	.1000E-01	14874.61	.1000E+00	107071.02	.1530E-02	8024.27	.2047E-01	-.01	.6130
.26	10740.01	.1000E-01	14160.70	.1000E+00	107071.02	.1530E-02	7400.70	.2101E-01	-.01	.6400
.28	10670.00	.1000E-01	13070.40	.1000E+00	107071.02	.1530E-02	6440.40	.2157E-01	-.01	.5000
.30	17004.64	.1000E-01	13114.43	.1000E+00	107071.02	.1530E-02	6440.53	.2300E-01	-.02	.6200
.32	17070.00	.1000E-01	12470.00	.1000E+00	107071.02	.1530E-02	5910.00	.2370E-01	-.00	.6000
.34	16340.00	.1000E-01	11750.70	.1000E+00	107071.02	.1530E-02	5304.71	.2670E-01	-.03	.7040
NU	S121 PSI	S122 PSI	S123 PSI	ETA DEGREES	EPS1 PERCENT	EPS2 PERCENT	EPS3 PERCENT	DATA DEGREES	EPSOC PERCENT	GAMOC PERCENT
.24	27.20	7.30	6.07	6.10	.4230E-01	.2470E-02	.1240E-01	17.50	.0000E-02	.4777E-01
.26	22.22	6.30	7.30	6.00	.4271E-01	.2810E-02	.1030E-01	14.30	.7000E-02	.3040E-01
.28	22.22	6.07	7.30	6.00	.4310E-01	.3070E-02	.1040E-01	10.40	.4000E-02	.3700E-01
.30	27.27	11.71	7.30	6.03	.4360E-01	.3730E-02	.2501E-01	10.20	.4700E-02	.1777E-01
.32	28.21	13.44	7.30	6.03	.4420E-01	.4300E-02	.3130E-01	12.40	.7000E-02	.4200E-01
.34	27.34	14.00	7.30	11.00	.4500E-01	.5100E-02	.3030E-01	10.70	.5710E-02	.0040E-01

## STRESS STATE AND ELASTIC CONSTANTS, DATA SET NO. 12

NU	WTOVT PSI	DEPRV PERCENT	MOVS PSI	PRSV PERCENT	MOOT PSI	THANT PERCENT	CHOOT PSI	CHANY PERCENT	MUC	STRAT
.24	13130.07	.1300E+00	11042.00	.1000E+00	90000.00	.1700E-02	6100.71	.2000E-01	-.00	.3000
.26	13020.00	.1300E+00	11110.00	.1000E+00	90000.00	.1700E-02	5700.00	.2000E-01	-.00	.3070
.28	14070.15	.1300E+00	11110.00	.1000E+00	90000.00	.1700E-02	5617.00	.2000E-01	-.00	.3010
.30	10000.00	.1300E+00	10000.00	.1000E+00	90000.00	.1700E-02	5310.00	.2000E-01	-.00	.4100
.32	11000.00	.1300E+00	10130.70	.1000E+00	90000.00	.1700E-02	7000.00	.2000E-01	-.00	.4000
.34	11700.00	.1300E+00	9150.31	.1000E+00	90000.00	.1700E-02	2700.00	.2000E-01	-.00	.4000
NU	S121 PSI	S122 PSI	S123 PSI	ETA DEGREES	EPS1 PERCENT	EPS2 PERCENT	EPS3 PERCENT	DATA DEGREES	EPSOC PERCENT	GAMOC PERCENT
.24	24.00	6.30	7.30	6.00	.1370E+00	.4070E-02	.0120E-01	6.00	.2070E-01	.1000E+00
.26	20.00	10.00	7.30	6.00	.1340E+00	.4070E-02	.0120E-01	6.00	.2110E-01	.1000E+00
.28	20.00	11.00	7.30	6.00	.1340E+00	.4070E-02	.0120E-01	6.00	.2110E-01	.1000E+00
.30	20.00	12.00	7.30	6.00	.1340E+00	.4070E-02	.0120E-01	6.00	.2110E-01	.1000E+00
.32	20.00	17.00	7.30	6.00	.1370E+00	.4070E-02	.0120E-01	6.00	.2110E-01	.1000E+00

[illegible]

~~9700 55 STATE AND CLASSIC CONSTANTS DATA SET NO. 1A~~

[illegible]

10	78.93	16.48	7.74	10.85	-191.40+0.0-	-190.00-0.1-	-193.75+0.3	10.74	-6.62+0.0-	-7.15+0.0-
11	78.46	16.39	7.75	14.85	-186.17+0.0-	-171.00-0.1-	-176.00-0.0	91.10	-1.17+0.0-	-0.45+0.0-

STP 99 STAFF AND PLASTIC CASTS. DATA SET NO. 19

[illegible]

STRESS RATE AND ELASTIC CONSTANTS, DATA SET NO. 10

01	020000 001	030000 00000000	040000 001	050000 00000000	060000 001	070000 00000000	080000 001	090000 00000000	100000 001	110000 00000000	120000 001	130000 00000000	140000 001	150000 00000000	160000 001	170000 00000000	180000 001	190000 00000000	200000 001	210000 00000000	220000 001	230000 00000000	240000 001	250000 00000000	260000 001	270000 00000000	280000 001	290000 00000000	300000 001	310000 00000000	320000 001	330000 00000000	340000 001	350000 00000000	360000 001	370000 00000000	380000 001	390000 00000000	400000 001	410000 00000000	420000 001	430000 00000000	440000 001	450000 00000000	460000 001	470000 00000000	480000 001	490000 00000000	500000 001	510000 00000000	520000 001	530000 00000000	540000 001	550000 00000000	560000 001	570000 00000000	580000 001	590000 00000000	600000 001	610000 00000000	620000 001	630000 00000000	640000 001	650000 00000000	660000 001	670000 00000000	680000 001	690000 00000000	700000 001	710000 00000000	720000 001	730000 00000000	740000 001	750000 00000000	760000 001	770000 00000000	780000 001	790000 00000000	800000 001	810000 00000000	820000 001	830000 00000000	840000 001	850000 00000000	860000 001	870000 00000000	880000 001	890000 00000000	900000 001	910000 00000000	920000 001	930000 00000000	940000 001	950000 00000000	960000 001	970000 00000000	980000 001	990000 00000000	1000000 001	1010000 00000000	1020000 001	1030000 00000000	1040000 001	1050000 00000000	1060000 001	1070000 00000000	1080000 001	1090000 00000000	1100000 001	1110000 00000000	1120000 001	1130000 00000000	1140000 001	1150000 00000000	1160000 001	1170000 00000000	1180000 001	1190000 00000000	1200000 001	1210000 00000000	1220000 001	1230000 00000000	1240000 001	1250000 00000000	1260000 001	1270000 00000000	1280000 001	1290000 00000000	1300000 001	1310000 00000000	1320000 001	1330000 00000000	1340000 001	1350000 00000000	1360000 001	1370000 00000000	1380000 001	1390000 00000000	1400000 001	1410000 00000000	1420000 001	1430000 00000000	1440000 001	1450000 00000000	1460000 001	1470000 00000000	1480000 001	1490000 00000000	1500000 001	1510000 00000000	1520000 001	1530000 00000000	1540000 001	1550000 00000000	1560000 001	1570000 00000000	1580000 001	1590000 00000000	1600000 001	1610000 00000000	1620000 001	1630000 00000000	1640000 001	1650000 00000000	1660000 001	1670000 00000000	1680000 001	1690000 00000000	1700000 001	1710000 00000000	1720000 001	1730000 00000000	1740000 001	1750000 00000000	1760000 001	1770000 00000000	1780000 001	1790000 00000000	1800000 001	1810000 00000000	1820000 001	1830000 00000000	1840000 001	1850000 00000000	1860000 001	1870000 00000000	1880000 001	1890000 00000000	1900000 001	1910000 00000000	1920000 001	1930000 00000000	1940000 001	1950000 00000000	1960000 001	1970000 00000000	1980000 001	1990000 00000000	2000000 001	2010000 00000000	2020000 001	2030000 00000000	2040000 001	2050000 00000000	2060000 001	2070000 00000000	2080000 001	2090000 00000000	2100000 001	2110000 00000000	2120000 001	2130000 00000000	2140000 001	2150000 00000000	
----	---------------	--------------------	---------------	--------------------	---------------	--------------------	---------------	--------------------	---------------	--------------------	---------------	--------------------	---------------	--------------------	---------------	--------------------	---------------	--------------------	---------------	--------------------	---------------	--------------------	---------------	--------------------	---------------	--------------------	---------------	--------------------	---------------	--------------------	---------------	--------------------	---------------	--------------------	---------------	--------------------	---------------	--------------------	---------------	--------------------	---------------	--------------------	---------------	--------------------	---------------	--------------------	---------------	--------------------	---------------	--------------------	---------------	--------------------	---------------	--------------------	---------------	--------------------	---------------	--------------------	---------------	--------------------	---------------	--------------------	---------------	--------------------	---------------	--------------------	---------------	--------------------	---------------	--------------------	---------------	--------------------	---------------	--------------------	---------------	--------------------	---------------	--------------------	---------------	--------------------	---------------	--------------------	---------------	--------------------	---------------	--------------------	---------------	--------------------	---------------	--------------------	---------------	--------------------	---------------	--------------------	---------------	--------------------	---------------	--------------------	----------------	---------------------	----------------	---------------------	----------------	---------------------	----------------	---------------------	----------------	---------------------	----------------	---------------------	----------------	---------------------	----------------	---------------------	----------------	---------------------	----------------	---------------------	----------------	---------------------	----------------	---------------------	----------------	---------------------	----------------	---------------------	----------------	---------------------	----------------	---------------------	----------------	---------------------	----------------	---------------------	----------------	---------------------	----------------	---------------------	----------------	---------------------	----------------	---------------------	----------------	---------------------	----------------	---------------------	----------------	---------------------	----------------	---------------------	----------------	---------------------	----------------	---------------------	----------------	---------------------	----------------	---------------------	----------------	---------------------	----------------	---------------------	----------------	---------------------	----------------	---------------------	----------------	---------------------	----------------	---------------------	----------------	---------------------	----------------	---------------------	----------------	---------------------	----------------	---------------------	----------------	---------------------	----------------	---------------------	----------------	---------------------	----------------	---------------------	----------------	---------------------	----------------	---------------------	----------------	---------------------	----------------	---------------------	----------------	---------------------	----------------	---------------------	----------------	---------------------	----------------	---------------------	----------------	---------------------	----------------	---------------------	----------------	---------------------	----------------	---------------------	----------------	---------------------	----------------	---------------------	--

10	20.72	10.12	7.35	17.07	1007E+00	7000E-01	1300E+00	25.25	1000E-01	1000E+00
10	20.72	10.12	7.35	17.07	1007E+00	7000E-01	1300E+00	25.25	1000E-01	1000E+00
10	20.72	10.12	7.35	17.07	1007E+00	7000E-01	1300E+00	25.25	1000E-01	1000E+00
10	20.72	10.12	7.35	17.07	1007E+00	7000E-01	1300E+00	25.25	1000E-01	1000E+00

Appendix CDerivations

The following derivations were made for use in this study:

- C-1 Strain Tensor for Resonant Column Specimen
- C-2 Strain Tensor for Hollow Cylinder Specimen
- C-3 Calculation of Moduli for Resonant Column Tests
- C-4 Principal Stresses for Resonant Column Specimen
- C-5 Principal Stresses for Hollow Cylinder Specimen
- C-6 Calculation of Compression Modulus for Hollow Cylinder Tests
- C-7 Calculation of Volume of Hollow Cylinder Specimen
- C-8 Calculation of Relative Density

### Appendix C-1

#### Strain Tensor for Resonant Column Specimen

From the expressions for the strains contained in Equations 2.5 through 2.11 and from the boundary conditions presented in Equations 2.12 and 2.13, the following expressions may be written:

$$\epsilon_{\theta} = \frac{u}{r}, \text{ because } \frac{\partial v}{\partial \theta} = 0 \quad (\text{C-1.1})$$

$$\epsilon_{R\theta} = \frac{1}{2} \left( \frac{\partial u}{r \partial \theta} + z \Delta \theta_o - z \Delta \theta_o \right) = \frac{1}{2} \frac{\partial u}{r \partial \theta} \quad (\text{C-1.2})$$

$$\epsilon_{Rz} = \frac{1}{2} \frac{\partial u}{\partial z}, \text{ because } \frac{\partial w}{\partial r} = 0 \quad (\text{C-1.3})$$

$$\epsilon_{\theta z} = \frac{1}{2} \frac{v}{z} = \frac{1}{2} r \Delta \theta_o, \text{ where } \frac{\partial w}{\partial \theta} = 0 \quad (\text{C-1.4})$$

and  $u$  is unknown, but

$$u = \int \epsilon_R dr \quad (\text{C-1.5})$$

From Hooke's Law, it is known that:

$$\epsilon_x = \epsilon_y = -\mu \epsilon_z \quad (\text{C-1.6})$$

and 
$$\epsilon_x + \epsilon_y + \epsilon_z = \epsilon_{vol} = (1 - 2\mu) \epsilon_z \quad (\text{C-1.7})$$

Also,

$$\epsilon_{vol} = \epsilon_R + \epsilon_{\theta} + \epsilon_z = (1 - 2\mu) \epsilon_z \quad (\text{C-1.8})$$

or 
$$\epsilon_R + \epsilon_{\theta} = -2\mu \epsilon_z \quad (\text{C-1.9})$$

Now, if one considers the new volume,  $V_N$ , and relates it to the old volume,  $V_o$ , it can be stated that:

$$V_N = V_O (1 + \epsilon_{vol}) = V_O [1 + (1 - 2\mu)\epsilon_z] \quad (C-1.10)$$

But  $V_N$  is also equal to:

$$V_N = H_O (1 + \epsilon_z) \cdot \pi R_N^2 \quad (C-1.11)$$

where  $H_O$  is the old height and  $R_N$  the new radius. We also know that  $V_O$  is a function of  $H_O$  and  $R_O$ , the old radius, as follows:

$$V_O = H_O \cdot \pi R_O^2 \quad (C-1.12)$$

Combining the last three equations, C-1.10 through C-1.12, the following expression for  $R_N$  may be developed:

$$R_N = R_O \cdot \left[ \frac{1 + (1 - 2\mu)\epsilon_z}{1 + \epsilon_z} \right]^{1/2} \quad (C-1.13)$$

and it is also known that:

$$R_N = R_O (1 + \epsilon_R) \quad (C-1.14)$$

It is now possible to write an expression for  $\epsilon_R$  as follows:

$$\epsilon_R = \left[ \frac{1 + (1 - 2\mu)\epsilon_z}{1 + \epsilon_z} \right]^{1/2} - 1 \quad (C-1.15)$$

Now, from Equation C-1.5:

$$u = \int \epsilon_R dr \quad (C-1.5)$$

$$\text{or} \quad u = r \cdot \left( \left[ \frac{1 + (1 - 2\mu)\epsilon_z}{1 + \epsilon_z} \right]^{1/2} - 1 \right) \quad (C-1.16)$$

It is possible now to write expressions for  $\epsilon_\theta$ ,  $\epsilon_{R\theta}$ , and  $\epsilon_{Rz}$ , and as follows:

$$\epsilon_{\theta} = \frac{u}{r} = \left[ \frac{1 + (1 - 2\mu)\epsilon_z}{1 + \epsilon_z} \right]^{1/2} - 1 = \epsilon_R \quad (\text{C-1.17})$$

$$\epsilon_{R\theta} = \frac{1}{2} \frac{\partial u}{r \partial \theta} = 0 \quad (\text{C-1.18})$$

and  $\epsilon_{Rz} = \frac{1}{2} \frac{\partial u}{\partial z} = 0 \quad (\text{C-1.19})$

It is also known that:

$$\epsilon_R + \epsilon_{\theta} = -2\mu\epsilon_z \quad (\text{C-1.19})$$

so that one may write:

$$\epsilon_R = \epsilon_{\theta} = -\mu\epsilon_z \quad (\text{C-1.20})$$

The strain tensor may now be written:

$$\epsilon = \begin{vmatrix} -\mu\epsilon_z & 0 & 0 \\ 0 & -\mu\epsilon_z & \frac{1}{2} r \Delta\theta_o \\ 0 & \frac{1}{2} r \Delta\theta_o & \epsilon_z \end{vmatrix} \quad (2.14)$$

It should be further noted that the  $\epsilon_{\theta z}$  component is a function of the radius  $r$ . For practical application purposes, the average  $\epsilon_{\theta z}$  will be assumed to exist at  $r = \frac{2}{3} R$ , and be considered a constant at that value.

Appendix C-2

Strain Tensor for Hollow Cylinder Specimen

From the expressions for the strain contained in Equations 2.5, 2.8 through 2.11, 2.15, and 2.16, and from the boundary conditions expressed in Equations 2.12 and 2.13, the following expressions may be written:

$$\epsilon_{R\theta} = \frac{1}{2} \left( \frac{\partial u}{r \partial \theta} + \Delta \theta_o z - \Delta \theta_o z \right) = \frac{1}{2} \frac{\partial u}{r \partial \theta} \quad (C-2.1)$$

$$\epsilon_{Rz} = \frac{1}{2} \frac{\partial u}{\partial z}, \text{ because } \frac{\partial w}{\partial r} = 0 \quad (C-2.2)$$

$$\epsilon_{\theta z} = \frac{1}{2} \frac{\partial v}{\partial z} = \frac{1}{2} R_{avg} \Delta \theta_o, \text{ where } \frac{\partial w}{\partial \theta} = 0 \quad (C-2.3)$$

and  $u$  is unknown, but

$$u = \int \epsilon_R dr \quad (C-2.4)$$

If it is assumed that Hooke's Law applies, the following expressions may be written:

$$\epsilon_R = \frac{1}{E} \sigma_R - \frac{\mu}{E} \sigma_z - \frac{\mu}{E} \sigma_\theta \quad (C-2.5)$$

$$\epsilon_z = \frac{1}{E} \sigma_z - \frac{\mu}{E} \sigma_R - \frac{\mu}{E} \sigma_\theta \quad (C-2.6)$$

and 
$$\epsilon_\theta = \frac{1}{E} \sigma_\theta - \frac{\mu}{E} \sigma_R - \frac{\mu}{E} \sigma_z \quad (C-2.7)$$

If  $\epsilon_\theta = 0$ , Equation C-2.7 may be rewritten as follows:

$$\sigma_\theta = \mu(\sigma_R + \sigma_z) \quad (C-2.8)$$

Now  $\epsilon_z$  and  $\epsilon_R$  may be written:

$$\epsilon_R = \frac{1}{E} \sigma_R - \frac{\mu}{E} \sigma_z - \frac{\mu}{E} [\mu (\sigma_R + \sigma_z)] \quad (C-2.9)$$

$$= \left( \frac{1 - \mu^2}{E} \right) \sigma_R - \left( \frac{\mu + \mu^2}{E} \right) \sigma_z$$

and

$$\epsilon_z = \frac{1}{E} \sigma_z - \frac{\mu}{E} \sigma_R - \frac{\mu}{E} [\mu (\sigma_R + \sigma_z)] \quad (C-2.10)$$

$$= \left( \frac{1 - \mu^2}{E} \right) \sigma_z - \left( \frac{\mu + \mu^2}{E} \right) \sigma_R$$

Now, the change in the radial strain,  $\Delta \epsilon_R$ , during loading may be written:

$$\Delta \epsilon_R = \left( \frac{1 - \mu^2}{E} \right) \Delta \sigma_R - \left( \frac{\mu + \mu^2}{E} \right) \Delta \sigma_z \quad (C-2.11)$$

And because  $\Delta \sigma_R = 0$  in this testing program,

$$\Delta \epsilon_R = \left( \frac{\mu + \mu^2}{E} \right) \Delta \sigma_z \quad (C-2.12)$$

Similarly,

$$\Delta \epsilon_z = \left( \frac{1 - \mu^2}{E} \right) \Delta \sigma_z \quad (C-2.13)$$

Combining the above two equations, C-2.12 and C-2.13 gives:

$$\Delta \epsilon_R = - \left( \frac{\mu + \mu^2}{1 - \mu^2} \right) \Delta \epsilon_z \quad (C-2.14)$$

Now, because

$$u = \int \epsilon_R \, dr \quad (C-2.4)$$

for  $R_{avg} \leq r \leq R_2$ ,

$$\begin{aligned} u &= \int_{R_{avg}}^r - \left( \frac{\mu + \mu^2}{1 - \mu^2} \right) \Delta \epsilon_z \, dr \\ &= - \left( \frac{\mu + \mu^2}{1 - \mu^2} \right) \Delta \epsilon_z [r - R_{avg}] \end{aligned} \quad (C-2.15)$$

for  $R_1 \leq r \leq R_{avg}$ ,

$$\begin{aligned} u &= \int_{R_{avg}}^r - \left( \frac{\mu + \mu^2}{1 - \mu^2} \right) \cdot \Delta \epsilon_z \, dr \\ &= - \left( \frac{\mu + \mu^2}{1 - \mu^2} \right) \cdot \Delta \epsilon_z \cdot [r - R_{avg}] \end{aligned} \quad (C-2.16)$$

The expressions for  $\epsilon_{R\theta}$  and  $\epsilon_{Rz}$  may now be written:

$$\epsilon_{R\theta} = \frac{1}{2} \frac{\partial u}{r \partial \theta} = 0 \quad (C-2.17)$$

$$\epsilon_{Rz} = \frac{1}{2} \frac{\partial u}{\partial z} = 0 \quad (C-2.18)$$

The strain tensor may now be written:

$$\epsilon = \begin{vmatrix} -\left( \frac{\mu + \mu^2}{1 - \mu^2} \right) \epsilon_z & 0 & 0 \\ 0 & 0 & \frac{1}{2} R_{avg} \Delta \theta_o \\ 0 & \frac{1}{2} R_{avg} \Delta \theta_o & \epsilon_z \end{vmatrix} \quad (2.17)$$

It is also worth noting that for the special condition where  $\Delta \theta_o = 0$ , Equation (2.17) is transformed so that the values of  $\epsilon_R$ ,  $\epsilon_\theta$ , and  $\epsilon_z$  are also the principal strain values,  $\epsilon_3$ ,  $\epsilon_2$ , and  $\epsilon_1$  respectively. In this special case the strain tensor is that of a plane strain condition.

### Appendix C-3

#### Calculation of Dynamic Moduli for Resonant Column Tests

##### Compression Modulus

The basic expression for the dynamic compression modulus,  $E$ , is as follows:

$$E = \rho \cdot v_p^2 \quad (C-3.1)$$

where  $\rho$  is the mass density of the specimen material, and where  $v_p$  is the "P-wave" (compression wave) velocity of propagation. For the solid cylindrical specimen,

$$\rho = \frac{W}{V \cdot g} \quad (C-3.2)$$

where  $W$  is the specimen weight,  $V$  is the specimen volume, and  $g$  is the acceleration of gravity. The value of  $v_p$  may be calculated from the following expression:

$$v_p = \frac{2 \cdot \pi \cdot f_v \cdot L}{\psi_v} \quad (C-3.3)$$

where  $f_v$  is the resonant frequency in compression,  $L$  is the length (or height) of the cylindrical specimen and where  $\psi_v$  is the root of the frequency equation:

$$\psi_v \cdot \tan \psi_v = \frac{W}{W_{TOP}} \quad (C-3.4)$$

where  $W_{TOP}$  is the top cap weight. The value of  $W_{TOP}$  in this testing series is 1576.6 gm.

During the resonant column test, the resonant frequency is influenced by dynamic coupling between the sample and the cap system. If a test could be conducted under ideal conditions, where the top cap weight was

negligible when compared with the specimen weight, there would be no coupling effect and  $f_v$  would reflect the true resonant frequency of the soil specimen. In this special case,  $\psi_v = \pi/2$ , and Equation C-3.3 reduces to the following:

$$V_p = 4 \cdot f_v \cdot L \quad (C-3.5)$$

In the more general case, the dynamic compression modulus may be calculated directly from Equations C-3.1 through C-3.4. The only difficulty in this calculation, albeit a minor one, is that the value of  $\psi_v$  must be calculated from Equation C-3.4 by an iterative process.

These calculations are made in Computer Program RC, which is included as Appendix D-1.

#### Shear Modulus

The basic expression for the dynamic shear modulus,  $G$ , is as follows:

$$G = \rho \cdot v_s^2 \quad (C-3.6)$$

where  $v_s$  is the "S-wave" (shear wave) velocity of propagation, and where  $\rho$  is the mass density of the specimen material and is defined in Equation C-3.2. The value of  $v_s$  may be calculated as follows:

$$v_s = \frac{2 \cdot \pi \cdot f_s \cdot L}{\psi_s} \quad (C-3.7)$$

where  $f_s$  is the resonant frequency in torsional shear,  $L$  is the length (or height) of the cylindrical specimen, and where  $\psi_s$  is the root of the frequency equation:

$$\psi_s \cdot \tan \psi_s = \frac{J}{J_0} \quad (C-3.8)$$

where  $J$  is the torsional moment of inertia of the specimen, and  $J_0$  is the torsional moment of inertia of the top cap system. The units of  $J$  and  $J_0$  are mass-length-time<sup>2</sup>. For a cylindrical specimen,  $J$  may be calculated as follows:

$$J = \frac{W \cdot D^2}{8 \cdot g} \quad (C-3.9)$$

where  $D$  is the diameter of the specimen.

As discussed earlier, the factor  $\psi_s$  is necessary to correct for the dynamic coupling influence of the top cap system upon the measured resonant frequency. If the torsional moment of inertia of the top cap system were negligible when compared with the torsional moment of inertia of the specimen,  $\psi_s = \pi/2$ , and Equation C-3.7 would reduce to:

$$V_s = 4 \cdot f_s \cdot L \quad (C-3.10)$$

In the more general case, the dynamic shear modulus may be calculated directly from Equations C-3.6 through C-3.9. The value of  $J_0$  in this testing series is:

$$J_0 = 31.45 \text{ gm-cm-sec}^2 \quad (C-3.11)$$

The value of  $\psi_s$  must be calculated from Equation C-3.8 by an iterative process.

These calculations are made in Computer Program RC, which is included as Appendix D-1.

# Appendix C-4

## Principal Stresses for Resonant Column Specimen

The Mohr's circle diagram in Figure C4-1 represents the state of stress within the resonant column specimen, viewed from the " $\theta z$  plane", for the condition of simultaneous maximum vertical compression and torsional shear stress. The principal stresses are shown on this figure as  $\sigma_1$ ,  $\sigma_2$ , and  $\sigma_3$ . The values  $\Delta\sigma_z$  and  $\Delta\tau_{\theta z}$  as recorded raw data were double amplitude values and thus must be divided by 2 for plotting on Mohr's circle.

The center of the Mohr's circle,  $\sigma_{ct}$ , may be calculated as follows

$$\sigma_{ct} = \sigma_{\theta} + \frac{\Delta\sigma_z}{4} \cdot \sin(\omega_z t) \quad (3.18)$$

where  $\omega_z$  is the rotational frequency of vertical loading and is constant.

Note that:

$$\sigma_{\theta} = \sigma_R = \sigma_{1c} = \sigma_{2c} = \sigma_{3c} \quad (C-4.1)$$

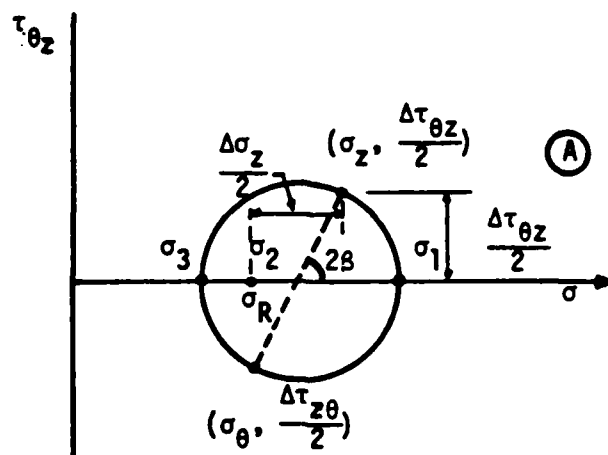
for this testing series, where  $\sigma_{1c}$ ,  $\sigma_{2c}$ , and  $\sigma_{3c}$  are the principal stresses during consolidation.

From the figure,

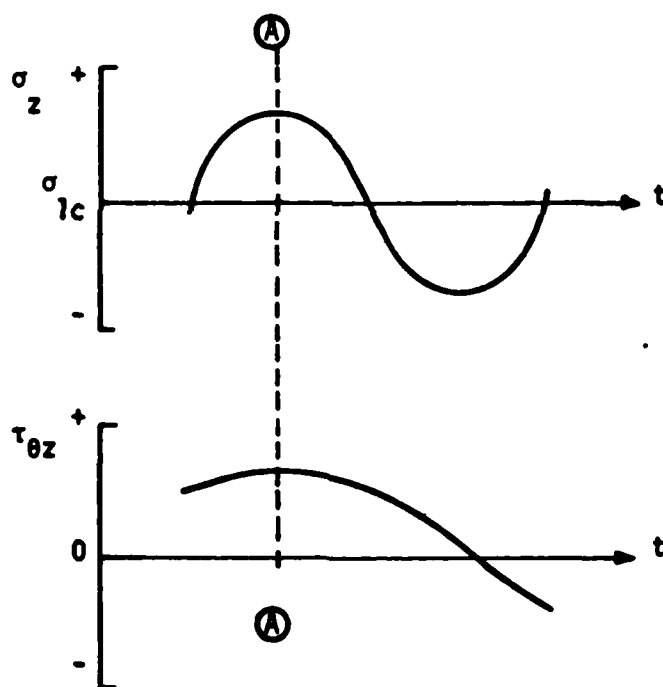
$$\tan(2\beta) = \left[ \frac{\frac{\Delta\tau_{\theta z}}{2} \cdot \sin(\rho \cdot \omega_z \cdot t)}{\frac{\Delta\sigma_z}{4} \cdot \sin(\omega_z \cdot t)} \right] \quad (C-4.2)$$

$$\text{where } \rho = \frac{f_T}{f_z} = \frac{\omega_T}{\omega_z}$$

$$\text{Now: } \beta = \frac{1}{2} \tan^{-1} \left[ \frac{2 \cdot \Delta\tau_{\theta z} \cdot \sin(\rho \cdot \omega_z \cdot t)}{\Delta\sigma_z \cdot \sin(\omega_z \cdot t)} \right] \quad (3.17)$$



(a)



(b)

FIGURE C4-1 MOHR'S CIRCLE IN STRESS (a) AND STRESS TIME HISTORIES (b) FOR SIMULTANEOUS DYNAMIC LOADING OF RESONANT COLUMN SPECIMENS UNDER CONDITION OF MAXIMUM INSTANTANEOUS VERTICAL AND TORSIONAL STRESS

Now:

$$\sigma_1 = \sigma_R + \frac{\Delta\sigma_z}{2} \cdot \sin(\omega_z \cdot t) + \frac{\Delta\tau_{\theta z}}{2} \cdot \sin(\rho \cdot \omega_z \cdot t) \cdot \tan(\beta) \quad (3.14)$$

Note that because of the geometry of the Mohr's circle,  $\sigma_1$  may also be written:

$$\sigma_1 = \sigma_R + \frac{\Delta\sigma_z}{4} \cdot \sin(\omega_z \cdot t) + \sqrt{\left[\frac{\Delta\sigma_z}{4} \cdot \sin(\omega_z \cdot t)\right]^2 + \left[\frac{\Delta\tau_{\theta z}}{2} \cdot \sin(\rho \cdot \omega_z \cdot t)\right]^2} \quad (C-4.3)$$

The remaining two principal stresses are as follows:

$$\sigma_2 = \sigma_R \quad (3.15)$$

and

$$\sigma_3 = 2\sigma_{ct} - \sigma_1 \quad (3.16)$$

It should be noted that  $\sigma_1$  and  $\sigma_3$  are the major and minor principal stresses at the condition of simultaneous maximum vertical compression and torsional shear stress as shown in Figure C4-1(a). As time goes on, however, the amplitude and direction of these principal stresses will change, and at some point " $\sigma_1$ " will be numerically smaller than " $\sigma_3$ ". At that point the principal stress directions "reverse" and  $\sigma_3$  becomes the new  $\sigma_1$ .

### Appendix C-5

#### Principal Stresses for Hollow Cylinder Specimen

The Mohr's circle diagram in Figure C5-1 represents the state of stress within the hollow cylinder specimen, viewed from the " $\theta z$  plane", for the condition of simultaneous maximum vertical compression and torsional shear stress. The principal stresses are shown on the figure as  $\sigma_1$  and  $\sigma_2$ . The minor principal stress,  $\sigma_3$ , is unchanged during loading and is:

$$\sigma_3 = \sigma_{3c} = \sigma_R \quad (C-5.1)$$

The vertical and torsional stresses shown in Figure C5-1(a) may be written

$$\frac{\partial \sigma_z}{\partial t} = \frac{\Delta \sigma_z}{2} \cdot \sin(\lambda \cdot t) \quad (C-5.2)$$

and

$$\frac{\partial \tau_{\theta z}}{\partial t} = \frac{\Delta \tau_{\theta z}}{2} \cdot \sin[(\lambda - \alpha) \cdot t] \quad (C-5.3)$$

where  $\lambda$  is the rotational frequency of loading and is constant.

The center of the Mohr's circle,  $\sigma_{ct}$ , at any time may be calculated as follows:

$$\sigma_{ct} = \frac{[\sigma_{1c} + \frac{\Delta \sigma_z}{2} \cdot \sin(\lambda \cdot t)] + [\sigma_{2c} + \frac{\Delta \sigma_\theta}{2} \cdot \sin(\lambda \cdot t)]}{2} \quad (C-5.4)$$

and because  $\sigma_{2c} = \mu(\sigma_{1c} + \sigma_{3c})$ , and  $\Delta \sigma_\theta = \mu \Delta \sigma_z$ ,

$$\sigma_{ct} = \frac{[\sigma_{1c} + \frac{\Delta \sigma_z}{2} \cdot \sin(\lambda \cdot t)] + [\mu(\sigma_{1c} + \sigma_{3c}) + \frac{\mu \Delta \sigma_z}{2} \cdot \sin(\lambda \cdot t)]}{2} \quad (C5-5.5)$$

which reduces to:

$$\sigma_{ct} = \left(\frac{1 + \mu}{2}\right) \sigma_{1c} + \left(\frac{1 + \mu}{4}\right) \Delta \sigma_z \cdot \sin(\lambda \cdot t) + \frac{\mu \sigma_{3c}}{2} \quad (3.37)$$

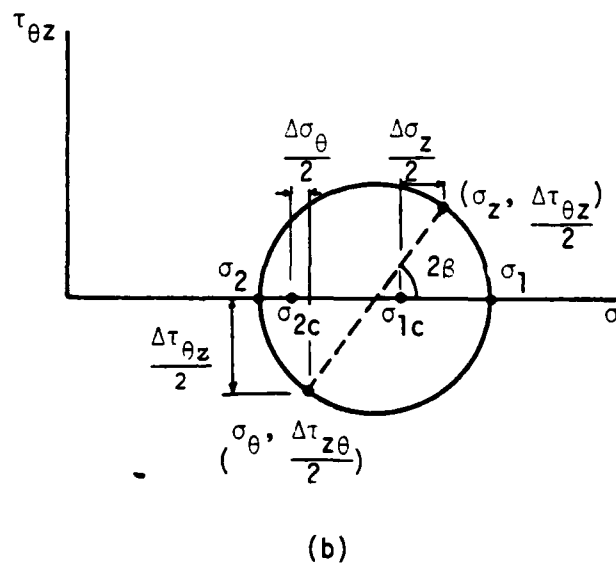
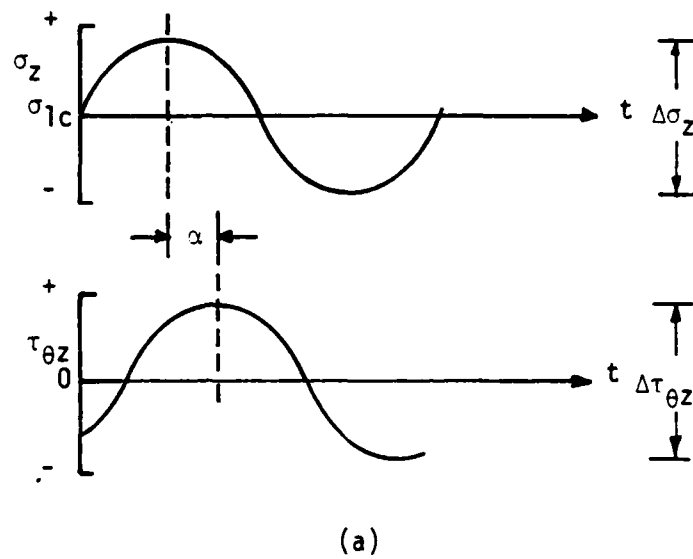


FIGURE C5-1 STRESS TIME HISTORIES (a) AND MOHR'S CIRCLE IN STRESS (b) FOR SIMULTANEOUS DYNAMIC LOADING OF HOLLOW CYLINDER SPECIMENS UNDER CONDITION OF MAXIMUM INSTANTANEOUS VERTICAL AND TORSIONAL STRESS

Now, from Figure C5-1, the following expression may be written:

$$\tan(2\beta) = \frac{\left( \frac{\Delta\tau_{\theta z}}{2} \cdot \sin[(\lambda-\alpha) \cdot t] \right)}{\left( \sigma_{1c} + \frac{\Delta\sigma_z}{2} \cdot \sin(\lambda \cdot t) - \sigma_{ct} \right)} \quad (C-5.6)$$

$$\text{or} \quad \beta = \frac{1}{2} \tan^{-1} \left\{ \frac{\Delta\tau_{\theta z} \cdot \sin[(\lambda-\alpha) \cdot t]}{2 \left[ \sigma_{1c} + \frac{\Delta\sigma_z}{2} \cdot \sin(\lambda \cdot t) - \sigma_{ct} \right]} \right\} \quad (3.36)$$

The principal stresses may now be written:

$$\sigma_1 = \sigma_{1c} + \frac{\Delta\sigma_z}{2} \cdot \sin(\lambda \cdot t) + \frac{\Delta\tau_{\theta z}}{2} \cdot \sin[(\lambda-\alpha) \cdot t] \cdot \tan(\beta) \quad (3.33)$$

$$\sigma_2 = 2\sigma_{ct} - \sigma_1 = \sigma_1 - 2(\sigma_1 - \sigma_{ct}) \quad (3.34)$$

$$\text{and} \quad \sigma_3 = \sigma_{3c} = \sigma_R \quad (3.35)$$

It should be noted that with time, the numerical values of the major and minor principal stresses will change. If  $\frac{\Delta\sigma_z}{2}$  exceeds  $0.85 \cdot \sigma_{3c}$  at any time, then the principal stress directions will "reverse" for a period during each cycle of loading, and  $\sigma_3$  will become the new  $\sigma_1$  for that period.

### Appendix C-6

#### Calculation of Compression Modulus for Hollow Cylinder Tests

From Hooke's Law the strains may be written as follows:

$$\epsilon_z = \frac{1}{E} \sigma_z - \frac{\mu}{E} (\sigma_R + \sigma_\theta) \quad (C-6.1)$$

$$\epsilon_R = \frac{1}{E} \sigma_R - \frac{\mu}{E} (\sigma_z + \sigma_\theta) \quad (C-6.2)$$

and

$$\epsilon_\theta = \frac{1}{E} \sigma_\theta - \frac{\mu}{E} (\sigma_z + \sigma_R) \quad (C-6.3)$$

Because  $\epsilon_\theta = 0$  in this testing series, Equation C-6.3 may be rewritten as follows:

$$\sigma_\theta = \mu (\sigma_z + \sigma_R) \quad (C-6.4)$$

Now Equation C-6.1 may be written:

$$\epsilon_z = \left( \frac{1 - \mu^2}{E} \right) \sigma_z - \left( \frac{\mu + \mu^2}{E} \right) \sigma_R \quad (C-6.5)$$

During dynamic loading, the change in vertical strain may be written as follows:

$$\Delta \epsilon_z = \left( \frac{1 - \mu^2}{E} \right) \Delta \sigma_z - \left( \frac{\mu + \mu^2}{E} \right) \Delta \sigma_R \quad (C-6.6)$$

but because  $\Delta \sigma_R = 0$ ,

$$\Delta \epsilon_z = \left( \frac{1 - \mu^2}{E} \right) \Delta \sigma_z \quad (C-6.7)$$

or

$$E = (1 - \mu^2) \frac{\Delta \sigma_z}{\Delta \epsilon_z} \quad (4.13)$$

# Appendix C-7

## Calculation of Volume of Hollow Cylinder Specimen

For most tests in this testing program, the specimen height,  $H$ , and thickness,  $T$ , were measured immediately following the initial isotropic increment of consolidation. For some earlier tests, only the sample height was accurately measured. Assuming the specimen in Figure C7-1(a) is typical, then:

$$T = R_2 - R_1 \quad (C-7.1)$$

$R_{avg}$  is approximately 10.0 cm (3.937 in) for all samples.

The volume of a specimen,  $V$ , is:

$$V = H \cdot \pi \cdot (R_2^2 - R_1^2) \quad (C-7.2)$$

but because  $R_2 = R_{avg} + \frac{T}{2}$ , and  $R_1 = R_{avg} - \frac{T}{2}$ ,

$$V = H \cdot \pi \cdot \left[ \left( R_{avg} + \frac{T}{2} \right)^2 - \left( R_{avg} - \frac{T}{2} \right)^2 \right] \quad (C-7.3)$$

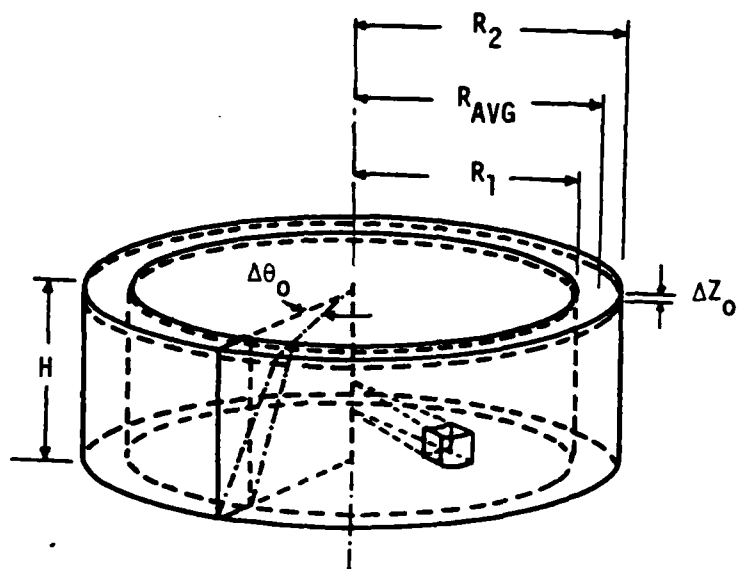
Expanding this expression gives:

$$V = H \cdot \pi \cdot \left[ \left( R_{avg}^2 + T \cdot R_{avg} + \frac{T^2}{4} \right) - \left( R_{avg}^2 - T \cdot R_{avg} + \frac{T^2}{4} \right) \right] \quad (C-7.4)$$

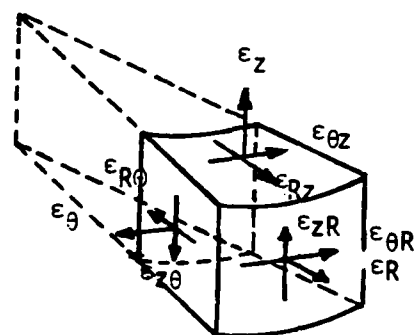
$$\text{or} \quad V = H \cdot \pi \cdot 2 \cdot T \cdot R_{avg} \quad (C-7.5)$$

To calculate the volume in cubic inches, since  $T$  and  $H$  are measured in inches, Equation C-7.5 may be written:

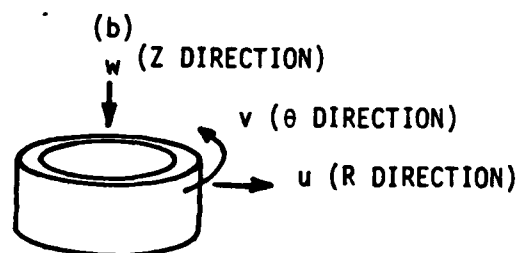
$$V = H \cdot T \cdot 24.73695 \quad (C-7.6)$$



(a)



(b)



(c)

FIGURE C7-1 FREE BODY DIAGRAM AND STATE OF STRAINS  
FOR HOLLOW CYLINDER SPECIMENS

If T was not recorded, an average value of  $T = 0.779$  in. may be used with good accuracy, and Equation C-7.5 may be written:

$$V \approx H \cdot 19.270084 \quad (C-7.7)$$

Equations C-7.6 and C-7.7 are used in Computer Program HC, included as Appendix D-2, to calculate the volume of hollow cylinder specimens.

### Appendix C-8

#### Calculation of Relative Density

The soil used in this study was Monterey No. 0 sand, a uniformly graded, fine grained quartz sand processed from beach sand. A gradation analysis of this sand is shown in Figure C8-1.

In order to calculate relative densities for the various specimens constructed through this study, laboratory tests were performed to determine the maximum and minimum densities,  $\gamma_{d \max}$  and  $\gamma_{d \min}$ , which could be achieved. These two limiting densities were found to be as follows:

$$\gamma_{d \max} = 1.70709 \text{ gm/cc} \quad (\text{C-8.1})$$

and 
$$\gamma_{d \min} = 1.42532 \text{ gm/cc} \quad (\text{C-8.2})$$

The relative density of a sand,  $D_R$ , is defined as follows:

$$D_R = \frac{e_{\max} - e}{e_{\max} - e_{\min}} \times 100\% \quad (\text{C-8.3})$$

where  $e$  is the void ratio and is defined as:

$$e = \frac{V_v}{V_s} \quad (\text{C-8.4})$$

where  $V_v$  is the volume of voids, and  $V_s$  the volume of solids, which may also be written:

$$V_s = \frac{W_s}{G_s \cdot \gamma_w} \quad (\text{C-8.5})$$

In this equation,  $W_s$  is the weight of soil (weight of voids is assumed negligible),  $G_s$  is the unit weight of the solid materials, and  $\gamma_w$  is the unit weight of water,  $\gamma_w = 1 \text{ gm/cc}$ . The volume,  $V$ , may be written:

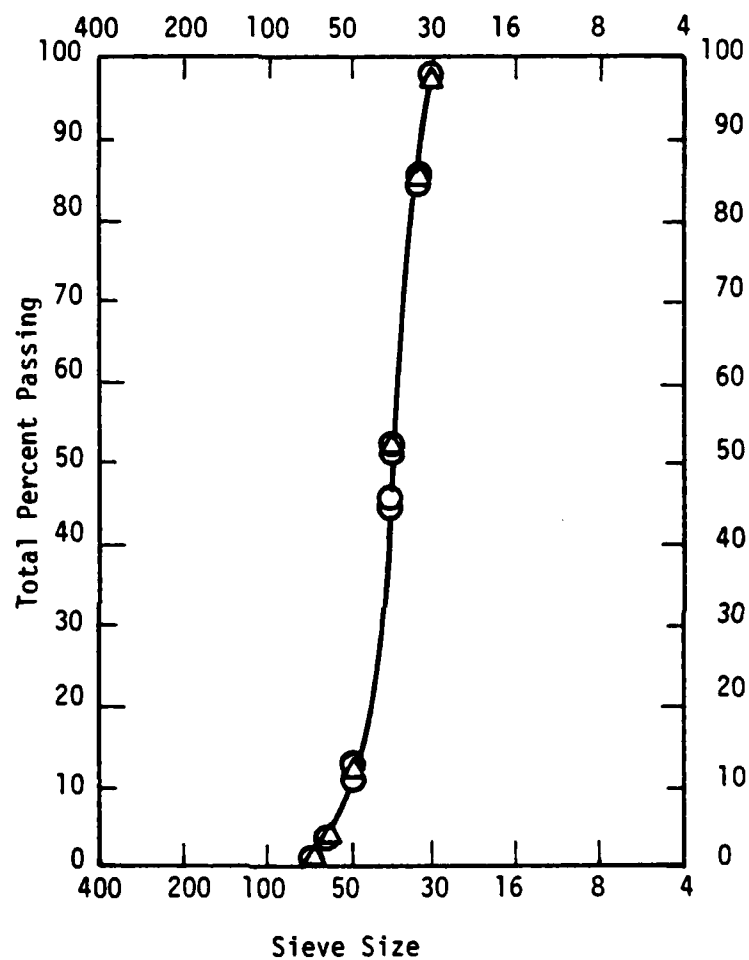


FIGURE C8-1 GRADATION ANALYSIS OF MONTEREY NO. 0 SAND USED IN THIS STUDY

$$V = V_v + V_s \quad (C-8.6)$$

Now  $e$  may be rewritten:

$$e = \frac{V_v}{V_s} = \frac{V_v \cdot G_s \cdot \gamma_w}{W_s} \quad (C-8.7)$$

Also, because  $\gamma_d = \frac{W_s}{V}$ ,

$$V_v = \frac{W_s}{\gamma_d} - V_s \quad (C-8.8)$$

and

$$e = \frac{G_s \cdot \gamma_w \cdot W_s}{\gamma_d \cdot W_s} - 1 \quad (C-8.9)$$

which reduces to:

$$e = \frac{G_s \cdot \gamma_w}{\gamma_d} - 1 \quad (C-8.10)$$

The relative density may now be written:

$$D_R = \frac{\left( \frac{G_s \cdot \gamma_w}{\gamma_{dmin}} - 1 \right) - \left( \frac{G_s \cdot \gamma_w}{\gamma_d} - 1 \right)}{\left( \frac{G_s \cdot \gamma_w}{\gamma_{dmin}} - 1 \right) - \left( \frac{G_s \cdot \gamma_w}{\gamma_{dmax}} - 1 \right)} \times 100\% \quad (C-8.11)$$

or

$$D_R = \frac{\left( \frac{1}{\gamma_{dmin}} \right) - \left( \frac{1}{\gamma_d} \right)}{\left( \frac{1}{\gamma_{dmin}} \right) - \left( \frac{1}{\gamma_{dmax}} \right)} \times 100\% \quad (C-8.12)$$

This Equation further reduces to:

$$D_R = \frac{0.701597 - \frac{1}{\gamma_d}}{0.1158046} \times 100\% \quad (C-8.13)$$

Equation C-8.13 was used to calculate relative density during this study.

Appendix D  
Computer Programs

The following computer programs were developed for use in this study:

D-1 Program RC--A Program to Reduce Data from the Triaxial Resonant Column Testing Series.

D-2 Program HC--A Program to Reduce Data from the Thin-Walled Hollow Cylinder Testing Series.

## APPENDIX D1

Program RC--A Program to Reduce Data from the  
Triaxial Resonant Column Testing Series

```

C      PROGRAM RC (INPUT,OUTPUT,PUNCH)
C
C      A COMPUTER PROGRAM TO REDUCE DATA FROM THE TRIAXIAL RESONANT COLUMN
C      TESTING SERIES.
C
C      CODED BY PAT GRIFFIN -- OCTOBER 20, 1979
C
C      THIS PROGRAM IS BASED ON CLASSICAL ELASTIC THEORY AND HOOKE'S LAW.
C      THE INPUT PARAMETERS INCLUDE THE SAMPLE PHYSICAL DIMENSIONS, THE
C      SYSTEM DYNAMIC PROPERTIES, CALIBRATION FACTORS AND THE RAW TEST
C      DATA, INCLUDING THE DRIVING VOLTAGE, ACCELEROMETER RESPONSE VOLTAGE,
C      AND THE RESONANT FREQUENCY IN VERTICAL AND TORSIONAL LOADING. THE
C      PROGRAM COMPUTES THE COMPRESSION AND SHEAR MODULI, STRAIN AMPLITUDES
C      AND DAMPING RATIOS, THE MAGNITUDE AND DIRECTION OF THE PRINCIPAL
C      STRESSES AND THE INCREMENTAL PRINCIPAL STRAINS, AND THE OCTAHEDRAL
C      STRAIN AND THE OCTAHEDRAL SHEARING STRAIN. WHERE THERE IS A
C      REDUNDANCY OF DATA, SUCH AS WITH THE COMBINED LOADING TESTS, THE
C      PROGRAM ALSO COMPUTES A POISSON'S RATIO AND THE AVERAGE RATIO OF
C      HORIZONTAL SHEAR STRAIN TO VERTICAL NORMAL STRAIN.
C
C      THE FOLLOWING IS A LISTING OF THE VARIABLE NAMES USED IN THIS
C      PROGRAM:
C
C      ACCEVT TORSIONAL ACCELERATION RESPONSE READING
C      ACCEV  VERTICAL ACCELERATION RESPONSE READING
C      ACFT   TORSIONAL ACCELERATION CALIBRATION FACTOR
C      ACFTV  VERTICAL ACCELERATION CALIBRATION FACTOR
C      BETA   ANGLE OF RE-ORIENTATION OF THE PRINCIPAL STRESS AXES
C      COILT  TORSIONAL DRIVING VOLTAGE READING
C      COILV  VERTICAL DRIVING VOLTAGE READING
C      DAMPT  TORSIONAL DAMPING
C      DAMPV  VERTICAL DAMPING
C      DCFT   TORSIONAL DAMPING CALIBRATION FACTOR
C      DCFV   VERTICAL DAMPING CALIBRATION FACTOR
C      DEPSV  VERTICAL STRAIN
C      DGAMT  TORSIONAL STRAIN
C      DIAM  DIAMETER OF SAMPLE
C      DSTGV  VERTICAL STRESS
C      DTAUT  TORSIONAL STRESS
C      EATA   ANGLE OF RE-ORIENTATION OF THE INCREMENTAL PRINCIPAL STRAINS
C      EPSCT  CENTER OF EPS1 - EPS2 MOHR'S CIRCLE
C      EPSOC  OCTAHEDRAL STRAIN
C      EPS1   MAJOR INCREMENTAL PRINCIPAL STRAIN
C      EPS2   INTERMEDIATE INCREMENTAL PRINCIPAL STRAIN
C      EPS3   MINOR INCREMENTAL PRINCIPAL STRAIN
C      FREQT  TORSIONAL RESONANT FREQUENCY
C      FREQV  VERTICAL RESONANT FREQUENCY
C      GAMOC  OCTAHEDRAL SHEARING STRAIN
C      HEIGHT HEIGHT
C      MODT   SHEAR MODULUS
C      MODV   YOUNG'S MODULUS
C      NU     POISSON'S RATIO
C      NUP    CALCULATED POISSON'S RATIO
C      NP     NUMBER OF DATA POINTS FOR A SAMPLE (MAXIMUM 50)
C      NS     NUMBER OF SAMPLES
C      PMI    ROLLED MASS OF INERTIA OF SAMPLE

```

```

      QMD  MASS DENSITY OF SAMPLE
      SIGCT CENTER OF SIG1 - SIG2 MOMENT CIRCLE
      SIG1  MAJOR PRINCIPAL STRESS
      SIG2  INTERMEDIATE PRINCIPAL STRESS
      SIG3  MINOR PRINCIPAL STRESS
      SIG3C CONFINING PRESSURE
      QMD  SYSTEM MASS RATIO
      SPMI  SYSTEM POLAR MASS OF INERTIA
      SPMIR SYSTEM POLAR MASS OF INERTIA RATIO
      STRAT RATIO OF AVG. DGAMI TO DEPSV
      TCM  TOP CAP WEIGHT
      UWT  UNIT WEIGHT OF SAMPLE
      VOL  VOLUME OF SAMPLE
      WT  WEIGHT OF SAMPLE

      DIMENSION COILV(50),ACCEV(50),PROV(50),COILT(50),ACCET(50),FROT(50)
      1)
      REAL MU,MUC,MDDV,MDDT
      200  FORMAT(16)
      201  FORMAT(4F10.4,14)
      202  FORMAT(4F10.4)
      203  FORMAT(1H,////)
      204  FORMAT(10X,TEST RESULTS FOR SAMPLE NO.,11)
      205  FORMAT(////14X,SIG3C WT DIAM HEIGHT NP//
      206  114X,KSC GRAMS CM CM)
      207  FORMAT(//,10X,4F10.2,16)
      208  FORMAT(////14X,TCW ACCEV DCEV ACFT DCFT P
      209  1H,114X,GRAMS)
      210  FORMAT(//,10X,4F10.2)
      211  FORMAT(////14X,VOL UWT SPMI SMR SPMIR//
      212  114X,CC G/CC)
      213  FORMAT(10X,6F10.2)
      214  FORMAT(////14X,COILV ACCEV PROV COILT ACCET F
      215  120T,114X,MV-DD MV-DD HERTZ MV-DD MV-DD HERTZ
      216  2//)
      217  FORMAT(14X,*** WARNING - SIG1 IS NOT MAXIMUM SIG1 ***
      218  200)
      219  FORMAT(////10X,CALCULATED STRESS STATE AND ELASTIC CONSTANTS, ON
      220  1TA SET NO.,13,11X,MDDV DEPSV DAVDV MDDT DGAM
      221  2T DAVDT MUC STRAT,11X,
      222  31PSI PERCENT PERCENT PSI PERCENT PERCENT//)
      223  FORMAT(15X,*** ERROR IN VERTICAL MODULUS CALCULATION ***
      224  200)
      225  FORMAT(15X,*** ERROR IN TORSIONAL MODULUS CALCULATION ***
      226  200)
      227  FORMAT(8X,F10.2,E10.4,2F10.2,E10.4,3F10.4)
      228  FORMAT(8X,F10.2,E10.4,F10.2)
      229  FORMAT(12X,F10.2,E10.4,F10.2)
      230  FORMAT(12X)
      231  1)
      232  FORMAT(//6X,MU SIG1 SIG2 SIG3 BETA FDC1
      233  1 EPS2 EPS3 EATA EPSCC GAYOC,14X,
      234  2,PSI PSI PSI DEGREES PERCENT PERCENT PERCENT
      235  1T DEGREES PERCENT PERCENT//)
      236  FORMAT(12X,FR,3,6F10.2,4F10.4,4F10.2,4F10.4)
      237  1)
      238  READ INPUT DATA
      239  1)
      240  READQ9,NS

```

[illegible]

	IF(J,ST,1000)GOTO14	1727
	J=J+1	1728
	GOTO11	1729
14	CONTINUE	1730
	MODV=0.	1731
	FRQV(1)=0.	1732
	DOINT=0	1733
	GOTO15	1734
17	MODV=((FRQV(1)*HEIGHT/R)**2.)*RWO*.569100	1735
	R=1./(1.-.27*(RV**92))	1736
	DAWV=DCRV*(COILV(1)/ACCEV(1))/R	1737
		1738
	CALCULATE TORSIONAL MODULUS AND DAMPING	1739
		1740
18	J=1	1741
	IF(FRQ(1),EQ,0.)GO=1.	1742
	IF(FRQ(1),EQ,0.)GOTO24	1743
	DEL=.001	1744
	DEL=ROT(PT)	1745
20	CAL=ROT*(R)	1746
	EQ=(CAL-ST)/ST	1747
	IF(ABS(EQ).LT,.001)GOTO16	1748
	IF(FR,ST,0.)GOTO17	1749
	R=R/(1.-DEL)	1750
	DEL=DEL*.2	1751
22	R=R*(1.-DEL)	1752
	IF(J,ST,1000)GOTO18	1753
	J=J+1	1754
	GOTO4	1755
24	CONTINUE	2017
	MODT=0.	2018
	FRQT(1)=0.	2019
	DOINT=0	2020
	GOTO12	2021
26	MODT=((FRQT(1)*HEIGHT/R)**2.)*RWO*.569100	2022
	R=1./(1.-.27*(RT**92))	2023
	DAWPT=DCFT*(COILT(1)/ACCEV(1))/R	2024
28	CONTINUE	2025
	IF(FRQV(1),EQ,0.)RO=1.	2026
	IF(FRQV(1),EQ,0.)GOTO28	2027
	RO=FRQT(1)/FRQV(1)	2028
30	CONTINUE	2029
	SIGPC=SIGPA	2030
	WJ=.10	2031
	IF(FRQT(1),EQ,0.)GOTO40	2032
		2033
	CALCULATE TORSIONAL STRESS	2034
		2035
	STAIT=CCANT*MODT/RO.	2036
	IF(FRQV(1),EQ,0.)GOTO41	2037
		2038
	CALCULATE POISSON'S RATIO AND STRAT	2039
		2040
	MUC=(MODV/(2.*MODT))-1.	2041
	STRAT=CCANT/(10*PSV*2.)	2042
		2043
	PRINT RESULTS	2044

```

PRINT211,MDDV,DEPSV,DAMPV,MDDT,DCAMT,DCAMOT,MDD,STRAT
GOTO22
CONTINUE
40 PRINT212,MDDV,DEPSV,DAMPV
GOTO23
41 CONTINUE
PRINT213,MDDT,DCAMT,DCAMOT
CONTINUE
22 IF(FRQ2(1),EQ,0,INTAUT=0,
PRINT214
C
C CALCULATE SIG1, SIG2, SIG3, AND BETA
C
D020J=1,4
VU=VU+.04
IF(FRQ2(1),EQ,0,GOTO24
DSIGV=(DEPSV*MDDV/87.1)+(2.0**J)*SIG20
LAMB=3.14159/180,
LAMBDA=LAM
SIG1=0,
L=1
20 L=L+1
IF(L,GT,99)GOTO200
IF(L,GT,99)GOTO201
LAMBDA=LAMBDA+LAM
SIGCT=SIG3C+(DSIGV*COS(LAMBDA)/4.)
Y=LAMBDA*90
X=DTAUT*COS(Y)/(DSIGV+COS(LAMBDA)/2.)
BETA=.8*ATAN(X)
SIG1=SIG3C+(DSIGV+COS(LAMBDA)/2.)
SIG1=SIG1+(DTAUT*COS(Y)*TAN(BETA)/2.)
IF(SIG1,GT,SIG1M)GOTO32
GOTO31
20 LAMBDA=LAMBDA
SIG1V=SIG1
GOTO30
21 SIGCT=SIG3C+(DSIGV+COS(LAMBDA)/4.)
Y=LAMBDA*90
X=DTAUT*COS(Y)/(DSIGV+COS(LAMBDA)/2.)
BETA=.8*ATAN(X)*180./3.14159
SIG1=SIG1M
SIG2=SIG3C
SIG3=SIG1-(2.0*(SIG1-SIGCT))
GOTO20
24 CONTINUE
SIG1=SIG3C+(DTAUT/2.)
SIG2=SIG3C
SIG3=SIG3C-(DTAUT/2.)
BETA=45,
BET1=45,
DEPSV=0,
GOTO44
43 CONTINUE
IF(FRQ2(1),EQ,0,GOTO40
GOTO45
43 BET1=0,

```

```

2200
2201
2202
2203
2204
2205
2206
2207
2208
2209
2210
2211
2212
2213
2214
2215
2216
2217
2218
2219
2220
2221
2222
2223
2224
2225
2226
2227
2228
2229
2230
2231
2232
2233
2234
2235
2236
2237
2238
2239
2240
2241
2242
2243
2244
2245
2246
2247
2248
2249
2250
2251
2252
2253
2254
2255
2256
2257
2258
2259
2260
2261
2262
2263
2264
2265
2266
2267
2268
2269
2270
2271
2272
2273
2274
2275
2276
2277
2278
2279
2280
2281
2282
2283
2284
2285
2286
2287
2288
2289
2290
2291
2292
2293
2294
2295
2296
2297
2298
2299
2300
2301
2302
2303
2304
2305
2306
2307
2308
2309
2310
2311
2312
2313
2314
2315
2316
2317
2318
2319
2320
2321
2322
2323
2324
2325
2326
2327
2328
2329
2330
2331
2332
2333
2334
2335
2336
2337
2338
2339
2340
2341
2342
2343
2344
2345
2346
2347
2348
2349
2350
2351
2352
2353
2354
2355
2356
2357
2358
2359
2360
2361
2362
2363
2364
2365
2366
2367
2368
2369
2370
2371
2372
2373
2374
2375
2376
2377
2378
2379
2380
2381
2382
2383
2384
2385
2386
2387
2388
2389
2390
2391
2392
2393
2394
2395
2396
2397
2398
2399
2400
2401
2402
2403
2404
2405
2406
2407
2408
2409
2410
2411
2412
2413
2414
2415
2416
2417
2418
2419
2420
2421
2422
2423
2424
2425
2426
2427
2428
2429
2430
2431
2432
2433
2434
2435
2436
2437
2438
2439
2440
2441
2442
2443
2444
2445
2446
2447
2448
2449
2450
2451
2452
2453
2454
2455
2456
2457
2458
2459
2460
2461
2462
2463
2464
2465
2466
2467
2468
2469
2470
2471
2472
2473
2474
2475
2476
2477
2478
2479
2480
2481
2482
2483
2484
2485
2486
2487
2488
2489
2490
2491
2492
2493
2494
2495
2496
2497
2498
2499
2500
2501
2502
2503
2504
2505
2506
2507
2508
2509
2510
2511
2512
2513
2514
2515
2516
2517
2518
2519
2520
2521
2522
2523
2524
2525
2526
2527
2528
2529
2530
2531
2532
2533
2534
2535
2536
2537
2538
2539
2540
2541
2542
2543
2544
2545
2546
2547
2548
2549
2550
2551
2552
2553
2554
2555
2556
2557
2558
2559
2560
2561
2562
2563
2564
2565
2566
2567
2568
2569
2570
2571
2572
2573
2574
2575
2576
2577
2578
2579
2580
2581
2582
2583
2584
2585
2586
2587
2588
2589
2590
2591
2592
2593
2594
2595
2596
2597
2598
2599
2600
2601
2602
2603
2604
2605
2606
2607
2608
2609
2610
2611
2612
2613
2614
2615
2616
2617
2618
2619
2620
2621
2622
2623
2624
2625
2626
2627
2628
2629
2630
2631
2632
2633
2634
2635
2636
2637
2638
2639
2640
2641
2642
2643
2644
2645
2646
2647
2648
2649
2650
2651
2652
2653
2654
2655
2656
2657
2658
2659
2660
2661
2662
2663
2664
2665
2666
2667
2668
2669
2670
2671
2672
2673
2674
2675
2676
2677
2678
2679
2680
2681
2682
2683
2684
2685
2686
2687
2688
2689
2690
2691
2692
2693
2694
2695
2696
2697
2698
2699
2700
2701
2702
2703
2704
2705
2706
2707
2708
2709
2710
2711
2712
2713
2714
2715
2716
2717
2718
2719
2720
2721
2722
2723
2724
2725
2726
2727
2728
2729
2730
2731
2732
2733
2734
2735
2736
2737
2738
2739
2740
2741
2742
2743
2744
2745
2746
2747
2748
2749
2750
2751
2752
2753
2754
2755
2756
2757
2758
2759
2760
2761
2762
2763
2764
2765
2766
2767
2768
2769
2770
2771
2772
2773
2774
2775
2776
2777
2778
2779
2780
2781
2782
2783
2784
2785
2786
2787
2788
2789
2790
2791
2792
2793
2794
2795
2796
2797
2798
2799
2800
2801
2802
2803
2804
2805
2806
2807
2808
2809
2810
2811
2812
2813
2814
2815
2816
2817
2818
2819
2820
2821
2822
2823
2824
2825
2826
2827
2828
2829
2830
2831
2832
2833
2834
2835
2836
2837
2838
2839
2840
2841
2842
2843
2844
2845
2846
2847
2848
2849
2850
2851
2852
2853
2854
2855
2856
2857
2858
2859
2860
2861
2862
2863
2864
2865
2866
2867
2868
2869
2870
2871
2872
2873
2874
2875
2876
2877
2878
2879
2880
2881
2882
2883
2884
2885
2886
2887
2888
2889
2890
2891
2892
2893
2894
2895
2896
2897
2898
2899
2900
2901
2902
2903
2904
2905
2906
2907
2908
2909
2910
2911
2912
2913
2914
2915
2916
2917
2918
2919
2920
2921
2922
2923
2924
2925
2926
2927
2928
2929
2930
2931
2932
2933
2934
2935
2936
2937
2938
2939
2940
2941
2942
2943
2944
2945
2946
2947
2948
2949
2950
2951
2952
2953
2954
2955
2956
2957
2958
2959
2960
2961
2962
2963
2964
2965
2966
2967
2968
2969
2970
2971
2972
2973
2974
2975
2976
2977
2978
2979
2980
2981
2982
2983
2984
2985
2986
2987
2988
2989
2990
2991
2992
2993
2994
2995
2996
2997
2998
2999
3000

```

```

      DGAMT=0.
      GOT044
      C
      C CALCULATE EPS1, EPS2, EPS3, FATA, EPSOC, AND GAMOC
      C
      42 EPSCT=(1.-MU)*DEPSV/2.
      Z=DGAMT/(4.+(DEPSV-EPSCT))
      FATA=.885TAN(Z)
      44 EPS1=DEPSV+(DGAMT*TAN(FATA)/4.)
      EPS2=-MU*DEPSV
      EPS3=((MU*DEPSV)+(DGAMT*TAN(FATA)/4.))
      EPSOC=(EPS1+EPS2+EPS3)*.333333
      F=((EPS1-EPS2)**2.)*((EPS1-EPS3)**2.)*((EPS2-EPS3)**2.)
      GAMOC=.564457*SQRT(F)
      C
      C PRINT RESULTS
      C
      PRINT311,MU,SIG1,SIG2,SIG3,BETA,EPS1,EPS2,EPS3,FATA,EPSOC,GAMOC
      99 CONTINUE
      97 CONTINUE
      98 CONTINUE
      99 STOP
      END

```

## APPENDIX D2

Program HC--A Program to Reduce Data From the  
Thin-Walled Hollow Cylinder Testing Series

```

PROGRAM HC (INPUT,OUTPUT)
C
C A COMPUTER PROGRAM TO REDUCE DATA FROM THE HOLLOW CYLINDER TESTING
C SERIES.
C
C CODED BY PAT SPIFFIN -- OCTOBER 25, 1970
C
C THIS PROGRAM IS BASED ON CLASSICAL ELASTIC THEORY AND HOOKE'S LAW.
C THE INPUT PARAMETERS INCLUDE THE CONFINING PRESSURE, THE VERTICAL
C AND TORSIONAL STRESS AND STRAIN READINGS, AND THE PHASE LAG BETWEEN
C VERTICAL AND TORSIONAL LOADING. THE PROGRAM CALCULATES THE
C MAGNITUDE AND DIRECTION OF THE PRINCIPAL STRESSES AND INCREMENTAL
C PRINCIPAL STRAINS, THE TANGENT AND SECANT COMPRESSION MODULI, THE
C SHEAR MODULUS, AND THE INCREMENTAL OCTAHEDRAL STRAIN AS A FUNCTION
C OF THE POISSON'S RATIO. WITH THE COMBINED LOADING TESTS THIS
C PROGRAM ALSO CALCULATES AN EFFECTIVE POISSON'S RATIO, THE SHEAR
C STRAIN, AND THE OCTAHEDRAL SHEARING STRAIN.
C
C THE FOLLOWING IS A LISTING OF THE VARIABLE NAMES USED IN THIS
C PROGRAM:
C
C
C ALPHA PHASE DIFFERENCE BETWEEN VERTICAL AND TORSIONAL LOADING
C BETA ANGLE OF REORIENTATION OF THE PRINCIPAL STRESSES
C GAMV CALCULATED SHEAR STRAIN ON VERTICAL PLANE AT MAX DEFSV
C MUVT CALCULATED SHEAR MODULUS - FROM MUVT AND MU
C DEFSV CYCLIC VERTICAL STRAIN
C DTAVT CYCLIC TORSIONAL STRAIN
C DSIGV CYCLIC VERTICAL STRESS
C DTAUT CYCLIC TORSIONAL STRESS
C DATA ANGLE OF REORIENTATION OF THE INCREMENTAL PRINCIPAL STRAINS
C EDCCT CENTER OF THE EPS1 - EPS2 MOHR'S CIRCLE
C EDCNC INCREMENTAL OCTAHEDRAL STRAIN
C EPSV MAXIMUM VERTICAL STRAIN
C EPSVC VERTICAL STRAIN DURING CONSOLIDATION
C EPS1 MAJOR INCREMENTAL PRINCIPAL STRAIN
C EPS2 INTERMEDIATE INCREMENTAL PRINCIPAL STRAIN
C EPS3 MINOR INCREMENTAL PRINCIPAL STRAIN
C GAMOC INCREMENTAL OCTAHEDRAL SHEARING STRAIN
C WEIGHT SAMPLE WEIGHT
C MUOT CALCULATED SHEAR MODULUS
C MUOVS CALCULATED SECANT COMPRESSION MODULUS
C MUOVT CALCULATED TANGENT COMPRESSION MODULUS
C MU POISSON'S RATIO
C MU* CALCULATED POISSON'S RATIO
C NP NUMBER OF DATA POINTS PER SAMPLE (MAXIMUM 40)
C NS NUMBER OF SAMPLES
C SIGCT CENTER OF SIG1 - SIG2 MOHR'S CIRCLE
C SIGV MAXIMUM VERTICAL STRESS
C SIGVC VERTICAL STRESS DURING CONSOLIDATION
C SIG1 MAJOR PRINCIPAL STRESS
C SIG2 INTERMEDIATE PRINCIPAL STRESS
C SIG3 MINOR PRINCIPAL STRESS
C SIGRC CONFINING PRESSURE
C STRAT RATIO OF GAMV TO DEFSV
C T SAMPLE THICKNESS
C UWT SAMPLE UNIT WEIGHT

```

```

C VOL SAMPLE VOLUME
C WT SAMPLE WEIGHT
C
C DIMENSION DSIGV(40),DEPSV(40),DTAUT(40),DCBMT(40),ALPHA(40)
C REAL MU,MUC,MOCVS,MODVT,MODT
60 FORMAT(1X)
100 FORMAT(4F10.4,15)
101 FORMAT(5F10.4)
102 FORMAT(8AH
1
103 FORMAT(14I1////)
200 FORMAT(10X,TEST RESULTS FOR SAMPLE NO.,1,13////14X,15I30 WT
1 HEIGHT T NP/14X,1XKG GRAMS INCHES IN
2CHES//)
201 FORMAT(10X,1STRESS STATE AND ELASTIC CONSTANTS, DATA SET N
10,1,13//)
202 FORMAT(10X,10DSIGV DEPSV DTAUT DCBMT ALPHAI//)
203 FORMAT(8X,4F10.2,5X,13)
204 FORMAT(10X,1VOL HWT/14X,1KG G/CM/10X,DETA,2
1//)
205 FORMAT(10X,5F10.4)
300 FORMAT(3X,2F10.2,2F10.4,2F10.2,2F10.4,2F10.2,2F10.4,2F10.2,2F
10.4)
301 FORMAT(11X,1MU MODVT DEPSV MOCVS EPSV MODT
1 DCBMT MODT MOCMV MUC STRATE/14X,1DSI DEF
2CENT PSI PERCENT DSI PERCENT DSI PERCENT//
3//)
302 FORMAT(11X,1MU SIG1 SIG2 SIG3 BETA EPS1,1
11 EPS2 EPS3 EPS4 DATA EPS500 GAMMA/14X,1DSI
2 PSI PSI DEGREES PERCENT PERCENT PERCENT DEGREE
3 PERCENT PERCENT//)
303 FORMAT(2X,5F10.2,2F10.4,2F10.2,2F10.4)
304 FORMAT(3X,2F10.2,2F10.4,2F10.2,2F10.4,2X,2F10.2)
400 FORMAT(5F10.4)
C
C READ INPUT DATA
C
C READ 00,NS
C D00BL=1,NS
C D00T102
C D00T102
C D00T102
C D00T102
C READ100,SIG30,WT,HEIGHT,T,ND
C PRINT200,L
C PRINT203,SIG30,WT,HEIGHT,T,ND
C
C CALCULATE SYSTEM CONSTANTS
C
C VOL=HEIGHT*T*405.14508
C IF(T.EQ.0.1)VOL=HEIGHT*715.7801
C HWT=WT/VOL
C IF(SIG30.EQ.0.4)EPSVC=.0015
C IF(SIG30.EQ.0.2)EPSVC=.0005
C IF(SIG30.EQ.0.1)EPSVC=.0001
C SIG30C=SIG30*10.0

```

```

1000 STQVC=1,DEFSVC30
1001 DDINT224,MVL,MVT
1002 DDINT220
1003 DDINT1=1,M0
1004 DDINT11,DSISV(1),DEFSV(1),DTAUT(1),DGAMT(1),ALPHA(1)
1005 DDINT224,DSISV(1),DEFSV(1),DTAUT(1),DGAMT(1),ALPHA(1)
1006 ALPHA(1)=ALPHA(1)*.6,DEFSV(1)
1007 DEFSV(1)=DEFSV(1)/(25,DEFTAUT)
1008 DTAUT(1)=DTAUT(1)*.44,DE
1009 DSGAMT(1)=DGAMT(1)*.00667888
1010 GAMT=M0E
1011 DDINT1=1,M0
1012 DDINT 221,1
1013 DDINT221
1014 MVL,10
1015 DDINTJ=1,4
1016 MVL=MVL+.2E
1017
1018
1019
1020
1021
1022
1023
1024
1025
1026
1027
1028
1029
1030
1031
1032
1033
1034
1035
1036
1037
1038
1039
1040
1041
1042
1043
1044
1045
1046
1047
1048
1049
1050
1051
1052
1053
1054
1055
1056
1057
1058
1059
1060
1061
1062
1063
1064
1065
1066
1067
1068
1069
1070
1071
1072
1073
1074
1075
1076
1077
1078
1079
1080
1081
1082
1083
1084
1085
1086
1087
1088
1089
1090
1091
1092
1093
1094
1095
1096
1097
1098
1099
1100
1101
1102
1103
1104
1105
1106
1107
1108
1109
1110
1111
1112
1113
1114
1115
1116
1117
1118
1119
1120
1121
1122
1123
1124
1125
1126
1127
1128
1129
1130
1131
1132
1133
1134
1135
1136
1137
1138
1139
1140
1141
1142
1143
1144
1145
1146
1147
1148
1149
1150
1151
1152
1153
1154
1155
1156
1157
1158
1159
1160
1161
1162
1163
1164
1165
1166
1167
1168
1169
1170
1171
1172
1173
1174
1175
1176
1177
1178
1179
1180
1181
1182
1183
1184
1185
1186
1187
1188
1189
1190
1191
1192
1193
1194
1195
1196
1197
1198
1199
1200
1201
1202
1203
1204
1205
1206
1207
1208
1209
1210
1211
1212
1213
1214
1215
1216
1217
1218
1219
1220
1221
1222
1223
1224
1225
1226
1227
1228
1229
1230
1231
1232
1233
1234
1235
1236
1237
1238
1239
1240
1241
1242
1243
1244
1245
1246
1247
1248
1249
1250
1251
1252
1253
1254
1255
1256
1257
1258
1259
1260
1261
1262
1263
1264
1265
1266
1267
1268
1269
1270
1271
1272
1273
1274
1275
1276
1277
1278
1279
1280
1281
1282
1283
1284
1285
1286
1287
1288
1289
1290
1291
1292
1293
1294
1295
1296
1297
1298
1299
1300
1301
1302
1303
1304
1305
1306
1307
1308
1309
1310
1311
1312
1313
1314
1315
1316
1317
1318
1319
1320
1321
1322
1323
1324
1325
1326
1327
1328
1329
1330
1331
1332
1333
1334
1335
1336
1337
1338
1339
1340
1341
1342
1343
1344
1345
1346
1347
1348
1349
1350
1351
1352
1353
1354
1355
1356
1357
1358
1359
1360
1361
1362
1363
1364
1365
1366
1367
1368
1369
1370
1371
1372
1373
1374
1375
1376
1377
1378
1379
1380
1381
1382
1383
1384
1385
1386
1387
1388
1389
1390
1391
1392
1393
1394
1395
1396
1397
1398
1399
1400
1401
1402
1403
1404
1405
1406
1407
1408
1409
1410
1411
1412
1413
1414
1415
1416
1417
1418
1419
1420
1421
1422
1423
1424
1425
1426
1427
1428
1429
1430
1431
1432
1433
1434
1435
1436
1437
1438
1439
1440
1441
1442
1443
1444
1445
1446
1447
1448
1449
1450
1451
1452
1453
1454
1455
1456
1457
1458
1459
1460
1461
1462
1463
1464
1465
1466
1467
1468
1469
1470
1471
1472
1473
1474
1475
1476
1477
1478
1479
1480
1481
1482
1483
1484
1485
1486
1487
1488
1489
1490
1491
1492
1493
1494
1495
1496
1497
1498
1499
1500
1501
1502
1503
1504
1505
1506
1507
1508
1509
1510
1511
1512
1513
1514
1515
1516
1517
1518
1519
1520
1521
1522
1523
1524
1525
1526
1527
1528
1529
1530
1531
1532
1533
1534
1535
1536
1537
1538
1539
1540
1541
1542
1543
1544
1545
1546
1547
1548
1549
1550
1551
1552
1553
1554
1555
1556
1557
1558
1559
1560
1561
1562
1563
1564
1565
1566
1567
1568
1569
1570
1571
1572
1573
1574
1575
1576
1577
1578
1579
1580
1581
1582
1583
1584
1585
1586
1587
1588
1589
1590
1591
1592
1593
1594
1595
1596
1597
1598
1599
1600
1601
1602
1603
1604
1605
1606
1607
1608
1609
1610
1611
1612
1613
1614
1615
1616
1617
1618
1619
1620
1621
1622
1623
1624
1625
1626
1627
1628
1629
1630
1631
1632
1633
1634
1635
1636
1637
1638
1639
1640
1641
1642
1643
1644
1645
1646
1647
1648
1649
1650
1651
1652
1653
1654
1655
1656
1657
1658
1659
1660
1661
1662
1663
1664
1665
1666
1667
1668
1669
1670
1671
1672
1673
1674
1675
1676
1677
1678
1679
1680
1681
1682
1683
1684
1685
1686
1687
1688
1689
1690
1691
1692
1693
1694
1695
1696
1697
1698
1699
1700
1701
1702
1703
1704
1705
1706
1707
1708
1709
1710
1711
1712
1713
1714
1715
1716
1717
1718
1719
1720
1721
1722
1723
1724
1725
1726
1727
1728
1729
1730
1731
1732
1733
1734
1735
1736
1737
1738
1739
1740
1741
1742
1743
1744
1745
1746
1747
1748
1749
1750
1751
1752
1753
1754
1755
1756
1757
1758
1759
1760
1761
1762
1763
1764
1765
1766
1767
1768
1769
1770
1771
1772
1773
1774
```

```

C      SIGIM=0.
C      CALCULATE SIGCT, BETA, AND SIGI
C      DOACK=1.0
C      LAMBDA=LAMBDA+LAMBDA
C      SIGCT=SIGCT+((1.0+VU)/4.0)*DSIGV(I)*COS(LAMBDA)
C      V=LAMBDA-ALPHA(I)
C      X=(DTAUT(I)*COS(V))/(3.7*SIGCT+DSIGV(I)*COS(LAMBDA))-(2.0*SIGCT)
C      BETA=(.5*ATAN(X))
C      SIGI=(1.0+DSIGCT+((DSIGV(I)*COS(LAMBDA))/2.0
C      SIGI=SIGI+((DTAUT(I)*COS(V)*TAN(BETA))/2.0)
C      CALCULATE MAXIMUM SIGI
C      IF(SIGI.GT.SIGIM)LAMBDA=LAMBDA
C      IF(SIGI.GT.SIGIM) SIGIM=SIGI
C      CONTINUE
C      CALCULATE MAXIMUM PRINCIPAL STRESSES AND BETA
C      SIGCT=SIGCT+((1.0+VU)/4.0)*DSIGV(I)*COS(LAMBDA)
C      V=LAMBDA-ALPHA(I)
C      X=(DTAUT(I)*COS(V))/(3.7*SIGCT+DSIGV(I)*COS(LAMBDA))-(2.0*SIGCT)
C      BETA=(.5*ATAN(X))
C      SIGI=SIGIM
C      SIG2=SIGI-(2.0*(SIGI-SIGCT))
C      IF(SIG2.GE.SIGCT)GOTO3
C      SIG2=SIGCT
C      SIG2=SIGCT
C      GOTO3
C      SIGI=SIGCT
C      CONTINUE
C      CALCULATE MAXIMUM INCREMENTAL PRINCIPAL STRAINS AND FATS
C      MODVT=(1.0-(MU*VU))*DSIGV(I)/DEDEV(I)
C      MODVT=MODVT/(2.0*(1.0+VU))
C      LAMBDA=LAMBDA+LAMBDA
C      LAMBDA=LAMBDA
C      V=LAMBDA-ALPHA(I)
C      CG=DTAUT(I)*COS(V)/MODVT
C      Z=CG/DEDEV(I)
C      FATA=(.5*ATAN(Z))
C      FDS1=(DEDEV(I)/2.0)*(CG*TAN(FATA)/4.0)
C      FDS2=CG*TAN(FATA)/4.0
C      FDS3=((MU*(MU*VU))/(1.0-(MU*VU))*DEDEV(I)/2.0
C      IF(FDS1.LT.FDS2)GOTO4
C      FDS1=FDS2
C      FDS2=FDS3
C      FDS3=FDS3
C      CONTINUE

```

```

      EDCNCL=(EDC1+EDC2+EDC3)*.33,3333
      E2=(EDC1-EDC3)*.07,1+((EDC1-EDC3)*.07,1+((EDC2-EDC3)*.07,1
      IF(F,DT,FH)GOTO45
      CONTINUE
41      LAMM=LSD
      E4=EAT2
      E1=EDC1
      E2=EDC2
      E3=EDC3
      E4=EDC4
      E5=EDC5
      E6=EDC6
      E7=E
      CONTINUE
      E2=E4+E1*100./3,34187
      EDC1=E1*100.
      EDC2=E2*100.
      EDC3=E3*100.
      EDC4=E4
      E5=E5*100
      E5=E5*66.6667*SQRT(FH)
      *
      *
      *
      PRINT DOIN[DOAL,CTDESSCS AND STOREING
      *
      *
      PRINTA33,'U,SIC],SIC2,SIC3,RET4,EDS1,EDS2,EDS3,FAT4,EDSC6,CAMOC
42      CONTINUE
43      CONTINUE
44      CONTINUE
      CT=0
      END

```

## EARTHQUAKE ENGINEERING RESEARCH CENTER REPORTS

NOTE: Numbers in parenthesis are Accession Numbers assigned by the National Technical Information Service; these are followed by a price code. Copies of the reports may be ordered from the National Technical Information Service, 5285 Port Royal Road, Springfield, Virginia, 22161. Accession Numbers should be quoted on orders for reports (PB --- ---) and remittance must accompany each order. Reports without this information were not available at time of printing. Upon request, EERC will mail inquirers this information when it becomes available.

- EERC 67-1 "Feasibility Study Large-Scale Earthquake Simulator Facility," by J. Penzien, J.G. Bouwkamp, R.W. Clough and D. Rea - 1967 (PB 187 905)A07
- EERC 68-1 Unassigned
- EERC 68-2 "Inelastic Behavior of Beam-to-Column Subassemblages Under Repeated Loading," by V.V. Bertero - 1968 (PB 184 888)A05
- EERC 68-3 "A Graphical Method for Solving the Wave Reflection-Refraction Problem," by H.D. McNiven and Y. Menqi - 1968 (PB 187 943)A03
- EERC 68-4 "Dynamic Properties of McKinley School Buildings," by D. Rea, J.G. Bouwkamp and R.W. Clough - 1968 (PB 187 902)A07
- EERC 68-5 "Characteristics of Rock Motions During Earthquakes," by H.B. Seed, I.M. Idriss and F.W. Kiefer - 1968 (PB 188 338)A03
- EERC 69-1 "Earthquake Engineering Research at Berkeley," - 1969 (PB 187 906)A11
- EERC 69-2 "Nonlinear Seismic Response of Earth Structures," by M. Dibaj and J. Penzien - 1969 (PB 187 904)A08
- EERC 69-3 "Probabilistic Study of the Behavior of Structures During Earthquakes," by R. Ruiz and J. Penzien - 1969 (PB 187 886)A06
- EERC 69-4 "Numerical Solution of Boundary Value Problems in Structural Mechanics by Reduction to an Initial Value Formulation," by N. Distefano and J. Schujman - 1969 (PB 187 942)A02
- EERC 69-5 "Dynamic Programming and the Solution of the Biharmonic Equation," by N. Distefano - 1969 (PB 187 941)A03
- EERC 69-6 "Stochastic Analysis of Offshore Tower Structures," by A.K. Malhotra and J. Penzien - 1969 (PB 187 903)A09
- EERC 69-7 "Rock Motion Accelerograms for High Magnitude Earthquakes," by H.B. Seed and I.M. Idriss - 1969 (PB 187 940)A02
- EERC 69-8 "Structural Dynamics Testing Facilities at the University of California, Berkeley," by R.M. Stephen, J.G. Bouwkamp, R.W. Clough and J. Penzien - 1969 (PB 189 111)A04
- EERC 69-9 "Seismic Response of Soil Deposits Underlain by Sloping Rock Boundaries," by H. Dezfulian and H.B. Seed - 1969 (PB 189 114)A03
- EERC 69-10 "Dynamic Stress Analysis of Axisymmetric Structures Under Arbitrary Loading," by S. Ghosh and E.L. Wilson - 1969 (PB 189 026)A10
- EERC 69-11 "Seismic Behavior of Multistory Frames Designed by Different Philosophies," by J.C. Anderson and V. V. Bertero - 1969 (PB 190 662)A10
- EERC 69-12 "Stiffness Degradation of Reinforcing Concrete Members Subjected to Cyclic Flexural Moments," by V.V. Bertero, B. Bresler and H. Ming Liao - 1969 (PB 202 942)A07
- EERC 69-13 "Response of Non-Uniform Soil Deposits to Travelling Seismic Waves," by H. Dezfulian and H.B. Seed - 1969 (PB 191 023)A03
- EERC 69-14 "Damping Capacity of a Model Steel Structure," by D. Rea, R.W. Clough and J.G. Bouwkamp - 1969 (PB 190 663)A06
- EERC 69-15 "Influence of Local Soil Conditions on Building Damage Potential during Earthquakes," by H.B. Seed and I.M. Idriss - 1969 (PB 191 036)A03
- EERC 69-16 "The Behavior of Sands Under Seismic Loading Conditions," by M.L. Silver and H.B. Seed - 1969 (AD 714 982)A07
- EERC 70-1 "Earthquake Response of Gravity Dams," by A.K. Chopra - 1970 (AD 709 640)A03
- EERC 70-2 "Relationships between Soil Conditions and Building Damage in the Caracas Earthquake of July 29, 1967," by H.B. Seed, I.M. Idriss and H. Dezfulian - 1970 (PB 195 762)A05
- EERC 70-3 "Cyclic Loading of Full Size Steel Connections," by E.P. Popov and R.M. Stephen - 1970 (PB 213 545)A04
- EERC 70-4 "Seismic Analysis of the Charaima Building, Caraballeda, Venezuela," by Subcommittee of the SEAONC Research Committee: V.V. Bertero, P.F. Fratessa, S.A. Mahin, J.H. Sexton, A.C. Scordelis, E.L. Wilson, L.A. Wyllie, H.B. Seed and J. Penzien, Chairman - 1970 (PB 201 455)A06

- EERC 70-5 "A Computer Program for Earthquake Analysis of Dams," by A.K. Chopra and P. Chakrabarti - 1970 (AD 723 994)A05
- EERC 70-6 "The Propagation of Love Waves Across Non-Horizontally Layered Structures," by J. Lysmer and L.A. Drake 1970 (PB 197 896)A03
- EERC 70-7 "Influence of Base Rock Characteristics on Ground Response," by J. Lysmer, H.B. Seed and P.B. Schnabel 1970 (PB 197 897)A03
- EERC 70-8 "Applicability of Laboratory Test Procedures for Measuring Soil Liquefaction Characteristics under Cyclic Loading," by H.B. Seed and W.H. Peacock - 1970 (PB 198 016)A03
- EERC 70-9 "A Simplified Procedure for Evaluating Soil Liquefaction Potential," by H.B. Seed and I.M. Idriss - 1970 (PB 198 009)A03
- EERC 70-10 "Soil Moduli and Damping Factors for Dynamic Response Analysis," by H.B. Seed and I.M. Idriss - 1970 (PB 197 869)A03
- EERC 71-1 "Koyna Earthquake of December 11, 1967 and the Performance of Koyna Dam," by A.K. Chopra and P. Chakrabarti 1971 (AD 731 496)A06
- EERC 71-2 "Preliminary In-Situ Measurements of Anelastic Absorption in Soils Using a Prototype Earthquake Simulator," by R.D. Borcherdt and P.W. Rodgers - 1971 (PB 201 454)A03
- EERC 71-3 "Static and Dynamic Analysis of Inelastic Frame Structures," by F.L. Porter and G.H. Powell - 1971 (PB 210 135)A06
- EERC 71-4 "Research Needs in Limit Design of Reinforced Concrete Structures," by V.V. Bertero - 1971 (PB 202 943)A04
- EERC 71-5 "Dynamic Behavior of a High-Rise Diagonally Braced Steel Building," by D. Rea, A.A. Shah and J.G. Bouwhuis 1971 (PB 203 584)A06
- EERC 71-6 "Dynamic Stress Analysis of Porous Elastic Solids Saturated with Compressible Fluids," by J. Ghaboussi and E. L. Wilson - 1971 (PB 211 396)A06
- EERC 71-7 "Inelastic Behavior of Steel Beam-to-Column Subassemblages," by H. Krawinkler, V.V. Bertero and E.P. Popov 1971 (PB 211 335)A14
- EERC 71-8 "Modification of Seismograph Records for Effects of Local Soil Conditions," by P. Schnabel, H.B. Seed and J. Lysmer - 1971 (PB 214 450)A03
- EERC 72-1 "Static and Earthquake Analysis of Three Dimensional Frame and Shear Wall Buildings," by E.L. Wilson and H.H. Dovey - 1972 (PB 212 904)A05
- EERC 72-2 "Accelerations in Rock for Earthquakes in the Western United States," by P.B. Schnabel and H.B. Seed - 1972 (PB 213 100)A03
- EERC 72-3 "Elastic-Plastic Earthquake Response of Soil-Building Systems," by T. Minami - 1972 (PB 214 868)A08
- EERC 72-4 "Stochastic Inelastic Response of Offshore Towers to Strong Motion Earthquakes," by M.K. Kaul - 1972 (PB 215 713)A05
- EERC 72-5 "Cyclic Behavior of Three Reinforced Concrete Flexural Members with High Shear," by E.P. Popov, V.V. Bertero and H. Krawinkler - 1972 (PB 214 555)A05
- EERC 72-6 "Earthquake Response of Gravity Dams Including Reservoir Interaction Effects," by P. Chakrabarti and A.K. Chopra - 1972 (AD 762 330)A08
- EERC 72-7 "Dynamic Properties of Pine Flat Dam," by D. Rea, C.Y. Liaw and A.K. Chopra - 1972 (AD 763 928)A05
- EERC 72-8 "Three Dimensional Analysis of Building Systems," by E.L. Wilson and H.H. Dovey - 1972 (PB 222 438)A06
- EERC 72-9 "Rate of Loading Effects on Uncracked and Repaired Reinforced Concrete Members," by S. Mahin, V.V. Bertero, D. Rea and M. Atalay - 1972 (PB 224 520)A08
- EERC 72-10 "Computer Program for Static and Dynamic Analysis of Linear Structural Systems," by E.L. Wilson, K.-J. Bathe, J.E. Peterson and H.H. Dovey - 1972 (PB 220 437)A04
- EERC 72-11 "Literature Survey - Seismic Effects on Highway Bridges," by T. Iwasaki, J. Penzien and R.W. Clough - 1972 (PB 215 613)A19
- EERC 72-12 "SHAKE-A Computer Program for Earthquake Response Analysis of Horizontally Layered Sites," by P.B. Schnabel and J. Lysmer - 1972 (PB 220 207)A06
- EERC 73-1 "Optimal Seismic Design of Multistory Frames," by V.V. Bertero and H. Kamil - 1973
- EERC 73-2 "Analysis of the Slides in the San Fernando Dams During the Earthquake of February 9, 1971," by H.B. Seed, K.L. Lee, I.M. Idriss and F. Makdisi - 1973 (PB 223 402)A14

- EERC 73-3 "Computer Aided Ultimate Load Design of Unbraced Multistory Steel Frames," by M.B. El-Hafez and G.H. Powell 1973 (PB 248 315)A09
- EERC 73-4 "Experimental Investigation into the Seismic Behavior of Critical Regions of Reinforced Concrete Components as Influenced by Moment and Shear," by M. Celebi and J. Penzien - 1973 (PB 215 884)A09
- EERC 73-5 "Hysteretic Behavior of Epoxy-Repaired Reinforced Concrete Beams," by M. Celebi and J. Penzien - 1973 (PB 239 568)A03
- EERC 73-6 "General Purpose Computer Program for Inelastic Dynamic Response of Plane Structures," by A. Kanaan and G.H. Powell - 1973 (PB 221 260)A08
- EERC 73-7 "A Computer Program for Earthquake Analysis of Gravity Dams Including Reservoir Interaction," by P. Chakrabarti and A.K. Chopra - 1973 (AD 766 271)A04
- EERC 73-8 "Behavior of Reinforced Concrete Deep Beam-Column Subassemblages Under Cyclic Loads," by O. Küstü and J.G. Bouwkamp - 1973 (PB 246 117)A12
- EERC 73-9 "Earthquake Analysis of Structure-Foundation Systems," by A.K. Vaish and A.K. Chopra - 1973 (AD 766 272)A07
- EERC 73-10 "Deconvolution of Seismic Response for Linear Systems," by R.B. Reimer - 1973 (PB 227 179)A08
- EERC 73-11 "SAP IV: A Structural Analysis Program for Static and Dynamic Response of Linear Systems," by K.-J. Bathe, E.L. Wilson and F.E. Peterson - 1973 (PB 221 967)A09
- EERC 73-12 "Analytical Investigations of the Seismic Response of Long, Multiple Span Highway Bridges," by W.S. Tseng and J. Penzien - 1973 (PB 227 816)A10
- EERC 73-13 "Earthquake Analysis of Multi-Story Buildings Including Foundation Interaction," by A.K. Chopra and J.A. Gutierrez - 1973 (PB 222 970)A03
- EERC 73-14 "ADAP: A Computer Program for Static and Dynamic Analysis of Arch Dams," by R.W. Clough, J.M. Raphael and S. Mojtahedi - 1973 (PB 223 763)A09
- EERC 73-15 "Cyclic Plastic Analysis of Structural Steel Joints," by R.B. Pinkney and R.W. Clough - 1973 (PB 226 843)A08
- EERC 73-16 "QUAD-4: A Computer Program for Evaluating the Seismic Response of Soil Structures by Variable Damping Finite Element Procedures," by I.M. Idriss, J. Lysmer, R. Hwang and H.B. Seed - 1973 (PB 229 424)A05
- EERC 73-17 "Dynamic Behavior of a Multi-Story Pyramid Shaped Building," by R.M. Stephen, J.P. Hollings and J.G. Bouwkamp - 1973 (PB 240 718)A06
- EERC 73-18 "Effect of Different Types of Reinforcing on Seismic Behavior of Short Concrete Columns," by V.V. Bertero, J. Hollings, O. Küstü, R.M. Stephen and J.G. Bouwkamp - 1973
- EERC 73-19 "Olive View Medical Center Materials Studies, Phase I," by B. Bresler and V.V. Bertero - 1973 (PB 235 986)A06
- EERC 73-20 "Linear and Nonlinear Seismic Analysis Computer Programs for Long Multiple-Span Highway Bridges," by W.S. Tseng and J. Penzien - 1973
- EERC 73-21 "Constitutive Models for Cyclic Plastic Deformation of Engineering Materials," by J.M. Kelly and P.P. Gillis 1973 (PB 226 024)A03
- EERC 73-22 "DRAIN - 2D User's Guide," by G.H. Powell - 1973 (PB 227 016)A05
- EERC 73-23 "Earthquake Engineering at Berkeley - 1973," (PB 226 033)A11
- EERC 73-24 Unassigned
- EERC 73-25 "Earthquake Response of Axisymmetric Tower Structures Surrounded by Water," by C.Y. Liaw and A.K. Chopra 1973 (AD 773 052)A09
- EERC 73-26 "Investigation of the Failures of the Olive View Stairtowers During the San Fernando Earthquake and Their Implications on Seismic Design," by V.V. Bertero and R.G. Collins - 1973 (PB 235 106)A13
- EERC 73-27 "Further Studies on Seismic Behavior of Steel Beam-Column Subassemblages," by V.V. Bertero, H. Krawinkler and E.P. Popov - 1973 (PB 234 172)A06
- EERC 74-1 "Seismic Risk Analysis," by C.S. Oliveira - 1974 (PB 235 920)A06
- EERC 74-2 "Settlement and Liquefaction of Sands Under Multi-Directional Shaking," by R. Pyke, C.K. Chan and H.B. Seed 1974
- EERC 74-3 "Optimum Design of Earthquake Resistant Shear Buildings," by D. Ray, K.S. Pister and A.K. Chopra - 1974 (PB 231 172)A06
- EERC 74-4 "LUSH - A Computer Program for Complex Response Analysis of Soil-Structure Systems," by J. Lysmer, T. Udaka, H.B. Seed and R. Hwang - 1974 (PB 236 796)A05

- EERC 74-5 "Sensitivity Analysis for Hysteretic Dynamic Systems: Applications to Earthquake Engineering," by D. Ray 1974 (PB 233 213)A06
- EERC 74-6 "Soil Structure Interaction Analyses for Evaluating Seismic Response," by H.B. Seed, J. Lysmer and R. Hwang 1974 (PB 236 519)A04
- EERC 74-7 Unassigned
- EERC 74-8 "Shaking Table Tests of a Steel Frame - A Progress Report," by R.W. Clough and D. Tang - 1974 (PB 240 869)A03
- EERC 74-9 "Hysteretic Behavior of Reinforced Concrete Flexural Members with Special Web Reinforcement," by V.V. Bertero, E.P. Popov and T.Y. Wang - 1974 (PB 236 797)A07
- EERC 74-10 "Applications of Reliability-Based, Global Cost Optimization to Design of Earthquake Resistant Structures," by E. Vitiello and K.S. Pister - 1974 (PB 237 231)A06
- EERC 74-11 "Liquefaction of Gravelly Soils Under Cyclic Loading Conditions," by R.T. Wong, H.B. Seed and C.K. Chan 1974 (PB 242 042)A03
- EERC 74-12 "Site-Dependent Spectra for Earthquake-Resistant Design," by H.B. Seed, C. Ugas and J. Lysmer - 1974 (PB 240 953)A03
- EERC 74-13 "Earthquake Simulator Study of a Reinforced Concrete Frame," by P. Hidalgo and R.W. Clough - 1974 (PB 241 944)A13
- EERC 74-14 "Nonlinear Earthquake Response of Concrete Gravity Dams," by N. Pal - 1974 (AD/A 006 583)A06
- EERC 74-15 "Modeling and Identification in Nonlinear Structural Dynamics - I. One Degree of Freedom Models," by N. Distefano and A. Rath - 1974 (PB 241 548)A06
- EERC 75-1 "Determination of Seismic Design Criteria for the Dumbarton Bridge Replacement Structure, Vol. I: Description, Theory and Analytical Modeling of Bridge and Parameters," by F. Baron and S.-H. Pang - 1975 (PB 259 407)A15
- EERC 75-2 "Determination of Seismic Design Criteria for the Dumbarton Bridge Replacement Structure, Vol. II: Numerical Studies and Establishment of Seismic Design Criteria," by F. Baron and S.-H. Pang - 1975 (PB 259 408)A11 (For set of EERC 75-1 and 75-2 (PB 259 406))
- EERC 75-3 "Seismic Risk Analysis for a Site and a Metropolitan Area," by C.S. Oliveira - 1975 (PB 248 134)A09
- EERC 75-4 "Analytical Investigations of Seismic Response of Short, Single or Multiple-Span Highway Bridges," by M.-C. Chen and J. Penzien - 1975 (PB 241 454)A09
- EERC 75-5 "An Evaluation of Some Methods for Predicting Seismic Behavior of Reinforced Concrete Buildings," by S.A. Mahin and V.V. Bertero - 1975 (PB 246 306)A16
- EERC 75-6 "Earthquake Simulator Study of a Steel Frame Structure, Vol. I: Experimental Results," by R.W. Clough and D.T. Tang - 1975 (PB 243 981)A13
- EERC 75-7 "Dynamic Properties of San Bernardino Intake Tower," by D. Rea, C.-Y. Liaw and A.K. Chopra - 1975 (AD/A008 406) A05
- EERC 75-8 "Seismic Studies of the Articulation for the Dumbarton Bridge Replacement Structure, Vol. I: Description, Theory and Analytical Modeling of Bridge Components," by F. Baron and R.E. Hamati - 1975 (PB 251 539)A07
- EERC 75-9 "Seismic Studies of the Articulation for the Dumbarton Bridge Replacement Structure, Vol. 2: Numerical Studies of Steel and Concrete Girder Alternates," by F. Baron and R.E. Hamati - 1975 (PB 251 540)A10
- EERC 75-10 "Static and Dynamic Analysis of Nonlinear Structures," by D.P. Mondkar and G.H. Powell - 1975 (PB 242 434)A08
- EERC 75-11 "Hysteretic Behavior of Steel Columns," by E.P. Popov, V.V. Bertero and S. Chandramouli - 1975 (PB 252 365)A11
- EERC 75-12 "Earthquake Engineering Research Center Library Printed Catalog," - 1975 (PB 243 711)A26
- EERC 75-13 "Three Dimensional Analysis of Building Systems (Extended Version)," by E.L. Wilson, J.P. Hollings and H.H. Dovey - 1975 (PB 243 989)A07
- EERC 75-14 "Determination of Soil Liquefaction Characteristics by Large-Scale Laboratory Tests," by P. De Alba, C.K. Chan and H.B. Seed - 1975 (NUREG 0027)A08
- EERC 75-15 "A Literature Survey - Compressive, Tensile, Bond and Shear Strength of Masonry," by R.L. Mayes and R.W. Clough - 1975 (PB 246 292)A10
- EERC 75-16 "Hysteretic Behavior of Ductile Moment Resisting Reinforced Concrete Frame Components," by V.V. Bertero and E.P. Popov - 1975 (PB 246 388)A05
- EERC 75-17 "Relationships Between Maximum Acceleration, Maximum Velocity, Distance from Source, Local Site Conditions for Moderately Strong Earthquakes," by H.B. Seed, R. Murarka, J. Lysmer and I.M. Idriss - 1975 (PB 248 172)A01
- EERC 75-18 "The Effects of Method of Sample Preparation on the Cyclic Stress-Strain Behavior of Sands," by J. Mulilis, C.K. Chan and H.B. Seed - 1975 (Summarized in EERC 75-28)

- EERC 75-19 "The Seismic Behavior of Critical Regions of Reinforced Concrete Components as Influenced by Moment, Shear and Axial Force," by M.B. Atalay and J. Penzien - 1975 (PB 258 842)A11
- EERC 75-20 "Dynamic Properties of an Eleven Story Masonry Building," by R.M. Stephen, J.P. Hollings, J.G. Bouwkamp and D. Jurukovski - 1975 (PB 246 945)A04
- EERC 75-21 "State-of-the-Art in Seismic Strength of Masonry - An Evaluation and Review," by R.L. Mayes and R.W. Clough - 1975 (PB 249 040)A07
- EERC 75-22 "Frequency Dependent Stiffness Matrices for Viscoelastic Half-Plane Foundations," by A.K. Chopra, P. Chakrabarti and G. Dasgupta - 1975 (PB 248 121)A07
- EERC 75-23 "Hysteretic Behavior of Reinforced Concrete Framed Walls," by T.Y. Wong, V.V. Bertero and E.P. Popov - 1975
- EERC 75-24 "Testing Facility for Subassemblages of Frame-Wall Structural Systems," by V.V. Bertero, E.P. Popov and T. Endo - 1975
- EERC 75-25 "Influence of Seismic History on the Liquefaction Characteristics of Sands," by H.B. Seed, K. Mori and C.K. Chan - 1975 (Summarized in EERC 75-28)
- EERC 75-26 "The Generation and Dissipation of Pore Water Pressures during Soil Liquefaction," by H.B. Seed, P.P. Martin and J. Lysmer - 1975 (PB 252 648)A03
- EERC 75-27 "Identification of Research Needs for Improving Aseismic Design of Building Structures," by V.V. Bertero - 1975 (PB 248 136)A05
- EERC 75-28 "Evaluation of Soil Liquefaction Potential during Earthquakes," by H.B. Seed, I. Arango and C.K. Chan - 1975 (NUREG 0026)A13
- EERC 75-29 "Representation of Irregular Stress Time Histories by Equivalent Uniform Stress Series in Liquefaction Analyses," by H.B. Seed, I.M. Idriss, F. Makdisi and N. Banerjee - 1975 (PB 252 635)A03
- EERC 75-30 "FLUSH - A Computer Program for Approximate 3-D Analysis of Soil-Structure Interaction Problems," by J. Lysmer, T. Udaka, C.-F. Tsai and H.B. Seed - 1975 (PB 259 332)A07
- EERC 75-31 "ALUSH - A Computer Program for Seismic Response Analysis of Axisymmetric Soil-Structure Systems," by E. Berger, J. Lysmer and H.B. Seed - 1975
- EERC 75-32 "TRIP and TRAVEL - Computer Programs for Soil-Structure Interaction Analysis with Horizontally Travelling Waves," by T. Udaka, J. Lysmer and H.B. Seed - 1975
- EERC 75-33 "Predicting the Performance of Structures in Regions of High Seismicity," by J. Penzien - 1975 (PB 248 130)A03
- EERC 75-34 "Efficient Finite Element Analysis of Seismic Structure - Soil - Direction," by J. Lysmer, H.B. Seed, T. Udaka, R.N. Hwang and C.-F. Tsai - 1975 (PB 253 570)A03
- EERC 75-35 "The Dynamic Behavior of a First Story Girder of a Three-Story Steel Frame Subjected to Earthquake Loading," by R.W. Clough and L.-Y. Li - 1975 (PB 248 841)A05
- EERC 75-36 "Earthquake Simulator Study of a Steel Frame Structure, Volume II - Analytical Results," by D.T. Tang - 1975 (PB 252 926)A10
- EERC 75-37 "ANSER-I General Purpose Computer Program for Analysis of Non-Linear Structural Response," by D.P. Mondkar and G.H. Powell - 1975 (PB 252 386)A08
- EERC 75-38 "Nonlinear Response Spectra for Probabilistic Seismic Design and Damage Assessment of Reinforced Concrete Structures," by M. Murakami and J. Penzien - 1975 (PB 259 530)A05
- EERC 75-39 "Study of a Method of Feasible Directions for Optimal Elastic Design of Frame Structures Subjected to Earthquake Loading," by N.D. Walker and K.S. Pister - 1975 (PB 257 781)A06
- EERC 75-40 "An Alternative Representation of the Elastic-Viscoelastic Analogy," by G. Dasgupta and J.L. Sackman - 1975 (PB 252 173)A03
- EERC 75-41 "Effect of Multi-Directional Shaking on Liquefaction of Sands," by H.B. Seed, R. Pyke and G.R. Martin - 1975 (PB 258 781)A03
- EERC 76-1 "Strength and Ductility Evaluation of Existing Low-Rise Reinforced Concrete Buildings - Screening Method," by T. Okada and B. Bresler - 1976 (PB 257 906)A11
- EERC 76-2 "Experimental and Analytical Studies on the Hysteretic Behavior of Reinforced Concrete Rectangular and T-Beams," by S.-Y.M. Ma, E.P. Popov and V.V. Bertero - 1976 (PB 260 843)A12
- EERC 76-3 "Dynamic Behavior of a Multistory Triangular-Shaped Building," by J. Petrovski, R.M. Stephen, E. Gartenbaum and J.G. Bouwkamp - 1976 (PB 273 279)A07
- EERC 76-4 "Earthquake Induced Deformations of Earth Dams," by N. Serff, H.B. Seed, F.I. Makdisi & C.-Y. Chang - 1976 (PB 292 065)A08

- EERC 76-5 "Analysis and Design of Tube-Type Tall Building Structures," by H. de Clercq and G.H. Powell - 1976 (PB 252 220) A10
- EERC 76-6 "Time and Frequency Domain Analysis of Three-Dimensional Ground Motions, San Fernando Earthquake," by T. Kudo and J. Penzien (PB 260 556)A11
- EERC 76-7 "Expected Performance of Uniform Building Code Design Masonry Structures," by R.L. Mayes, Y. Omote, S.W. Chen and R.W. Clough - 1976 (PB 270 098)A05
- EERC 76-8 "Cyclic Shear Tests of Masonry Piers, Volume 1 - Test Results," by R.L. Mayes, Y. Omote, R.W. Clough - 1976 (PB 264 424)A06
- EERC 76-9 "A Substructure Method for Earthquake Analysis of Structure - Soil Interaction," by J.A. Gutierrez and A.K. Chopra - 1976 (PB 257 783)A08
- EERC 76-10 "Stabilization of Potentially Liquefiable Sand Deposits using Gravel Drain Systems," by H.B. Seed and J.R. Booker - 1976 (PB 258 820)A04
- EERC 76-11 "Influence of Design and Analysis Assumptions on Computed Inelastic Response of Moderately Tall Frames," by G.H. Powell and D.G. Row - 1976 (PB 271 409)A06
- EERC 76-12 "Sensitivity Analysis for Hysteretic Dynamic Systems: Theory and Applications," by D. Ray, K.S. Pister and E. Polak - 1976 (PB 262 859)A04
- EERC 76-13 "Coupled Lateral Torsional Response of Buildings to Ground Shaking," by C.L. Kan and A.K. Chopra - 1976 (PB 257 907)A09
- EERC 76-14 "Seismic Analyses of the Banco de America," by V.V. Bertero, S.A. Mahin and J.A. Hollings - 1976
- EERC 76-15 "Reinforced Concrete Frame 2: Seismic Testing and Analytical Correlation," by R.W. Clough and J. Gidwani - 1976 (PB 261 323)A08
- EERC 76-16 "Cyclic Shear Tests of Masonry Piers, Volume 2 - Analysis of Test Results," by R.L. Mayes, Y. Omote and R.W. Clough - 1976
- EERC 76-17 "Structural Steel Bracing Systems: Behavior Under Cyclic Loading," by E.P. Popov, K. Takanashi and C.W. Roeder - 1976 (PB 260 715)A05
- EERC 76-18 "Experimental Model Studies on Seismic Response of High Curved Overcrossings," by D. Williams and W.G. Godden - 1976 (PB 269 548)A08
- EERC 76-19 "Effects of Non-Uniform Seismic Disturbances on the Dumbarton Bridge Replacement Structure," by F. Baron and R.E. Hamati - 1976 (PB 282 981)A16
- EERC 76-20 "Investigation of the Inelastic Characteristics of a Single Story Steel Structure Using System Identification and Shaking Table Experiments," by V.C. Matzen and H.D. McNiven - 1976 (PB 258 453)A07
- EERC 76-21 "Capacity of Columns with Splice Imperfections," by E.P. Popov, R.M. Stephen and R. Philbrick - 1976 (PB 260 378)A04
- EERC 76-22 "Response of the Olive View Hospital Main Building during the San Fernando Earthquake," by S. A. Mahin, V.V. Bertero, A.K. Chopra and R. Collins - 1976 (PB 271 425)A14
- EERC 76-23 "A Study on the Major Factors Influencing the Strength of Masonry Prisms," by N.M. Mostaghel, R.L. Mayes, R. W. Clough and S.W. Chen - 1976 (Not published)
- EERC 76-24 "GADFLA - A Computer Program for the Analysis of Pore Pressure Generation and Dissipation during Cyclic or Earthquake Loading," by J.R. Booker, M.S. Rahman and H.B. Seed - 1976 (PB 263 947)A04
- EERC 76-25 "Seismic Safety Evaluation of a R/C School Building," by B. Bresler and J. Axley - 1976
- EERC 76-26 "Correlative Investigations on Theoretical and Experimental dynamic Behavior of a Model Bridge Structure," by K. Kawashima and J. Penzien - 1976 (PB 263 388)A11
- EERC 76-27 "Earthquake Response of Coupled Shear Wall Buildings," by T. Srichatrapimuk - 1976 (PB 265 157)A07
- EERC 76-28 "Tensile Capacity of Partial Penetration Welds," by E.P. Popov and R.M. Stephen - 1976 (PB 262 899)A03
- EERC 76-29 "Analysis and Design of Numerical Integration Methods in Structural Dynamics," by H.M. Hilber - 1976 (PB 264 410)A06
- EERC 76-30 "Contribution of a Floor System to the dynamic Characteristics of Reinforced Concrete Buildings," by L.E. Malik and V.V. Bertero - 1976 (PB 272 247)A13
- EERC 76-31 "The Effects of Seismic Disturbances on the Golden Gate Bridge," by F. Baron, M. Arikan and R.E. Hamati - 1976 (PB 272 279)A09
- EERC 76-32 "Infilled Frames in Earthquake Resistant Construction," by R.E. Klingner and V.V. Bertero - 1976 (PB 265 892)A13

- UCB/EERC-77/01 "PLUSH - A Computer Program for Probabilistic Finite Element Analysis of Seismic Soil-Structure Interaction," by M.P. Romo Organista, J. Lysmer and H.B. Seed - 1977
- UCB/EERC-77/02 "Soil-Structure Interaction Effects at the Humboldt Bay Power Plant in the Ferndale Earthquake of June 7, 1975," by J.E. Valera, H.B. Seed, C.F. Tsai and J. Lysmer - 1977 (PB 265 795)A04
- UCB/EERC-77/03 "Influence of Sample Disturbance on Sand Response to Cyclic Loading," by K. Mori, H.B. Seed and C.K. Chan - 1977 (PB 267 352)A04
- UCB/EERC-77/04 "Seismological Studies of Strong Motion Records," by J. Shoja-Taheri - 1977 (PB 269 655)A10
- UCB/EERC-77/05 "Testing Facility for Coupled-Shear Walls," by L. Li-Hyung, V.V. Bertero and E.P. Popov - 1977
- UCB/EERC-77/06 "Developing Methodologies for Evaluating the Earthquake Safety of Existing Buildings," by No. 1 - B. Bresler; No. 2 - B. Bresler, T. Okada and D. Zisling; No. 3 - T. Okada and B. Bresler; No. 4 - V.V. Bertero and B. Bresler - 1977 (PB 267 354)A08
- UCB/EERC-77/07 "A Literature Survey - Transverse Strength of Masonry Walls," by Y. Omote, R.L. Mayes, S.W. Chen and R.W. Clough - 1977 (PB 277 933)A07
- UCB/EERC-77/08 "DRAIN-TABS: A Computer Program for Inelastic Earthquake Response of Three Dimensional Buildings," by R. Guendelman-Israel and G.H. Powell - 1977 (PB 270 693)A07
- UCB/EERC-77/09 "SUBWALL: A Special Purpose Finite Element Computer Program for Practical Elastic Analysis and Design of Structural Walls with Substructure Option," by D.Q. Le, H. Peterson and E.P. Popov - 1977 (PB 270 567)A05
- UCB/EERC-77/10 "Experimental Evaluation of Seismic Design Methods for Broad Cylindrical Tanks," by D.P. Clough (PB 272 280)A13
- UCB/EERC-77/11 "Earthquake Engineering Research at Berkeley - 1976," - 1977 (PB 273 507)A09
- UCB/EERC-77/12 "Automated Design of Earthquake Resistant Multistory Steel Building Frames," by N.D. Walker, Jr. - 1977 (PB 276 526)A09
- UCB/EERC-77/13 "Concrete Confined by Rectangular Hoops Subjected to Axial Loads," by J. Vallenias, V.V. Bertero and E.P. Popov - 1977 (PB 275 165)A06
- UCB/EERC-77/14 "Seismic Strain Induced in the Ground During Earthquakes," by Y. Sugimura - 1977 (PB 284 201)A04
- UCB/EERC-77/15 "Bond Deterioration under Generalized Loading," by V.V. Bertero, E.P. Popov and S. Viathanatepa - 1977
- UCB/EERC-77/16 "Computer Aided Optimum Design of Ductile Reinforced Concrete Moment Resisting Frames," by S.W. Zagajeski and V.V. Bertero - 1977 (PB 280 137)A07
- UCB/EERC-77/17 "Earthquake Simulation Testing of a Stepping Frame with Energy-Absorbing Devices," by J.M. Kelly and D.F. Tzstoo - 1977 (PB 273 506)A04
- UCB/EERC-77/18 "Inelastic Behavior of Eccentrically Braced Steel Frames under Cyclic Loadings," by C.W. Roeder and E.P. Popov - 1977 (PB 275 526)A15
- UCB/EERC-77/19 "A Simplified Procedure for Estimating Earthquake-Induced Deformations in Dams and Embankments," by F.I. Makdisi and H.B. Seed - 1977 (PB 276 820)A04
- UCB/EERC-77/20 "The Performance of Earth Dams during Earthquakes," by H.B. Seed, F.I. Makdisi and P. de Alba - 1977 (PB 276 821)A04
- UCB/EERC-77/21 "Dynamic Plastic Analysis Using Stress Resultant Finite Element Formulation," by P. Lukkunapvasit and J.M. Kelly - 1977 (PB 275 453)A04
- UCB/EERC-77/22 "Preliminary Experimental Study of Seismic Uplift of a Steel Frame," by R.W. Clough and A.A. Huckelbridge 1977 (PB 278 769)A08
- UCB/EERC-77/23 "Earthquake Simulator Tests of a Nine-Story Steel Frame with Columns Allowed to Uplift," by A.A. Huckelbridge - 1977 (PB 277 944)A09
- UCB/EERC-77/24 "Nonlinear Soil-Structure Interaction of Skew Highway Bridges," by M.-C. Chen and J. Penzien - 1977 (PB 276 176)A07
- UCB/EERC-77/25 "Seismic Analysis of an Offshore Structure Supported on Pile Foundations," by D.D.-N. Liou and J. Penzien 1977 (PB 283 180)A06
- UCB/EERC-77/26 "Dynamic Stiffness Matrices for Homogeneous Viscoelastic Half-Planes," by G. Dasgupta and A.K. Chopra - 1977 (PB 279 654)A06
- UCB/EERC-77/27 "A Practical Soft Story Earthquake Isolation System," by J.M. Kelly, J.M. Eidinger and C.J. Derham - 1977 (PB 276 814)A07
- UCB/EERC-77/28 "Seismic Safety of Existing Buildings and Incentives for Hazard Mitigation in San Francisco: An Exploratory Study," by A.J. Meltsner - 1977 (PB 281 970)A05
- UCB/EERC-77/29 "Dynamic Analysis of Electrohydraulic Shaking Tables," by D. Rea, S. Abedi-Hayati and Y. Takahashi 1977 (PB 282 569)A04
- UCB/EERC-77/30 "An Approach for Improving Seismic - Resistant Behavior of Reinforced Concrete Interior Joints," by B. Galunic, V.V. Bertero and E.P. Popov - 1977 (PB 290 870)A06

- UCB/EERC-78/01 "The Development of Energy-Absorbing Devices for Aseismic Base Isolation Systems," by J.M. Kelly and D.F. Tsztoo - 1978 (PB 284 978)A04
- UCB/EERC-78/02 "Effect of Tensile Prestrain on the Cyclic Response of Structural Steel Connections," by J.G. Bouwkamp and A. Mukhopadhyay - 1978
- UCB/EERC-78/03 "Experimental Results of an Earthquake Isolation System using Natural Rubber Bearings," by J.M. Eiding and J.M. Kelly - 1978 (PB 281 686)A04
- UCB/EERC-78/04 "Seismic Behavior of Tall Liquid Storage Tanks," by A. Niwa - 1978 (PB 284 917)A14
- UCB/EERC-78/05 "Hysteretic Behavior of Reinforced Concrete Columns Subjected to High Axial and Cyclic Shear Forces," by S.W. Zagajski, V.V. Bertero and J.G. Bouwkamp - 1978 (PB 283 858)A13
- UCB/EERC-78/06 "Inelastic Beam-Column Elements for the ANSR-I Program," by A. Riahi, D.G. Row and G.H. Powell - 1978
- UCB/EERC-78/07 "Studies of Structural Response to Earthquake Ground Motion," by O.A. Lopez and A.K. Chopra - 1978 (PB 282 790)A05
- UCB/EERC-78/08 "A Laboratory Study of the Fluid-Structure Interaction of Submerged Tanks and Caissons in Earthquakes," by R.C. Byrd - 1978 (PB 284 957)A08
- UCB/EERC-78/09 "Model for Evaluating Damageability of Structures," by I. Sakamoto and B. Bresler - 1978
- UCB/EERC-78/10 "Seismic Performance of Nonstructural and Secondary Structural Elements," by I. Sakamoto - 1978
- UCB/EERC-78/11 "Mathematical Modelling of Hysteresis Loops for Reinforced Concrete Columns," by S. Nakata, T. Sproul and J. Penzien - 1978
- UCB/EERC-78/12 "Damageability in Existing Buildings," by T. Blejwas and B. Bresler - 1978
- UCB/EERC-78/13 "Dynamic Behavior of a Pedestal Base Multistory Building," by R.M. Stephen, E.L. Wilson, J.G. Bouwkamp and M. Button - 1978 (PB 286 650)A08
- UCB/EERC-78/14 "Seismic Response of Bridges - Case Studies," by R.A. Imbsen, V. Nutt and J. Penzien - 1978 (PB 286 503)A10
- UCB/EERC-78/15 "A Substructure Technique for Nonlinear Static and Dynamic Analysis," by D.G. Row and G.H. Powell - 1978 (PB 288 077)A10
- UCB/EERC-78/16 "Seismic Risk Studies for San Francisco and for the Greater San Francisco Bay Area," by C.S. Oliveira - 1978
- UCB/EERC-78/17 "Strength of Timber Roof Connections Subjected to Cyclic Loads," by P. Gülkan, R.L. Mayes and R.W. Clough - 1978
- UCB/EERC-78/18 "Response of K-Braced Steel Frame Models to Lateral Loads," by J.G. Bouwkamp, R.M. Stephen and E.P. Popov - 1978
- UCB/EERC-78/19 "Rational Design Methods for Light Equipment in Structures Subjected to Ground Motion," by J.L. Sackman and J.M. Kelly - 1978 (PB 292 357)A04
- UCB/EERC-78/20 "Testing of a Wind Restraint for Aseismic Base Isolation," by J.M. Kelly and D.E. Chitty - 1978 (PB 292 833)A03
- UCB/EERC-78/21 "APOLLO - A Computer Program for the Analysis of Pore Pressure Generation and Dissipation in Horizontal Sand Layers During Cyclic or Earthquake Loading," by P.P. Martin and H.B. Seed - 1978 (PB 292 835)A04
- UCB/EERC-78/22 "Optimal Design of an Earthquake Isolation System," by M.A. Bhatti, K.S. Pister and E. Polak - 1978 (PB 294 735)A06
- UCB/EERC-78/23 "MASH - A Computer Program for the Non-Linear Analysis of Vertically Propagating Shear Waves in Horizontally Layered Deposits," by P.P. Martin and H.B. Seed - 1978 (PB 293 101)A05
- UCB/EERC-78/24 "Investigation of the Elastic Characteristics of a Three Story Steel Frame Using System Identification," by I. Kaya and H.D. McNiven - 1978
- UCB/EERC-78/25 "Investigation of the Nonlinear Characteristics of a Three-Story Steel Frame Using System Identification," by I. Kaya and H.D. McNiven - 1978
- UCB/EERC-78/26 "Studies of Strong Ground Motion in Taiwan," by Y.M. Hsiung, B.A. Bolt and J. Penzien - 1978
- UCB/EERC-78/27 "Cyclic Loading Tests of Masonry Single Piers: Volume 1 - Height to Width Ratio of 2," by P.A. Hidalgo, R.L. Mayes, H.D. McNiven and R.W. Clough - 1978
- UCB/EERC-78/28 "Cyclic Loading Tests of Masonry Single Piers: Volume 2 - Height to Width Ratio of 1," by S.-W.J. Chen, P.A. Hidalgo, R.L. Mayes, R.W. Clough and H.D. McNiven - 1978
- UCB/EERC-78/29 "Analytical Procedures in Soil Dynamics," by J. Lysmer - 1978

- UCB/EERC-79/01 "Hysteretic Behavior of Lightweight Reinforced Concrete Beam-Column Subassemblages," by B. Forzani, E.P. Popov, and V.V. Bertero - 1979
- UCB/EERC-79/02 "The Development of a Mathematical Model to Predict the Flexural Response of Reinforced Concrete Beams to Cyclic Loads, Using System Identification," by J.F. Stanton and H.D. McNiven - 1979
- UCB/EERC-79/03 "Linear and Nonlinear Earthquake Response of Simple Torsionally Coupled Systems," by C.L. Kan and A.K. Chopra - 1979
- UCB/EERC-79/04 "A Mathematical Model of Masonry for Predicting Its Linear Seismic Response Characteristics," by Y. Mengi and H.D. McNiven - 1979
- UCB/EERC-79/05 "Mechanical Behavior of Light Weight Concrete Confined by Different Types of Lateral Reinforcement," by M.A. Manrique, V.V. Bertero and E.P. Popov - 1979
- UCB/EERC-79/06 "Static Tilt Tests of a Tall Cylindrical Liquid Storage Tank," by R.W. Clough and A. Niwa - 1979
- UCB/EERC-79/07 "The Design of Steel Energy Absorbing Restrainers and Their Incorporation Into Nuclear Power Plants for Enhanced Safety: Volume 1 - Summary Report," by P.N. Spencer, V.F. Zackay, and E.R. Parker - 1979
- UCB/EERC-79/08 "The Design of Steel Energy Absorbing Restrainers and Their Incorporation Into Nuclear Power Plants for Enhanced Safety: Volume 2 - The Development of Analyses for Reactor System Piping," "Simple Systems" by M.C. Lee, J. Penzien, A.K. Chopra, and K. Suzuki "Complex Systems" by G.H. Powell, E.L. Wilson, R.W. Clough and D.G. Row - 1979
- UCB/EERC-79/09 "The Design of Steel Energy Absorbing Restrainers and Their Incorporation Into Nuclear Power Plants for Enhanced Safety: Volume 3 - Evaluation of Commercial Steels," by W.S. Owen, R.M.N. Pelloux, R.O. Ritchie, M. Faral, T. Ohhashi, J. Toplosky, S.J. Hartman, V.F. Zackay, and E.R. Parker - 1979
- UCB/EERC-79/10 "The Design of Steel Energy Absorbing Restrainers and Their Incorporation Into Nuclear Power Plants for Enhanced Safety: Volume 4 - A Review of Energy-Absorbing Devices," by J.M. Kelly and M.S. Skinner - 1979
- UCB/EERC-79/11 "Conservatism In Summation Rules for Closely Spaced Modes," by J.M. Kelly and J.L. Sackman - 1979

- UCB/EERC-79/12 "Cyclic Loading Tests of Masonry Single Piers Volume 3 - Height to Width Ratio of 0.5," by P.A. Hidalgo, R.L. Mayes, H.D. McNiven and R.W. Clough - 1979
- UCB/EERC-79/13 "Cyclic Behavior of Dense Coarse-Grain Materials in Relation to the Seismic Stability of Dams," by N.G. Banerjee, H.B. Seed and C.K. Chan - 1979
- UCB/EERC-79/14 "Seismic Behavior of R/C Interior Beam Column Subassemblages," by S. Viwathanatepa, E.P. Popov and V.V. Bertero - 1979
- UCB/EERC-79/15 "Optimal Design of Localized Nonlinear Systems with Dual Performance Criteria Under Earthquake Excitations," by M.A. Bhatti - 1979
- UCB/EERC-79/16 "OPTDYN - A General Purpose Optimization Program for Problems with or without Dynamic Constraints," by M.A. Bhatti, E. Polak and K.S. Pister - 1979
- UCB/EERC-79/17 "ANSR-II, Analysis of Nonlinear Structural Response, Users Manual," by D.P. Mondkar and G.H. Powell - 1979
- UCB/EERC-79/18 "Soil Structure Interaction in Different Seismic Environments," A. Gomez-Masso, J. Lysmer, J.-C. Chen and H.B. Seed - 1979
- UCB/EERC-79/19 "ARMA Models for Earthquake Ground Motions," by M.K. Chang, J.W. Kwiatkowski, R.F. Nau, R.M. Oliver and K.S. Pister - 1979
- UCB/EERC-79/20 "Hysteretic Behavior of Reinforced Concrete Structural Walls," by J.M. Vallenias, V.V. Bertero and E.P. Popov - 1979
- UCB/EERC-79/21 "Studies on High-Frequency Vibrations of Buildings I: The Column Effects," by J. Lubliner - 1979
- UCB/EERC-79/22 "Effects of Generalized Loadings on Bond Reinforcing Bars Embedded in Confined Concrete Blocks," by S. Viwathanatepa, E.P. Popov and V.V. Bertero - 1979
- UCB/EERC-79/23 "Shaking Table Study of Single-Story Masonry Houses, Volume 1: Test Structures 1 and 2," by P. Güllkan, R.L. Mayes and R.W. Clough - 1979
- UCB/EERC-79/24 "Shaking Table Study of Single-Story Masonry Houses, Volume 2: Test Structures 3 and 4," by P. Güllkan, R.L. Mayes and R.W. Clough - 1979
- UCB/EERC-79/25 "Shaking Table Study of Single-Story Masonry Houses, Volume 3: Summary, Conclusions and Recommendations," by R.W. Clough, P. Güllkan and R.L. Mayes

- UCB/EERC-79/26 "Recommendations for a U.S.-Japan Cooperative Research Program Utilizing Large-Scale Testing Facilities," by U.S.-Japan Planning Group - 1979
- UCB/EERC-79/27 "Earthquake-Induced Liquefaction Near Lake Amatitlan, Guatemala," by H.B. Seed, I. Arango, C.K. Chan, A. Gomez-Masso and R. Grant de Ascoli - 1979
- UCB/EERC-79/28 "Infill Panels: Their Influence on Seismic Response of Buildings," by J.W. Axley and V.V. Bertero - 1979
- UCB/EERC-79/29 "3D Truss Bar Element (Type 1) for the ANSR-II Program," by D.P. Mondkar and G.H. Powell - 1979
- UCB/EERC-79/30 "2D Beam-Column Element (Type 5 - Parallel Element Theory) for the ANSR-II Program," by D.G. Row, G.H. Powell and D.P. Mondkar
- UCB/EERC-79/31 "3D Beam-Column Element (Type 2 - Parallel Element Theory) for the ANSR-II Program," by A. Riahi, G.H. Powell and D.P. Mondkar - 1979
- UCB/EERC-79/32 "On Response of Structures to Stationary Excitation," by A. Der Kiureghian - 1979
- UCB/EERC-79/33 "Undisturbed Sampling and Cyclic Load Testing of Sands," by S. Singh, H.B. Seed and C.K. Chan - 1979
- UCB/EERC-79/34 "Interaction Effects of Simultaneous Torsional and Compressional Cyclic Loading of Sand," by P.M. Griffin and W.N. Houston - 1979

